Light-Harvesting Studies in Electrostatically Bonded All-Quantum Dot Assemblies

विद्या वाचस्पति की

उपाधि की अपेक्षाओं की आंशिक पूर्ति में प्रस्तुत शोध प्रबंध

A thesis submitted in partial fulfilment of the requirements of the degree of Doctor of Philosophy

द्वारा / By

प्रद्युत रॉय / Pradyut Roy

पंजीकरण सं. २०१७२०२२/ Registration No.: 20172022

शोध प्रबंध पर्यवेक्षक / Thesis Supervisor:

डॉ. प्रमोद पी. पिल्लई / Dr. Pramod P. Pillai

भारतीय विज्ञान शिक्षा एवं अनुसंधान संस्थान पुणे

INDIAN INSTITUTE OF SCIENCE EDUCATION AND RESEARCH PUNE

2024

Dedicated to

'Maa, Baba, &

My Entire Family'

Certificate

Certified that the work incorporated in the thesis entitled "***Light-Harvesting Studies in Electrostatically Bonded All-Quantum Dot Assemblies***" submitted by **Pradyut Roy** was carried out by the candidate, under my supervision. The work presented here or any part of it has not been included in any other thesis submitted previously for the award of any degree or diploma from any other University or institution.

Pramod P

Dr. Pramod P. Pillai
(Thesis Supervisor)

Date: 22/07/2024

Declaration by Student

Name of Student: **Pradyut Roy**

Reg. No.: **20172022**

Thesis Supervisor(s): Dr. Pramod P. Pillai

Department: Department of Chemistry

Date of joining program: 01st August 2017

Date of Pre-Synopsis Seminar: 25th January 2024

Title of Thesis: '**Light-Harvesting Studies in Electrostatically Bonded All-Quantum Dot Assemblies**'

I declare that this written submission represents my idea in my own words and where others' ideas have been included; I have adequately cited and referenced the original sources. I declare that I have acknowledged collaborative work and discussions wherever such work has been included. I also declare that I have adhered to all principles of academic honesty and integrity and have not misrepresented or fabricated or falsified any idea/data/fact/source in my submission. I understand that violation of the above will be cause for disciplinary action by the Institute and can also evoke penal action from the sources which have thus not been properly cited or from whom proper permission has not been taken when needed.

The work reported in this thesis is the original work done by me under the guidance of Dr. Pramod P. Pillai

Date: 22/07/2024

Signature of the student

Acknowledgement

As a famous quote says, '*we never thank the Sun enough for all it does for us, for all the light it shines around, for the warmth, beauty, and love*'. Just the same, I am very sure that no amount of phrases could express all the gratitude I have to the people around me who have made immense contributions in my life and in my career. So, I would like to state right at the beginning of the acknowledgement section that '*I am grateful forever to IISER, and everyone'* for making my PhD life enjoyable and fruitful.

First and foremost, I would like to express my cordial gratitude to my PhD supervisor**, Dr. Pramod P. Pillai**, for his constant support and guidance throughout my PhD journey. I am very thankful to him for all his patience and effort to encourage me to improve my research and presentation skills. You always motivated me, Sir, to be professional and taught me to understand the tips and tricks of science. I am deeply grateful to you for being a great mentor. I consider myself lucky to be part of your esteemed research group, and it's been a wonderful experience for me to work under your guidance.

I was also fortunate enough to have fantastic labmates during my PhD journey. A special thanks to all my super-seniors (**Soumendu da**, **Anisha bhaiya**, and **Gayatri di**). I started my research career under the mentorship of this trio. I always feel relaxed and overwhelmed whenever I talk with you guys. I appreciate all the help and suggestions that you guys have given me since the start of my PhD. I would also like to thank my other seniors (**Sumit da** and **Indra da**) for treating me as a friend and creating a pleasant environment to work in the lab, especially all the scientific discussions and gossip. I have learned a lot from all my five seniors. I am also thankful to all the excellent present (**Kashyap**, **Vanshika**, **Ankit**, **Shreya**, **Adhra**, and **Mridul**) and past (**Sarah**, **Shana**, **Rohit**, **Jibin**, **Sriram**, **Aiswarya**, **Aparna**, **Namitha**, **Anjela**, **Sruthy**, and **Sandhra**) lab members for their support and contributions. A special thanks goes to **Kashyap**, **Vanshika**, and **Ankit** for being wonderful friends. It would be ungrateful if I didn't acknowledge **Kashyap** and **Ankit** for the brotherhood they provided, and in particular, Ankit for helping me capture beautiful photographs for my papers, especially the '*pure-blues*'. I am happy to be part of the 'NanoAlchemy team.

I would like to thank my Research Advisory Committee (RAC) members, **Prof. Nirmalya Ballav** and **Dr. Arup Kumar Rath**, for managing their time to conduct my RAC meetings and

giving valuable comments and suggestions on my research. I am also thankful to my collaborators, **Prof. Manickam Jayakannan** and **Prof. Jyotishman Dasgupta**, **Mishika Virmani**, and **Kishan K. Yadav**, for the amazing collaborative experiences, insightful discussions, and enriching outputs.

My sincere gratitude to **Prof. Sujit Kumar Ghosh**, **Prof. Partha Hazra**, and **Dr. Boopathy Gnanaprakasam** for giving me the opportunity to work in their labs during the lab rotation project. Interactions with you as well as with your group members helped me a lot in learning different skills, which was extremely useful throughout my PhD career.

I would also like to express my gratitude to **Prof. Sunil S. Bhagwat**, Director of IISER Pune; **Prof. Jayant B. Udgaonkar**, former Director of IISER Pune; **Prof. Krishna N. Ganesh**, Founder Director of IISER Pune; **Prof. Nirmalya Ballav**, Chair Chemistry; and past chairs of our department for providing excellent research facilities as well as maintaining a healthy environment in the department and in the institute. I would like to thank all staff members of our department, especially **Mr. Mayuresh Kulkarni**, **Mr. Sanjay Kumar Meena**, **Mr. Ganesh Dimbar**, **Dr. Abhijit Biswas**, and **Mr. Ravinder Malothu**, for generously helping out during our needs. I would also like to thank **Mr. Nilesh Dumbre**, a staff member of the Physics Department, for helping us repair our instruments during the fire incident at the Department of Chemistry.

I would also like to thank all my integrated PhD batchmates (**Sumit**, **Souvik**, **Sourav**, **Abhijit**, **Sandip**, **Pratim** & **Harshit**) and friends from different disciplines at IISER Pune (**Tamaghna**, **Ratheejit**, **Arnab**) who have helped me in my good and bad times. My sincere gratitude to all my teachers (**Mr. Supriya Bisoi**, **Dr. Batul Chandra Santra**, **Mr. Krishnendu Roy**, **Dr. Kanchan Bag**, **Dr. Abhinandan Rana**, **Dr. Mahadeb Maity**, **Dr. Hariprasad Sarkar**, **Dr. Subhas Mondal**, and **Dr. Shaishab Kumar Dinda**) for sharing their knowledge and experiences with me and for developing my interest in and love for science. I am truly grateful to all of my teachers; without their active role in my career, I would not have been able to achieve the successes that I have today.

I am immensely grateful to my parents and my entire family, **Mr. Uttam Roy** and **Mrs. Kajal Roy**, **Mr. Bidyut Kumar Roy**, **Mrs. Supriya Roy**, and our newest member, **Rohit (*putu*)**, for their love, blessing, and support throughout my entire life. It would have been impossible for me to reach this position without their unconditional love and care. You all are the inspiration

for me to do great in life. I have always learned from you, always to live by the truth and to never give up in life. I am also thankful to my brother for teaching me many valuable life lessons, such as ‘more than perfection, it is the intention, attitude, and determination that make a person successful’. Bless me more, Maa and Baba, so that I can achieve more success in my life and become a good human being.

I am also very grateful to all my dearest friends (**Mr. Debiprasad Ghosh**, **Mr. Deepak Sarkar**, **Dr. Suman Manna**, **Dr. Susmita Bhowmik**, **Mr. Joy Chatterjee**, and **Ms. Anwesha Bera**) for providing some of the happiest moments of my life. A special thanks to **Rimi**, **Sumit da**, and **Susmita di** for providing all the emotional supports and cares, which I would like to nourish for my entire life.

Finally, I would like to thank Mother Nature and want to stay blessed forever by Almighty God for the rest of the journey of my life.

Table of Contents

Thesis Synopsis

The diligent utilisation of sunlight by green plants has essentially paved the way for the existence of life on Earth. This interplay between light and matter is one of nature's most fascinating phenomena, which has motivated researchers to make important discoveries. Thus, in a route to mimic famous photosynthetic machinery to harvest solar energy, it is extremely necessary to gain insights into the fundamental photophysical processes that complete the process of photosynthesis. Additionally, one must acquire the skill to create structures based on governable forces such as non-covalent interactions, as preferred in nature. Our understanding of natural photosynthesis reveals that the assembly and appropriate interaction between several light-harvesting components are of prime importance for carrying out any meaningful processes. Hence, the creation of novel light harvesters, and connecting them in a precise fashion are key characteristics to mimic photosynthesis in artificial materials. In this direction, many artificial light-harvesting materials based on organic dyes, organic–inorganic hybrid metal complexes, polymers, organic/inorganic nanomaterials, etc., have been developed with the goal of simulating the fundamental mechanisms of natural photosynthetic systems, particularly photoinduced electron and energy transfer processes. Among them, colloidal semiconductor quantum dots (QDs) have emerged as exciting materials of choice, due to their impact in a wide range of fundamental, as well as applied research. This includes sensors, photovoltaic diodes, display devices, photodetectors, and so on. Besides the size-dependent quantum confinement effect, QD also possesses several other advantages, such as large absorption cross-section, narrow emission bandwidth, superior photostability, and high quantum yield, which makes them an ideal alternative to existing luminescent materials such as organic dyes, inorganic-organic complexes, and so on. Additionally, the surface ligands of QDs can also be fine-tuned to impart various non-covalent interactions to regulate their light-harvesting properties. This drives the development of donor-acceptor assemblies solely based on QDs for energy harvesting and solid-state lighting applications, a move towards mimicking natural light-harvesting system. To date, the majority of the developed all-QD based nanohybrid systems are composed of Cd- and Pb-based toxic metal ions, which restricts their use in commercial and industrial applications. In this direction, our main objective was to introduce InP-based all-QD assemblies as an environmentally friendly alternative to state-of-the-art Cd-based QDs. However, this requires addressing one of the core issues that the InP family was confronting, which was the lack of complete colour gamut in the visible region. Here, the missing piece of the jigsaw was to generate pure-blue emitting InP QDs in an aqueous

medium. Thus, the proposed thesis aims to develop strategies for the preparation of pure-blue emitting InP QDs, and examine the exciton dynamics in fundamental photophysical processes. Light-induced energy and electron transfer processes were chosen as two key photophysical processes for this investigation.

Chapter 1 begins with an overview of solar energy harvesting and an in-depth understanding of the principles of photosynthetic machinery. This is followed by the introduction of multicomponent donor-acceptor system based on traditional chromophores. Subsequently, the emergence of semiconductor QDs as an alternative luminescent material is introduced, in the context of rational design of superior multicomponent systems. The progress in the field of all-QD based multicomponent systems was then succinctly outlined. Finally, we proposed our idea to mimic photosynthesis in a more sustainable way with environmentally benign QDs, along with addressing a few important challenges that impede research on all-QD based multicomponent systems, such as the lack of availability of all primary colors, and a proper roadmap for photophysical investigations.

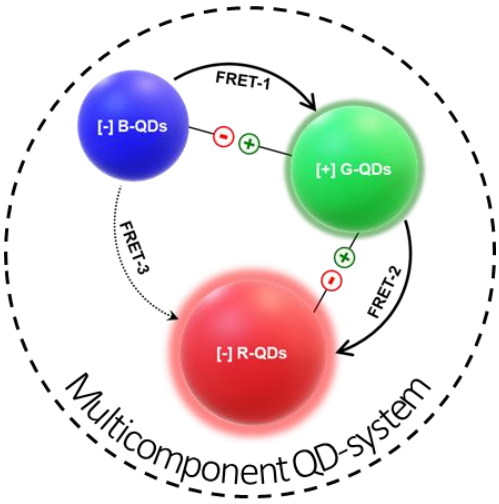

Scheme 1. Schematics of multicomponent donor–acceptor system based on all-QD assembly. Chakraborty, I. N.; **Roy, P.**; Rao, A.; Devatha, G.; Roy, S.; Pillai, P. P. The Unconventional Role of Surface Ligands in Dictating the Light Harvesting Properties of Quantum Dots. *J. Mater. Chem. A* **2021**, *9*, 7422–7457.

Chapter 2 provides a detailed description of the reagents used, instrumentations, experimental techniques, synthesis procedures of QDs, ligand exchange process, and concentration calculation of QDs. In addition, a brief overview of the formalisms for Förster resonance energy transfer and photoinduced electron transfer processes is also summarized to provide a better understanding about these processes.

In **Chapter 3**, a synthetic strategy is reported to produce InP/ZnS QDs in water, emitting in the pure-blue region. The developed water-dispersed blue-emitting InP/ZnS QDs exhibited excellent cell viability and multicolour bio-imaging ability inside the HeLa cells. Moreover, the ability of InP based pure-blue emitters to participate in an efficient Förster resonance energy transfer (FRET) process was demonstrated in the QD-dye model donor-acceptor system. Installing a favorable electrostatic interaction turned out to be crucial in achieving an efficient FRET process (E ~75%) from blue-emitting InP/ZnS QDs to rhodamine B dye (Rh B) in water.

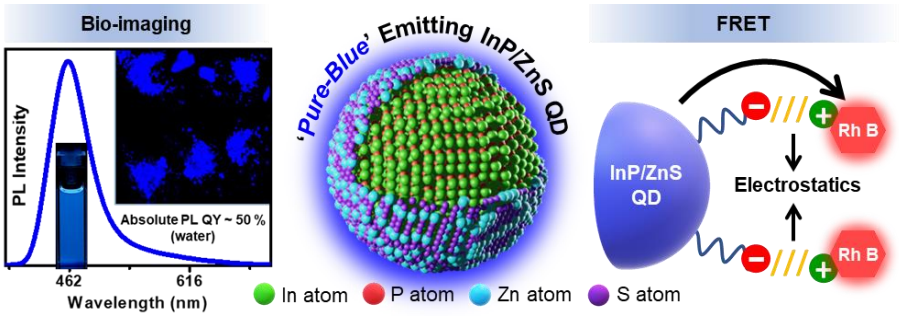

Scheme 2. Pure-blue emitting InP/ZnS QDs in water expands the scope of InP QDs for energy application and bioimaging research. **Roy, P.**; Virmani, M.; Pillai, P. P. Blue-Emitting InP Quantum Dots Participate in an Efficient Resonance Energy Transfer Process in Water. *Chem. Sci.* **2023**, *14*, 5167–5176.

Next, in **Chapter 4**, blue-emitting InP/ZnS QDs participated in an efficient electron transfer process in a model QD-dye nanohybrid system composed of blue-emitting InP/ZnS QDs donor and methylene blue acceptor dye. Steady-state and time-resolved spectroscopic studies confirms an efficient electron transfer from blue QDs to methylene blue dye in water.

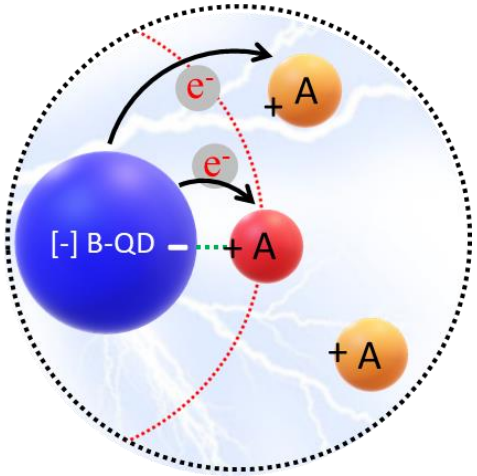

Scheme 3. Photoinduced electron transfer study in an electrostatically-assembled blue-emitting InP/ZnS QD donor and MB dye acceptor. (Manuscript under preparation).

After successful demonstration of energy and electron transfer processes with blue emitting InP/ZnS QDs, in the final **Chapter 5**, a series of all-QD based energy transfer systems were developed at the dyad level, based on blue-, green-, & red-emitting InP/ZnS QD and $CuInS_2$/ZnS QDs (blue-green, green-red, and blue-red all-QD assemblies). Detailed steady-state, and time-resolved spectroscopic experiments were performed to conclude the process of energy transfer in all-QD systems. The demonstration of resonance energy transfer process in all-QD based donor–acceptor systems is fundamentally intriguing and can have far-reaching applications in the areas of biophysics as well as other light-harvesting studies including photovoltaics and photocatalysis.

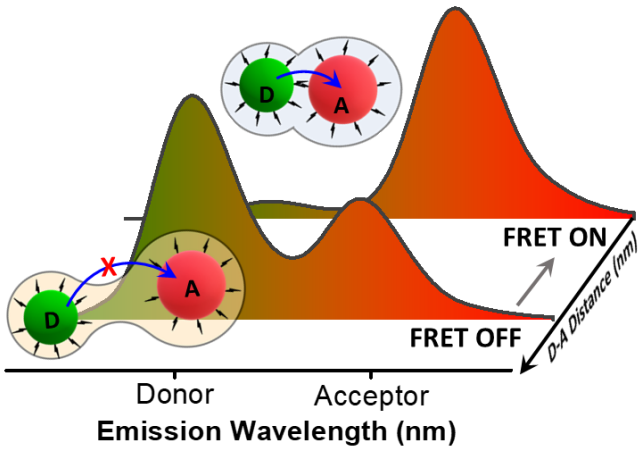

Scheme 4. Electrostatically assembled all-QD dyad assembly for FRET study. **Roy, P.**; Devatha, G.; Roy, S.; Rao, A.; Pillai, P. P. Electrostatically Driven Resonance Energy Transfer in an All-Quantum Dot Based Donor–Acceptor System. *J. Phys. Chem. Lett.* **2020**, *11*, 5354–5360. **Roy, P.**; Sury, A. S.; Pillai, P. P. Resonance Energy Transfer in Electrostatically Assembled Donor–Acceptor System based on Blue-Emitting InP Quantum Dots. *Chem. Phys. Impact* **2023**, *7*, 100334. **Roy, P.**; Sury, A. S.; Pillai, P. P. Electrostatics Enable Resonance Energy Transfer in InP Based All-Quantum Dot Donor–Acceptor Assembly. *Appl. Phys. Lett.* **2024**, *124*, 222104.

In summary, the proposed thesis work introduces environmentally friendly InP/ZnS QDs as blue emitter and completes the color gamut. It also showcases the potential of InP QDs as an alternative to the existing luminescent materials for future light-harvesting studies.

Chapter – 1

Introduction to Multicomponent Light Harvesting Systems

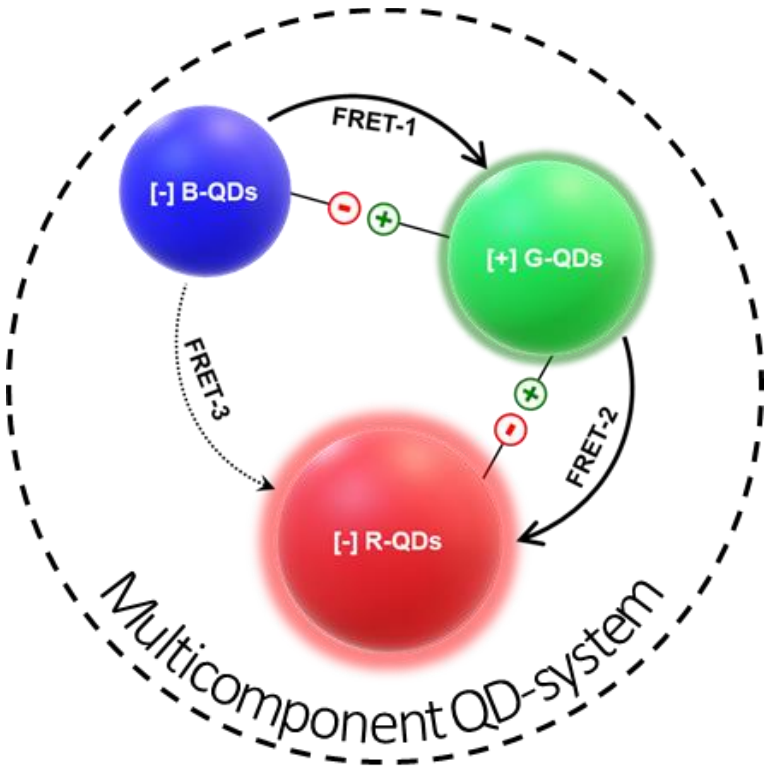

Part of this Chapter has been adapted from the following paper with permission. Copyright 2021, Royal Society of Chemistry.

Chakraborty, I. N.; **Roy, P.**; Rao, A.; Devatha, G.; Roy, S.; Pillai, P. P. The Unconventional Role of Surface Ligands in Dictating the Light Harvesting Properties of Quantum Dots. *J. Mater. Chem. A* **2021**, *9*, 7422–7457.

1.1 Introduction

Historically, 'Sun' has been one of the most important natural resources used by mankind to meet their daily needs.[1–2] In ancient era, the enormous energy stored in the sunlight was used for many intuitive daily applications such as lighting purposes, controlling the temperature inside the rooms (both heating and cooling, as required), concentrating sunlight to torch fire, and so on.[1–4] The ever-increasing energy demand to meet the rapid rise of technology in the 20th century led to the uncontrolled and careless use of non-renewable sources (like coal, natural gas, fossil fuels, oil and petroleum, etc.).[5–7] The excess consumption of fossil fuels has resulted in their rapid depletion as well as serious environmental hazards.[6] These alarming situations have led to the increasing interest in alternate power/fuel research such as bio-fuel, solar energy, geothermal energy, nuclear energy, and wind energy research (**Figure 1.1**).[7] For instance, the annual production of renewable energy worldwide rises at a rate of ~7%, and currently supplies 8,000 TWh of electricity. Among these, renewable solar energy is a promising alternative, since the supply of energy from Sun to the Earth is surplus: 3 x 10^{24} Joules a year or about 10,000 times more than the global population currently consumes.[8]

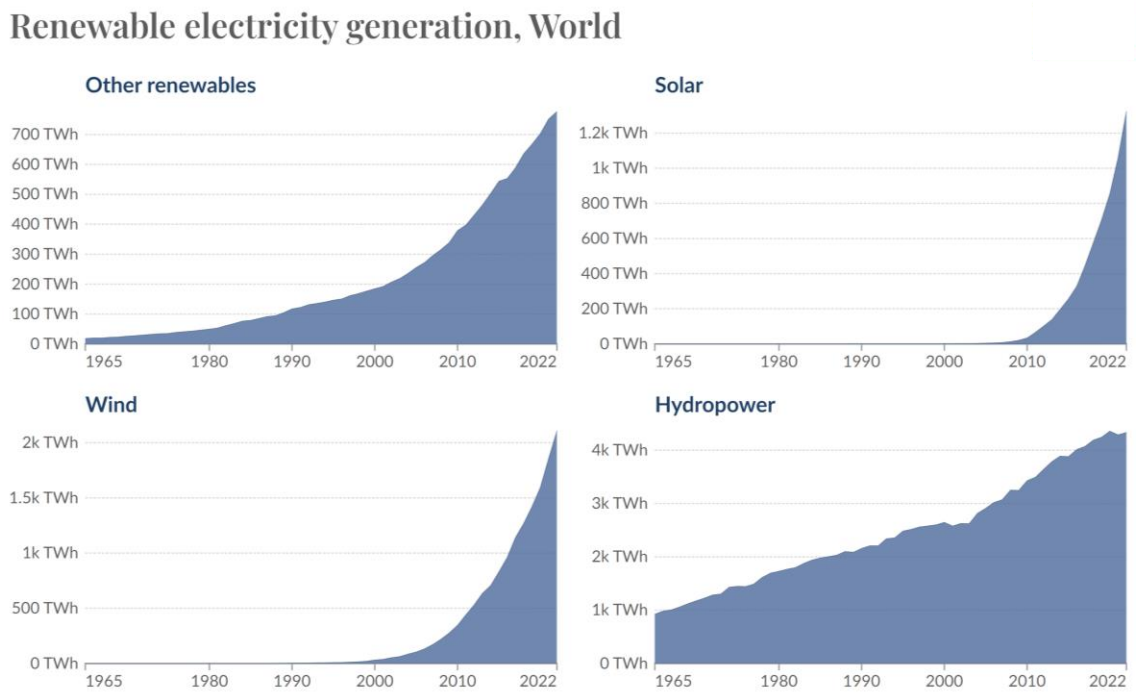

Figure 1.1 Plots showing various renewable energy sources, and their production growth over time (years). Here, other renewables refer to geothermal, waste, wave, tidal, etc. All forms of renewable energy collectively produce 8,000 TWh of electricity all over the world. TWh stands for Terawatt hours. Reproduced with permission from reference 7. Energy Institute – Statistical Review of World Energy (2023) – with major processing by Our World in Data.

In another words, covering 0.1 % of the Earth's surface with solar cells with an efficiency of ~10 % would satisfy our needs.[8] Thus, in the last few decades the focus has once again shifted to Sun, and how to harvest the sunlight in an efficient, large-scale, and affordable way. This has led to the emergence of modern energy research that spans from gaining fundamental understandings to commercialization of light harvesting devices.[8–10] Technically, the energy from the Sun can be used to drive three main processes in materials: (i) change in temperature, (ii) funnelling of energy, and (iii) movement of electrons.[11–12] Even though temperature changes in materials are often ungovernable, recent advances have led to the regulation of temperatures using plasmonic materials.[13–14] On the other hand, the extensive research in the last three decades has led to a precise control on the movements of energy and electrons through materials.[15–16] An understanding of the energy and electron transfer processes within artificial materials are the key to any light harvesting technology.

1.2 Mimicking the Process of Photosynthesis

As in any other area of science, energy research has been inspired by natural phenomena, like photosynthesis, vision, bioluminescence, etc.[17–20] For instance, the efficient movement of energy and electrons in natural photosynthetic reaction centres still remains the benchmark for energy researchers to follow.[12,21–23] The mimicking of natural processes, like photoinduced energy and electron transfer during photosynthesis, is a logical strategy adopted by researchers to achieve efficient light-harvesting using artificial materials.[12,15] Dedicated efforts in this direction have helped us to gain deeper understanding into the various mechanisms involved in photoinduced energy and electron transfer processes (**Figure 1.2**).[12] Among the many mechanisms, Förster resonance energy transfer (FRET) is a well-understood example, and it has been explored in many artificial materials to funnel photonic energy across long distances (10–100 Å).[12,29–30] A FRET process involves the non-radiative transfer of energy from an excited donor through a dipole–dipole interaction, triggering coupled transitions in an acceptor (**Figure 1.2a**).[18,24–25] Some of the important factors that govern the FRET process include the spectral overlap integral, donor–acceptor distance, and orientation factor. Generally, FRET results in the formation of a fluorescent complex. On the other hand, the photoinduced electron transfer (PET) process involves the transfer of an electron from a donor to an acceptor, and this is mainly governed by the energetics of the donor–acceptor pair. The transfer of electrons from a donor to an acceptor should be thermodynamically feasible for an efficient PET to happen.[12,25]

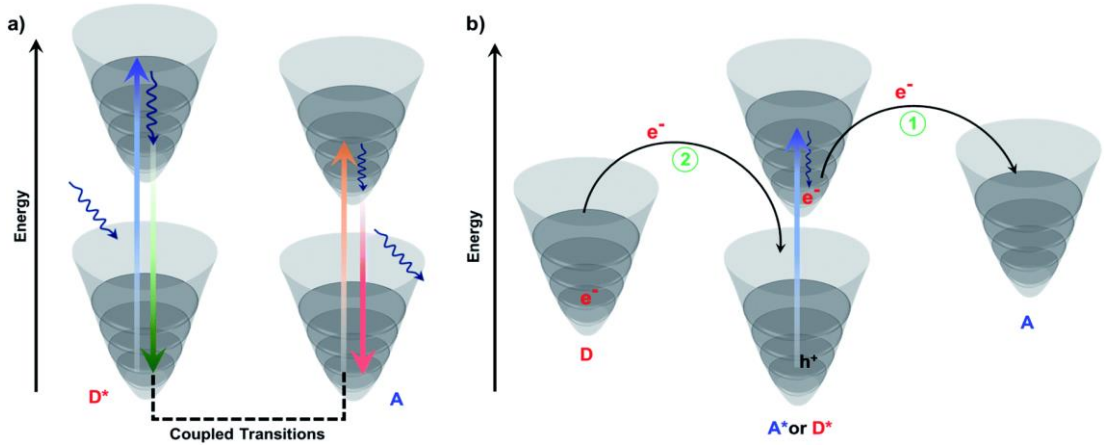

Figure 1.2 General schemes of (a) Förster resonance energy transfer (FRET) and (b) photoinduced electron transfer (PET) processes are shown in terms of potential energy diagram (Note: Only the bottom part of the potential energy surface is shown, here). A PET process can occur either through the photoexcitation of the donor (photooxidation, labelled as '1') or the acceptor (photoreduction, labelled as '2'). The photooxidation process involves the transfer of electrons from an excited donor (D^*) to a ground state acceptor (A). On the other hand, the photoreduction process involves the transfer of electrons from a ground state donor (D) to an excited state acceptor (A^*). Reproduced in part from reference 25. Copyright 2021, Royal Society of Chemistry.

A PET process can occur either through the photoexcitation of the donor (photooxidation) or the acceptor (photoreduction), as shown in **Figure 1.2b**. In most cases, a PET process results in the formation of a non-luminescent charge-separated complex.[12] Both these governable light-induced energy and electron transfer processes form an integral part of photosynthesis.[12,17–20] As per the understanding of photosynthetic machinery, there is no single champion component that is *solely* responsible for the efficient transport of energy and electrons during the photosynthesis (**Figure 1.3**).[12,17] Rather, nature has assembled a series of champion components in a precise fashion, which work in tandem to maximise the efficiency of the respective photophysical process.[21–22] During photosynthesis, long-range energy transfer occurs from light-absorbing pigments to the reaction centre, followed by a long-range electron-transfer process (**Figure 1.3**).[21–23] Such long-range processes demand effective communication between individual light-harvesting components. Nature has built a self-assembled masterpiece (*the photosynthetic reaction centre*) to allow control over long-range energy and electron transfer processes through the precise control of various interparticle interactions.[17–22]

How to mimic the photosynthesis in achieving a precise assembly of different artificial light harvesting components is of prime importance, to carry out any meaningful process. Moreover, connecting the individual champion materials (pigment-pigment and pigment-protein interactions) can allow us to get a grasp on a broader ground of action to address various complex photophysical processes during artificial light-harvesting.[26–29] One of the most

modular ways to assemble more than one system is via non-covalent interactions, which are often used by nature to devise its self-assembled machinery.[12,25] The proper tuning of non-covalent interactions can bring the light-harvesting components close to each other in a precise orientation, which in turn regulate various photophysical processes or chemical transformations.[29–35] Thus, it is essential to select suitable artificial light harvesting materials that can exhibit both photophysical properties and provide flexibility for tuning interparticle interactions.

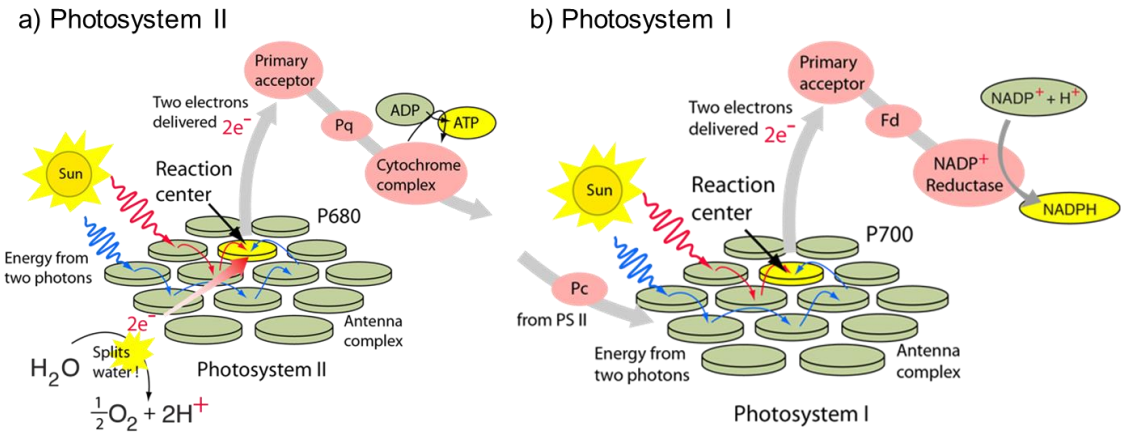

Figure 1.3 Schematics of photosynthetic reaction center. Cooperative efforts from the sensitive combination of pigment dyes and antenna complexes drives energy and electrons towards the primary reaction centre, thus replenishing the 'energy currency of the cell' (ATP), and NADPH cofactor in (a) Photosystem II, and (b) Photosystem I, respectively. Reproduced with permission from reference 17. Copyright 1995, William C. Brown Publishers.

1.3 Multicomponent Donor – Acceptor systems

An ideal light-harvesting material should exhibit properties such as a high molar extinction coefficient, excellent photo/thermal stability, easily tuneable absorption/emission profiles, high electron–hole mobility, and long–lived charge-separated states.[29–34] Aimed at this, many artificial materials have been developed in the last few decades, including organic, inorganic, polymeric, and biomolecular materials, and metallic/semiconductor nanomaterials.[29–34] In one such example, Rosławska, Schull, and co-workers have developed a light-harvesting triad assembly based on the derivatives of phthalocyanine chromophores.[33] It has been observed that metalation with palladium and zinc ions significantly alters the optical energy-gap of the phthalocyanine moiety. Both metal-phthalocyanines displayed enhancements in the optical energy gap in comparison with free-base phthalocyanine (H_2Pc) (~1.81 eV). Palladium-phthalocyanine (PdPc) and zinc-phthalocyanine (ZnPc) are characterized by emission lines at

~1.92 eV and ~1.90 eV, respectively. Accordingly, an energy relay trimer was developed, where the larger energy gap PdPc molecule was separated from the smaller energy gap H_2Pc by the intermediate energy gap ZnPc molecule (**Figure 1.4a**). The cascade resonance energy transfer (RET) was investigated based on the scanning tunnelling microscopy-induced luminescence (STML) spectrum (**Figure 1.4b**). The obtained emission characteristics for the three chromophores confirm a sequential energy transfer process from donor PdPc molecules to acceptor H_2Pc molecule, via ZnPc ancillary unit. A detailed STML spectral study in this energy cascade configuration demonstrates that sequential energy transfer is more advantageous to funnel energy between distant centres with high efficiency, a concept at play in photosynthetic machinery as well. In another study by Wasielewski and co-workers, light harvesting antenna structure was developed via the self-assembly of perylenediimide chromophores that has optoelectronic characteristics analogous to chlorophyll a unit (**Figure 1.5a**).[26] The self-assembling antenna reactor array exhibited sequential energy and electron transfer processes at time scales of 21 ps and 7 ps, respectively. This combination of energy and electron transfer processes in a single integrated assembly is the closest replica to the photosynthetic reaction center (**Figure 1.5a**).

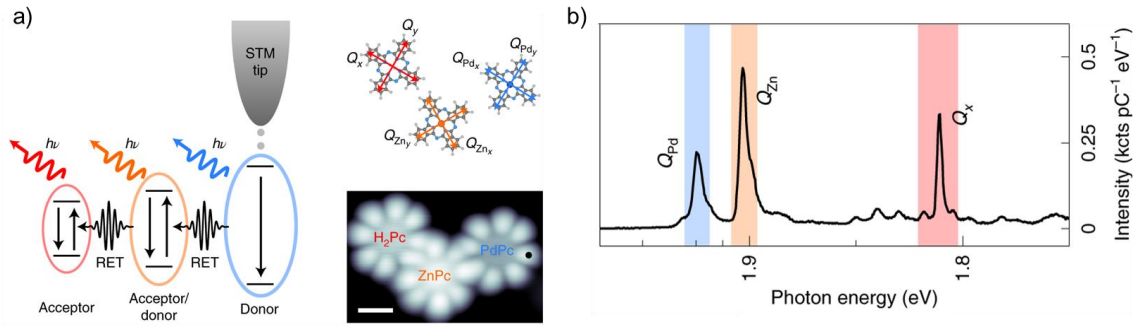

Figure 1.4 (a) Schematics of sequential energy transfer process from high to moderate to low energy gap chromophores. STM-image of model trimer array based on PdPc:::ZnPc:::H_2Pc assembly on NaCl substrate (right portion). The black dot on STM image describe the STM tip position used to measure the STM spectrum as described in (b) (I = 10 pA, V = –2.5 V). The presence of characteristics emission from all three chromophores upon photoexcitation of only PdPc chromophore confirm the cascade energy transfer process from donor PdPc to ancillary ZnPc to acceptor H_2Pc chromophore. Reproduced with permission from reference 33. Copyright 2021, Springer Nature.

Nevertheless, a fully functional artificial light-harvesting system demands combinations of light capture, energy funneling, electron transfer, and solar-to-chemical transformation. In that direction, Meyer and co-workers have developed an 'integrated modular assembly' via coupling the light harvesting antenna array and energy gradient long-range electron transfer system to create oxidative and reductive equivalents for relevant half-cell reactions (**Figure**

1.5b).[31] Here, the integrated assembly is designed based on derivatives of porphyrins, metalloporphyrins, and metal-polypyridyl complexes. The light absorption by the antenna array, followed by the sensitization of reactive chromophore (C) in the donor-chromophore-acceptor array drives the photochemical splitting of water into H_2 and O_2 products (**Figure 1.5b**). Perhaps, it is the best analogy with the natural photosynthetic machinery where light absorption and excited state electron transfer to distant reaction centres trigger the CO_2 reduction and water oxidation in PS I and PS II, respectively. Continuing in this direction, in a recent study by Niu, Yang, and co-workers reports a different form of artificial light harvesting system based on tetraphenylethylene derivative (D) as antenna chromophores, and iodide BODIPY (A) as a sensitizer for the charge separation process (**Figure 1.5c**).[34] The photoexcitation of 'D' in supramolecular assembly undergoes an excitonic energy transfer process to 'A', followed by excited A^* capturing an electron from ground state 'D' and leading to charge separation and chemical reactions. The designed supramolecular artificial light-harvesting system produces valuable hydrogen peroxides, and is utilized in photodynamic therapy by NADH oxidation and production of reactive oxygen species (**Figure 1.5c**). Thus, it is evident that the goal to mimic the photosynthetic machinery is extremely challenging, because it requires to integrate multiple functions in a stable chemical environment. As a result, developing a fully functional artificial light-harvesting system usually takes longer times than alternative approaches to solar energy conversion, like solar cells, photovoltaic cells, and organic thin film devices.[29]

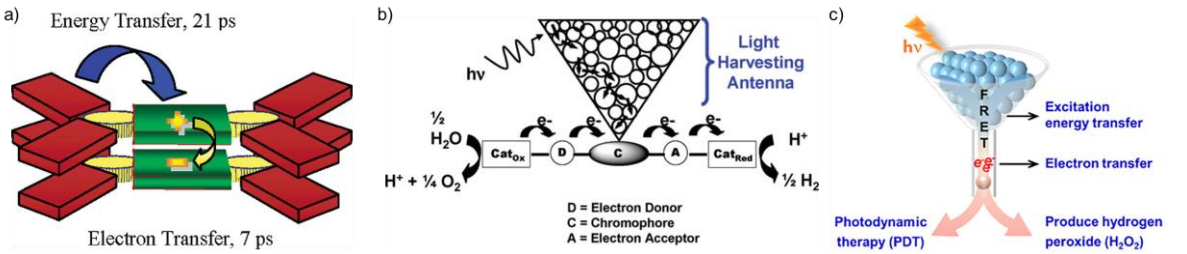

Figure 1.5 Schematics of artificial photosynthetic systems, combining (a) light harvesting antenna and charge transfer system, (b, c) energy funneling, electron transfer, and chemical transformation. The supramolecular assembly of various light absorbing chromophores, energy transfer and electron transfer components, and catalysts drive the essential sequence of events for solar-to-chemical transformation. Reproduced in part with from references 26, 31 and 34. Copyright 2004, 2005, and 2024, American Chemical Society.

1.4 Quantum Dot: An Alternative Light-Harvesting Material

Along with having the above-mentioned ideal characteristics for artificial light-harvesting materials, the easy tunability and flexibility of the surface chemistry of quantum dots (QDs) have earned them special importance in the area of light-harvesting studies.[15,16,25,35] QDs are luminescent semiconductor nanomaterials that have sizes comparable to their Bohr-exciton radius, which results in the quantum confinement of energy levels.[35] As a result, QDs are well-known to exhibit unique size-, shape-, and composition-dependent optoelectronic properties (**Figure 1.6**).[15,16,35,36] As the size of the QD decreases the band gap increase, following the Brus equation (equation 1 in **Figure 1.6**).[35] Alongside, their broad absorbance in the visible region, high tuneability, and narrow emission make QDs ideal candidates for many light-harvesting studies. Further, the photostability and tuneable surface chemistry of QDs are added advantages over traditional chromophores for the design of light-harvesting arrays.[25] A photoexcited QD can follow different decay pathways, as summarised in **Figure 1.7**; the efficiencies of these pathways will ultimately decide their role in light-harvesting studies. One of the common pathways is the radiative recombination of excitons, called photoluminescence (PL; marked '1' in **Figure 1.7**), which finds use in sensing, imaging, and solid-state display applications.[25]

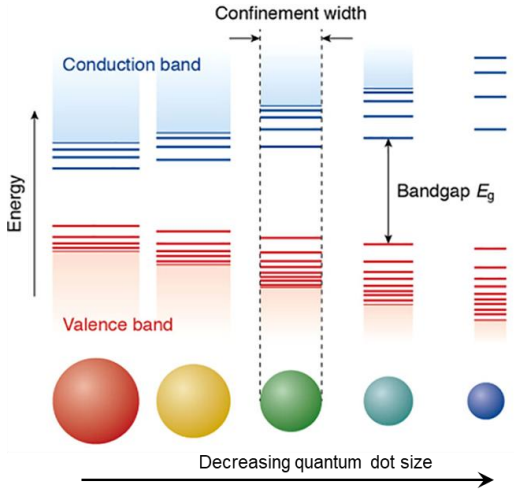

$$E_g(QD) = E_g(bulk) + \frac{h^2}{8R^2}\left(\frac{1}{m_e^*} + \frac{1}{m_h^*}\right) - \frac{1.78e^2}{4\pi\varepsilon_0\varepsilon_r R}$$

Figure 1.6 Schematics of size-dependent 'quantum confinement' effect in QD, indicating that the smaller QD have larger band gap and more discrete energy level. Representative Brus equation defining the size-dependent band gap of QDs. Where, R is the QD's radius, $m_{e(h)}^*$ is effective mass of electron (hole) in QD, and $\varepsilon_{0(r)}$ is the permittivity of vacuum (QD). Reproduced in part with permission from reference 36. Copyright 2011, Royal Society of Chemistry.

The photoexcited charge pairs can also participate in energy and electron transfer processes in the presence of appropriate acceptor moieties (marked '2' and '5' in **Figure 1.7**, respectively).[15,16,25] Likewise, the excitons in QDs can also be extracted for the photovoltaic applications and to drive various photo-redox transformations (marked '3' and '4' in **Figure 1.7**, respectively).[25,37] Most of the photophysical processes in QDs emerge from their core, and extensive studies have been performed to maximize the light harvesting properties by tuning their size, shape, composition, and crystallinity. As mentioned earlier, assembling and integration of champion materials is as equally important as developing a new champion material. This is where the ligands on the surface QDs can play a crucial role. Traditionally, surface ligands have been given only a secondary role, in terms of providing a stable dispersion in a particular medium. However, recent studies have proved that the surface ligands can be transformed to play a major role in directing the extraction of energy and electrons from a photoexcited QD.[14,25] The ligands on the surface of QDs can be appropriately decorated to bring various covalent and non-covalent interactions into action, which in turn can assist in maximizing their light harvesting properties. More importantly, a judicious control over such interparticle interactions (emanating from surface ligands) can help in realizing attractive light harvesting applications from QDs. Thus, along with the primary objective of stable dispersion in respective medium, the surface ligands in QDs can impart various non-covalent interactions into action and channelize the photoinduced electron and energy transfer processes.[25]

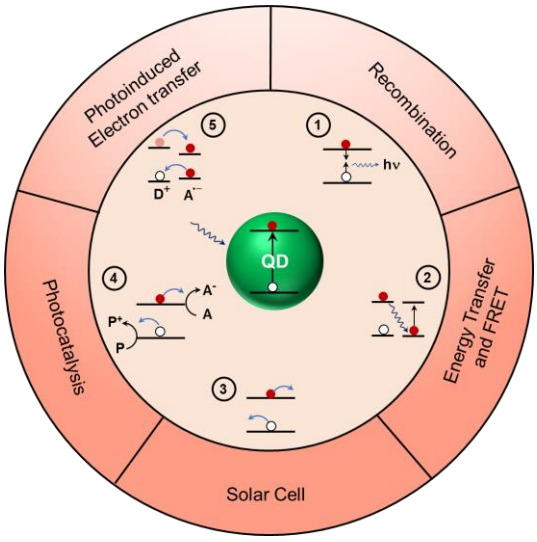

Figure 1.7 A summary of the relaxation pathways in a photoexcited QD, which forms the basis of various energy-related applications. Reproduced with permission from reference 25. Copyright 2021, Royal Society of Chemistry.

1.5 Surface Ligands and Interparticle Interactions

The individual engineering of both components of QDs – the core and the ligands – is essential for maximising the light–harvesting efficiencies of QDs. Most of the photophysical properties of QDs are dependent on their core parameters (such as size, shape, composition, crystallinity, etc.), which have been extensively studied and well-documented in literature.[38–39] On the contrary, the surface ligands have been primarily viewed from the perspective of being stabilising or capping agents. It was believed that surface ligands were important mainly for providing stability to a nanoparticle system in a particular medium. However, recent studies have revealed that the rational design of surface ligands can turn out to have a critical impact on various optoelectronic properties at the nanoscale, including light harvesting.[14,25,37,40–42] In general, a surface ligand has three sub-units: a binding (or head) group; a spacer; and a terminal group (**Figure 1.8**).[41] Dedicated research has been carried out to tune these individual components of surface ligands so as to achieve properties of interest in nanomaterials. Specifically, the terminal groups of ligands have been transformed to carry out an unconventional role via bringing various covalent and non-covalent interactions into play, thereby dictating the fate of photophysical processes in QDs and nanoparticles in general.[15,25,41–42]

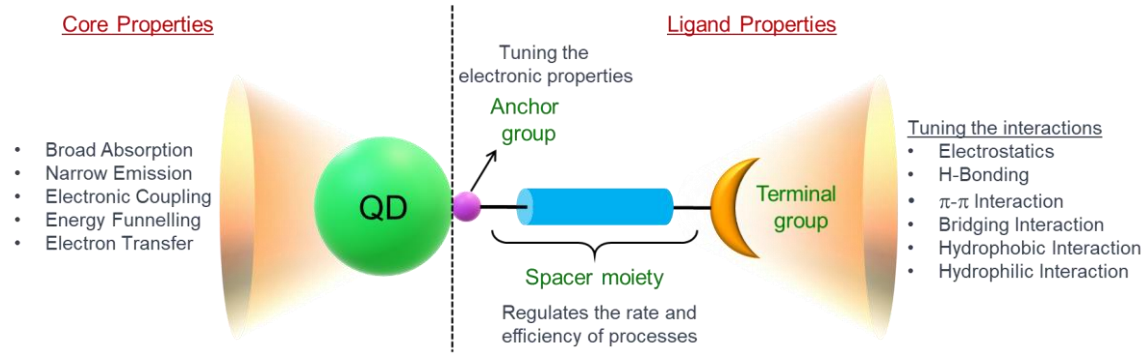

Figure 1.8 Schematics showing the general structure of a colloidal QD, emphasising various processes emanating from the core and from surface ligands. Reproduced with permission from references 25. Copyright 2021, Royal Society of Chemistry.

1.5.1 Anchoring Group

The primary job of the binding group is to anchor the ligand onto the surface of the QD. Often, binding groups coordinate with unpassivated atomic orbitals (or "dangling orbitals") on the surfaces of QDs, which are formed from low coordinating surface atoms.[41,43] As a result, the

anchoring of the binding group reduces the surface-centred excitonic trap states. Along with surface passivation, the nature of the binding group can influence the photophysical properties of QDs as well.[43–48] For instance, Wuister and co-workers observed that ligand exchange with thiol molecules resulted in the PL quenching of CdSe QDs, whereas the PL of CdTe QDs was enhanced after place exchange with thiolated ligands.[46] This striking discrepancy in PL behaviour was explained based on the trapping of photogenerated holes by the thiol groups, as the HOMO energy level of thiols lie above the valence band maximum of CdSe QDs (**Figure 1.9a**). Likewise, the concentration and nature of surface ligands can also influence the PL properties of QDs. Whitten, McLendon, and co-workers observed a PL enhancement in CdS QDs in the presence of low concentrations of trimethylamine, which was attributed to the usual surface passivation of trap states by the amine groups.[44] On the contrary, the excess use of amine ligands can suppress radiative emission from CdS QDs via electron transfer from amines to QDs.[45] Further, Kamat and co-workers explored the anchor-group-dependent excited state dynamics and interfacial electron transfer (ET) in QD–TiO_2 heterostructures (**Figure 1.9b**).[48] The use of amines as the binding group to link QDs and TiO_2 enhanced the rate of electron transfer (k_{et}) due to the confinement of the electron wave function via the passivation of intrinsic trap states.[47–48] On the other hand, electron trap states were created when thiol was used as the binding group of the linker, which suppressed the rate of interfacial electron transfer (**Figure 1.9c**).[48–50] Apart from influencing the efficiency, binding groups can control the nature of photophysical processes as well. Tang and co-workers studied the effects of binding groups in controlling the nature of energy transfer between CdS QD donor and boron dipyrromethane dye acceptors (**Figure 1.9e**).[51] The carboxylic-acid-functionalised acceptor dyes could attach themselves to multiple identical binding sites on the surfaces of the QDs, resulting in FRET being the sole quenching process. In contrast, both FRET and static quenching processes were observed when amine-functionalised dyes were used as acceptors. This was explained based on the existence of two available sites for the attachment of amine-functionalised dyes on QDs. The bright sites participated in a FRET process, whereas the dark sites were involved in charge transfer from the QDs through static interactions.

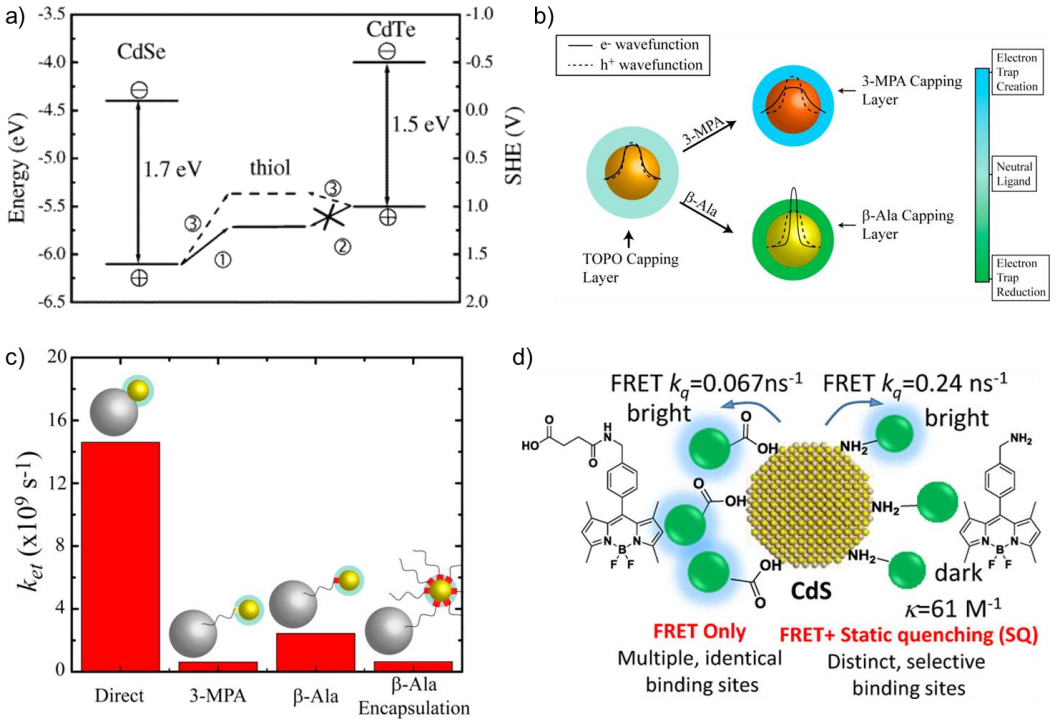

Figure 1.9 (a) The band-edge positions of CdSe and CdTe QDs shown against vacuum and standard hydrogen electrode. Thiols can quench the PL of CdSe QDs via scavenging holes from the valence band of CdSe QDs, but cannot quench the PL of CdTe QDs (solid line). Reproduced with permission from reference 46. Copyright 2004, American Chemical Society. (b) A schematic representation of the delocalisation and confinement of the electronic wave function in the core of a QD, by thiolated and amine ligands, respectively. (c) Variations in the rate of electron transfer as a function of the surface ligand used to adsorb CdS onto TiO_2. MPA and Ala contain thiol and amine as binding groups, respectively. Reproduced with permission from reference 48. Copyright 2013, American Chemical Society. (d) A schematic representation of energy transfer from a CdS QD to molecular acceptors that were functionalised with acid and amine binding groups. Reproduced with permission from reference 51. Copyright 2015, American Chemical Society.

1.5.2 Spacer Moiety

A spacer acts as a bridge between the binding and terminal groups of a ligand, and it essentially controls the distance between the QD core and its surroundings. Commonly, long alkyl chains are used as spacers to prevent any undesirable loss of excitons via spatially separating the QDs from other interfering species. Both FRET and PET processes are highly dependent on the distance between the donor and the acceptor. Thus, varying the spacer length of the ligand is a convenient way to regulate these photophysical processes in QDs as required.[30,52–56] In one example, Sugimura and co-workers studied the dependence of PL on the interparticle distance between two sizes of CdSe QDs.[54] The QD–QD system showed two types of energy-transfer processes as a function of different inter-QD distances. Förster-type coupling was responsible for PL quenching at shorter inter-QD distances (below 10 nm), and the efficiency was

dependent on the inverse of the sixth power of the distance.[12,15,25] However, weak dipole–dipole interactions, known as retarded light-field coupling, were observed at longer inter-QD distances, with the quenching efficiency dependent on the inverse of the square of the distance.[52–56] Similar to FRET, the charge transfer efficiency also has an exponential dependence on the donor–acceptor distance. A decrease in the spacer length led to strong electronic coupling between the donor and acceptor moieties, allowing for the efficient flow of electrons with negligible resistance.[53] A series of examples in this regard has been reported in QD-metal-oxide nanocomposites.[52–56] In one effort, Kamat and co-workers demonstrated a tunnelling model for the electron transfer process from CdSe QD to TiO_2 with bifunctional aliphatic ligands (**Figure 1.10a**).[56] Detailed spectroscopic studies revealed that the rate of PET, k_{et}, decreased with an increase in the spacer length, which was in good agreement with the predicted results (**Figure 1.10b**). Along with the length, the nature of the spacer plays a crucial role in deciding the fate of a photophysical process. Watson and co-workers have compared the kinetics and efficiencies of excited-state interfacial electron transfer in CdS QD donor-TiO_2 NP acceptor systems connected through aromatic and aliphatic bifunctional spacers.[52] Injection of electrons from the CdS QD to the TiO_2 NP occurred on multiple time scales. The fast component ($<10^{-8}$ s) was attributed to the tunnelling of electrons through excitonic states, which was more efficient during the use of an aromatic linker due to the presence of better electronic coupling in comparison with the aliphatic linker. However, the slow component (10^{-7} to 10^{-6} s) was due to trap-state-mediated electron injection, which had negligible dependence on the nature of the linker molecule. The distance dependence of electron-transfer processes was observed in the case of aromatic linkers as well.[52] Likewise, Cánovas and co-workers used molecular bridges to control the electron transfer rates in a covalently connected PbS QD-TiO_2 NP nanocomposite system (**Figure 1.10c**).[55] At a given donor–acceptor distance, stronger electronic coupling via the conductive aromatic phenyl bridge facilitates a faster electron transfer process than the use of a methylene spacer (**Figure 1.10d**).

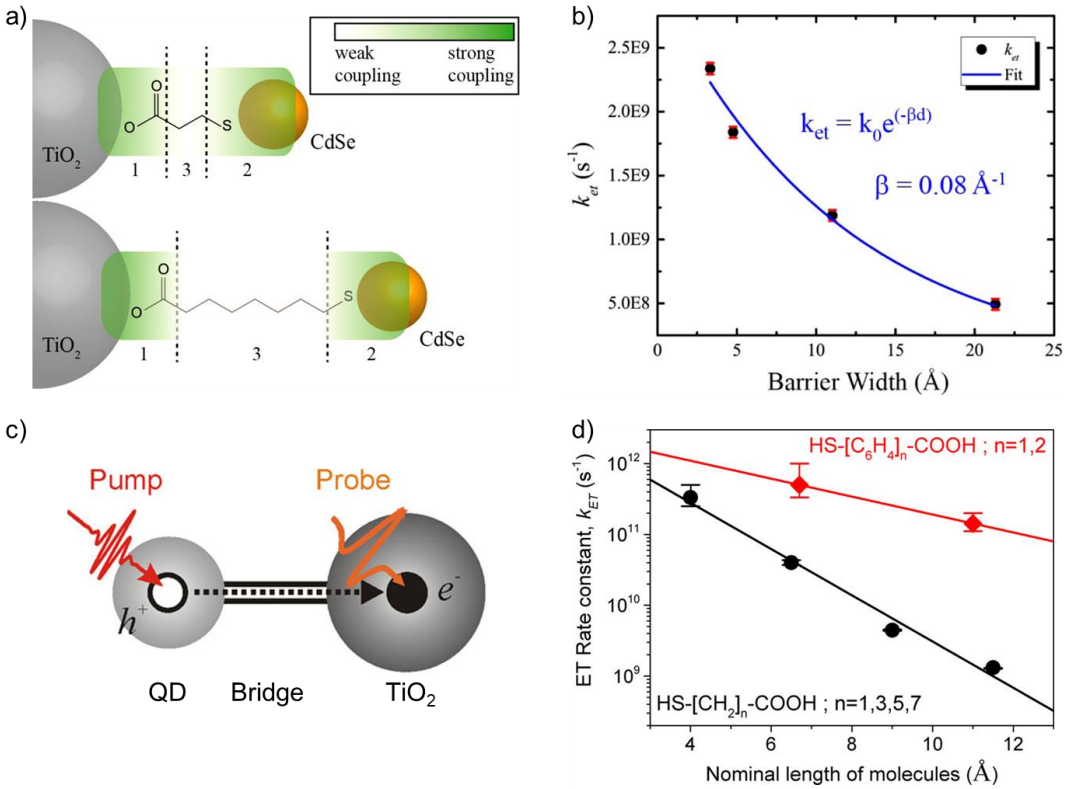

Figure 1.10 (a) A schematic representation of PET process from a CdSe QD to a TiO_2 through an aliphatic mercaptoalkanoic acid spacer. (b) A plot showing the variations of the experimentally calculated rates of PET, k_{et}, as a function of the spacer length. Reproduced with permission from reference 56. Copyright 2015, American Chemical Society. (c) Schematic of PET process from a QD to TiO_2 through a rigid aromatic spacer (bridge). (d) The variation in the rates of PET (k_{et}), as a function of spacer length for n-methylene-based aliphatic bridges (HS–$[CH_2]_n$–COOH, black dots) and n-phenylene-based aromatic bridges (HS–$[C_6H_4]_n$–COOH, red squares). Reproduced with permission from reference 55. Copyright 2013, American Chemical Society.

1.5.3 Terminal Group

Understanding of natural photosynthetic reaction centres has revealed that establishing precise control over the interactions between different champion materials is crucial for maximising the efficiency of photophysical processes.[12,21–22] However, how to achieve such finely tuned interactions in QDs still remains an open question. Here, the terminal groups of ligands have the potential to control the assembly of QDs with other light-harvesting materials via bringing various covalent and non-covalent interactions into play.[14–15,25] Specifically, a terminal group can be conveniently modified to achieve a particular interparticle interaction in a QD-based nanohybrid system, as per the demand. In comparison with covalent interactions, non-covalent interactions can offer additional advantages in terms of flexibility and ease of reversibility when it comes to fine-tuning the interparticle interactions. Some key non-covalent forces include electrostatics, H-bonding, bridging/coordination, and π–π stacking (**Figure 1.11**).[25,42,57]

Thus, thoughtful design of surface ligands and use of these non-covalent forces in the regulation of interparticle interactions will impact the outcome of photophysical processes in QD-based nanohybrid systems. Therefore, the photophysical processes can be conveniently controlled via bringing various non-covalent interactions into play through the appropriate surface functionalisation of QDs.

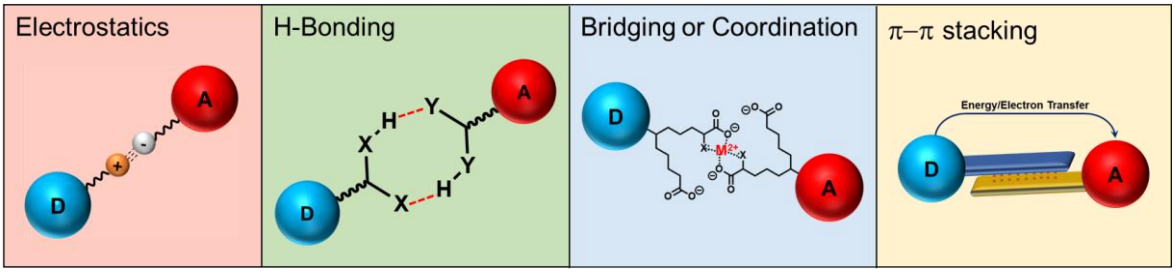

Figure 1.11 Representation of commonly used non-covalent interactions, which can arise through the judicious choice of surface ligands, for assembling QD-based donor–acceptor pairs. Reproduced with permission from reference 25. Copyright 2021, Royal Society of Chemistry.

1.6 All-QD based Light-Harvesting systems

As discussed, close-proximity and systematic co-ordination between various champion components make the process of photosynthesis unique and efficient. The mimicking of such machinery in artificial systems will require materials that interact in predefined ways with each other. Specifically, the regulation of interactions between donors and acceptors can ultimately dictate the outcome of light-induced electron or energy transfer processes. To achieve this control, the surfaces of QDs can be functionalised with appropriately charged ligands to impart attractive or repulsive interactions between QD-based donor–acceptor systems.[14.25] Thus, the donor–acceptor distance can be regulated via varying the surface chemistry of QDs. In an early report, Nabiev and co-workers investigated an energy-transfer process between oppositely charged CdSe/ZnS QDs of different sizes in an aqueous medium (**Figure 1.12a**).[58] Cysteamine and a mixture of mercaptosuccinic/mercaptosulphonic acid ligands were functionalised on the surfaces of differently sized CdSe/ZnS QDs to prepare positively and negatively charged QDs, respectively (**Figure 1.12a**). Strong electrostatic attraction between the two oppositely charged QDs resulted in efficient resonance energy transfer from green to red-emitting QDs (~100%). Following this work, a series of other studies was performed using electrostatic interactions as a tool to develop solid-state assemblies of various QDs, with fine control over their photophysical processes.[59–63] Later, Rogach and co-workers extended the idea of electrostatic interaction to obtain a compact layer-by-layer (LBL) assembly of oppositely charged CdTe

QDs deposited on a polymer-coated glass substrate.[60] Thioglycolic acid (TGA) and 2-mercaptoethylamine (MEA) were used as ligands to impart negative and positive charges, respectively, on the surfaces of QDs. Profound electrostatic interactions between the QD layers facilitated the energy transfer process, with an efficiency of ~80 % in the LBL system. In another study, Weiss and co-workers used bridging interactions to achieve efficient FRET in QD aggregates formed between two different sizes of NIR-emitting glutathione (GSH) capped PbS QDs (**Figure 1.12c,d**).[62] Binding studies confirmed that QD aggregates were formed due to preferential coordination between the Zn^{2+} ions and the glutamine residue of GSH (rather than the carboxylate residue). Upon increasing the concentration of Zn^{2+} ions, the continuous quenching of the PL of the donor QDs was observed, along with growth in the PL of the acceptor QDs. A FRET efficiency of as high as ~97 % with a rate of 14 ns^{-1} was estimated in these Zn^{2+}-ion bridged QD assemblies. Also, coordination with Zn^{2+} ions helped to achieve the long-range diffusion of excitons in these NIR QD assemblies (~11.2 nm at a DQD to AQD ratio of 3.5: 1, corresponding to 2.3 hopping steps before emission). Continuing in this direction, coordination-based bridging was further extended to mercaptoalkanoic acid capped PbS QDs to study distance-dependent near-infrared energy transfer rate.[63] A gradual decrease in QD–QD separation distance from 5.8 ± 0.3 nm to 3.7 ± 0.3 nm resulted in a dramatic increase in the energy transfer (EnT) rate was observed from ~150 ± 2 ns^{-1} to ~2 ± 0.3 ns^{-1}.

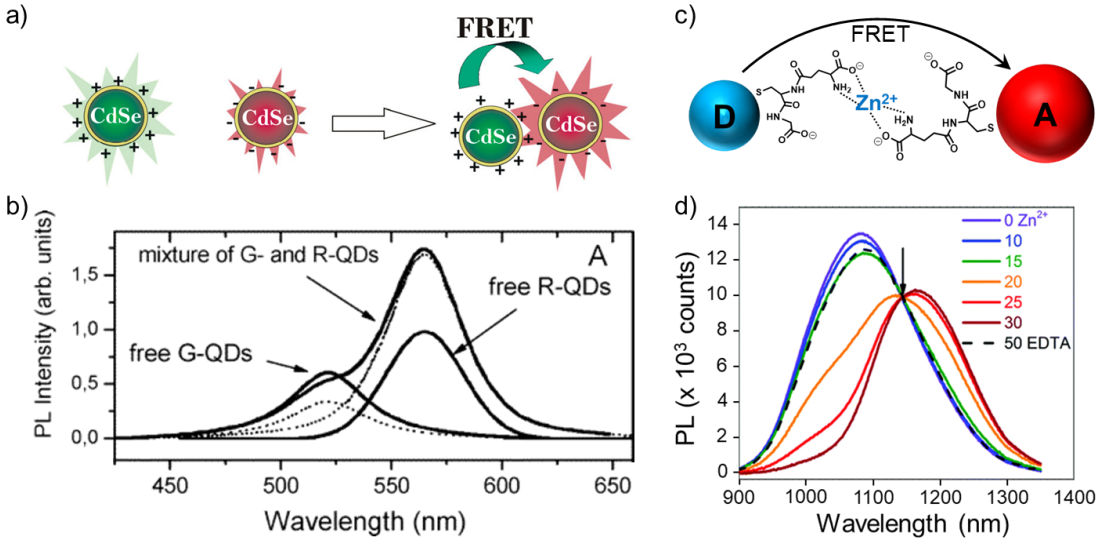

Figure 1.12 (a) Schematic representation of a FRET process, and (b) corresponding PL intensity profile in an electrostatically assembled QD–QD donor–acceptor pair. The positive and negative charges on the green- and red-emitting CdSe QDs arise from surface-bound cysteamine and mercaptosuccinic/mercaptosulfonic acid ligands, respectively. Reproduced with permission from reference 58. Copyright 2004, American Chemical Society. (c) A schematic diagram of a GSH-capped donor and acceptor PbS QD complex coupled through Zn^{2+} coordination. (b) Spectral changes in the PL of the donor–acceptor mixture upon the addition of varying amounts of Zn^{2+} ions, followed by the

recovery of the initial PL in the presence of EDTA molecules. The presence of Zn^{2+} ions facilitate an efficient FRET process from the donor–to–acceptor QD. Reproduced with permission from reference 62. Copyright 2017, Royal Society of Chemistry.

Furthermore, the idea of all–QD assembly was expanded in more complex geometry beyond the dyad assembly, and funnel–like energy band cascade assembly was developed with various band gap QDs.[64–68] The arrangement of multicomponent system in appropriately aligned manner was always challenging task to do. To achieve so, Knoll and co-workers used dendrimer functionalized nanotubes (NTs) to combine customized properties of different QDs using electrostatic force of interactions.[65] In a typical fabrication process, the NT template's wall was modified with 3-aminopropyl dimethylethoxysilane (3-APS) followed by deposition of positively charged dendrimer (G_4^+). Then graded bandgap assembly of three $Zn_xCd_{(1-x)}Se$ alloy QD, such as QD_{561}, QD_{594}, QD_{614} (subscript refers the emission maxima of QD) were deposited over dendrimer coated NTs with positively charged dendrimer (G_4^+) as a spacing layer (**Figure 1.13a**). The assembly was started with deposition of negatively charged green emitting QDs (QD_{561}) closest to the pore walls, followed by orange (QD_{594}) and red (QD_{614}) emitting QDs, overall system abbreviated as NTs2. Those arrangement of different QDs in NTs was associated with a decrease of bandgap energy from outer to the inner surface of NTs walls. The possibility of efficient direct FRET was ensured by strong spectral overlap integral in QD_{561}:::QD_{594} and QD_{594}:::QD_{614} system, resulted in amplified emission peak corresponding to 614 nm. The PL intensity of red emitting QD_{614} in NTs2 assembly was found to 3.6 times higher than the PL intensity in comparison with control NTs1 assembly, which do not contain intermediate QD_{594} layer (**Figure 1.13b**). This discrepancy was attributed to the absence of QD_{594} and poor spectral overlap between QD_{561} and QD_{614}, which apparently prevented the efficient energy transfer through the walls of the NTs. In a different approach, Lesnyak and co-workers developed novel hybrid QDs aerogels based on the controllable and reversible assembly of QDs via metal-tetrazole complexation (**Figure 1.13c**).[67] The tetrazole ligands on QD surface can initiate the aggregation/gelation process in presence of Zn^{2+} ions. The process of gelation enables an efficient FRET process between closely-spaced QDs in All-QD assembly. Finally, 3D assembling of different band gap QDs such as blue-emitting ZnSe, yellow- and red-emitting CdTe QDs resulted in formation of pure white light emitting aerogels (**Figure 1.13c**). This study revealed the potential of metal-ion-based coordination in assembling different QDs and their use in the area of light-emitting devices. In contrary to the interaction driven assembly of QDs, PL decay dynamics and nonradiative photoexcitation energy transfer was also investigated in a system of randomly distributed, and densely packed

PbS QDs film (**Figure 1.13d**).[68] The cascade energy transfer was monitored by analysing the PL intensity and PL decay dynamics of smaller and larger size QDs. A decrease in the PL intensity and lifetime of smallest donor QDs (1020 nm), and drastic increase in PL intensity and the lifetime of larger acceptor QDs (1500 nm) was observed in solid state film of mixture of three variable sizes of QDs (**Figure 1.13d**). The intermediate one (1240 nm) played the role for ancillary unit, and complete an arc of both energy donor and energy acceptor. The energy transfer process was attributed to happen from both the fundamental excitonic state and the long-lived gap-state (trap electronic level within the band gap) of the donor QDs to acceptor QDs. As a result, this observation was interpretated as FRET-assisted delayed fluorescence in densely packed film of three distinct sizes of PbS QDs.[68] In another set of studies, all–QD based energy transfer structure was prepared by applying the techniques of LBL assembly on a solid substate.[64,66] In one such example, Klar and co-worker realized cascade energy transfer process in a LBL assembly with four different sizes of CdTe QDs.[64] The efficient transfer of higher energy exciton towards the lower energy gap QD was observed in the funnel-like energy cascade structure. This leads to drastically enhanced red fluorescence (28 times) from center layer (larger size QDs), and to an almost complete quenching of orange, yellow, and green fluorescence streaming from the outer layer (donor and ancillary units). Similarly, Cloutier and co-workers have investigated the energy cascade process in LBL assembly with three different sizes of PbS QDs (PL maxima of QD_1, QD_2, and QD_3 are 980 nm, 1055 nm, and 1240 nm, respectively).[66] Here, the aromatic and aliphatic dithiol surfactant was used to cross-link the QDs layers, and the energy transfer mechanism was probed through each step of assembly process. The formation of multilayer QD_1:::QD_2:::QD_3:::QD_2:::QD_1 cascade structure resulted in 19-fold enhancement in the PL intensity at acceptor emission (1240 nm) compared to single layer acceptor QDs (**Figure 1.13e**). The efficient exciton funneling and recycling of trap state-bound excitons in cascade geometry was attributed to the main process that contributes to huge emission enhancement.

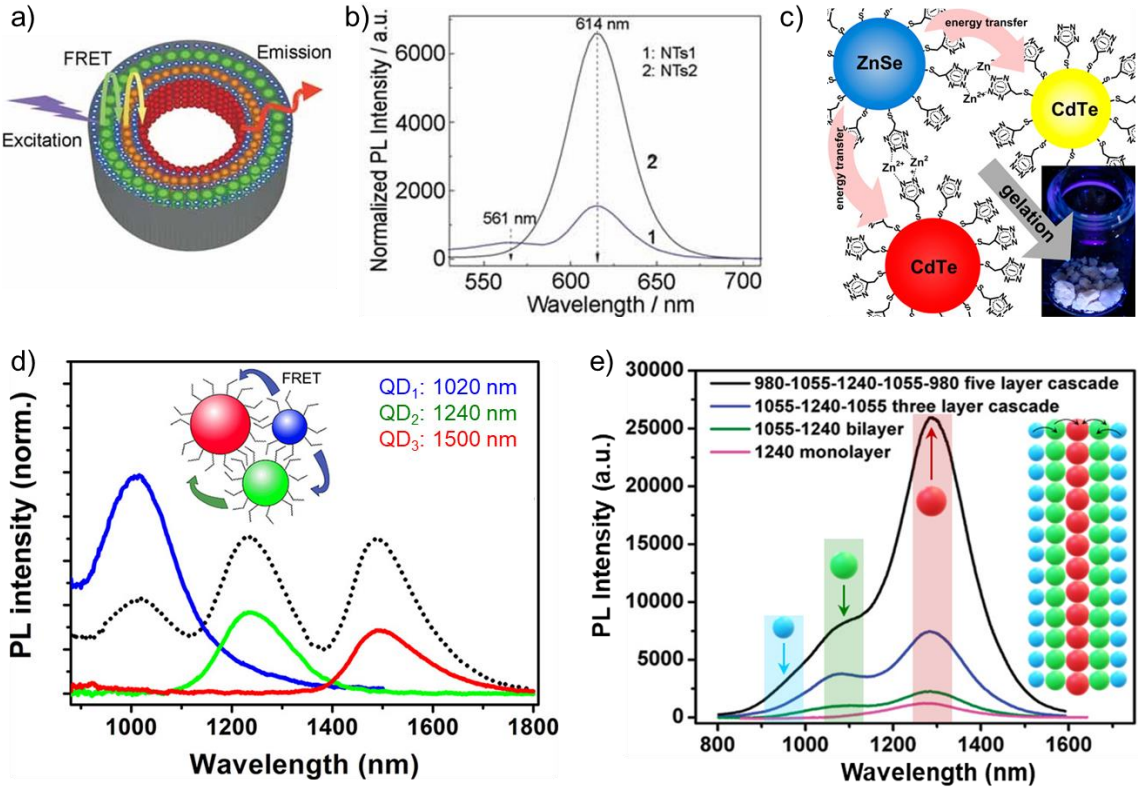

Figure 1.13 (a) Schematics of multicomponent of donor–acceptor system based on All–QD assembly in a dendrimer functionalized nanotube (NT) template. (b) Corresponding PL spectral responses showed an enhanced emission for acceptor QD_{614} in case of cascade energy transfer process (NTs2). Reproduced with permission from reference 65. Copyright 2008, WILEY-VCH Verlag GmbH & Co. KGaA, Weinheim. (c) A schematic diagram of zinc-ion-coordination-based gelation between different sizes of CdTe QDs, resulting in efficient FRET from smaller to bigger QDs. Inset showed the white emissive aerogel composed of blue-green-&-red emitting QDs. Reproduced with permission from reference 67. Copyright 2012, American Chemical Society. (d) PL spectra of densely packed film made from the mixture of three different sizes of PbS QDs proved to have cascade energy transfer process from smallest-to-medium-to-largest PbS QD. Reproduced with permission from reference 68. Copyright 2015, American Chemical Society. (e) PL spectra of multilayer QD-cascade structure (in LBL fashion) showed ~19-fold enhancement in the emission intensity for acceptor QDs (~1240 nm emission). Reproduced with permission from reference 66. Copyright 2011, American Chemical Society.

1.7 Objectives: Need of Environmentally Friendly All–QD Assembly

Most of the above-mentioned applications have been achieved with QDs that contain toxic metal ions like Cd, Pb, Hg, Se, Te, etc., because of their easy tunability in size and outstanding optical performances, projecting them toward ideal system to work.[58–68] Indeed, the decades of research on developing high quality QDs and fabrication methods paved the foundation for Cd- and Pb-chalcogenide based QDs.[15–16,25] Nevertheless, toxicity of Cd- and Pb-heavy metal restricts their use in commercial and industrial applications. According to the order of restriction of hazardous substances (RoHS), the content of Cd cannot exceed 100 ppm (0.01

%). Despite of having European RoHS Exemptions, we should also be aware of the environmental risk and hazards to human health of producing large quantity of Cd- and Pb-containing materials (**Figure 1.15**).[69] Because of the growing apprehension for environmental issues, the development of the heavy-metal-free QDs with optical properties near to state-of-the-art Cd-based QDs have received considerable attention.

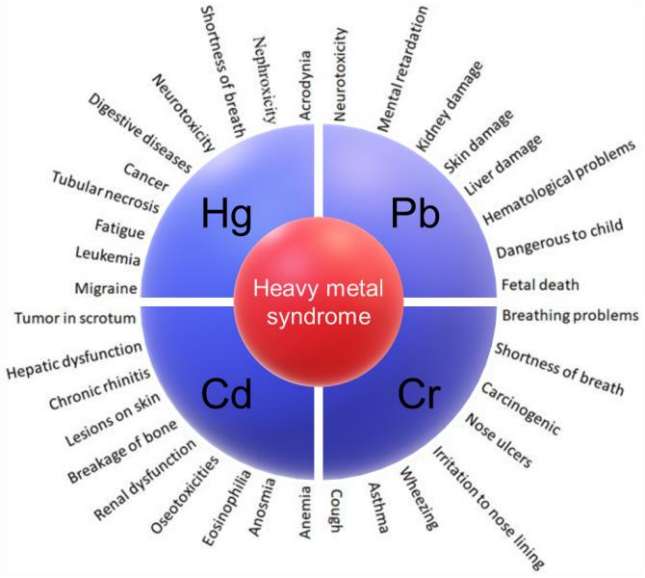

Figure 1.14 Hazards to health posed by lead, cadmium, mercury, and chromium in the human body. Reproduced with permission from reference 69. Copyright 2022, Scientific Electronic Library Online.

In family of environmentally friendly QDs, indium phosphide (InP) is considered as one of the most promising alternatives for CdX QD, which exhibits tunable emission spectrum in broad region from the visible to near-infrared (NIR).[70–72] In contrast to ionic II-VI QDs, the III-V InP QD is more covalent in nature, which make them structurally robust and nontoxic by preventing leakage of ions. Therefore, in multidisciplinary research from device to biology, environmentally benign InP QD have significant advantages over the state-of-the-art Cd-based QDs.[14,71–74] However, there is a lack of light-harvesting studies on all-QD assemblies based on environmentally friendly InP QDs. This could possibly because of the lack of availability of all primary colors (blue, green, and red emissions) with InP QDs and their sensitive surface chemistry (prone to oxidation).[75] In general, the challenges associated with the lack of selective excitation of donor QDs (because of broad absorption of QDs) have prevented elaborate FRET studies in an all-QD based donor-acceptor system.[12,14–16,25] These are the major limitations in all–QD based light harvesting studies. This motivated us to develop strategies to design all–

QD multicomponent assemblies based on InP QDs, and prepare a roadmap for FRET investigation in all–QD donor:::acceptor systems.

This essentially demands the availability of all primary color-emitting InP QDs, such as in the blue, green, and red regions for completing the wide color gamut. As discussed in the **Section 1.2**, the outcome of a multicomponent system should be a relay of energy, and electron in unidirectional fashion. This essentially means to have control over the arrangement of different band gap QDs, like the directional assembly. One of the ways to achieve such inter-QD interaction is to functionalize the QDs with ligand of choice and regulate the non-covalent forces emanating from the ligands. This will ensure that the higher band gap InP QD (preferably blue-emitting) will predominantly interact with another moderately-low band gap InP QD (preferably green-emitting) and followed by interaction with lower band gap InP QD (preferably red-emitting) (**Figure 1.15**). The mode of interaction was selected as the electrostatics to choreograph the all–InP QD based donor:::acceptor assembly for studying various photophysical interactions.

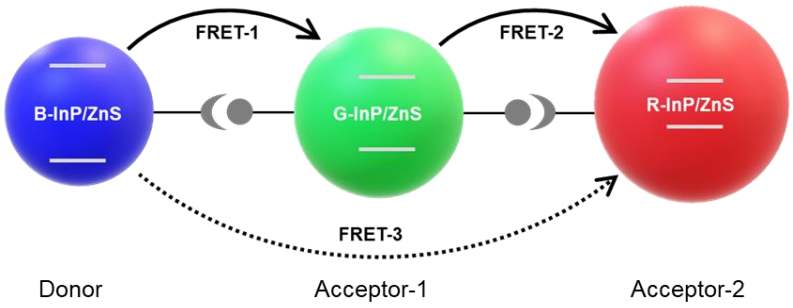

Figure 1.15 Schematic representation of interaction driven all–InP/ZnS QD based multicomponent system for FRET study.

In accordance with literature, there were enough studies on the development and use of green and red emitting InP QDs. The corresponding reported PL QY for InP QDs with green and red emission has been pushed up to near unity even at the device level (theoretical maximum EQE, 21.4 %).[73–74] However, there is a scarcity of blue emitting InP QDs. One of the biggest challenges in developing a wide color gamut multicomponent system is the lack of blue emitting InP QDs.

Based on these challenges, the objectives of the proposed thesis are summaries here. Our very first objective was to develop InP/ZnS QDs emitting in the pure-blue region and functionalize the QDs with appropriate ligands. The successful synthesis of blue emitting InP/ZnS QDs will

fill the gap in the required wide color gamut (one of the primary colors). Our next objective was to explore the potential of the newly developed pure-blue emitting InP QDs in fundamental photophysical processes such as FRET and PET process. Once it has been established, our final objective was to develop all–QD based multicomponent system via ligand directed electrostatics forces. To achieve this, one need to have to establish protocols to study and understand energy and electron transfer processes at dyad levels based on all–QD donor–acceptor system. In this direction, we have studied inter-QD energy transfer process at dyad level in blue-green, green-red, and blue-red emitting all–InP/ZnS QD donor–acceptor assemblies, and green-red [-] InP/ZnS:::[+] CIS/ZnS QD nanohybrid assembly. Optimization of all dyad systems enables us to design the road-map for FRET study in all–QD based donor:::acceptor system, which in future shall facile the formation of multicomponent triad assemblies.

1.8 Brief Overview of the Chapters

The overall objective of the thesis is to develop InP QDs emitting primary colors and use them in donor–acceptor systems to study light-induced energy and electron transfer processes. **Chapter 1** provides a brief introduction of photoinduced energy and electron transfer processes, uniqueness of QDs in light harvesting studies, and literature background on all–QD-based multicomponent systems. Alongside, objectives of the thesis aimed towards overcoming some of the challenges associated with studying photophysical processes in all–QD based donor-acceptor system is highlighted. **Chapter 2** summarizes the synthetic protocols, methodology, instrumentation and formalism of FRET and PET processes. In **Chapter 3**, the focus was on creating stable and highly efficient pure-blue emitters based on environmentally friendly InP/ZnS QD, especially in water. A fine control over the growth kinetics of the core InP as well as the shell ZnS, and a rational combination of metal-halides, less-reactive aminophosphine and sulfur precursors was the key to achieve a strong and stable PL in the pure-blue region. Following this, the newly developed blue-emitting InP/ZnS QDs was explored in FRET and bioimaging studies. **Chapter 4** describes the suitability of newly developed blue-emitting InP/ZnS QDs for PET study. In **Chapter 5**, electrostatically driven all–QD dyad assembly was developed based on blue-green, green-red, and blue-red environmentally benign QDs. Optimization of dyad assembly established the roadmap for FRET investigation in inter-QD system. Now, all the primary colors are available, and groundwork is done for the future realization of InP-QD based multicomponent system.

1.9 References

(1) Cleveland, C. J. *Concise Encyclopedia of the History of Energy*; Academic Press, 2009.

(2) Maeda, M. *How to Solar Power Your Home : Everything You Need to Know Explained Simply*; Atlantic Publishing Group: Ocala, 2019.

(3) Denzer, A. *The Solar House : Pioneering Sustainable Design*; Rizzoli: New York, 2013.

(4) Perlin, J. *Let It Shine : The 6,000-Year Story of Solar Energy*; New World Library: S.L., 2022.

(5) Sarkar, D. K. *Thermal Power Plant : Design and Operation*; Elsevier: Amsterdam ; Boston, 2015.

(6) Perera, F. Pollution from Fossil-Fuel Combustion is the Leading Environmental Threat to Global Pediatric Health and Equity: Solutions Exist. *Int. J. Environ. Res. Public Health* **2018**, *15*, 16.

(7) Ritchie, H.; Roser, M.; Rosado, P. *Renewable Energy*. Our World in Data, 2023. https://ourworldindata.org/renewable-energy

(8) Grätzel, M. Photoelectrochemical cells. *Nature* **2001**, *414*, 338–344.

(9) Solak, E. K.; Irmak, E. Advances in organic photovoltaic cells: a comprehensive review of materials, technologies, and performance. *RSC Adv.* **2023**, *13*, 12244–12269.

(10) Rehman, F.; Syed, I. H.; Khanam, S.; Ijaz, S.; Mehmood, H.; Zubair, M.; Massoud, Y.; Mehmood, M. Q. Fourth-generation solar cells: a review. *Energy Adv.* **2023**, *2*, 1239–1262.

(11) Jauffred, L.; Samadi, A.; Klingberg, H.; Bendix, P. M.; Oddershede, L. B. Plasmonic Heating of Nanostructures. *Chem. Rev.* **2019**, *119*, 8087–8130.

(12) Lakowicz, J. R. *Principles of Fluorescence Spectroscopy*, 3rd ed.; Springer: New York, 1999.

(13) Baffou, G.; Cichos, F.; Quidant, R. Applications and challenges of thermoplasmonics. *Nat. Mater.* **2020**, *19*, 946–958.

(14) Jain, V.; Kashyap, R. K. Pillai, P. P. Plasmonic Photocatalysis: Activating Chemical Bonds through Light and Plasmon. *Adv. Optical Mater.* **2022**, *10*, 2200463.

(15) Hildebrandt, N.; Spillmann, C. M.; Algar, W. R.; Pons, T.; Stewart, M. H.; Oh, E.; Susumu, K.; Díaz, S. A.; Delehanty, J. B.; Medintz, I. L. Energy Transfer with Semiconductor Quantum Dot Bioconjugates: A Versatile Platform for Biosensing, Energy Harvesting, and Other Developing Applications. *Chem. Rev.* **2017**, *117*, 536–711.

(16) Pietryga, J. M.; Park, Y.-S.: Lim, J.; Fidler, A. F.; Bae, W. K.; Brovelli, S.; Klimov, V. I. Spectroscopic and Device Aspects of Nanocrystal Quantum Dots. *Chem. Rev.* **2016**, *116*, 10513–10622.

(17) Moore, R.; Clark, W. D.; Kingsley, R. S.; Vodopich, D. *Botany: Plant Diversity-Botany*; Wm. C. Brown, 1995.

(18) Romero, E.; Novoderezhkin, V. I.; van Grondelle, R. Quantum design of photosynthesis for bio-inspired solar-energy conversion. *Nature* **2017**, *543*, 355–365.

(19) Martino, N.; Ghezzi, D.; Benfenati, F.; Lanzani, G.; Antognazza, M. R. Organic semiconductors for artificial vision. *J. Mater. Chem. B* **2013**, *1*, 3768–3780.

(20) Samanta, A.; Medintz, I. L. Bioluminescence-Based Energy Transfer Using Semiconductor Quantum Dots as Acceptors. *Sensors* **2020**, *20*, 2909.

(21) Huber, R. A Structural Basis of Light Energy and Electron Transfer in Biology (Nobel Lecture). *Angew. Chem., Int. Ed. Engl.* **1989**, *28*, 848–869.

(22) Deisenhofer, J.; Michel, H. The Photosynthetic Reaction Center from the Purple Bacterium Rhodopseudomonas viridis (Nobel Lecture). *Angew. Chem., Int. Ed. Engl.* **1989**, *28*, 829–847.

(23) Gust, D.; Moore, T. A.; Moore, A. L. Molecular mimicry of photosynthetic energy and electron transfer. *Acc. Chem. Res.* **1993**, *26*, 198–205.

(24) Fŏrster, T. 10th Spiers Memorial Lecture. Transfer mechanisms of electronic excitation. *Discuss. Faraday Soc.* **1959**, *27*, 7–17.

(25) Chakraborty, I. N.; Roy, P.; Rao, A.; Devatha, G.; Roy, S.; Pillai, P. P. The Unconventional Role of Surface Ligands in Dictating the Light Harvesting Properties of Quantum Dots. *J. Mater. Chem. A* **2021**, *9*, 7422–7457.

(26) Rybtchinski, B.; Sinks, L. E.; Wasielewski, M. R. Combining Light-Harvesting and Charge Separation in a Self-Assembled Artificial Photosynthetic System Based on Perylenediimide Chromophores. *J. Am. Chem. Soc.* **2004**, *126*, 12268–12269.

(27) Wasielewski, M. R. Self-Assembly Strategies for Integrating Light Harvesting and Charge Separation in Artificial Photosynthetic Systems. *Acc. Chem. Res.* **2009**, *42*, 1910–1921.

(28) Gust, D.; Moore, T. A.; Moore, A. L. Mimicking Photosynthetic Solar Energy Transduction. *Acc. Chem. Res.* **2001**, *34*, 40–48.

(29) Mirkovic, T.; Ostroumov, E. E.; Anna, J. M.; van Grondelle, R.; Govindjee,; Scholes, G. D. Light Absorption and Energy Transfer in the Antenna Complexes of Photosynthetic Organisms. *Chem. Rev.* **2017**, *117*, 249–293.

(30) Kuciauskas, D.; Liddell, P. A.; Lin, S.; Johnson, T. E.; Weghorn, S. J.; Lindsey, J. S.; Moore, A. L. Thomas A. Moore, and Devens Gust, An Artificial Photosynthetic Antenna-Reaction Center Complex. *J. Am. Chem. Soc.* **1999**, *121*, 8604–8614.

(31) Alstrum-Acevedo, J. H.; Brennaman, M. K.; Meyer, T. J. Chemical Approaches to Artificial Photosynthesis. 2. *Inorg. Chem.* **2005**, *44*, 6802–6827.

(32) Xue, B.; Li, Y.; Yang, F.; Zhang, C.; Qin, M.; Cao, Y.; Wang, W. An integrated artificial photosynthesis system based on peptide nanotubes. *Nanoscale* **2014**, *6*, 7832–7837.

(33) Cao, S.; Rosławska, A.; Doppagne, B.; Romeo, M.; Féron, M.; Chérioux, F.; Bulou, H.; Scheurer, F.; Schull, G. Energy funnelling within multichromophore architectures monitored with subnanometre resolution. *Nat. Chem.* **2021**, *13*, 766–770.

(34) Teng, K.-X.; An, Z.-P.; Niu, L.-Y.; Yang, Q.-Z. A Supramolecular Artificial Light-Harvesting System with Excitation Energy and Electron Transfer. *ACS Mater. Lett.* **2024**, *6*, 290–297.

(35) Brus, L. E. Electron–Electron and Electron-Hole Interactions in Small Semiconductor Crystallites: The Size Dependence of the Lowest Excited Electronic State. *J. Chem. Phys.* **1984**, *80*, 4403–4409.

(36) Donegá, C. de M. Synthesis and properties of colloidal heteronanocrystals. *Chem. Soc. Rev.* **2011**, *40*, 1512–1546.

(37) Kodaimati, M. S.; McClelland, K. P.; He, C.; Lian, S.; Jiang, Y.; Zhang, Z.; Weiss, E. A. Viewpoint: Challenges in Colloidal Photocatalysis and Some Strategies for Addressing Them. *Inorg. Chem.* **2018**, *57*, 3659–3670.

(38) Yuan, X.; Zhao, J.; Jing, P.; Zhang, W.; Li, H.; Zhang, L.; Zhong, X.; Masumoto, Y. Size- and Composition-Dependent Energy Transfer from Charge Transporting Materials to ZnCuInS Quantum Dots. *J. Phys. Chem. C* **2012**, *116*, 11973–11979.

(39) Chung, H.; Cho, K.-S.; Koh, W.-K.; Kim, D.; Kim, J. Composition-dependent trap distributions in CdSe and InP quantum dots probed using photoluminescence blinking dynamics. *Nanoscale* **2016**, *8*, 14109–14116.

(40) Hines, D. A.; Kamat, P. V. Recent Advances in Quantum Dot Surface Chemistry. *ACS Appl. Mater. Interfaces* **2014**, *6*, 3041–3057.

(41) Giansante, C. Library Design of Ligands at the Surface of Colloidal Nanocrystals. *Acc. Chem. Res.* **2020**, *53*, 1458–1467.

(42) Bishop, K. J. M.; Wilmer, C. E.; Soh, S.; Grzybowski, B. A. Nanoscale Forces and Their Uses in Self-Assembly. *Small* **2009**, *5*, 1600–1630.

(43) Azpiroz, J. M.; Angelis, F. D. Ligand Induced Spectral Changes in CdSe Quantum Dots.

ACS Appl. Mater. Interfaces **2015**, *7*, 19736–19745.

(44) Dannhauser, T.; O'Neil, M.; Johansson, K.; Whitten, D.; McLendon, G. Photophysics of quantized colloidal semiconductors. Dramatic luminescence enhancement by binding of simple amines. *J. Phys. Chem.* **1986**, *90*, 6074–6076.

(45) Cowdery-Corvan, J. R.; Whitten, D. G.; McLendon, G. L. Electron transfer reactions at CdS semiconductor cluster interfaces. Adsorption and microenvironment effects on oxidative reactions. *Chem. Phys.* **1993**, *176* , 377–386.

(46) Wuister, S. F.; Donegá, C. de M.; Meijerink, A. Influence of Thiol Capping on the Exciton Luminescence and Decay Kinetics of CdTe and CdSe Quantum Dots. *J. Phys. Chem. B* **2004**, *108*, 17393–17397.

(47) Frederick, M. T.; Amin, V. A.; Swenson, N. K.; Ho, A. Y.; Weiss, E. A. Control of Exciton Confinement in Quantum Dot–Organic Complexes through Energetic Alignment of Interfacial Orbitals. *Nano Lett.* **2013**, *13*, 287–292,

(48) Hines, D. A.; Kamat, P. V. Quantum Dot Surface Chemistry: Ligand Effects and Electron Transfer Reactions. *J. Phys. Chem. C* **2013**, *117*, 14418–14426.

(49) Watson, D. F. Linker-Assisted Assembly and Interfacial Electron-Transfer Reactivity of Quantum Dot−Substrate Architectures. *J. Phys. Chem. Lett.* **2010**, *1*, 2299–2309.

(50) Pernik, D. R.; Tvrdy, K.; Radich, E. J.; Kamat, P. V. Tracking the Adsorption and Electron Injection Rates of CdSe Quantum Dots on TiO_2: Linked versus Direct Attachment. *J. Phys. Chem. C* **2011**, *115*, 13511–13519.

(51) Li, X.; Slyker, L. W.; Nichols, V. M.; Pau, G. S. H.; Bardeen, C. J.; Tang, M. L. Ligand Binding to Distinct Sites on Nanocrystals Affecting Energy and Charge Transfer. *J. Phys. Chem. Lett.* **2015**, *6*, 1709–1713.

(52) Dibbell, R. S.; Youker, D. G.; Watson, D. F. Excited-State Electron Transfer from CdS Quantum Dots to TiO_2 Nanoparticles via Molecular Linkers with Phenylene Bridges. *J. Phys. Chem. C* **2009**, *113*, 18643–18651.

(53) Dibbell, R. S.; Watson, D. F. Distance-Dependent Electron Transfer in Tethered Assemblies of CdS Quantum Dots and TiO2 Nanoparticles. *J. Phys. Chem. C* **2009**, *113*, 3139–3149.

(54) Tai, K.; Lü, W.; Umezu, I.; Sugimura, A. Inter-Dot Distance Dependence of Photoluminescence Properties in CdSe Quantum Dot Systems. *Appl. Phys. Express* **2010**, *3*, 035202.

(55) Wang, H.; McNellis, E. R.; Kinge, S.; Bonn, M.; Cánovas, E. Tuning Electron Transfer Rates through Molecular Bridges in Quantum Dot Sensitized Oxides. *Nano Lett.* **2013**,

13, 5311–5315.

(56) Hines, D. A.; Forrest, R. P.; Corcelli, S. A.; Kamat, P. V. Predicting the Rate Constant of Electron Tunneling Reactions at the CdSe–TiO2 Interface. *J. Phys. Chem. B* **2015**, *119*, 7439–7446.

(57) Walker, D. A.; Kowalczyk, B.; de la Cruz, M. O.; Grzybowski, B. A. Electrostatics at the nanoscale. *Nanoscale* **2011**, *3*, 1316–1344.

(58) Wargnier, R.; Baranov, A. V.; Maslov, V. G.; Stsiapura, V.; Artemyev, M.; Pluot, M.; Sukhanova, A.; Nabiev, I. Energy Transfer in Aqueous Solutions of Oppositely Charged CdSe/ZnS Core/Shell Quantum Dots and in Quantum Dot−Nanogold Assemblies. *Nano Lett.* **2004**, *4*, 451–457.

(59) Crooker, S. A.; Hollingsworth, J. A.; Tretiak, S.; Klimov, V. I. Spectrally Resolved Dynamics of Energy Transfer in Quantum-Dot Assemblies: Towards Engineered Energy Flows in Artificial Materials. *Phys. Rev. Lett.* **2002**, *89*, 186802.

(60) Franzl, T.; Shavel, A.; Rogach, A. L.; Gaponik, N.; Klar, T. A.; Eychmüller, A.; Feldmann, J. High-Rate Unidirectional Energy Transfer in Directly Assembled CdTe Nanocrystal Bilayers. *Small* **2005**, *1*, 392–395.

(61) Lutich, A. A.; Jiang, G.; Susha, A. S.; Rogach, A. L.; Stefani, F. D.; Feldmann, J. Energy Transfer versus Charge Separation in Type-II Hybrid Organic−Inorganic Nanocomposites. *Nano Lett.* **2009**, *9*, 2636–2640.

(62) Wang, C.; Kodaimati, M. S.; Schatz, G. C.; Weiss, E. A. The photoluminescence spectral profiles of water-soluble aggregates of PbS quantum dots assembled through reversible metal coordination. *Chem. Commun.* **2017**, *53*, 1981–1984.

(63) Kodaimati, M. S.; Wang, C.; Chapman, C.; Schatz, G. C.; Weiss, E. A. Distance-Dependence of Interparticle Energy Transfer in the Near-Infrared within Electrostatic Assemblies of PbS Quantum Dots. *ACS Nano* **2017**, *11*, 5041–5050.

(64) Franzl, T.; Klar, T. A.; Schietinger, S.; Rogach, A. L.; Feldmann, J. Exciton Recycling in Graded Gap Nanocrystal Structures. *Nano Lett.* **2004**, *4*, 1599–1603.

(65) Feng, C. L.; Zhong, X. H.; Steinhart, M.; Caminade, A.-M.; Majoral, J. P.; Knoll, W. Functional Quantum-Dot/Dendrimer Nanotubes for Sensitive Detection of DNA Hybridization. *Small* **2008**, *4*, 566–571.

(66) Xu, F.; Ma, X.; Haughn, C. R.; Benavides, J.; Doty, M. F.; Cloutier, S. G. Efficient Exciton Funneling in Cascaded PbS Quantum Dot Superstructures. *ACS Nano* **2011**, *5*, 9950–9957.

(67) Wolf, A.; Lesnyak, V.; Gaponik, N.; Eychmüller, A. Quantum-Dot-Based (Aero)gels:

Control of the Optical Properties. *J. Phys. Chem. Lett.* **2012**, *3*, 2188–2193.

(68) Litvin, A. P.; Parfenov, P. S.; Ushakova, E. V.; Vorsina, T. A.; Gamboa, A. L. S.; Fedorov, A. V.; Baranov, A. V. FRET-Activated Delayed Fluorescence in Densely Packed PbS Quantum-Dot Ensembles. *J. Phys. Chem. C* **2015**, *119*, 17016–17022.

(69) Naqvi, S. A. R.; Idrees, F.; Sherazi, T. A.; Shahzad, S. A.; Hassan, S. U.; Ashraf, N. Toxicology Associated with Heavy Metals Found in Cosmetics. *J. Chil. Chem. Soc.* **2022**, *67*, 5615–5622.

(70) Xie, R.; Battaglia, D.; Peng, X. Colloidal InP Nanocrystals as Efficient Emitters Covering Blue to Near-Infrared. *J. Am. Chem. Soc.* **2007**, *129*, 15432–15433.

(71) Li, L.; Reiss, P. One-pot Synthesis of Highly Luminescent InP/ZnS Nanocrystals without Precursor Injection. *J. Am. Chem. Soc.* **2008**, *130*, 11588–11589.

(72) Tessier, M. D.; Dupont, D.; Nolf, K. D.; Roo, J. D.; Hens, Z. Economic and Size-Tunable Synthesis of InP/ZnE (E = S, Se) Colloidal Quantum Dots. *Chem. Mater.* **2015**, *27*, 4893–4898.

(73) Won, Y.-H.; Cho, O.; Kim, T.; Chung, D.-Y.; Kim, T.; Chung, H.; Jang, H.; Lee, J.; Kim, D.; Jang, E. Highly efficient and stable InP/ZnSe/ZnS quantum dot light-emitting diodes. *Nature* **2019**, *575*, 634–638.

(74) Jang, E.; Kim, Y.; Won, Y.-H.; Jang, H.; Choi, S. M.; Environmentally Friendly InP-Based Quantum Dots for Efficient Wide Color Gamut Displays. *ACS Energy Lett.* **2020**, *5*, 1316–1327.

(75) Cros-Gagneux, A.; Delpech, F.; Nayral, C.; Cornejo, A.; Coppel, Y.; Chaudret, B.Surface Chemistry of InP Quantum Dots: A Comprehensive Study. *J. Am. Chem. Soc*. **2010**, *132*, 18147–18157.

Chapter – 2

Materials, Methods, and Instrumental Techniques

2.1 Materials and Reagents

Indium iodide (InI_3), indium chloride ($InCl_3$), indium acetate ($In(Ac)_3$), zinc iodide (ZnI_2), zinc chloride ($ZnCl_2$), zinc stearate ($Zn(St)_2$), copper acetate ($Cu(Ac)_2$), olylamine (OAm), myristic acid (MA), oleic acid (OA), 1-octadecene (ODE), 1-dodecanethiol (DDT), tris(dimethylamino)phosphine (($P(DMA)_3$), 6-mercaptohexanoic acid (MHA), 11-mercaptoundecanoic acid (MUA), rhodamine B dye, and methylene blue dye were purchased from Sigma-Aldrich and were used without further purification. Tris (trimethylsilyl)phosphine, $P(TMS)_3$) was purchased from Strem chemicals. N,N,N-trimethyl(11-mercaptoundecyl)ammonium chloride (TMA) was synthesized using a reported procedure.[1]

2.2 Synthesis of Environmentally Friendly Quantum Dots (QDs)

2.2.1 Synthesis of Green-Emitting InP/ZnS QDs:

The green-emitting InP/ZnS core/shell QDs were synthesized by following a reported one-pot synthetic protocol.[2] In a typical reaction, myristic acid (0.7 mmol, 157 mg), $In(Ac)_3$ (0.2 mmol, ~58 mg), and 1-octadecene (6 mL) were taken in a 100 mL three-neck RB and heated to ~110 ^{0}C under N_2 flow with gentle stirring, till a clear solution was formed. The reaction mixture was then degassed for ~2 h at ~110 ^{0}C followed by cooling to room temperature. Next, a mixture of zinc stearate (0.2 mmol, 125 mg), DDT (0.2 mmol, 48 µL) and $P(TMS)_3$ (0.2 mmol, 580 µL) in 2 mL ODE were prepared under inert atmosphere, and was injected into the reaction mixture, followed by heating to ~270 ^{0}C for ~1 h. At ~60 ^{0}C, the reaction mixture turned yellow indicating the decomposition of $P(TMS)_3$. Then the color slowly changed from yellow to dark-orange with increasing the reaction temperature, indicating the growth of InP QDs. When the temperature reached to ~230 ^{0}C, DDT started to decompose, leading to the formation of the ZnS shell over the InP QD core. After keeping for ~1 h at ~270 ^{0}C, the reaction mixture was quenched rapidly with a cold-water bath followed by the addition of 5 mL of hexane to arrest the growth of QDs. The resultant green-emitting InP/ZnS QDs were purified two times by precipitating with excess ethanol and re-dispersing back in chloroform, and used for further studies.

2.2.2 Synthesis of Red-Emitting InP/ZnS QDs:

Following the above described one pot synthetic method, red-emitting InP/ZnS QDs were synthesized with acid free indium-halide precursor and aminophosphine as the source of phosphorus precursor.[3] In a typical synthesis, indium (III) chloride (0.45 mmol, 100 mg), zinc chloride (2.2 mmol, 300 mg) and olylamine (15 mmol, 5.0 mL) were taken in a 100 mL three-neck RB and heated to ~120 ^{0}C under Ar atmosphere with gentle stirring, till a clear solution was formed. The reaction mixture was degassed for ~30 min at 120 ^{0}C and the temperature was raised further to ~200 ^{0}C under inert atmosphere. Upon reaching 200 ^{0}C, 350 µL of tris-(dimethylamino) phosphine (1.93 mmol) in 1.0 mL of olylamine was quickly injected into the reaction mixture, and the temperature was maintained at 200 ^{0}C for 1 h for the growth of InP core QDs. At the end, the reaction mixture was cooled down to room temperature with a cold-water bath and further proceeded for ZnS shell coating.

For the growth of ZnS shell, zinc stearate in octadecene (0.05 M, 2 mL) and DDT (0.1 mmol, 24 µL) was injected into the reaction mixture at room temperature under inert atmosphere, followed by increasing the temperature to 300 ^{0}C, and kept for 20 min. Finally, the reaction mixture was quenched with water bath followed by addition of 5 mL of hexane. The prepared red-emitting InP/ZnS core/shell QDs were purified by precipitating in ethanol and redispersed back in chloroform and used for further studies.

The green, and red emitting InP/ZnS QDs are abbreviated as G-QDs, and R-QDs, respectively, throughout the thesis.

2.2.3 Synthesis of Red-Emitting $CuInS_2$/ZnS QDs (CIS/ZnS QDs):

The synthesis was carried out by following a reported procedure.[4] Briefly, $In(Ac)_3$ (1.0 mmol, 292 mg), $Cu(Ac)_2$ (1.0 mmol, 182 mg) and 5 mL DDT were loaded in a 100 mL three-neck RB and heated to ~100 ^{0}C under N_2 flow with gentle stirring for ~10 minutes until a clear solution was obtained. The reaction mixture was degassed for ~30 min at ~100 ^{0}C, and the temperature was further raised to ~230 ^{0}C under continuous N_2 flow to allow the growth of $CuInS_2$ core for ~15 min. Here, DDT acts as a solvent as well as the sulfur precursor. With increase in temperature, a series of colour changes from golden-yellow to yellow to orange to dark-red were observed which indicates the nucleation and formation of $CuInS_2$ (CIS) QDs. The reaction mixture was then quenched rapidly with cold-water bath.

The as-synthesised CIS core QDs were further over coated with ZnS shell to improve the quantum yield and stability. For an in-situ ZnS overcoating, a solution of ODE and OA (4:1 ratio, 1.6 mL and 0.4 mL respectively) containing $Zn(St)_2$ (0.2 mmol, ~126 mg) was added dropwise to the reaction mixture at ~160 ^{0}C under N_2 flow over a period of 30 min. Afterward, the reaction temperature was raised to ~210 ^{0}C for about 15 min to allow for shell growth. The reaction mixture was quenched rapidly with water bath followed by the addition of 5 mL toluene to arrest the shell growth. The resultant solution was purified two times with acetone and finally redispersed back in chloroform for further studies.

The red-emitting R-CIS/ZnS QDs is abbreviated as R_{CIS}-QDs, throughout the thesis.

2.3 Preparation of Water Dispersed Environmentally Friendly QDs

Water dispersed charged QDs were prepared via the ligand exchange with MUA, MHA, and TMA ligand,.[5–6] Here, the MUA and MHA ligands impart negative charge, and the TMA ligand imparts positive charge to the QDs.

In a typical place exchange protocol, MUA (~100 mg, 0.46 mmol) was dissolved in 1:4 v/v ratio of water/methanol mixture (300 µL and 1.2 mL), and the pH of the solution was adjusted to ~12 using 3N NaOH solution. To the above solution of negatively charged MUA ligands, ~150 mmol of QD solution in chloroform was added, and stirred vigorously for ~5 min. Then, the solution was stirred for overnight followed by addition of 2 mL of water and 6 mL of chloroform, to facilitate the complete transfer of QDs from organic to aqueous phase. The success of place exchange reaction can be easily monitored by observing the phase transfer of photoluminescence (PL) from chloroform (luminescent to non-luminescent) and water (non-luminescent to luminescent) layers. Then, the aqueous phase was carefully separated and precipitated with acetone, to remove the unreacted MUA ligands via centrifugation. Finally, the anionic MUA capped [-] QDs were redispersed in milli-Q water for further studies.

The MHA capped [-] QD in water was prepared by replacing MUA ligand with MHA ligand in the above-mentioned ligand exchange procedure.

A similar procedure was adopted to prepare [+] charged QDs using an aqueous solution of [+] N,N,N-trimethyl(11-mercaptoundecyl)ammonium chloride (TMA) ligand, where the thiol group aided in surface functionalization, and quaternary ammonium group imparted cationic surface charge and dispersion in water.

[-] blue-emitting InP/ZnS QDs, [-]/[+] green-emitting InP/ZnS QDs, [-]/[+] red-emitting InP/ZnS QDs, and [-]/[+] red-emitting CIS/ZnS QDs are abbreviated as [-] B-QDs, [-]/[+] G-QDs, [-]/[+] R-QDs, and [-]/[+] R_{CIS}-QDs respectively, throughout the thesis.

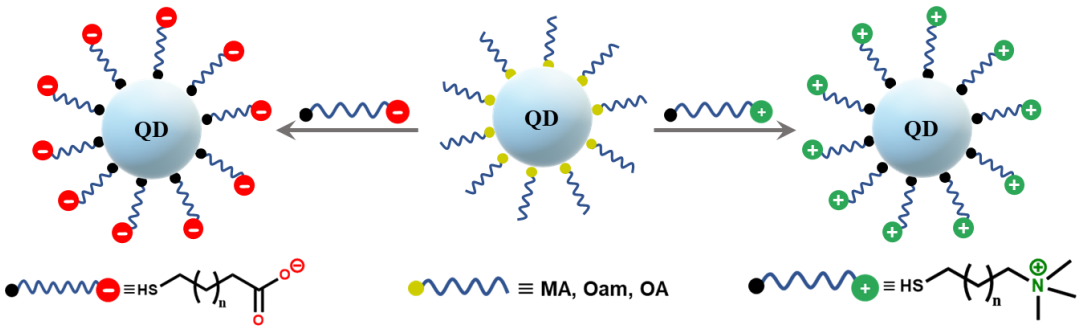

Scheme 2.1 Schematic representation of place exchange process with [-] and [+] charged ligands.

2.4 Biocompatibility and Cellular Bioimaging Studies

2.4.1 Cell Viability Assay:

MTT assay was employed to study cellular viability of QDs.[7] Briefly, a 96-well glass bottom plate was seeded with HeLa cells at a density of ~1000 cells per well. The cells were allowed to grow and adjust to the artificially created atmosphere in a humidified environment balanced with 5% CO_2 and maintained at 37 ºC. After 24 h, the wells were aspirated off the media and replenished with [-] B-QDs containing fresh media at various concentrations. Twelve concentrations were triplicated per QD and, were added for a given 96-well experiment. The first row of 6-well plate was kept as a control wherein no QD addition was made. The cells incubated with the QDs were left undisturbed under standard culture conditions for a period of 72 h. Towards the end of 72 h, the media in the plates were aspirated and a 50 µg/mL solution of MTT (3-(4,5-dimethylthiazol-2-yl)-2,5-diphenyltetrazolium bromide) in complete media was added per well for a period of 4 h. After 4 h, the plates were carefully aspirated off the media without disturbing the settled formazan crystals and 100 µL of HPLC grade DMSO was then added to each well. The plate was then transferred to a microplate shaker and allowed the crystals to dissolve in DMSO for a total of 30 min. Next, the plate was then subjected under a Varioscan machine, wherein the absorbance per well was then measured at 570 nm. The absorbance readout was then converted into the relative cellular viability with respect to the control, and was then plotted against the concentration.

2.4.2 Concentration-Dependent Cellular Imaging:

The six well sterile mammalian culture plate was employed for cellular uptake experiment of the [-] B-QDs. A thoroughly cleaned and UV sterile coverslip was placed per well of a 6-well plate. Next the plate was left under the conditions of UV for a period of 30 min inside the laminar flow hood. A total of 105 cells dispersed in 2 mL of complete media were added per well on top of coverslip. The cells were then allowed to grow for a period of 16–24 h. Once the cells adhered with a visible and healthy cytoskeleton, the compound addition was attempted. For concentration optimization, cells were treated with different concentrations of [-] B-QDs (20 µg/mL and 40 µg/mL) for a period of 6 h. At the end of 6 h, the media containing the compound was aspirated and washed 3 times with 2 mL warm HBBS buffer (Hank's balanced salt solution) to wash off the uninternalized QDs. Next, the cells were added with 1 mL of 4 % paraformaldehyde (PFA) solution and left undisturbed at room temperature for a period of 10 min. After 10 min, the cells were washed off with 2 mL warm HBBS solution twice to remove the PFA. The coverslip containing the fixed cells were then inverted onto a glass slide containing a drop (40 µL) of mounting media (70 % glycerol in water). The seals of the glass slides to cover slips were carefully sealed using a transparent nail paint. The slides were then imaged under a confocal microscope.

2.4.3 Multicolor Bio-Imaging:

Multicolor imaging experiments were performed via co-localization study with QD concentration of 40 µg/mL. Initially, a 6-well plate with a coverslip was added with 105 cells and then allowed to adhere. Next, the media was replenished with fresh media containing 40 µg/mL of [-] B-QD system. After 6 h, the media was aspirated, and cells were washed thrice with 2 mL of HBBS buffer. Next, the cells were incubated with SYTO^{TM} Deep Red at a concentration of 0.1 µg/mL in complete media for a total of 30-40 min. The cells were then washed twice with warm HBBS solution and fixed using paraformaldehyde fixation as described previously. Next, 100 µL of phalloidin (PHD) solution at 0.01 µM concentration was then added onto the cover slip and was allowed to incubate under toom temperature conditions in dark for 2 h. Next, the cover slips containing cells were then rinsed off with warm HBBS solution and inverted onto a glass slide using 70 % glycerol in water as mounting media. The prepared glass slides were then imaged under a confocal microscope using 405 nm (Laser Power: 2%, Gain: 600) excitation laser for QD and collection from 415–500 nm range. The

FITC conjugated phalloidin was excited using a 488 nm laser (Laser Power: 6%, Gain: 700) and the emission was collected in 510–560 nm range. The nuclear staining SYTO dye was excited using a 633 nm (Laser Power: 4%, Gain: 700). Stacks of dept 0.3 µm were collected per channel. The multicolour scanning was done on Zeiss Confocal instrument. The images collected were then processed using an ImageJ software for image processing and quantification.

2.5 Instrumentation and Software

2.5.1 UV-vis Absorption Studies:

UV-vis absorption studies were carried out on a Shimadzu UV-3600 Plus absorption spectrophotometer in an optical quartz cuvette of 1 cm path length over the range of 200–800 nm.

2.5.2 Steady-State Photoluminescence Studies:

The photoluminescence experiments were performed on Fluorolog-3 spectrofluorometer (HORIBA Scientific) with Xe-lamp as excitation source.

2.5.3 Absolute Photoluminescence Quantum Yield Measurements:

The absolute PL quantum yield (PL QY_A) measurement was carried out by using an integrating sphere on Fluoromax-4 spectrofluorometer (Horiba Jobin Yvon) with Xe-lamp as excitation source. The wavelength of excitation was 350 nm for blue QDs and 370 nm for green and red QDs, respectively. The emission monochromator was set in between 340–690 nm for blue QDs and 360–720 nm for green and red QDs, for measuring the scattering for solvent, and QY for QD sample.

2.5.4 Excitation Spectra:

The excitation spectra were recorded using a Fluorolog-3 spectrofluorometer (Horiba Scientific) with Xe lamp as excitation source. The excitation monochromator was set over the range below the emission maxima for QDs and dyes. The emission monochromator was set at the PL maxima of the corresponding QDs and dyes.

2.5.5 Time-Corelated Single Photon Count (TCSPC) Measurements:

Time-resolved PL studies were performed in a HORIBA DeltaFlex Time-Correlated Single Photon Counting system using 370 nm and 405 nm Delta-diodes as the excitation sources, with a time to amplitude converter (TAC) range of 800 nm and 3.2 μs, respectively, for 10,000 counts. The decay curve was deconvoluted using EZ analysis software and data was fit with multi exponential curves. The average lifetime was calculated using the following equation.

$$\boldsymbol{\tau_{Avg}} = \frac{\sum_{i=1}^{i=n} \boldsymbol{\alpha_i \tau_i^2}}{\sum_{i=1}^{i=n} \boldsymbol{\alpha_i \tau_i}} \quad \ldots (1)$$

Where τ_i is the lifetime and α_i is the pre-exponential factor.

The fractional contribution of each decay time (f_i) in the fit was calculated using the following equation.

$$\boldsymbol{f_i} = \frac{\boldsymbol{\alpha_i \tau_i}}{\sum \boldsymbol{\alpha_i \tau_i}} \quad \ldots (2)$$

2.5.6 Zeta Potential Measurements:

The zeta potential (ζ) measurement of charged QDs was performed in Zetasizer Nano series, Nano-2590 (Malvern instruments, U.K.) with a 655 nm laser. The optical density of the solution was maintained ~0.03 during all the measurements. The ζ value was estimated from the electrophoretic mobility (U_E) (the velocity with which the charged particles are attracted to the oppositely charged electrodes) and is calculated using Henry's equation:

$$\boldsymbol{U_E} = \frac{\boldsymbol{2\varepsilon\zeta f(K_a)}}{\boldsymbol{3\eta}} \quad \ldots (3)$$

Where,

ε is the dielectric constant.

ζ is the zeta potential (mV).

η is the viscosity coefficient of the medium (Pa.s).

f(ka) is Henry's function determined using Smoluchowski approximation.

2.5.7 X-Ray Diffraction (XRD) Measurements:

X-ray diffraction patterns were measured on Bruker D8 Advanced X-Ray diffractometer using Cu K_α (λ = 1.54 Å) rays. The samples for XRD analysis were prepared by drop casting the as-synthesized QDs on a clean glass substrate.

2.5.8 High Resolution Transmission Electron Microscopy (HRTEM):

The samples for microscopy measurements were prepared by drop casting QD solution on a 400-mesh carbon coated copper TEM grid (Ted Pella, Inc.). The samples were allowed to dry under ambient conditions, and were further dried under vacuum. The high-resolution images were recorded on a JEOL JEM- 2200FS (200 keV) HRTEM instrument.

2.5.9 Fourier-Transform Infrared Spectroscopy (FTIR) Studies:

Fourier transform infrared spectroscopy (FTIR) experiments were performed to confirm the presence of ligands on the surface of QDs. The measurements were performed on NICOLET 6700 FTIR instrument, using solid KBr disc.

2.5.10 X-ray Photoelectron Spectroscopy (XPS) Studies:

The XPS studies was performed by drop casting the QDs on silicon wafer, dispersed in IPA solvent, followed by drying under the vacuum. Then the measurements were performed in Thermo Fisher Scientific Instrument, Leicestershire, UK (Model: K-Alpha+) equipment using Al-Kα anode (1486.6 eV) in a transmission lens mode and multi-channel plate (MCP) detector. The binding energy scale was calibrated using standard C 1s peak (284.6 eV) and the elemental peaks were analysed using non-linear Shirley background correction. The peak positions fitting was performed by using XPSpeak41 software and optimized by a weight least-square fitting method using Gaussian and Lorentzian lineshapes.

2.5.11 Nuclear Magnetic Resonance Spectroscopy (NMR) Studies:

The ^{1}H NMR data was recorded on Brucker Ascend ^{TM} 400 MHz spectrometer.

2.5.12 Inductively Coupled Plasma-Mass Spectrometry (ICP-MS):

The ICP-MS analysis was performed to determine the concentration of In^{3+} ion in B-QD. At first, the QD sample was digested in 0.3 N HNO_3 solution, followed by filtration through syringe filter to remove any dust particles present in the solution. The amount of In^{3+} in the digested samples was quantified using ICP-MS analysis, performed on Quadrupole-ICP MS (Thermo iCAP-Q) instrument.

2.5.13 Cyclic Voltammetry (CV) Experiments:

The CV measurements were performed using Metrohm DropSens µStat400 electrochemical workstation and Dropview 8400 software of version 2.215B1204. Glassy carbon was used as the working electrode, non-aqueous $Ag/AgNO_3$ as the reference electrode and Pt wire was used as the counter electrode.

The onset oxidation and reduction potential for QDs *vs* vacuum was determined by following below equations.[8]

$$\boldsymbol{E_{VB} = -I_P = -\left(eE_{Ox} + E_{Ref}\right)eV} \quad \ldots (4)$$

$$\boldsymbol{E_{CB} = -E_A = -\left(eE_{Red} + E_{Ref}\right)eV} \quad \ldots (5)$$

Where, E_{Ox}, and E_{Red} are the onset redox potential relative to the reference electrode, while E_{ref} is the potential difference between the selected reference electrode and the vacuum energy level. I_P, and E_A represents the ionization potential and electron affinity, respectively.

2.5.14 Cytotoxicity and Bio-Imaging Studies:

The MTT assay was measured using a Varioscan™ plate reader instrument. For bio-imaging study, Zeiss LSM 780 confocal microscopy was used. Alongside, for maintaining the cells in tissue culture, we routinely use the following instruments: CO_2 incubator (galaxy 170, Eppendorf), centrifuge machines (5910 Ri, Eppendorf).

2.5.15 Droplet Experiments:

In a typical experiment, a glass slide was wrapped with a Teflon tape to increase the hydrophobicity of the substrate, so that uniform droplets can be prepared from aqueous samples. Following this, ~10 µL of (i) different ratios of donor–acceptor solution, (ii) only

donor, and (iii) only acceptor solution was placed over the Teflon coated glass slide and allowed them for normal evaporation. The true colour PL images were taken at different time intervals.

2.5.16 Preparation of Agarose Gel:

In a typical procedure, ~30 mg of agarose powder was taken in 3 mL water (1.0 % w/v), and heated at ~90 ºC, till the agarose completely solubilize. The clear solution was then cooled to 50 ºC and mixed with aqueous solutions of (i) different ratios of donor-acceptor, (ii) only donor, and (iii) only acceptor. Finally, the agarose mixture was poured into petri dish and kept overnight at ~50 ^{0}C for film casting. The film was thoroughly characterised using steady-state and time-resolved spectroscopic techniques.

2.5.17 Commission Internationale de l'Elcairage (CIE) Plot:

The CIE plot was generated from GOCIE-1931 software.[9] The complete PL spectrum of pure-blue emitting InP/ZnS QD was used to generate the coordinate in CIE spectrum and, accordingly the colour purity was determined by calculating the deviation of the measured coordinate (for sample) from the boundary of chromaticity diagram with respect to pure white region (0.33,0.33). Purity of colour, C_s, was determined by following the equation below.

$$\boldsymbol{Color\ Purity} = \left(\frac{C_s - C}{C_b - C}\right) * \mathbf{100}\ \% \qquad \ldots (6)$$

Where, C_s, C_b, and C represents the coordinates for sample, boundary, and centre of chromaticity diagram, respectively. The coordinates for boundary (C_b) were determined by connecting the sample point with the centre followed by extrapolating towards the boundary.

2.6 Concentration Calculation for QDs

2.6.1 Calculation of Concentration for Green- and Red-emitting InP/ZnS QDs:

The concentration of green- and red-emitting InP/ZnS QDs were calculated from absorption spectra using Beer lambert Law.[10]

$$\boldsymbol{A = \varepsilon \cdot c \cdot l} \qquad \ldots (7)$$

Where, A= absorbance or optical density

ε = Absorption coefficient or molar extinction coefficient ($M^{-1}cm^{-1}$)

c = Concentration of the solution (mol L^{-1})

l = Optical path length = 1 cm

ε was calculated from the following equation.[11]

$$\boldsymbol{\varepsilon = 3046.1(D)^3 - 76532(D)^2 + (5.5137\ X\ 10^5)(D) - (8.9839\ X\ 10^5)} \quad \ldots (8)$$

Here, D is the diameter of InP/ZnS QD, which was estimated to be 2.9 and 4.1 nm for G-QDs and R-QDs, respectively, from the following equation.

$$\boldsymbol{D = (-3.7707\ X10^{-12})\lambda^5 + (1.0262\ X10^{-8})\lambda^4 - (1.0781\ X10^{-5})\lambda^3 + (5.4550\ X10^{-3})\lambda^2 - (1.3122)\lambda + 119.9} \quad \ldots (9)$$

Here, λ is the wavelength at first excitonic peak in nm (452 nm and 570 nm for green- and red-emitting QDs, respectively). The ε value was calculated to be 128498 $M^{-1}cm^{-1}$ and 277528 $M^{-1}cm^{-1}$ for G-QDs and R-QDs respectively.

The concentration of green- and red-emitting InP/ZnS QDs was calculated by substituting ε and A value in equation (7).

2.6.2 Calculation of Concentration of CIS/ZnS QDs:

The concentration of CIS/ZnS QDs was calculated by using the equation (7). The ε was calculated from the following equation.[12–13]

$$\boldsymbol{\varepsilon = 830 d^{3.7}} \quad \ldots (10)$$

Here, d is the diameter of QDs, and was calculated by using the equation below.

$$\boldsymbol{d = 68.952 - 0.2136\ X\ \lambda_{PL} + (1.717\ X\ 10^{-4})\ \lambda_{PL}^2} \quad \ldots (11)$$

Here, ($\lambda_{(PL)}$) is the emission wavelength of QDs (631 nm).

The ε was calculated to be 25625 $M^{-1}cm^{-1}$ and the concentration was estimated by substituting the ε and A value in equation (7).

2.7 Background of Förster Resonance Energy Transfer (FRET) Formalism

The Förster resonance energy transfer (FRET) process is a non-radiative transfer of energy from an excited state donor to a ground state acceptor (**Scheme 2.2**).[10,14] It is driven by the long-range dipole–dipole interaction, and thus is strongly dependent on the donor–acceptor distance. Also, it demands an appreciable spectral overlap between the emission of donor and absorption of acceptor fluorophores.

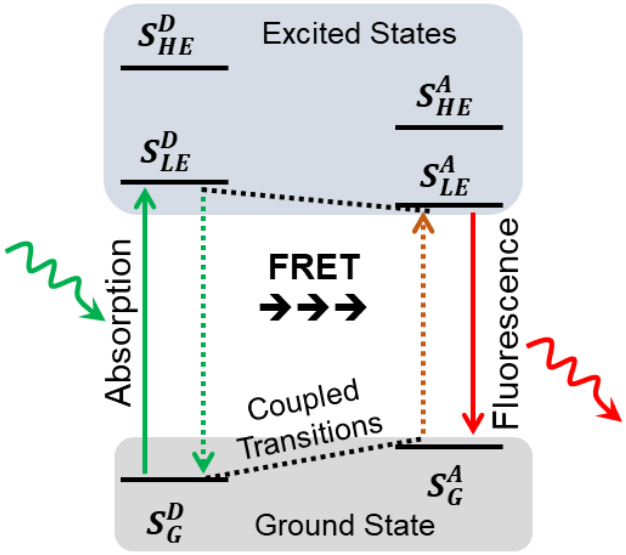

Scheme 2.2 Schematic representation of the Förster resonance energy transfer (FRET) process, where non-radiative transfer of energy leads to higher fluorescence from the acceptor. The terms S_G, S_{LE}, and S_{HE} stand for singlet ground state, singlet lowest excited state, and singlet higher excited state, respectively, while D and A refers to donor and acceptor, respectively.

The rate of energy transfer between donor and acceptor at a distance r can be expressed as:[10]

$$k_T(r) = \frac{B\Phi_D J(\lambda)}{\tau_D r^6} = \frac{1}{\tau_D}\left(\frac{R_0}{r}\right)^6 \quad \ldots (12)$$

Where, R_0 is the Förster distance at which FRET efficiency is 50%, r is the distance between donor and acceptor, and J(λ) is the spectral overlap integral between emission of donor and absorption of acceptor. Φ_D and τ_D are the PL quantum yield and lifetime of donor, respectively.

B is a constant that can be written as a function of refractive index of the medium η_D, Avogadro's number N_A and dipole orientation parameter κ_p:[14]

$$B = \frac{[9000(ln10)]\kappa_p^2}{128\pi^5\eta_D^4 N_A} \quad \ldots (13)$$

The orientation factor (κ_p) varies from 0 (for perpendicular alignment of the D–A dipoles) to 4 (for parallel orientation). The dynamic average value of k_p was assumed to be 2/3.[10,14]

Here, the Förster distance R_0 is given by[10]

$$\boldsymbol{R_0 = \left(B\phi_D J(\lambda)\right)^{1/6} = 0.2018\left(\frac{\phi_D \kappa_p^2 J(\lambda)}{\eta^4}\right)^{1/6}} \text{ Å} \quad \ldots (14)$$

Calculation of spectral overlap integral

The spectral overlap integral was estimated using the well-accepted equation, which takes account of the donor fluorescence and acceptor absorption properties, respectively.[10,14]

$$\boldsymbol{J(\lambda) = \int_0^\infty F_D(\lambda)\, \epsilon_A(\lambda)\, \lambda^4\, d\lambda \quad M^{-1}cm^{-1}nm^4} \quad \ldots (15)$$

Where, $F_D(\lambda)$ is the normalized fluorescence intensity of donor at a particular wavelength (λ), ϵ_A is the molar extinction coefficient of the acceptor at a particular wavelength. Higher the value of $J(\lambda)$, better the probability for a donor–acceptor system to become an efficient FRET pair.

Calculation of efficiency of energy transfer process

The efficiency of FRET can be calculated from steady-state PL and as well as from PL lifetime experiments.[10]

From steady-state PL quenching,

$$\boldsymbol{E = 1 - \frac{I_{DA}}{I_D}} \quad \ldots (16)$$

From lifetime quenching studies,

$$\boldsymbol{E = 1 - \frac{\tau_{DA}}{\tau_D}} \quad \ldots (17)$$

The I_{DA}, τ_{DA} are the PL intensity and lifetime of the donor in presence of acceptor and I_D, τ_D are PL intensity of lifetime of the donor in absence of acceptor.

Efficiency of energy transfer strongly depends on the distance between donor and acceptor. It varies inversely with sixth power to the distance between donor and acceptor ($E \alpha 1/r^6$).

However, for unlinked donor–acceptor system, the extent of energy transfer also depends on the concentration of acceptor. This can, for example, be realized by arraying multiple acceptors around a single donor QD. In this configuration, the QD donor plays a dual role: (i) a nanoscale scaffold by assembling multiple acceptors through the electrostatic attraction emanating from its surface, and (ii) a central exciton donor of energy to the surrounding acceptors. Such configuration produces a proportional increase in the FRET cross-section with increasing the number of acceptors. As a result, there will be a substantial enhancement in the overall energy transfer efficiency compared to one-to-one donor–acceptor pair. The overall energy transfer efficiency can be expressed as:[15]

$$\boldsymbol{E = \frac{nR_0^6}{nR_0^6 + r^6}} \quad \ldots (18)$$

Where, E is the energy transfer efficiency calculated from equations (16) and (17), R_0 is the Förster distance at which FRET efficiency is 50% (calculated from equation (14), r is the distance between donor and acceptor and the term n represents the total number of acceptors interacting with the same donor.

For non-covalently bonded donor–acceptor system, the critical concentration of acceptor (A_0) can be calculated from the Forster distance (R_0) of the system, by using the following equations.[10,16]

$$\boldsymbol{A_0 = \frac{3000}{2\pi^{3/2} N_A R_0^3}} \quad \ldots (19)$$

If R_0 is expressed in cm, the value of A_0 will be in mole/L, that is molarity (M).

The term A_0 represents the concentration at which the intramolecular energy transfer efficiency among the acceptors will be 76 %. Thus, when the acceptor concentration exceeds one hundredth of its critical concentration, possible intramolecular process will start to contribute.

2.8 Background of Photoinduced Electron Transfer (PET) Formalism

The photoinduced electron transfer (PET) process involves the transfer of an electron from a donor to an acceptor, and this is mainly governed by the energetics of the donor–acceptor pair.[10] The transfer of electrons from a donor to an acceptor should be thermodynamically feasible for an efficient PET to happen. A PET process can occur either through the photoexcitation of the donor (photooxidation) or the acceptor (photoreduction), as shown in **Scheme 2.3a**.[10,17] After the photoexcitation process, the electron is getting transfer from donor to acceptor, via formation of a charge transfer complex $[D^{+}:::A^{-}]^{*}$. In most cases, the charge transfer complex results in the formation of a non-luminescent charge-separated complex (D^{+} and A^{-}), but in some cases exciplex is observed. Finally, the extra electron on the acceptor is transferred back to donor, leaving the system in the initial phase (**Scheme 2.3b**).[10,17]

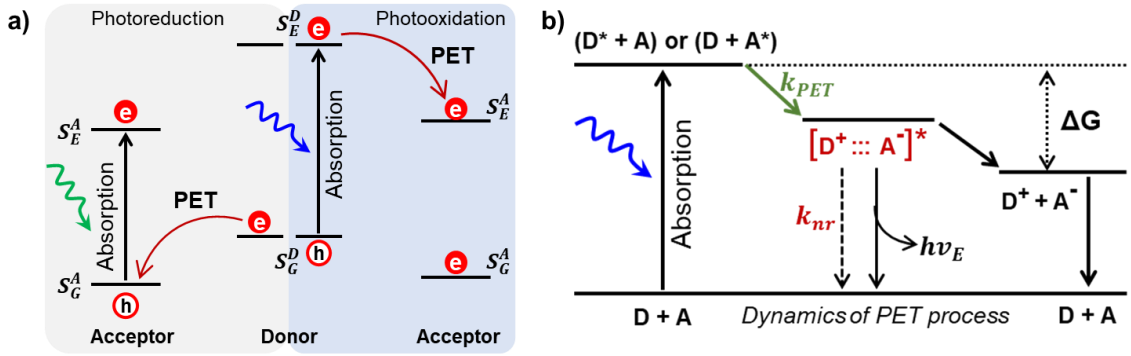

Scheme 2.3 Schematic representation of photoinduced electron transfer (PET) process. (a) A PET process can occur either through the photoexcitation of the donor (photooxidation) or the acceptor (photoreduction). The photooxidation process involves the transfer of electrons from an excited donor (D*) to a ground state acceptor (A). On the other hand, the photoreduction process involves the transfer of electrons from a ground state donor (D) to the ground state of the excited acceptor (A*). The terms S_G, and S_E stand for singlet ground state and singlet excited state, while D and A refers to donor and acceptor for PET process, respectively. (b) The dynamics of PET process in either case of donor or acceptor excitation. The k_{PET} describes the rate of PET process. Upon photoexcitation the electron donor transfers an electron to the acceptor with a rate of k_{PET}, forming the charge transfer complex $[D^{+}:::A^{-}]^{*}$. The formed charge transfer complex may emit as an exciplex or be quenched and finally returns to the ground state via charge separated state (D^{+} and A^{-}).

Thus, the process of PET can be easily monitored by analysing the PL intensity and PL lifetime quenching process for both donor and acceptor. The efficiency of PET process can be determined from the steady-state and time-resolved studies by using equations (16) and (17).

For nearly seven decades, Marcus theory has been effective for understanding and predicting kinetics of electron transfer reactions.[18-20] In this theory, electron transfer systems are well represented by harmonic free energy curves for donor (D) and acceptor (A) states. The

harmonic free energy curve provides the free energy of donor and acceptor as a function of nuclear distortion from equilibrium position, and largely depends on the reorganization energy λ, and Gibbs free energy change between donor and acceptor at equilibrium ΔG°. In accordance with the Marcus theory, electron transfer occurs by tunnelling from nuclear configurations when donor and acceptor have equivalent energy (intersection of two harmonic parabola; **Scheme 2.4a**).

The expression of rate constant for the PET process can be derived from the Eyring equation, such as,[10]

$$\boldsymbol{k_{PET} = Ae^{-\frac{\Delta G^*}{k_B T}}} \quad \ldots (20)$$

Where, ΔG^* represent the Gibbs free energy of activation, in turn, is given by,

$$\boldsymbol{\Delta G^* = \frac{\lambda}{4}\left[1 + \frac{\Delta G^o}{\lambda}\right]^2} \quad \ldots (21)$$

and 'A' is the pre-exponential factor, which depends on the nature of the electron transfer process, electronic coupling, and reorganization factor.

Therefore, the rate of PET process (k_{PET}) can be expressed as a function of a combination of electronic and nuclear factors:[18–21]

$$\boldsymbol{k_{PET} = \frac{2\pi H_{DA}^2}{h}\left[\frac{\pi}{\lambda k_B T}\right]^{1/2} e^{\left[-\frac{(\lambda+\Delta G^o)^2}{4\lambda k_B T}\right]}} \quad \ldots (22)$$

Here, H_{DA} is the electronic coupling between the donor and acceptor, λ is the nuclear reorganization parameter, h is Planck's constant, k_B is the Boltzmann constant, and ΔG° is the standard free-energy change for the electron transfer process at equilibrium.

The rate of PET process is predicted to increase as −ΔG° approaches λ and reach a maximum when −ΔG° = λ. When −ΔG° increases beyond λ, the rate of electron transfer is, counterintuitively, predicted to decrease described in the Marcus inverted region (**Scheme 2.4b**).

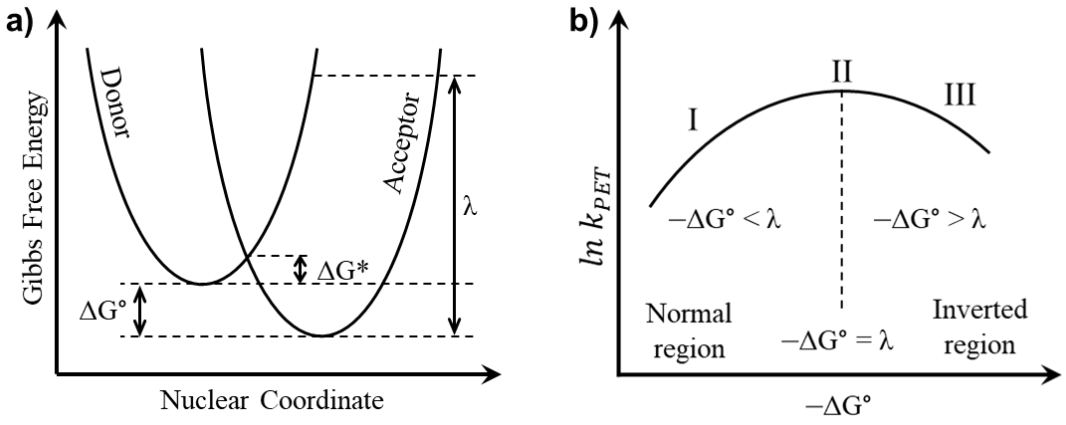

Scheme 2.4 Schematic representation of Marcus model for photoinduced electron transfer (PET) process. (a) Gibbs free energy parabolas *vs* nuclear coordinate for PET donor–acceptor system. The free energy for donor and acceptor states are equal at intersection point, and the electron tunnels through the barrier. (b) The inverted Marcus plot (plot of $\ln k_{PET}$ *vs* $-\Delta G°$): Regions-I & III are normal and inverted regions, respectively. The rate will be maximum at region-II, where $-\Delta G° = \lambda$

In general, the mechanism of electron transfer process depends on the nature, magnitude, and energetics of the electronic interaction of the separated donor–acceptor moieties. In the case of QD-based PET systems, in which an aliphatic linker separates the donor and acceptor, the electron transfer proceeds by a simple model of tunnelling process, following the Marcus model. In tunnelling process, the rate of electron transfer process varies exponentially on the separation distance, and the electron or hole never resides on the bridge. The exponential dependence of the PET rate constant is commonly expressed as:[21–22]

$$\boldsymbol{k_{PET} = k_0 e^{(-\beta d_{DA})}} \quad \ldots (23)$$

Here, k_0 is the pre-exponential constant, β is the tunnelling decay constant, and d_{DA} is the donor–acceptor separation distance.

Calculation of photoinduced electron transfer rate

The rate of PET process can be easily calculated from time-resolved experiments by monitoring the average lifetime of donor in absence and presence of acceptor.[10,22]

The average lifetime of donor in absence of acceptor:

$$\boldsymbol{\tau_D = \frac{1}{k_r + k_{nk}}} \quad \ldots (24)$$

The average lifetime of donor in presence of acceptor:

$$\boldsymbol{\tau_{DA} = \frac{1}{k_r + k_{nk} + k_{PET}}} \quad \ldots (25)$$

Here, K_r, and K_{nr} are the radiative and non-radiative decay rate for donor.

By combining the equation (24) and (25), the rate of PET process can be calculated, such as:

$$\boldsymbol{k_{PET} = \frac{1}{\tau_D}\left(\frac{\tau_D}{\tau_{DA}} - 1\right)} \quad \ldots (26)$$

In contrast, the process of PET can be extensively studied with the help of steady-state and time-resolved spectroscopic techniques. The electron transfer starts with the basic principle of electrochemistry. It is more predictable because the possibility of PET can be predicted from the redox potential of donor and acceptor. The Gibbs free energy change for PET process can be calculated as:[10]

$$\boldsymbol{\Delta G^o = -nF\Delta E} \quad \ldots (27)$$

Where, n is the number of electron involve in the process, ΔE is the difference in redox potential, and F is the Faraday constant.

For a given process, the value of ΔG° can be calculated form electrochemistry. When $\Delta G° < 0$, the process is thermodynamically favoured.

2.9 References

(1) Tien, J.; Terfort, A.; Whitesides, G. M. Microfabrication through Electrostatic Self-Assembly. *Langmuir* **1997**, *13*, 5349–5355.

(2) Li, L.; Reiss, P. One-Pot Synthesis of Highly Luminescent InP/ZnS Nanocrystals without Precursor Injection. *J. Am. Chem. Soc.* **2008**, *130*, 11588–11589.

(3) Tessier, M. D.; Dupont, D.; De Nolf, K.; De Roo, J.; Hens, Z. Economic and Size-Tunable Synthesis of InP/ZnE (E = S, Se) Colloidal Quantum Dots. *Chem. Mater.* **2015**, *27*, 4893–4898.

(4) Deng, D.; Chen, Y.; Cao, J.; Tian, J.; Qian, Z.; Achilefu, S.; Gu, Y. High-Quality CuInS2/ZnS Quantum Dots for In vitro and In vivo Bioimaging. *Chem. Mater.* **2012**, *24*, 3029–3037.

(5) Talapin, D. V.; Rogach, A. L.; Mekis, I.; Haubold, S.; Kornowski, A.; Haase, M.; Weller, H. Synthesis and Surface Modification of Amino-Stabilized CdSe, CdTe and InP Nanocrystals. *Colloids Surf. A: Physicochem. Eng. Asp.* **2002**, *202*, 145–154

(6) Devatha, G.; Roy, S.; Rao, A.; Mallick, A.; Basu, S.; Pillai, P. P. Electrostatically Driven Resonance Energy Transfer in "Cationic" Biocompatible Indium Phosphide Quantum Dots. *Chem. Sci.* **2017**, *8*, 3879–3884.

(7) Michalet, X.; Pinaud, F. F.; Bentolila, L. A.; Tsay, J. M.; Doose, S.; Li, J. J.; Sundaresan, G.; Wu, A. M.; Gambhir, S. S.; Weiss, S. Quantum Dots for Live Cells, in Vivo Imaging, and Diagnostics. *Science*, **2005**, *307*, 538–544.

(8) Liu, J.; Yang, W.; Li, Y.; Fan, L. Li, Y. Electrochemical Studies of the Effects of the Size, Ligand and Composition on the Band Structures of CdSe, CdTe and Their Alloy Nanocrystals. *Phys. Chem. Chem. Phys.* **2014**, *16*, 4778–4788.

(9) Choudhury, A. K. R. Using instruments to quantify colour. In *Principles of Colour and Appearance Measurement*, 1st ed.; Woodhead Publishing, UK, 2014; pp 270–317.

(10) Lakowicz, J. R. *Principles of Fluorescence Spectroscopy*, 3rd ed.; Springer: New York, 1999.

(11) Reiss, P.; Protière, M.; Li, L. Core/Shell Semiconductor Nanocrystals. *Small* **2009**, *5*, 154–168.

(12) Xia, C.; Wu, W.; Yu, T.; Xie, X.; van Oversteeg, C.; Gerritsen, H. C.; de Mello Donega, C. Size-Dependent Band-Gap and Molar Absorption Coefficient of Colloidal $CuInS_2$ Quantum Dots. *ACS Nano* **2018**, *12*, 8350–8361.

(13) Booth, M.; Brown, A. P.; Evans, S. D.; Critchley, K. Determining the Concentration of $CuInS_2$ Quantum Dots from the Size-Dependent Molar Extinction Coefficient. *Chem. Mater.* **2012**, *24*, 2064–2070.

(14) Sapsford, K. E.; Berti, L.; Medintz, I. L. Materials for Fluorescence Resonance Energy Transfer Analysis: Beyond Traditional Donor–Acceptor Combinations. *Angew. Chem. Int. Ed.* **2006**, *45*, 4562–4588.

(15) Clapp, A. R.; Medintz, I. L.; Mauro, J. M.; Fisher, B. R.; Bawendi, M. G.; Mattoussi, H. Fluorescence Resonance Energy Transfer Between Quantum Dot Donors and Dye-Labeled Protein Acceptors. *J. Am. Chem. Soc.* **2004**, *126*, 301–310.

(16) Wu, P. G.; Brand, L. Resonance Energy Transfer: Methods and Applications. *Anal Biochem.* **1994**, *218*, 1–13.

(17) Chakraborty, I. N.; Roy, P.; Rao, A.; Devatha, G.; Roy, S.; Pillai, P. P. The Unconventional Role of Surface Ligands in Dictating the Light Harvesting Properties of Quantum Dots. *J. Mater. Chem. A*, **2021**, *9*, 7422–7457.

(18) Marcus, R. A. On the Theory of Oxidation-Reduction Reactions Involving Electron Transfer. I. *J. Chem. Phys.* **1956**, *24*, 966–978.

(19) Marcus, R. A. On the Theory of Oxidation-Reduction Reactions Involving Electron Transfer. II. Applications to Data on the Rates of Isotopic Exchange Reactions. *J. Chem. Phys.* **1957**, *26*, 867–871.

(20) Marcus, R. A. Electron Transfer Reactions in Chemistry: Theory and Experiment (Nobel Lecture). *Angew. Chem. Int. Ed. Engl.* **1993**, *32*, 1111–1121.

(21) Adams, D. M.; Brus, L.; Chidsey, C. E. D.; Creager, S.; Creutz, C.; Kagan, C. R.; Kamat, P. V.; Lieberman, M.; Lindsay, S.; Marcus, R. A.; Metzger, R. M.; Michel-Beyerle, M. E.; Miller, J. R.; Newton, M. D.; Rolison, D. R.; Sankey, O.; Schanze, K. S.; Yardley, J.; Zhu, X. Charge transfer on the Nanoscale: Current Status. *J. Phys. Chem. B* **2003**, *107*, 6668–6697.

(22) Tagliazucchi, M.; Tice, D. B.; Sweeney, C. M.; Morris-Cohen, A. J.; Weiss, E. A. Ligand-Controlled Rates of Photoinduced Electron Transfer in Hybrid CdSe Nanocrystal/Poly(viologen) Films. *ACS Nano* **2011**, *5*, 9907–9917.

Chapter – 3

Blue Emitting InP/ZnS Quantum Dots: Expanding the Spectrum of Environmentally Friendly Quantum Dots for FRET Studies

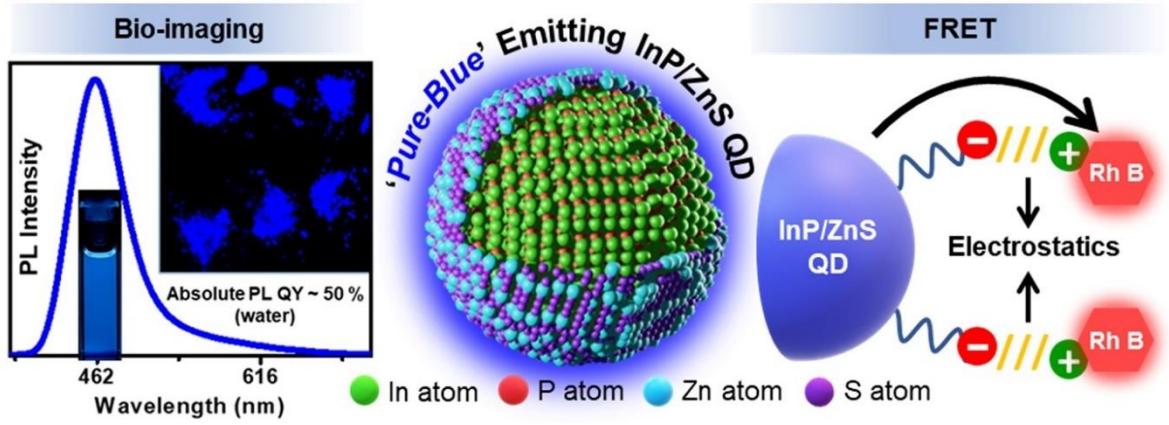

This Chapter has been adapted from the following paper with permission. Copyright 2023, The Royal Society of Chemistry (RSC):

Roy, P.; Virmani, M.; Pillai, P. P. Blue-emitting InP quantum dots participate in an efficient resonance energy transfer process in water. *Chem. Sci.* **2023**, *14*, 5167–5176.

3.1 Abstract

Development of stable blue-emitting materials has always been a challenging task because of the necessity of high crystal quality and good optical properties. We have developed a highly efficient blue-emitter, based on environmentally friendly indium phosphide/zinc sulphide quantum dots (InP/ZnS QDs) in water, by controlling the growth kinetics of the core as well as the shell. A rational combination of less-reactive metal-halides, phosphorus, and sulphur precursors is the key for achieving the uniform growth of InP core and ZnS shell. The InP/ZnS QD showed a long-term stable photoluminescence (PL) in the pure-blue region (~462 nm), with an absolute PL quantum yield of ~50 % and a colour purity of ~80 % in water. Cytotoxicity studies revealed that the cells can withstand up to ~2 micromolar concentration of pure-blue emitting InP/ZnS QD (~120 µg/mL). Multicolour imaging studies show that the PL of InP/ZnS QDs was well-retained inside the cells as well, without interfering with the fluorescence signal of commercially available biomarkers. Moreover, the ability of InP based pure-blue emitters to participate in an efficient Förster resonance energy transfer (FRET) process is demonstrated. Installing a favorable electrostatic interaction turned out to be crucial in achieving an efficient FRET process (E ~75 %) from blue-emitting InP/ZnS QDs to rhodamine B dye (Rh B) in water. The quenching dynamics fits well with the Perrin formalism and distance-dependent quenching (DDQ) model, which confirms an electrostatically driven multi-layer assembly of Rh B acceptor molecules around the InP/ZnS QD donor. Furthermore, the process of FRET was successfully translated into solid-state, proving their suitability for device-level studies as well. In short, our study expands the spectrum of aqueous QDs based on InP towards the blue-region for future biological and light harvesting studies.

3.2 Introduction

Luminescent materials find applications in broad areas of science and technology including full-color display devices, photovoltaics, bioimaging and targeting, sensing, and so on.[1-3] The diversity of modern science demand for the need of luminescent materials that emit in all regions of the visible and near-infrared spectra.[1-5] But, it is challenging to prepare ‘pure’ blue-emitting luminescent materials as they often fail to meet the stringent requirement of colour purity, high and stable quantum yield, and long-term photostability.[1,2] This has been an obstacle in realizing the full use of luminescent materials in different areas of energy and medical research. Quantum dots (QDs) can be one class of materials that could solve this challenge, as

they possess unique optoelectronic properties, such as large absorption cross-section, tunable and narrow emission bandwidth, high photoluminescence quantum yield (PL QY), and enhanced photostability.[3-13] In this direction, indium phosphide (InP) based QDs are emerging as one of the luminescent materials of choice because of their intrinsically lower toxicity over traditional Cd- and Pb-based QDs.[14-24] Having a bulk band gap of 1.35 eV and Bohr exciton radius of ~9.6 nm, the emission wavelength of InP QDs can be tuned throughout the full-visible color gamut and near-infrared region by varying their size.[4,14,16] However, the creation of highly luminescent blue-emitting InP QDs is not a straight-forward task in QD research because of the necessity of ultra-small sized QD core (<2 nm) (**Figure 3.1a**).[6,18] The ultra-small QDs are prone to contain more crystal defects that could hamper their luminescent properties, and this demands for the improved synthetic strategies. Moreover, the high covalent nature of InP QDs makes them more vulnerable towards oxidizing environments.[25] Additionally, covalent bond formation usually demands higher reaction temperatures, long reaction times, and more reactive precursors. As a result, the generation of monodispersed and smaller sized QD is significantly challenging in III-V semiconductors.[18] Thus, reliable synthesis protocols are required for achieving emission at a shorter wavelength with a higher reaction yield and improved electronic properties. In that direction, a seminal work by LaMer and Dinegar forms the foundation for understanding the desired need at nucleation and growth rates.[18,26] In general, the solution-process synthesis of QDs is governed by two distinct stages of nucleation and growth. Understanding the kinetics of these processes and their underlying chemical reactions is primordial for the rational design of synthesis methods. In according to the LaMer plot, as depicted in **Figure 3.1b**, a high precursor to monomer conversion rate and easy temporal separation between nucleation and the growth process are essential for obtaining smaller size QDs.[18,26] A few protocols are available to prepare blue-emitting InP QDs in organic medium, wherein the growth kinetics of QDs is slowed-down by controlling the reaction temperature, precursor reactivity, surface etching, shell growth, competitive secondary nucleation process, etc.[27-34] In one of the early report by Ning, Tian and co-workers, a unique synthetic methodology was introduced for the preparation of blue-emitting InP/ZnS QDs, with the aid of copper ions. Here, the presence of copper ion in reaction mixture assists a competitive secondary nucleation event towards the formation of hexagonal $Cu_{3-x}P$ nanocrystals.[29] This resulted in poor supply of phosphorous precursors, which in turn causes slow growth, and the smaller sized InP QDs with blue PL (**Figure 3.2a**).

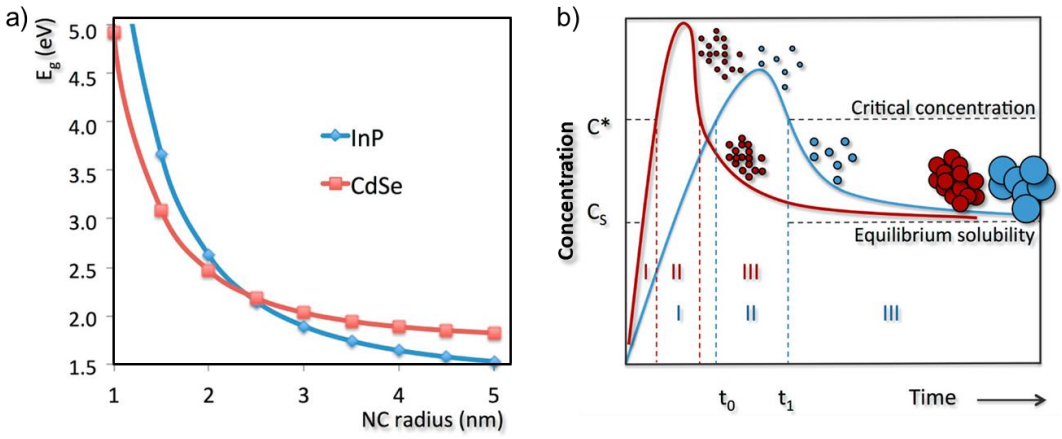

Figure 3.1 (a) Corelation between band gap vs diameter of InP and CdSe QDs, calculated using the effective mass approximation (used parameters: band gap (E_g) = 1.35/1.74 eV; dielectric constant (ε_r) = 12.4/9.5; Bohr excitonic radius (r_{Bohr}) = 9.6/4.6 nm for InP/CdSe). (b) Schematic representation of LaMer plot for the monodispersed colloidal synthesis of nanocrystals (NCs), following three distinct stages: (I) precursor conversion raises monomer concentration above the critical concentration threshold, C*; (II) nucleation, and (III) growth stages while the monomer concentration is in the regime of supersaturation (Cs< C < C*). A decrease in precursor-to-monomer conversion rate leads to adverse changes in QDs concentration and size (red to blue curve). Reproduced with permission from references 18. Copyright 2016 American Chemical Society.

In another elegant work, Chae and co-workers have regulated the size of InP QDs by controlling the reaction kinetics of ZnS shelling by varying the hydrocarbon ligand length (alkanethiols).[30] The reactive shorter alkanethiol allowed for rapid shelling of ZnS, and inhibits the growth of the InP core, thus reducing the emission wavelength (exhibiting PL peak at 485 nm; **Figure 3.2b**). In addition to that, the length of fatty acid can also alter the nucleation kinetics for the core synthesis. Large steric hindrance from longer fatty acid ligands restricts the In-P-Zn complexation, and thus, the nucleation and growth rates for InP core QD increases, resulted in red shift in PL wavelength. Likewise, Woo and co-workers added an important insight into the mechanism for the formation of smaller sized InP QDs, in presence of acetate salt of indium ion (**Figure 3.2c**).[27] Accordingly, holding of reaction temperature at 130 ^{0}C is crucial to restrict the growth of InP core into the blue region. This is because, in presence of acetate salt, ultra-small InP cores remain at constant competition between etching and growth processes. The process of etching was dominant at temperatures below 150 °C, whereas the growth process outperformed at above 150 °C. Therefore, as expected, lower the reaction temperature (130 °C), smaller the size of the synthesized QDs (band edge emission, BEM at 475 nm), and the emission red shifted to 497 nm when the reaction temperature was increased to 170 ^{0}C.

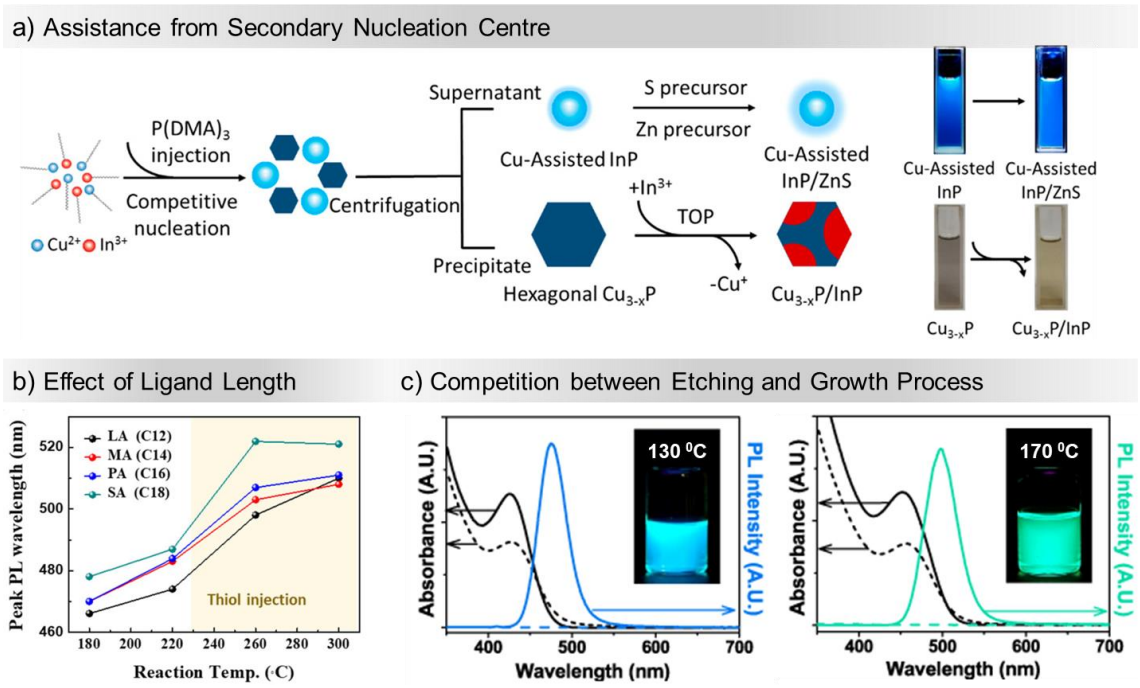

Figure 3.2 Methodologies for production of blue-emitting InP/ZnS QDs. (a) Schematic for preparation of blue InP QDs assisted by Cu ions. The competitive secondary nucleation centre restricts the precursor concentration for the growth process, leading to creation of smaller sized QDs. PL (upper), and optical (lower) photograph for InP QD and InP/ZnS QD are given at the right side of scheme. Reproduced in part with permission from reference 29. Copyright 2019 American Chemical Society. (b) Effect of ligand length, and (c) the reaction temperature on the size of InP QDs. Lower reaction temperature (etching dominated) and smaller ligand length (less steric hindrance for In-P-Zn complexation, thus, favors ZnS shelling) are essential components to regulate the growth rate of QDs synthesis. In presence of long chain alkanethiols, emission maxima are red shifted (LA<MA<PA<SA). Similarly, the band edge emission remains in the blue region at 130 ^{0}C, and shits to green region at 170 ^{0}C. Parts adapted with permission from references 30 and 27. Copyright 2020 Multidisciplinary Digital Publishing Institute and Copyright 2012 IOP Publishing Ltd.

The development of these procedures was very helpful in comprehending the dynamics of the nucleation and growth processes. Nonetheless, majority of them are constrained by the colour purity, photostability, or emission maxima of the QDs (usually at around sky-blue region). This necessitates the development of new techniques for the flawless replication of the LaMer model, which are only possible with complete control over the reactivity of each precursor which in turn provide controls over breaking and making of bonds. In that direction, Yang and coworkers and Hens and co-workers have introduced an innovative and potentially efficient alternative methods for preparation of InP QDs.[16,35] At the first place, they demonstrate that the size of the InP QDs can be regulated with various combinations of InX_3 (X = Cl, Br, I) and aminophosphine (amino = dimethylamino [DMA]) (**Figure 3.3**). As the bond strength drops on moving from indium chloride ($InCl_3$) to indium bromide ($InBr_3$) to indium iodide (InI_3), the process of bond breaking and bond making fastens, providing a complete control over the rate

of the nucleation process.[16] As a result, the chemical reactivity-based size-tuning method enabled the production of InP/ZnS and InP/ZnSe QDs with an emission range encompassing a significant portion of the visible spectrum (**Figure 3.3**). However, the blue emission was missing, probably a right and rational combination of indium and zinc halide precursors requires to be optimized. In one such example, stable blue-emitting InP/ZnS/ZnS QD (λ_{em} ~475 nm) was prepared by fine-tuning the inherent reactivity between phosphorus and indium precursors, thereby achieving a control over nucleation and growth processes.[31] This has led to the development of efficient blue-emitting light emitting diodes (LEDs) based on InP/ZnS/ZnS core/shell/shell QDs. The use of a double layer of a very thick ZnS shell was crucial in this study for stabilizing the QDs and achieving high PL QY. The presence of a thick ZnS shell in this study (~8 monolayers), eventually increasing the overall size of the QD to ~6.8 nm, which might have inherent limitations in light-harvesting (poor energy transfer efficiency because of the thick shell)[36] as well as in biological studies (poor renal clearance because of the large size).[37] In a very recent study, Douhal and co-workers were successful in preparing a smaller sized InP/ZnS/ZnS QDs (~4 nm) with the PL centered in the deep-blue region in organic medium, by fine-tuning the growth kinetics and ZnS shell-thickness.[34] The other demand in the area is to retain the high PL of blue-emitting InP/ZnS QDs in aqueous medium to expand their scope in diverse areas of science. Therefore, there is a necessity to optimize the synthetic protocol further for preparing stable pure-blue emitting InP/ZnS QDs in the aqueous medium, along with demonstrating their versatile applied properties in water.

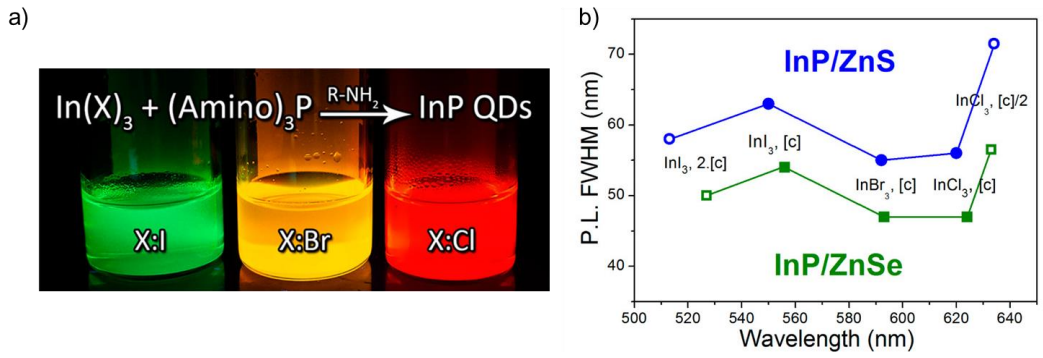

Figure 3.3 Chemical reactivity-based size-tunning of InP QDs. The size of the InP QDs can be regulated with various combinations of InX_3 (X = Cl, Br, I) and aminophosphine. (a) PL photograph and (b) emission line width of developed InP QDs in relation to different Indium halide precursor salts, indicating that a large part of the visible spectra can be addressed by fine-tunning the inherent reactivity among the precursors. Here, [c] correspond to 0.45 mmol of indium precursor in 5 mL of olylamine. Reproduced with permission from reference 16. Copyright 2015 American Chemical Society.

Here, we report the preparation of highly luminescent pure-blue emitting InP/ZnS QDs (~462 nm) in organic medium and their successful transfer to aqueous phase, with an absolute PL quantum yield of ~50 % and a colour purity of ~80 % (CIE 0.16,0.15) in water. These InP QDs contain a thin shell of ZnS compared to previous reports (3 vs 8 monolayers), which motivated us to test their suitability for both bioimaging as well as light induced Förster resonance energy transfer studies (FRET). Majority of the QD based FRET donors used so far emits from the green region, which limits the use of acceptor molecules that emit from yellow region and above. In other words, the unavailability of pure-blue emitting QD donors restricts the use of acceptor molecules (biomolecules, organic and inorganic chromophores) that absorb in blue to cyan regions. Thus, there is a high demand for the demonstration of a FRET system based on a pure-blue emitting QD donor, and this forms the focus of the present Chapter. As a proof of concept, we have demonstrated an efficient FRET from blue-emitting InP/ZnS QD donor to red-emitting rhodamine B dye acceptor. This system also serves as an example for long-range FRET process (here, long-range is in terms of wide color gamut).

A fine-control over the core size and shell thickness of InP/ZnS QDs, by optimizing the precursor amounts and the growth kinetics, enabled us to achieve a strong and stable PL in the pure-blue region. A rational combination of less-reactive metal-halides, phosphorus, and sulphur precursors was the key for achieving the uniform growth of InP core and ZnS shell. For instance, the dual role of aminophosphine as both precursor and reducing agent (disproportionation), coupled with the weak bond strength of iodide salts of indium and zinc was crucial in achieving the desired control over the growth kinetics of the core. The as-synthesized InP/ZnS QDs (3.55 ± 0.41 nm diameter) exhibited a first excitonic peak at ~410 nm with the peak-to-valley ratio of 1.45, and a sharp PL peak at ~462 nm (full-width half-maxima of ~58 nm). The uniformity in the ZnS shell led to the proper surface modification with 11-mercaptoundecanoic acid ([-], MUA), which imparted the much-required colloidal stability to pure-blue emitting InP/ZnS QDs in water as well as in biological media. Importantly, there was only a marginal decrease in the absolute PL quantum yield (QY) of blue-emitting InP/ZnS QDs after the surface functionalization and dispersion in water (~60 % in chloroform and ~50 % in water). The blue-emitting InP/ZnS QDs retained their strong PL inside the biological cells without interfering with the fluorescence signal of commercial dyes. Moreover, the InP/ZnS QDs participated in an efficient FRET process, which expands the spectrum of aqueous QDs towards the blue-region for future light harvesting studies. The presence of negative surface charges on QDs led to the formation of an electrostatically

bounded donor-acceptor system consisting of [-] pure-blue emitting InP/ZnS QDs donor and [+] rhodamine B dye (Rh B) acceptor. Installing a favourable electrostatic interaction turned out to be crucial in achieving ~75 % efficient FRET process from InP/ZnS QDs to Rh B dye, in water. Furthermore, the process of FRET was successfully translated into solid-state as well, which proves their suitability for device level studies. Thus, the bioimaging and FRET studies showcase the potency of water-stable pure-blue emitting InP/ZnS QDs for future biological as well as light harvesting studies.

3.3 Experimental Section

3.3.1 Synthesis of Pure-Blue Emitting InP/ZnS QDs:

The synthesis of pure-blue emitting InP/ZnS QDs was carried out by following a modified one-pot synthetic procedure.[38] In a typical synthesis, indium (III) iodide (0.34 mmol, 169 mg), zinc iodide (2.2 mmol, 703 mg) and olylamine (15 mmol, 5.0 mL) were taken in 100 mL three-neck RB and heated to ~140 ^{0}C under Ar atmosphere with gentle stirring, till a clear solution was formed. The reaction mixture was degassed for ~60 min at 140 ^{0}C and the temperature was raised further to ~200 ^{0}C under inert atmosphere. Upon reaching 200 ^{0}C, 450 µL of tris-(dimethylamino) phosphine (2.47 mmol) in 1.0 mL of olylamine was quickly injected into the reaction mixture and kept for ~20 min for the growth of InP core QDs. An in-situ ZnS shell coating was performed to stabilize the QDs and improve the PL QY.

After 20 min, a solution of zinc and sulphur precursor was quickly injected into the reaction mixture at ~200 ^{0}C, which contained 2.7 mmol of DDT (~645 µL) and 1.0 mmol of zinc stearate in 4 mL ODE. Then the reaction temperature was raised to ~300 ^{0}C and allowed to react for ~45 min. At the end, the reaction mixture was quenched with water bath followed by addition of 5.0 mL hexane to arrest the growth of ZnS Shell. The obtained QD solution was centrifuged at 7000 rpm for 10 min to remove excess indium and zinc precursor. The resultant supernatant was purified by precipitating with ethanol and redispersed back in chloroform, and used for the further studies. The combination of DDT and zinc stearate was crucial in getting fine-control over the thickness of ZnS shell.

#Tips and Tricks to the Underlying Synthesis Protocol:

In our protocol, a fine control over the shell growth and thickness led to the formation of high-quality pure-blue emitting InP/ZnS QDs. In general, the InP core is overcoated with a ZnS shell

via hot-injection techniques. Important point to be mentioned here is that the high temperature crystallization process continues even during the cooling process.[39] With this thought in mind, instead of cooling the reaction system after the successful formation of InP core, a quick and direct injection of Zn- and S-precursors was done at high temperature and inert atmosphere. As mentioned in the above typical procedure, after the successful synthesis of InP core at 200 ^{0}C, Zn-precursor dissolved in octadecene (ODE) and dodecanethiol (DDT, S-precursor) was added to the reaction mixture. Then, the reaction temperature was increased to 300 ^{0}C and allowed to react for 45 min. Here, an optimized Zn- and S-precursor amount provides a fine control over the thickness of the ZnS shell. This allowed us to restrict the growth of the ZnS shell to ~3 monolayers. The consequence of having a small InP core size and a thin ZnS shell is as follows. The energy difference between small InP core and ZnS shell is not significant enough to form a typical type-I core-shell QDs. Instead, they form a quasi-type-II core-shell QDs.[40] As the shell thickness is less, the excitons will be mainly confined within the InP core.[40-41] As a result, the PL QY will be high, and the PL maxima will be centered around the band edge emission of the core QDs (~462 nm in the present study). Otherwise, a thicker shell will lead to the delocalization of the electron wave function to the shell, which compromises the photophysical properties of the QDs.

For energy transfer studies, the as-synthesized blue emitting InP/ZnS QD was ligand exchanged [-] MUA ligand, by following the place exchange protocol as described in **Chapter–2**. The negatively charged water dispersed [-] B-InP/ZnS QD is abbreviated as [-] B-QD, throughout the thesis.

3.3.2 Resonance Energy Transfer Studies between Pure-Blue Emitting InP/ZnS QD and Rhodamine B Dye:

The energy transfer experiments were performed with [-] B-QD and Rh B dye in water. In a typical energy transfer experiment, a 2.7 mL aqueous solution of donor [-] B-QDs was prepared with an absorbance of ~0.1 at the first excitonic peak (~410 nm), corresponding to ~4 μM of QD concentration. Next, different aliquots of acceptor Rh B dye (3 μL of ~700 μM) were sequentially added to donor [-] B-QD, and the spectral changes were monitored using Shimadzu UV-3600 Plus absorption spectrophotometer and Fluorolog-3 spectrofluorometer (HORIBA Scientific) under 370 nm excitation. The corresponding lifetime experiments were carried out in a HORIBA DeltaFlex Time-Correlated Single Photon Counting system using a

370 nm Delta-Diode source. The fluorescence decay was deconvoluted using EZ software, and fit with exponential decay, minimizing the χ^2 values.

3.3.3 Instrument and Techniques:

Details of all other experimental methods, instrumental techniques, and formalism for the Förster resonance energy transfer (FRET) process were already discussed in **Chapter -2**

3.4 Results and Discussion

3.4.1 Synthesis and Characterization of Pure-Blue Emitting InP/ZnS QDs:

One of the main challenges in the preparation of stable blue-emitting InP/ZnS QDs was controlling the growth kinetics of the core as well as the shell. In literature, the control over the growth kinetics of the InP core has been achieved by the appropriate choice of metal-ion precursors in combination with aminophosphine.[14,31,42] For instance, the emission of InP/ZnS QDs shifts from red to green to blue regions, by changing the halide salts of In and Zn precursors from chloride to bromide to iodide, respectively.[14] Likewise, the moderate disproportionation reaction of aminophosphine controls the speed of the reaction, and thus, the emission colour of InP QDs.[42] By adopting this approach, stable blue-emitting InP/ZnS/ZnS QDs (λ_{em} ~475 nm) have already been prepared by Sun and co-workers.[34] Our first attempt was to use these blue-emitting InP/ZnS/ZnS QDs as a model system for energy transfer studies with appropriate acceptor molecules. However, the thick double ZnS shell (~8 monolayers) prevented any photophysical interaction between the blue-emitting InP core and the acceptor molecules. Consequently, our efforts were to fine-tune the kinetics of shell growth to generate a thin layer of ZnS around the blue-emitting InP core. Decreasing the reaction temperature and time of the shell formation failed to reduce the shell thickness, and the emission was still centered around 475 nm (even non-uniform shell growth was observed in some cases). Next, the ratio of Zn:S precursors were optimized to obtain a thin shell of ZnS (~3 monolayers), which allowed the InP core to participate in an efficient FRET process with rhodamine B acceptor (*vide infra*). Along with reducing the shell thickness, the optimization of Zn:S precursors resulted in lowering the emission maxima of the InP/ZnS QDs to the pure-blue region (~462 nm). To the best of our knowledge, this is the shortest wavelength reported so far for environmentally friendly blue-emitting InP/ZnS QDs in water.

The as-synthesized InP/ZnS QDs exhibited a sharp first excitonic peak at ~410 nm with a peak-to-valley ratio of 1.45, indicating a high degree of size homogeneity (**Figure 3.4a).**[22] The PL of InP/ZnS QDs was centered around the pure-blue region (~462 nm) in chloroform, with a colour purity of ~80 % (CIE 0.16,0.15) and a full-width half-maxima of ~58 nm (**Figures 3.4a,b**). The absolute PL QY of InP/ZnS QDs was estimated to be ~0.6 in chloroform, which is significant for this class of blue-emitting QDs (inset of **Figure 3.4a**). Now, it is essential to disperse these blue-emitting QDs in aqueous medium to expand their scope beyond organic medium. However, it is often difficult to retain the excellent PL properties of QDs in aqueous medium, especially for blue-emitting QDs. In this regard, a place exchange protocol was developed to replace olylamine ligands on blue-emitting InP/ZnS QDs with 11-mercaptoundecanoic acid ([-], MUA) (**Scheme 3.1**).[18,43] The transfer of the blue PL from the chloroform to the aqueous phase indicates the successful dispersion of QDs in water (**Scheme 3.1**). Zeta potential studies revealed that the surface of the QDs is negatively charged (-45.8 ± 1.8 mV), which confirms the success of the place exchange reaction (**Figure 3.5a**). The presence of MUA ligands on the surface of blue-emitting InP/ZnS QDs was further confirmed using standard analytical techniques (**Figure 3.6**). The thiol groups in MUA ligands bind on the surface of ZnS shell, whereas the terminal carboxylate groups provide the much-needed dispersion in aqueous medium.

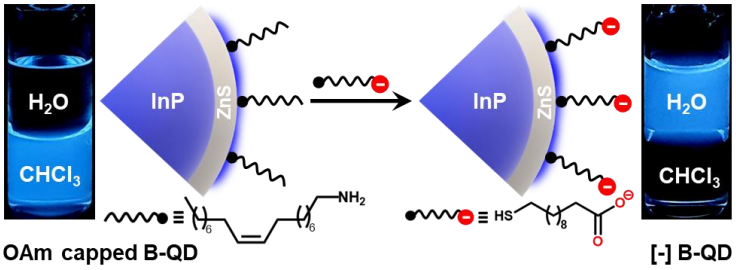

Scheme 3.1 Schematic representation of the ligand exchange process, along with the optical photographs showing the transfer of pure-blue emitting InP/ZnS QDs from the chloroform to the aqueous layer.

All the photophysical properties of pure-blue emitting InP/ZnS QDs were well-retained even after the place exchange reaction (**Figures 3.4a,c** and **Table 3.1**). The multiexponential PL decay of blue-emitting InP/ZnS QDs was preserved in the aqueous medium, with an average lifetime of ~212 ns (**Figure 3.4c** and **Table 3.1**). Importantly, the absolute PL QY was estimated to be 0.47 ± 0.2 in water for blue-emitting [-] B-QDs (~85 % retention) (inset of **Figure 3.4a**).

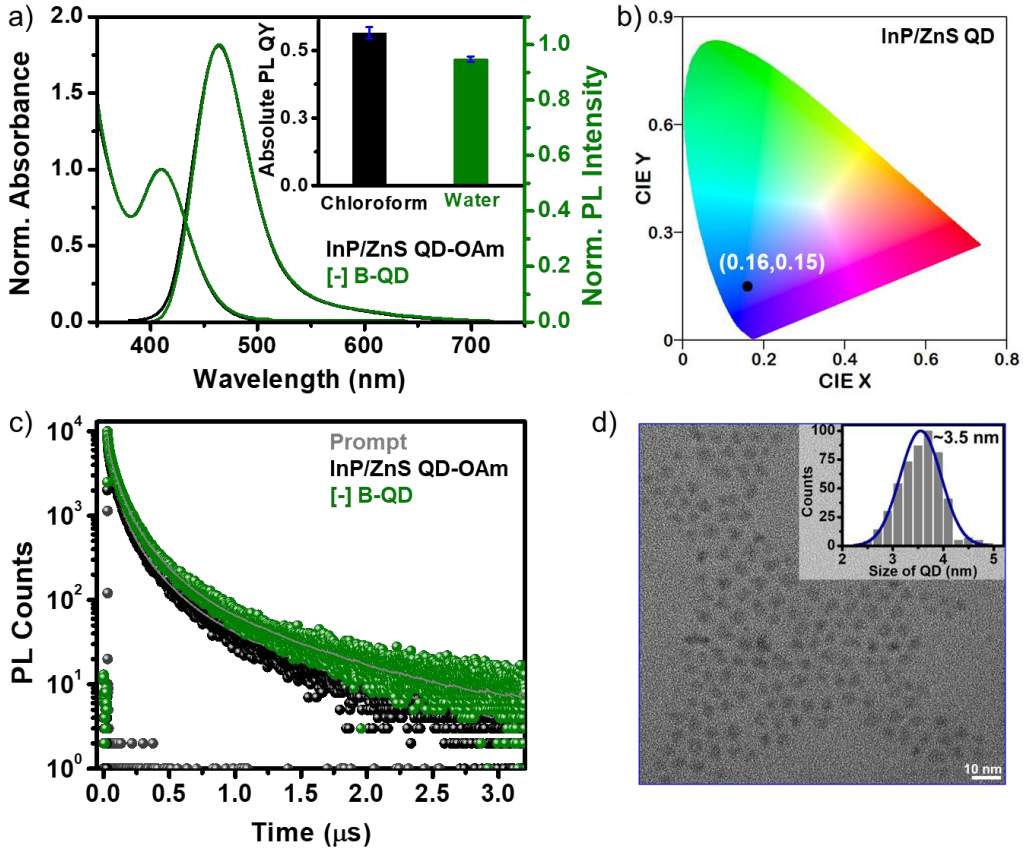

Figure 3.4 Spectroscopic and microscopic characterization of pure-blue emitting InP/ZnS QDs. (a) The normalized UV-vis absorption and PL spectra of InP/ZnS QDs before (black) and after (olive) ligand exchange with [-] MUA ligands. The corresponding absolute PL QY_A data shown in the inset prove ~85% retention of PL in water. (b) The CIE 1931 plot for pure-blue emitting InP/ZnS QD. The corresponding fluorescence spectra to CIE axis point was estimated to be (0.16,0.15). The complete PL spectrum of pure-blue emitting InP/ZnS QD was used to generate the coordinate in CIE spectrum. The measured colour purity was ~80 %. (c) The PL decay profiles of InP/ZnS QDs before (black) and after (olive) place exchange with [-] MUA ligands. (d) A representative TEM image of [-] B-QDs. The corresponding size distribution histogram (from ~500 QDs) is shown in the inset.

Table 3.1 PL decay analysis of pure-blue emitting InP/ZnS QDs before and after surface functionalization with MUA ligands, in a time window of 3.2 μs.

System	τ_1 (ns)	α_1	τ_2 (ns)	α_2	τ_3 (ns)	α_3	τ_4 (ns)	α_4	$\tau_{avg.}$ (ns)	χ^2
InP/ZnS-OAm	4.21	0.47	46.46	0.37	143.61	0.14	585.15	0.02	206.80	1.14
	f_1 = 0.04		f_2 = 0.34		f_3 = 0.39		f_4 = 0.23			
[-] InP/ZnS-MUA	8.98	0.46	58.42	0.37	167.09	0.15	629.70	0.02	211.63	1.12
	f_1 = 0.06		f_2 = 0.34		f_3 = 0.39		f_4 = 0.21			

The photostability experiment shows that the PL of [-] B-QD blue-emitter was preserved for at least ~10 h under continuous illumination with a 365 nm xenon lamp (the power measured at the cuvette wall was ~6.2 mW/cm^2) (**Figure 3.5b**). Thus, the phase transfer, IR, and NMR

studies confirm the successful ligand exchange of OAm with MUA ligands on the surface of pure-blue emitting InP/ZnS QDs (**Figures 3.6**). High-resolution transmission electron microscopy (HRTEM) studies confirm the formation of uniform sized [-] B-QDs having an average diameter of 3.5 ± 0.4 nm (**Figures 3.4d** and **A3.1**). Further, the powder X-ray diffraction (PXRD) studies confirm the zinc blend phase for the InP core (**Figure A3.2**).[21] A large shift in the diffraction peaks toward the ZnS planes was observed for the core/shell [-] InP/ZnS QDs. The shell thickness was determined to be ~0.85 nm (~3 monolayers) (See the detailed discussion in **Appendix Section**). The average diameter of the blue-emitting [-] B-QDs was estimated to be 3.5 ± 0.2 nm from PXRD study, which corroborates well with the TEM data. The elemental analyses from X-ray photoelectron spectroscopy (XPS) and energy dispersive X-ray spectroscopy (EDAX) confirm the presence of all the major elements in [-] B-QDs **(Figures A3.3-A3.4**). The valence and conduction band positions of [-] B-QDs were estimated to be at -6.33 eV and -3.63 eV (vs vacuum), respectively, with the combination of cyclic voltammetry and absorption studies (**Figure A3.5**). These values are in good agreement with literature reports on sky-blue emitting InP/ZnS/ZnS QD.[31] It is worth mentioning that the molar extinction coefficient (ε) for small InP/ZnS QDs are not available in the literature. In the present study, the ε of pure-blue emitting [-] InP/ZnS QDs was estimated to be ~2.5 x 10^4 $M^{-1}cm^{-1}$, from the combination of inductively coupled plasma- mass spectroscopy (ICP-MS), PXRD, and UV-vis absorption spectroscopy (details are provided in **Appendix Section**). In literature, the ε of InP magic-sized clusters at the first excitonic peak ~390 nm is reported to be ~2.8 x 10^4 $M^{-1}cm^{-1}$.[44] Thus, the ε of pure-blue emitting [-] InP/ZnS QDs is within the range of small sized InP QDs.

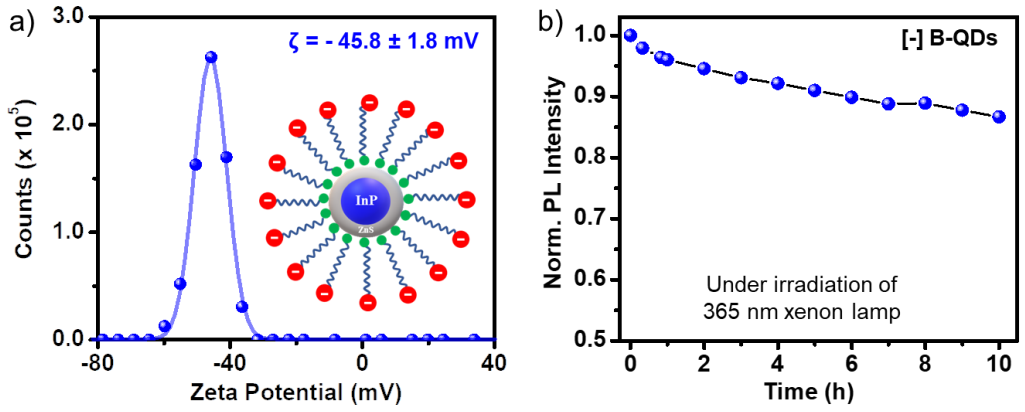

Figure 3.5 (a) Representative zeta potential (ζ) plot of [-] B-QDs. The error in ζ value was estimated from three different measurements on three different samples. (b) A plot showing the long-term PL stability of [-] B-QDs, under continuous irradiation with ~365 nm UV light for ~10 h (the power measured at the cuvette wall was ~6.2 mW/cm^2).

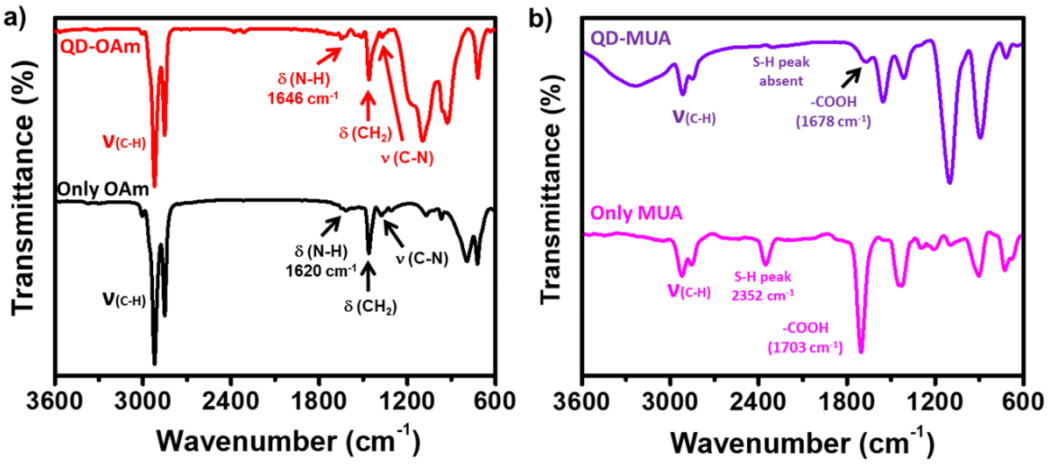

Figure 3.6 FTIR spectra of (a) OAm ligand (black) and OAm capped InP/ZnS QD (red), (b) [-] MUA ligand (magenta) and [-] B-QD (violet).

The photophysical properties of QD depend on the quality of the crystals formed, which is governed by the kinetics of nucleation and crystallization growth processes. In the present study, the less reactive aminophosphine and weak In/Zn-I bond strength led to the balance between the nucleation and growth rates.[31,42] As a result, the size of the core InP QD was controlled below 2 nm. Further, a fine control over the shell growth and thickness was achieved, which led to the unusually high photophysical performance of blue-emitting InP/ZnS QDs. This was achieved by optimizing the amount of Zn- and S-precursors and growing the ZnS shell at a high temperature (details are provided in **Chapter 2**). The consequence of having a small InP core size and a thin ZnS shell is as follows. The energy difference between small InP core (~1.8 nm) and ZnS shell is not significant enough to form a typical type-I core-shell QDs. Instead, they form a quasi-type-II core-shell QDs.[34] As the shell thickness is less, the excitons will be mainly confined within the InP core.[34,44] As a result, the PL QY will be high, and the PL maxima will be centered around the band edge emission of the core QDs (~462 nm in the present study). A thicker shell will lead to the delocalization of the electron wave function to the shell, which compromises the photophysical properties of the QDs.[44] Furthermore, the uniformity in the ZnS shell and the robust nature of the core-shell QD allowed for the transfer of blue-emitting InP/ZnS QDs to aqueous medium (via place exchange reaction), without compromise in their photophysical properties.

Thus, the blue-emitting InP/ZnS QDs exhibit all the fundamental characteristics that a QD should possess for studying the applied properties. Accordingly, the InP QD based pure-blue emitters were used in multicolour bioimaging and resonance energy transfer studies, as

representative examples, to prove their potency for future biological and light harvesting applications.

3.4.2. Biocompatibility and Cellular Bioimaging Studies:

First, the compatibility of blue-emitting [-] B-QDs as bioimaging agents was tested. The colloidal stability as well as the PL of [-] B-QDs was well-retained in buffer and biological media for a long time (~30 h) (**Figure 3.7**). Next, the cytotoxicity of [-] B-QDs was tested in HeLa cell lines using the MTT assay.[18] Up to ~95 % cell viability was exhibited by [-] B-QDs till ~120 µg/mL concentration (~2 µM), beyond which a mild toxicity was observed (~75 % cell viability at ~300 µg/mL) (**Figures 3.7** and **3.8a**). It can be concluded that the blue-emitting [-] B-QDs are less cytotoxic compared to the traditional Cd based QDs.[18] The less toxic metal ions and anionic charges displayed on the surface of the QDs prevent their unwarranted interactions with a multitude of cytosolic proteins and other biomolecules inside the cells, thereby preserving the cellular viability. Inspired by the excellent cell viability data, detailed imaging experiments were then carried out. As seen in **Figure A3.6**, the PL signals emanating from the cells intensified as the concentration of [-] B-QD blue-emitter was increased.

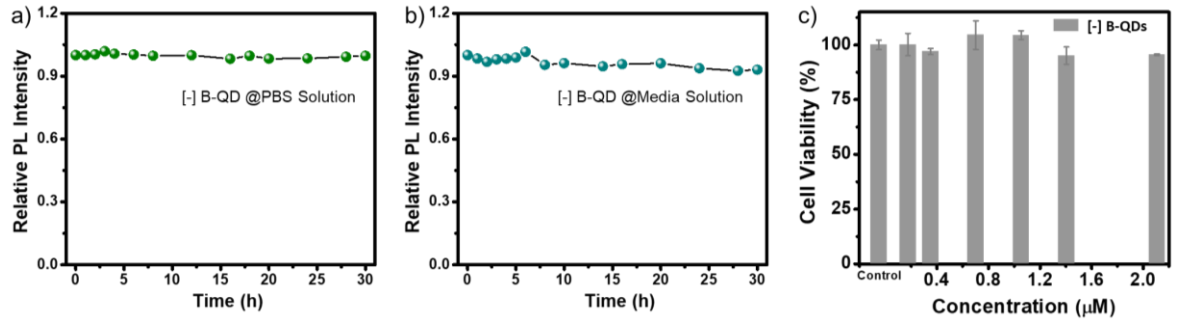

Figure 3.7 The plots showing the PL stability of [-] B-QDs in (a) PBS buffer and (b) biological media solution (5 % FBS in media solution). (c) MTT assay with [-] B-QDs, showed ~95 % viability of HeLa cell with 120 µg/mL QD (~2.1 µM).

The observed images were then quantified, and the resultant corrected total cell fluorescence (CTCF) values were coherent with the physical inspection (**Figures 3.8b** and **A3.6**). The narrow absorption and emission features of blue-emitting [-] B-QDs motivated us to check their compatibility with other commercially available fluorophores. For this, the cells were treated with blue-emitting [-] B-QDs for a period of 6 h, followed by the sequential staining of the nuclei as well as the actin and filaments with commercially available SYTO-dye and phalloidin green (PHD), respectively. The cells were visualized using a Zeiss confocal

microscopy under simultaneous excitations with 3 different laser sources (405 nm, 488 nm, and 633 nm). The QDs and the commercial markers fluoresce individually at their respective excitation wavelengths. The presence of QDs did not interfere with the fluorescence signals of the other two dyes (**Figure 3.8c**). Thus, the blue-emitting [-] B-QDs displayed excellent multicolour bioimaging abilities, which is essential for any optical probes in cellular imaging studies.

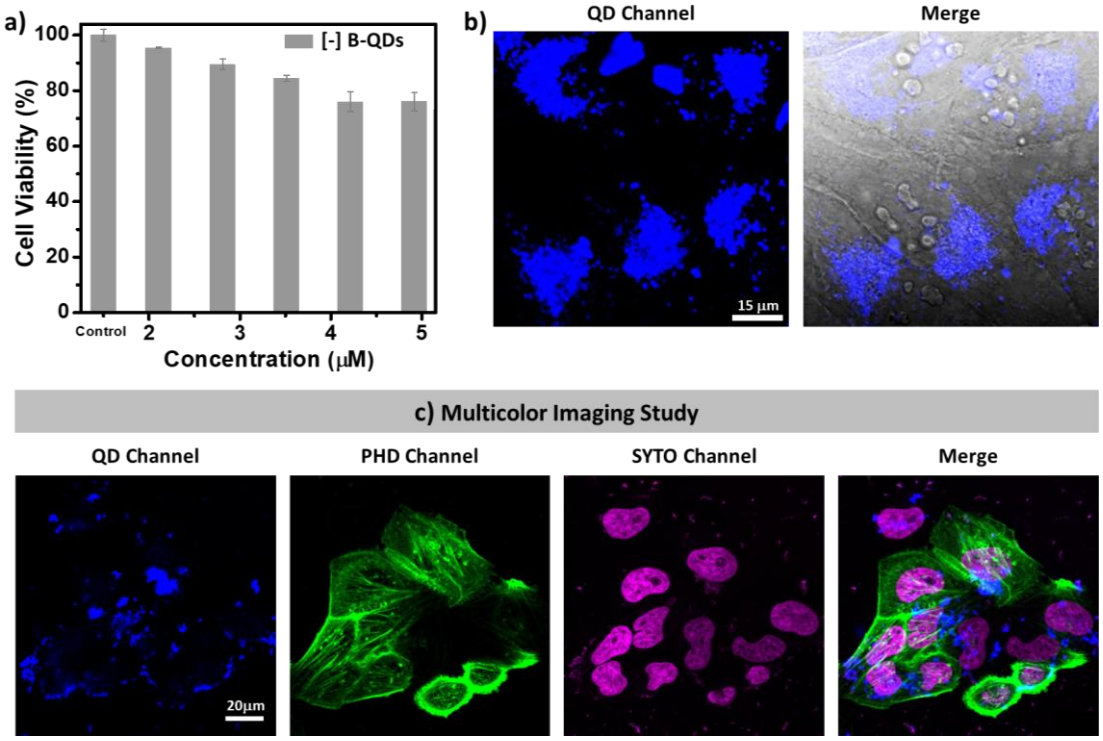

Figure 3.8 Biocompatibility and bioimaging studies with pure-blue emitting [-] B-QDs. (a) MTT assay showing the viability of HeLa cells incubated with different concentrations of [-] B-QDs for ~72 h (higher concentration region). (b) Representative confocal images of HeLa cells recorded, after internalizing with 0.70 μM [-] B-QDs for ~7 h. (c) Multicolor imaging of pure-blue emitting [-] B-QDs with PHD and SYTO-Deep Red commercial dyes.

3.4.3 Light Induced Resonance Energy Transfer Studies:

3.4.3.1. Steady-State Experiments

The stable and high PL quantum yield of the blue-emitting [-] B-QDs motivated us to test their suitability for light harvesting studies as well. The light induced Förster resonance energy transfer (FRET) process was selected as the case study, because of its wide applicability in biology and energy research.[46-55] It is worth mentioning that most of the QD based FRET studies that have been reported so far in water, are with QDs emitting in the green or higher

wavelength regions.[13,18-20,56] Thus, the suitability of [-] B-QDs to participate as an efficient FRET donor was studied in the present work, in view of expanding the spectrum of environmentally friendly QDs towards the blue-region in energy transfer studies. Rhodamine B (Rh B) having emission in the red region (575–625 nm) was chosen as the energy acceptor, to test the suitability of blue-emitting [-] B-QDs in participating wide-range FRET process (**Figure 3.9a**). A large spectral overlap integral value of ~8 x 10^{14} $M^{-1}cm^{-1}nm^4$ indicates that the pure-blue emitting [-] B-QDs and Rh B dye form a good donor-acceptor pair for FRET studies (details are provided in the **Appendix Section**).[46] Moreover, the presence of a permanent positive charge on Rh B (because of the quaternary ammonium group) will ensure a strong electrostatic attraction with [-] B-QDs, which will be crucial in realizing an efficient FRET process. In a typical PL quenching study, different aliquots of Rh B acceptor dye (3 µL each from ~700 µM stock solution) were added to ~4 µM of blue-emitting [-] B-QDs (the optical density at the first excitonic peak was fixed at ~0.1). The corresponding spectral changes were monitored through steady-state and time-resolved spectroscopic techniques (**Figures 3.9** and **A3.7**). The [-] B-QD:::Rh B complex was excited at 370 nm, in order to achieve the selective excitation of the QD donor (Rh B has negligible absorption at ~370 nm). Upon successive additions of the Rh B dye, a gradual decrease in the PL of blue-emitting [-] B-QD was observed, along with a concomitant increase in the emission corresponding to the Rh B dye (λ_{max} ~575 nm) (**Figure 3.9b**). The PL quenching efficiency was estimated to be ~92 % from steady-state studies ($E = 1 - I/I_0$, where I and I_0 are the PL intensities of QDs in presence and absence of acceptor, respectively).[46] The non-linear Stern-Volmer (SV) plot, with upward-exponential curvature, indicates the involvement of both static and dynamic components in the PL quenching mechanism (inset of **Figure 3.9b**). This upward-exponential variation in PL quenching can be treated within the framework of Perrin formalism,[46,47] where the logarithm of the relative PL of the donor shows a linear variation with acceptor concentration (**Figure 3.10**). The quenching volume and radius for [-] B-QD::: Rh B dye donor-acceptor system was estimated to be ~6.62 x 10^{-16} cm^3 and ~54.1 nm, respectively (**Figure 3.10**). This essentially means that any acceptor molecule in this quenching volume can diffuse close to the surface of the QD donor and participate in an efficient FRET process within the lifetime of the donor. This large value for the quenching volume can be attributed to the presence of strong electrostatic interaction in the [-] B-QD:::Rh B dye donor-acceptor system (*vide infra*). The relative PL of donor and acceptor, as well as the PL quenching efficiency were saturated after the addition of ~6.5 µM of Rh B dye (**Figure 3.9c**). The emission intensity of the only Rh B dye (~7.5 µM) under direct excitation at 370 nm was much lower than that in the [-] B-QD:::Rh

B complex (red and orange traces, respectively in **Figure 3.9b**), confirming the transfer of energy from the QD donor to the Rh B acceptor.

In another set of studies, the reverse addition experiments were performed to rule out the interference from the direct excitation of Rh B dye acceptors. Here, the PL of the acceptor Rh B dye (~7.5 µM) was monitored upon successive addition of the donor QDs (4 µL each of ~418 µM QD). A steady increase in the PL of Rh B dye was observed (~4.5 times, $I/I_0 = 4.5$) in presence of ~6 µM of [-] B-QDs (**Figure 3.9d**), which further confirms an efficient energy transfer process from QDs to Rh B dye. Likewise, detailed excitation spectroscopy studies reaffirm the involvement of an efficient energy transfer process in [-] B-QD:::Rh B dye donor-acceptor system (**Figure 3.11**). A high efficiency in the energy transfer process (~92 %) proves a strong interaction between the blue-emitting [-] B-QD and Rh B dye. The presence of opposite charges on both [-] B-QD and Rh B point towards the involvement of electrostatic attraction in achieving an efficient PL quenching in [-] B-QD:::Rh B dye donor-acceptor system.

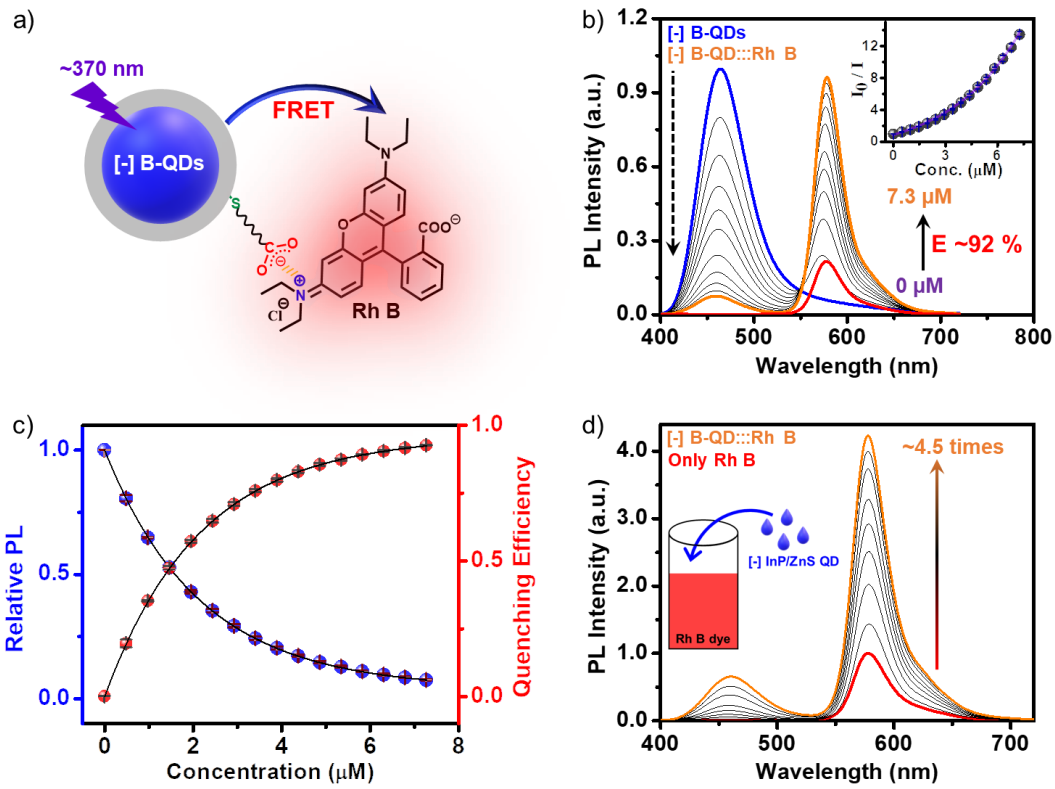

Figure 3.9 Steady-state FRET studies in [-] B-QD:::Rh B donor-acceptor system. (a) Schematic representation of electrostatically driven FRET process from pure-blue emitting [-] B-QDs donor to Rh B acceptor dye. (b) The PL spectral changes in [-] InP/ZnS QDs upon addition of varying concentrations of Rh B dye. The inset shows the corresponding Stern-Volmer plot. (c) A saturation in both the relative PL intensity of donor [-] B-QDs and the quenching efficiency was observed after ~6.5 µM addition of

acceptor Rh B dye. (d) Reverse addition experiment: A steady enhancement in the PL of ~7.5. µM acceptor Rh B dye was observed, upon addition of varying concentrations of [-] B-QDs donor. Excitation wavelength was 370 nm in all these studies.

Accordingly, PL quenching experiments were performed in buffer to weaken the electrostatic interactions in [-] B-QD:::Rh B dye donor-acceptor system.[57-58] An increase in the ionic strength of the medium will weaken the electrostatic interaction due to the screening of charges on both the donor and the acceptor.[58] As predicted, the PL enhancement for acceptor Rh B dye showed a substantial decrease from 5.5 to 3.4 times, as the ionic strength of the medium was increased from 0.05 mM (basic water, pH ~10) to 0.85 M (5X PBS) (**Figure A3.8** in the **Appendix Section**). This confirms an electrostatically driven energy transfer from the InP/ZnS QD donor to the Rh B dye acceptor.

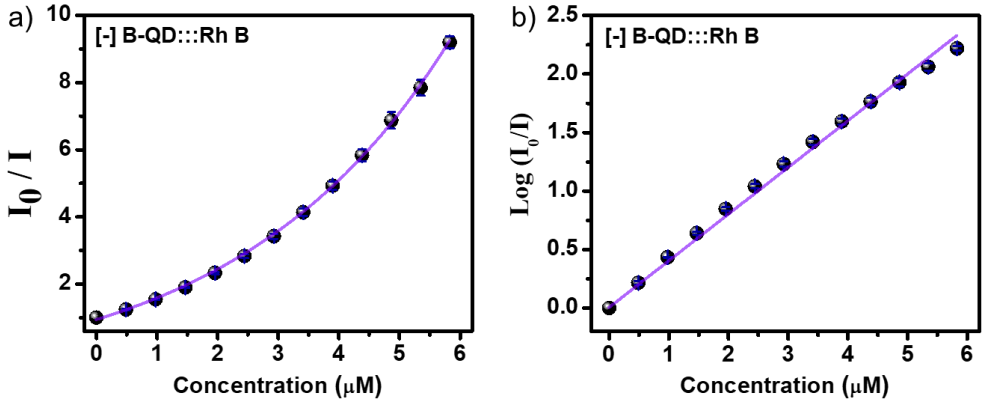

Figure 3.10 Stern-Volmer analysis treated within the framework of Perrin formalism. (a) Relative PL intensity (I_0/I) of [-] B-QD as a function of Rh B concentration. (b) The plot for log(I_0/I) *vs* concertation of acceptor Rh B dye.

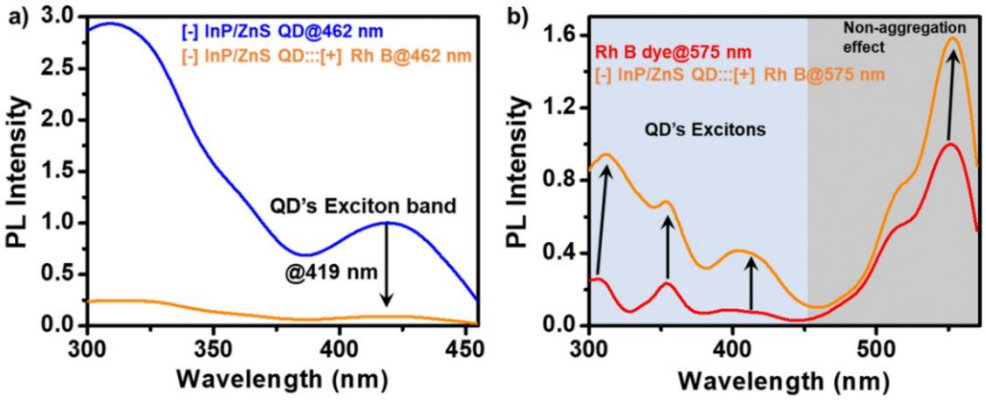

Figure 3.11 PLE study for [-] InP/ZnS QD:::Rh B dye complex in water. (a) The excitation spectra of donor [-] InP/ZnS QD in presence (orange) and absence (blue) of acceptor Rh B dye, collected at 462 nm (emission wavelength of donor QD). (b) The excitation spectra of Rh B dye in presence (orange) and absence (red) of donor [-] InP/ZnS QD, collected at 575 nm (emission wavelength of acceptor Rh

B dye). The PL intensity collected at the donor emission wavelength (~462 nm) in [-] InP/ZnS QD:::Rh B dye donor-acceptor system was lower in the region of QD exciton and lower wavelengths, compared to only [-] InP/ZnS QD. However, the PL intensity collected at the acceptor emission wavelength (~575 nm) showed an enhancement at the QD exciton band in [-] InP/ZnS QD:::Rh B complex, compared to only Rh B dye. This confirms that the light absorbed by the QD donor is transferring to the Rh B dye acceptor, resulting in the enhanced emission from the acceptor.

3.4.3.2. Time-Resolved Experiments

Detailed time-resolved PL decay kinetic studies were carried out to confirm the energy transfer process in electrostatically bounded [-] B-QD:::Rh B dye donor-acceptor system. A clear quenching in the average PL lifetime of the donor QD was observed in the presence of acceptor Rh B dyes (from ~212 ns to ~61 ns), with the quenching efficiency estimated to be ~73 % ($E = 1 - \tau/\tau_0$, where τ and τ_0 are the average lifetimes of QDs in presence and absence of Rh B dye, respectively) (**Figure 3.12a** and **Table 3.2**).[46] Stern-Volmer plot constructed from the time-resolved PL data showed a non-linear variation of the relative QD donor lifetime as a function of acceptor concentration (**Figure 3.12b** and **Table A3.1**). The non-linear nature of the SV plot suggests the involvement of factors beyond the normal diffusional or collisional quenching process. Accordingly, the relative PL lifetime data was analysed with other models to explain the non-linear Stern-Volmer plot. The variation in the relative QD donor lifetime fit well with the model of distance-dependent quenching (DDQ) (**Figure A3.9**).[58] The bimolecular quenching constant was estimated to be ~1.24 x 10^{12} $M^{-1}s^{-1}$ using the DDQ model, which is higher than the typical diffusion-only controlled quenching process (~10^{10} $M^{-1}s^{-1}$). Detailed analysis of the DDQ model prove the involvement of a distance-dependent quenching, and formation of multiple layers of Rh B dye acceptors around the [-] B-QD donor. The presence of both positive and negative charges on Rh B dye can be the driving force for the formation of multi-layer arrangement of the dyes around the QD (**Figures A3.9b,c**). A negligible change in the negative zeta potential of [-] B-QD:::Rh B dye complex at different donor-acceptor ratios supports the formation of multiple layers of the acceptor dyes (**Figure A3.10** in the **Appendix Section**).

The ultimate proof for the FRET in [-] B-QD:::Rh B dye donor-acceptor system was obtained from the temperature dependent PL lifetime studies. Typically, the PL lifetime increases upon decreasing the temperature, since the non-radiative recombination channels will be inhibited because of the suppression of phonon vibrations.[59] On the other hand, FRET is a non-radiative process which will be independent of the temperature, at a given donor-acceptor distance.[56,59] Thus, performing temperature dependent PL lifetime studies is a common practice

to confirm the process of FRET in a donor-acceptor system.[59,62] In the present study as well, a linear increase was observed in the individual PL lifetime of [-] B-QD donor and [-] B-QD:::Rh B complex as the temperature was lowered (**Figure A3.11**). Whereas, negligible changes were observed in the efficiency of PL lifetime quenching as a function of temperature, which confirms the prominent involvement of non-radiative resonance energy transfer process in the PL quenching of [-] B-QD by Rh B dye (**Figure 3.12c** and **A3.12**, and, **Table A3.2**). Accordingly, different energy transfer parameters were calculated for the [-] B-QD:::Rh B dye donor-acceptor system using the FRET formalism, as summarized in **Figure 3.12d** (details of each parameter calculation are given in **Chapter 2**).

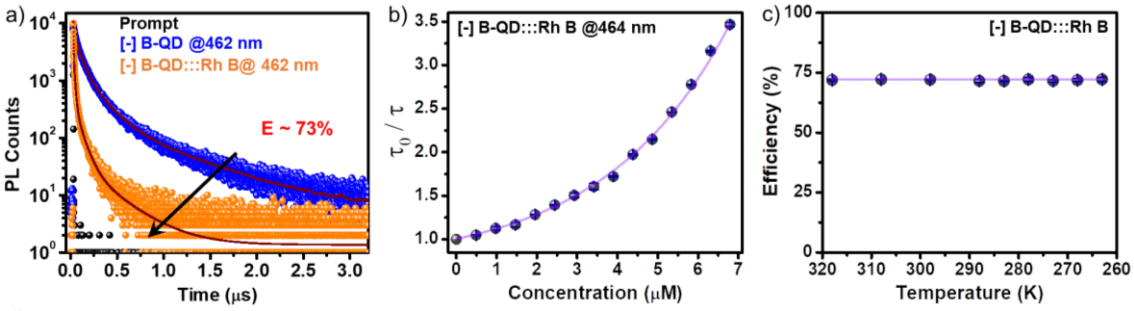

d)

Nanohybrid System	J(λ) $M^{-1}cm^{-1}nm^4$	R_0 (Å)	E (%)	$k_T(r)$ (s^{-1})	V (cm^3)	r_q (nm)	K_a ($M^{-1}s^{-1}$)
[-] B-QD:::[+] Rh B	~7.95 x 10^{14}	90	~75	~1.21 x 10^7	~6.62 x 10^{-16}	54.1	~1.24 x 10^{12}

Figure 3.12 Time-resolved FRET studies in [-] B-QD:::Rh B dye donor-acceptor system. (a) PL decay profiles of [-] B-QDs in presence (orange) and absence (blue) of ~7.5 μM Rh B dye (excitation wavelength was 370 nm). (b) The corresponding Stern-Volmer plot based on relative PL lifetime values of [-] B-QD. (c) A plot of FRET efficiency (estimated from lifetime quenching) *vs* temperature. Negligible effect of temperature on the FRET efficiency confirms the process of resonance energy transfer in [-] B-QD:::Rh B dye donor-acceptor system. (d) Table summarizing various quenching parameters estimated based on FRET formalism: the spectral overlap integral [J(λ)]; Förster radius (R_0); FRET efficiency (E); rate of energy transfer (k_T); quenching volume (V); quenching radius (r_q), and bimolecular quenching constant (k_a).

Table 3.2 PL decay analysis of pure-blue emitting [-] B-QDs and [-] B-QD:::Rh B dye complex, in a time window of 3.2 μs.

System	τ_1 (ns)	α_1	τ_2 (ns)	α_2	τ_3 (ns)	α_3	τ_4 (ns)	α_4	$\tau_{avg.}$ (ns)	χ^2
[-] B-QDs	8.98	0.46	58.42	0.37	167.09	0.15	629.70	0.02	211.63	1.12
[-] B-QD:::Rh B	2.13	0.74	10.40	0.21	47.55	0.04	184.32	0.01	60.80	1.24

3.4.3.3. FRET in Solid State

Demonstration of the FRET process in solid-state is essential to prove the suitability of pure-blue emitting InP/ZnS QDs for device level applications, such as in full-color display and photovoltaic devices. As a result, FRET studies were performed by preparing thin films of donor, acceptor, and donor-acceptor complex in agarose. The pure-blue PL of the [-] B-QDs was well-retained in the agarose film prepared with the only donor, overruling the inter-QD energy transfer in the system (**Figure 3.13**). On the contrary, the PL of the agarose film containing only the Rh B dye was completely quenched because of the inter-molecular aggregation (aggregation induced quenching). Interestingly, the PL of the Rh B dye was dominating in the agarose film prepared from a mixture of [-] B-QD + Rh B dye (inset of **Figure 3.14a**). Steady-state and time-resolved PL studies confirm an efficient FRET process in [-] B-QD:::Rh B dye donor-acceptor system in agarose film as well (**Figure 3.14a,b**). For instance, the PL lifetime of the [-] B-QD decreased from ~217 ns to ~5 ns (~98 %) in the presence of Rh B dye in the agarose film (**Table 3.3**). The electrostatic assembly between [-] B-QDs and Rh B dye prevents the dye from undergoing aggregation within themselves, thereby preserving the process of FRET in agarose film.

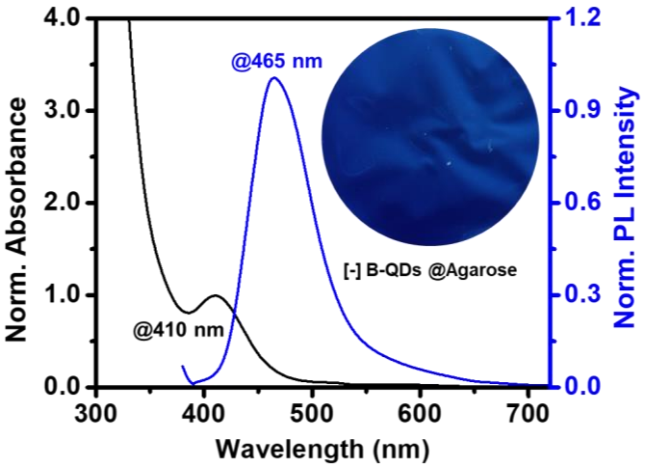

Figure 3.13 Characterization of [-] B-QDs in agarose film. Normalized absorption and PL spectra of [-] B-QDs in agarose film (1%, w/v).

Finally, a temporal evolution of the FRET process was visualized via the droplet-evaporation method. In a typical experiment, droplets (~10 µL) of different donor: acceptor (D:A) ratios were placed on a Teflon-coated glass slide, and the PL colour of the droplet was monitored in UV-chamber as a function of time/evaporation. At the initial stage, the droplet showed a PL colour corresponding to the mixing of donor and acceptor colours (such as magenta, pink, and

orange corresponding to the D:A of 1:0.3, 1:0.6, and 1:1.3, respectively). As the time proceeds, the drying of the droplet occurs, and the colour of the droplet shift towards the red (corresponding to the Rh B dye) on complete evaporation of water (**Figure 3.14c**). This PL colour change of the droplets can be explained based on Förster formalism.[43] The efficiency of the FRET process is extremely sensitive towards the distance between the donor and the acceptor (E α $1/r^6$, where r is the donor-acceptor distance).[46] In the present study, the evaporation of the droplet decreases the D-A distance, resulting in an increase in the FRET efficiency. This will be accompanied with a temporal colour change towards the PL of the Rh B acceptor, which once again ascertains the involvement of an efficient FRET process in [-] B-QD:::Rh B dye donor-acceptor system.

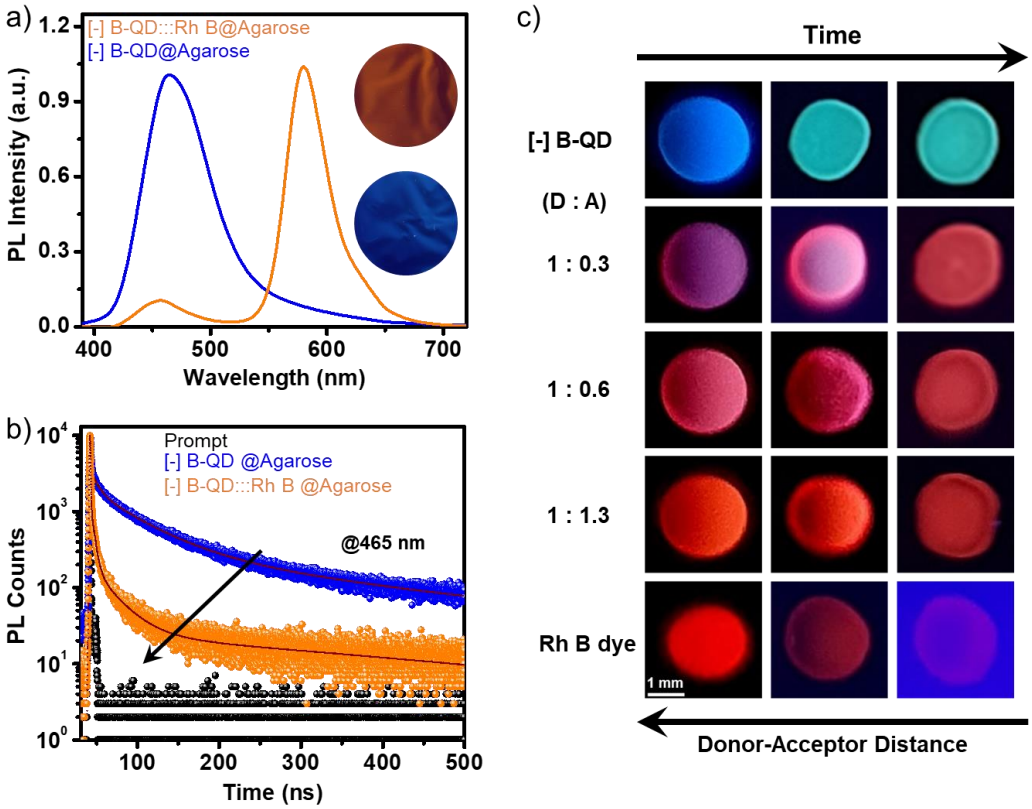

Figure 3.14 FRET studies in solid-state. (a) Steady-state and (b) time-resolved PL of [-] B-QDs in absence (blue) and presence (orange) of Rh B dye, in 1% agarose gel. The inset of (a) shows the true colour PL image of pure-blue emitting [-] B-QDs and [-] B-QD:::Rh B complex agarose film. (c) Temporal evolution of FRET in solid-state: True colour PL images of [-] B-QD (first row), 1:0.3 molar ratio of QD:Dye (second row), 1:0.6 molar ratio of QD:Dye (third row), 1:1.3 molar ratio of QD:Dye (fourth row), and only Rh B dye (fifth row), as a function of drying. The first and the third columns correspond to liquid drop (0 h) and solid film (~12 h), respectively. The donor-acceptor distance decreases as drying proceeds, resulting in an increase in the FRET efficiency. Consequently, the colour of the droplet shifts towards the red region corresponding to the Rh B dye (rows 2-4). First row: The blue PL of the [-] B-QDs shifts towards the cyan colour upon complete drying, indicating inter-QD interactions. Last row: The background of the last image was intentionally changed to blue to improve the visibility of the dried droplet.

Table 3.3 PL decay analysis of pure-blue emitting InP/ZnS QDs and [-] InP/ZnS QD:::Rh B dye complex in agarose film, in a time window of 500 ns.

System	τ_1 (ns)	α_1	τ_2 (ns)	α_2	τ_3 (ns)	α_3	τ_4 (ns)	α_4	$\tau_{avg.}$ (ns)	χ^2
[-] B-QDs	0.70	0.07	8.39	0.08	52.77	0.43	253.27	0.42	216.85	1.15
[-] B-QD:::Rh B	0.21	0.97	2.50	0.02	12.80	0.01	---	---	4.81	1.40

3.5 Conclusions

Our work introduces environmentally friendly InP/ZnS QDs to the family of pure-blue emitting luminescent materials. A fine control over the growth kinetics of the core as well as the shell was crucial in achieving a stable PL in blue-emitting InP/ZnS QDs (PL QY_A ~60 % at 462 nm). The retention of the strong PL of blue-emitting InP/ZnS QDs in the aqueous medium enabled their use in diverse areas including cellular bioimaging and light harvesting. Cytotoxicity and bioimaging experiments showcase the potency of blue-emitting InP/ZnS QDs as optical probes for multicolour cellular imaging studies. As part of light harvesting studies, an efficient FRET process from blue-emitting [-] B-QDs to Rh B dye was demonstrated in water. Detailed steady-state and time-resolved photophysical studies show that the non-linear Stern-Volmer (SV) plots fit well with the Perrin formalism and DDQ model, which further confirms a multi-layer assembly of Rh B acceptor molecules in the quenching radius. The large values of bimolecular quenching constant (~1.24 x 10^{12} $M^{-1}s^{-1}$) and quenching radius (~54 nm) reveal the involvement of electrostatic attraction between the oppositely charged InP/ZnS QDs and Rh B dyes. This turned out to be a crucial factor in achieving an efficient FRET process in blue-emitting [-] B-QD::: Rh B dye donor-acceptor system. The process of FRET was demonstrated in solid state as well, in a temporal fashion, which enhances the prospects of blue-emitting [-] B-QDs for device level applications. The successful demonstration of a FRET process based on blue-emitting InP/ZnS QDs opens various possibilities in energy transfer studies with a wide range of acceptors emitting from the cyan region onwards. A logical extension will be to check the suitability of blue-emitting InP/ZnS QDs in photocatalysis and photovoltaics, to establish them as an efficient light harvester. Looking forward, the blue-emitting InP/ZnS QD developed in this work can potentially be an alternative to the existing luminescent materials for both biological as well as energy applications.

3.6 Future Direction

As the Chapter discusses, the optimized synthesis procedure allows us the stabilize the QDs with thinnest layer of ZnS shell (possible so far). The consequence of having such thin shell, especially for blue InP core resulted in divergence from so called typical type-I architecture of core-shell QDs. Instead, a quasi-type-II core-shell structure was formed because of smaller energy differences (less than 0.2 eV) between the small InP core (~1.8 nm) and thin ZnS shell. This means that the exciton with high energy can effortlessly cross the energy barrier and tunnel out to QDs. This provides opportunities to investigate the exciton dynamics with pure-blue emitting InP/ZnS QDs in water. Furthermore, the model study with [-] B-QD:::Rh B dye donor-acceptor system proves the capabilities of pure-blue emitting InP/ZnS QDs as an efficient FRET donor. Now, the next feat will be to investigate the energy transfer process with more intricate all-QD assembly. Therefore, opportunities to investigate the exciton dynamics, and to create multicomponent donor-acceptor system in an all-QD system could be the future, with the developed blue-emitting InP/ZnS QDs, and this forms the basis of upcoming Chapters.

3.7 References

(1) Nakamura, S. Background Story of the Invention of Efficient InGaN Blue-Light-Emitting Diodes (Nobel Lecture). *Angew. Chem. Int. Ed.* **2015**, *54*, 7770–7788.

(2) Shen, Z.; Burrows, P. E.; Bulović, V.; Forrest, S. R.; Thompson, M. E. Three-Color, Tunable, Organic Light-Emitting Devices. *Science* **1997**, *276*, 2009–2011.

(3) Wang, Y.; Fedin, I.; Zhang, H.; Talapin, D. V. Direct optical lithography of functional inorganic nanomaterials. *Science* **2017**, *357*, 385–388.

(4) Xie, R.; Battaglia, D.; Peng, X. Colloidal InP Nanocrystals as Efficient Emitters Covering Blue to Near-Infrared. *J. Am. Chem. Soc.* **2007**, *129*, 15432–15433.

(5) Wolf, A.; Lesnyak, V.; Gaponik, N.; Eychmüller, A. Quantum–Dot-Based (Aero)gels: Control of the Optical Properties. *J. Phys. Chem. Lett.* **2012**, *3*, 2188–2193.

(6) Brus, L. E. Electron–Electron and Electron–Hole Interactions in Small Semiconductor Crystallites: The Size Dependence of the Lowest Excited Electronic State. *J. Chem. Phys.* **1984**, *80*, 4403–4409.

(7) Vossmeyer, T.; Katsikas, L.; Giersig, M.; Popovic, I. G.; Diesner, K.; Chemseddine, A.; Eychmüller, A.; Weller, H. CdS Nanoclusters: Synthesis, Characterization, Size

Dependent Oscillator Strength, Temperature Shift of the Excitonic Transition Energy, and Reversible Absorbance Shift. *J. Phys. Chem.* **1994**, *98*, 7665–7673.

(8) Medintz, I. L.; Mattoussi, H. Quantum Dot-Based Resonance Energy Transfer and Its Growing Application in Biology. *Phys. Chem. Chem. Phys.* **2009**, *11*, 17–45.

(9) Sarkar, S.; Bose,R.; Jana, S.; Jana, N. R.; Pradhan, N. Doped Semiconductor Nanocrystals and Organic Dyes: An Efficient and Greener FRET System. *J. Phys. Chem. Lett.* **2010**, *1*, 636–640.

(10) Wu, M.; Mukherjee, P.; Lamont, D. N.; Waldeck, D. H. Electron Transfer and Fluorescence Quenching of Nanoparticle Assemblies. *J. Phys. Chem. C* **2010**, *114*, 5751–5759.

(11) Pietryga, J. M.; Park, Y.-S.: Lim, J.; Fidler, A. F.; Bae, W. K.; Brovelli, S.; Klimov, V. I. Spectroscopic and Device Aspects of Nanocrystal Quantum Dots. *Chem. Rev.* **2016**, *116*, 10513–10622.

(12) Chakraborty, I. N.; Roy, P.; Rao, A.; Devatha, G.; Roy, S.; Pillai, P. P. The Unconventional Role of Surface Ligands in Dictating the Light Harvesting Properties of Quantum Dots. *J. Mater. Chem. A* **2021**, *9*, 7422–7457.

(13) Jain, V.; Roy, S.; Roy P.; Pillai, P. P. When Design Meets Function: The Prodigious Role of Surface Ligands in Regulating Nanoparticle Chemistry. *Chem. Mater.* **2022**, *34*, 7579–7597.

(14) Li, L.; Reiss, P. One-Pot Synthesis of Highly Luminescent InP/ZnS Nanocrystals without Precursor Injection. *J. Am. Chem. Soc.* **2008**, *130*, 11588–11589.

(15) Thomas, A.; Nair, P. V.; Thomas, K. G. InP Quantum Dots: An Environmentally Friendly Material with Resonance Energy Transfer Requisites. *J. Phys. Chem. C* **2014**, *118*, 3838–3845.

(16) Tessier, M. D.; Dupont, D.; De Nolf, K.; De Roo, J.; Hens, Z. Economic and Size-Tunable Synthesis of InP/ZnE (E = S, Se) Colloidal Quantum Dots. *Chem. Mater.* **2015**, *27*, 4893–4898.

(17) Gary, D. C.; Terban, M. W.; Billinge, S. J. L.; Cossairt, B. M. Two-Step Nucleation and Growth of InP Quantum Dots via Magic-Sized Cluster Intermediates. *Chem. Mater.* **2015**, *27*, 1432–1441.

(18) Tamang, S.; Lincheneau, C.; Hermans, Y.; Jeong, S.; Reiss, P. Chemistry of InP Nanocrystal Syntheses. *Chem. Mater.* **2016**, *28*, 2491–2506.

(19) Devatha, G.; Roy, S.; Rao, A.; Mallick, A.; Basu, S.; Pillai, P. P. Electrostatically Driven Resonance Energy Transfer in "cationic" Biocompatible Indium Phosphide Quantum Dots. *Chem. Sci.* **2017**, *8*, 3879–3884.

(20) Thirunavukkuarasu, S.; George, A.; Thomas, A.; Thomas, A.; Vijayan, V.; Thomas, K. G. InP Quantum Dots: Probing the Active Domain of Tau Peptide Using Energy Transfer. *J. Phys. Chem. C* **2018**, *122*, 14168–14176.

(21) Devatha, G.; Rao, A.; Roy S.; Pillai, P. P. Förster Resonance Energy Transfer Regulated Multicolor Photopatterning from Single Quantum Dot Nanohybrid Films. *ACS Energy Lett.* **2019**, *4*, 1710–1716.

(22) Won, Y.-H.; Cho, O.; Kim, T.; Chung, D.-Y.; Kim, T.; Chung, H.; Jang, H.; Lee, J.; Kim, D.; Jang, E. Highly Efficient and Stable InP/ZnSe/ZnS Quantum Dot Light-Emitting Diodes. *Nature* **2019**, *575*, 634–638.

(23) Devatha, G.; Roy, P.; Rao, A.; Roy S.; Pillai, P. P. Multicolor Luminescent Patterning via Photoregulation of Electron and Energy Transfer Processes in Quantum Dots. *J. Phys. Chem. Lett.* **2020**, *11*, 4099–4106.

(24) Nguyen, H. A.; Dou, F. Y.; Park, N.; Wu, S.; Sarsito, H.; Diakubama, B.; Larson, H.; Nishiwaki, E.; Homer, M.; Cash, M.; Cossairt, B. M. Predicting Indium Phosphide Quantum Dot Properties from Synthetic Procedures Using Machine Learning. *Chem. Mater.* **2022**, *34*, 6296–6311.

(25) Cros-Gagneux, A.; Delpech, F.; Nayral, C.; Cornejo, A.; Coppel, Y.; Chaudret, B. Surface Chemistry of InP Quantum Dots: A Comprehensive Study. *J. Am. Chem. Soc.* **2010**, *132*, 18147–18157.

(26) LaMer, V. K.; Dinegar, R. H. Theory, Production and Mechanism of Formation of Monodispersed Hydrosols. *J. Am. Chem. Soc.* **1950**, *72*, 4847–4854.

(27) Lim, K.; Jang, H. S.; Woo, K. Synthesis of Blue Emitting InP/ZnS Quantum Dots through Control of Competition between Etching and Growth. *Nanotechnology* **2012**, *23*, 485609.

(28) Shen, W.; Tang, H.; Yang, X.; Cao, Z.; Cheng, T.; Wang, X.; Tan, Z.; You, J.; Deng, Z. Synthesis of Highly Fluorescent InP/ZnS Small-Core/Thick-Shell Tetrahedral-Shaped Quantum Dots for Blue Light-Emitting Diodes. *J. Mater. Chem. C* **2017**, *5*, 8243–8249.

(29) Huang, F.; Bi, C.; Guo, R.; Zheng, C.; Ning, J.; Tian, J. Synthesis of Colloidal Blue-Emitting InP/ZnS Core/Shell Quantum Dots with the Assistance of Copper Cations. *J. Phys. Chem. Lett.* **2019**, *10*, 6720–6726.

(30) Lee, W.; Lee, C.; Kim, B.; Choi, Y.; Chae, H. Synthesis of Blue-Emissive InP/GaP/ZnS Quantum Dots via Controlling the Reaction Kinetics of Shell Growth and Length of Capping Ligands. *Nanomaterials* **2020**, *10*, 2171.

(31) Zhang, W.; Ding, S.; Zhuang, W.; Wu, D.; Liu, P.; Qu, X.; Liu, H.; Yang, H.; Wu, Z.; Wang, K.; Sun, X. W. InP/ZnS/ZnS Core/Shell Blue Quantum Dots for Efficient Light-Emitting Diodes. *Adv. Funct. Mater.* **2020**, *30*, 2005303.

(32) Cui, Z.; Mei, S.; Wen, Z.; Yang, D.; Qin, S.; Xiong, Z.; Yang, B.; He, H.; Bao, R.; Qiu, Y.; Chen, Y.; Zhang, W.; Xie, F.; Xing, G.; Guo, R. Synergistic Effect of Halogen Ions and Shelling Temperature on Anion Exchange Induced Interfacial Restructuring for Highly Efficient Blue Emissive InP/ZnS Quantum Dots. *Small 2022*, **18**, 2108120.

(33) Zhang, H.; Ma, X.; Lin, Q.; Zeng, Z.; Wang, H.; Li, L. S.; Shen, H.; Jia, Y.; Du, Z. High-Brightness Blue InP Quantum Dot-Based Electroluminescent Devices: The Role of Shell Thickness. *J. Phys. Chem. Lett.* **2020**, *11*, 960–967.

(34) Rakshit, S.; Cohen, B.; Gutiérrez, M.; El-Ballouli, A. O.; Douhal, A. Deep Blue and Highly Emissive ZnS-Passivated InP QDs: Facile Synthesis, Characterization, and Deciphering of Their Ultrafast-to-Slow Photodynamics. *ACS Appl. Mater. Interfaces* **2023**, *15*, 3099–3111.

(35) Song, W.-S.; Lee, H.-S.; Lee, J. C.; Jang, D. S.; Choi, Y.; Choi, M.; Yang, H. Amine-Derived Synthetic Approach to Color-Tunable InP/ZnS Quantum Dots with High Fluorescent Qualities. *J. Nanoparticle Res.* **2013**, *15*, 1750.

(36) Jalali, H. B.; Melikov, R.; Sadeghi, S.; Nizamoglu, S. Excitonic Energy Transfer within InP/ZnS Quantum Dot Langmuir–Blodgett Assemblies. *J. Phys. Chem. C* **2018**, *122*, 11616–11622.

(37) Choi, H. S.; Liu, W.; Misra, P.; Tanaka, E.; Zimmer, J. P.; Ipe, B. I.; Bawendi, M. G.; Frangioni, J. V. Renal Clearance of Quantum Dots. *Nat. Biotechnol.* **2007**, *25*, 1165–1170.

(38) Zhang, W.; Ding, S.; Zhuang, W.; Wu, D.; Liu, P.; Qu, X.; Liu, H.; Yang, H.; Wu, Z.; Wang K. Sun, X. W. InP/ZnS/ZnS Core/Shell Blue Quantum Dots for Efficient Light-Emitting Diodes. *Adv. Funct. Mater.* **2020**, *30*, 2005303.

(39) Bagdasarov, K. S. Fundamentals of High-Temperature Crystallization. *Crystallogr. Rep.* **2002**, *47*, S27–S34.

(40) Rakshit, S.; Cohen, B.; Gutiérrez, M.; El-Ballouli, A. O.; Douhal, A. Deep Blue and Highly Emissive ZnS-Passivated InP QDs: Facile Synthesis, Characterization, and

Deciphering of Their Ultrafast-to-Slow Photodynamics. *ACS Appl. Mater. Interfaces* **2023**, *15*, 3099–3111.

(41) Jia, Y.; Chen, J.; Wu, K.; Kaledin, A.; Musaev, D. G.; Xie, Z.; Lian, T. Enhancing photo-reduction quantum efficiency using quasi-type II core/shell quantum dots. *Chem. Sci.* **2016**, *7*, 4125–4133.

(42) Tessier, M. D.; De Nolf, K.; Dupont, D.; Sinnaeve, D.; De Roo, J.; Hens, Z. Aminophosphines: A Double Role in the Synthesis of Colloidal Indium Phosphide Quantum Dots. *J. Am. Chem. Soc.* **2016**, *138*, 5923–5929.

(43) Talapin, D. V.; Rogach, A. L.; Mekis, I.; Haubold, S.; Kornowski, A.; Haase, M.; Weller, H. Synthesis and surface modification of amino-stabilized CdSe, CdTe and InP nanocrystals. *Colloids and Surfaces, A: Physicochemical and Engineering Aspects* **2002**, *202*, 145–154.

(44) Brown, R. P.; Gallagher, M. J.; Fairbrother, D. H.; Rosenzweig, Z. Synthesis and Degradation of Cadmium-Free InP and InPZn/ZnS Quantum Dots in Solution. *Langmuir* **2018**, *34*, 13924–13934.

(45) Jia, Y.; Chen, J.; Wu, K.; Kaledin, A.; Musaev, D. G.; Xie, Z.; Lian, T. Enhancing photo-reduction quantum efficiency using quasi-type II core/shell quantum dots. *Chem. Sci.* **2016**, *7*, 4125–4133.

(46) Lakowicz, J. R. *Principles of Fluorescence Spectroscopy*, 3rd ed.; Springer: New York, 1999.

(47) Thomas, A.; Sandeep, K.; Somasundaran, S. M.; Thomas, K. G. How Trap States Affect Charge Carrier Dynamics of CdSe and InP Quantum Dots: Visualization through Complexation with Viologen. *ACS Energy Lett.* **2018**, *3*, 2368–2375.

(48) Wargnier, R.; Baranov, A. V.; Maslov, V. G.; Stsiapura, V.; Artemyev, M.; Pluot, M.; Sukhanova, A.; Nabiev, I. Energy Transfer in Aqueous Solutions of Oppositely Charged CdSe/ZnS Core/Shell Quantum Dots and in Quantum Dot−Nanogold Assemblies. *Nano Lett.* **2004**, *4*, 451–457.

(49) Franzl, T.; Shavel, A.; Rogach, A. L.; Gaponik, N.; Klar, T. A.; Eychmüller, A.; Feldmann, J. High-Rate Unidirectional Energy Transfer in Directly Assembled CdTe Nanocrystal Bilayers. *Small* **2005**, *1*, 392–395.

(50) Sapsford, K. E.; Berti, L.; Medintz, I. L. Materials for Fluorescence Resonance Energy Transfer Analysis: Beyond Traditional Donor-Acceptor Combinations. *Angew. Chem. Int. Ed.* **2006**, *45*, 4562–4588.

(51) Freeman, R.; Willner, B.; Willner, I. Integrated Biomolecule–Quantum Dot Hybrid Systems for Bioanalytical Applications. *J. Phys. Chem. Lett.* **2011**, *2*, 2667–2677.

(52) Chou, K. F.; Dennis, A. M. Förster Resonance Energy Transfer Between Quantum Dot Donors and Quantum Dot Acceptors. *Sensors* **2015**, *15*, 13288–13325.

(53) Ji, X.; Wang, W.; Mattoussi, H. Controlling the Spectroscopic Properties of Quantum Dots via Energy Transfer and Charge Transfer Interactions: Concepts and Applications. *Nano Today* **2016**, *11*, 98–121.

(54) Sarkar, A.; Dhiman, S.; Chalishazar, A.; George, S. J. Visualization of Stereoselective Supramolecular Polymers by Chirality-Controlled Energy Transfer. *Angew. Chem. Int. Ed.* **2017**, *56*, 13767−13771.

(55) Kodaimati, M. S.; Lian, S.; Schatz, G. C.; Weiss, E. A. Energy Transfer-Enhanced Photocatalytic Reduction of Proton within Quantum Dot Light-Harvesting-Catalyst Assemblies. *Proc. Natl. Acad. Sci. U. S. A.* **2018**, *115*, 8290– 8295.

(56) Roy, P.; Devatha, G.; Roy, S.; Rao, A.; Pillai, P. P. Electrostatically Driven Resonance Energy Transfer in an All-Quantum Dot Based Donor–Acceptor System. *J. Phys. Chem. Lett.* **2020**, *11*, 5354–5360.

(57) He, C.; Nguyen, T. D.; Edme, K.; Olvera de la Cruz, M.; Weiss, E. A. Noncovalent Control of the Electrostatic Potential of Quantum Dots through the Formation of Interfacial Ion Pairs. *J. Am. Chem. Soc.* **2017**, *139*, 10126–10132.

(58) Zelent, B.; Kuśba, J.; Gryczynski, I.; Johnson, M. L.; Lakowicz, J. R. Distance-Dependent Fluorescence Quenching of p-Bis[2-(5-phenyloxazolyl)]benzene by Various Quenchers. *J. Phys. Chem.* **1996**, *100*, 18592–18602.

(59) Mutlugun, E.; Hernandez-Martinez, P. L.; Eroglu, C.; Coskun, Y.; Erdem, T.; Sharma, V. K.; Unal, E.; Panda, S. K.; Hickey, S. G.; Gaponik, N.; Eychmüller, A.; Demir, H. V. Large-Area (over 50 cm × 50 cm) Freestanding Films of Colloidal InP/ZnS Quantum Dots. *Nano Lett.* **2012**, *12*, 3986–3993.

3.8. Appendix

HRTEM Measurements:

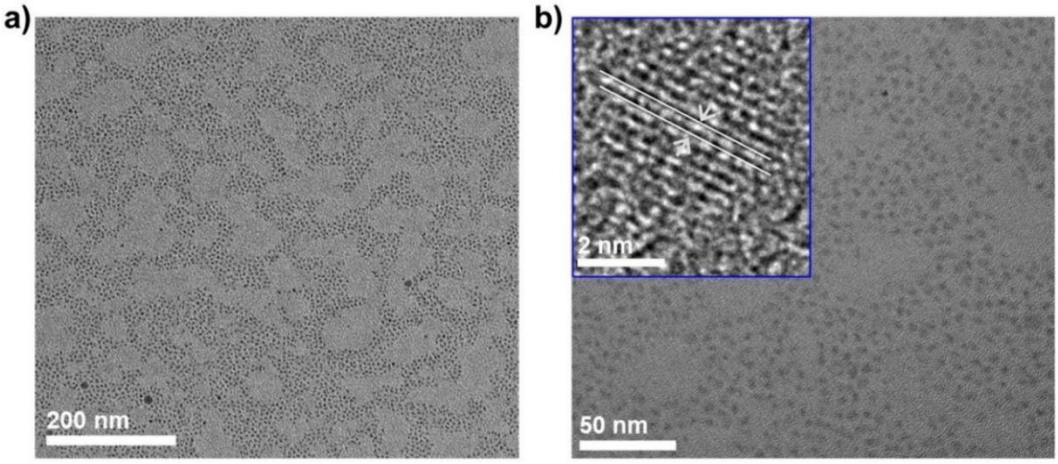

Figure A3.1 High resolution transmission electron microscopy (HRTEM) analysis of pure-blue emitting [-] B-QDs. Representative large area TEM images at resolution of (a) 200 nm, and (b) 100 nm, showing the uniformity in size and shape distribution. The inset of (b) shows the lattice fringes in single [-] B-QDs

Powder XRD Analysis:

The crystallite size of the core InP and core-shell InP/ZnS QDs was determined from PXRD peaks using Scherrer equation.

$$\boldsymbol{D = \frac{k\lambda}{\beta \cos \theta}} \quad \ldots (28)$$

Where, D = Crystallite size

k = Scherrer constant, is typically considered to be 0.94 for spherical particles

λ = Wavelength of Cu k_α X-ray = 1.5406 Å

β = FWHM of the PXRD peak in radian.

θ = Bragg angle

The Scherrer equation quantitatively describes the broadening of a peak at a particular angle (θ), as it relates the crystalline domain size (D) to the width of the peak (β). By using the above equation 28, the crystallite size of the InP-core and InP/ZnS core-shell QDs was determined to 1.8 ± 0.1 nm and 3.5 ± 0.2 nm, respectively.

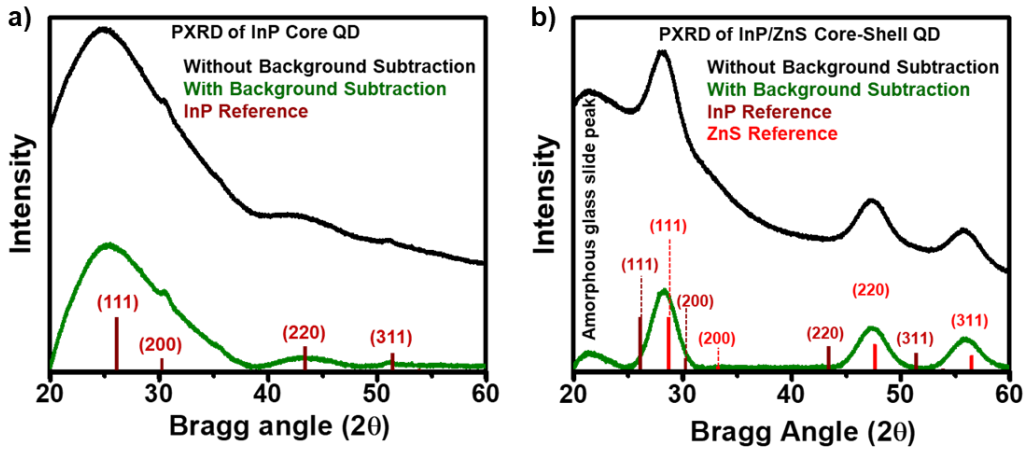

c)

System	(111) plane	(220) plane	(311) plane	Average size
InP core QD	---	L = 5.02° 2θ = 43.47° D = 1.78 nm	---	1.79 nm
InP/ZnS core-shell QD	L = 2.63° 2θ = 28.28° D = 3.26 nm	L = 2.65° 2θ = 47.40° D = 3.42 nm	L = 2.56° 2θ = 55.94° D = 3.66 nm	3.45 nm

Figure A3.2 Powder X-ray diffraction (PXRD) patterns of (a) InP-core and (b) InP/ZnS core-shell QDs without (black) and with (olive) background subtraction. Comparison of PXRD patterns of QDs with bulk InP (wine-solid) and ZnS (red-solid) reference reveals the presence of zinc blend phase in InP-core and InP/ZnS core-shell QD. The broadness of the first peak (around 2θ = 25 degrees) in InP-core is due to the combination of signal from (111) and (200) planes of zinc blend phase and the underlying amorphous glass slide. (c) Table for the calculation of diameter of InP-core and InP/ZnS core-shell QDs from Scherrer equation.

XPS studies for [-] InP/ZnS QDs:

A detailed elemental analysis of [-] B-QD was performed using of X-ray photoelectron spectroscopy (XPS). The In 3d, P 2p, Zn 2p, Zn 3s, and S 2p core peaks as well as the peaks for the surface ligands O 1s, C 1s and Na KLL Auger are present in the system. For the analysis, the charge correction for the all the spectral peaks was performed according to the carbon-1s standard peak (284.6 eV).

For, [-] B-QD, the In 3d and P 2p spectrum exhibits one doublet corresponding to In-P bond. The doublet for In was located at 443.26 eV ($3d_{5/2}$) and 450.86 eV ($3d_{3/2}$), respectively (spin-orbit splitting of 7.6 eV between $3d_{5/2}$ and $3d_{3/2}$). The doublet for P appears at 133.44 eV ($2p_{3/2}$) and 134.34 eV ($2p_{1/2}$), respectively (spin-orbit splitting of 0.9 eV between $2p_{3/2}$ and $2p_{1/2}$). The presence of single doublet for In 3d and P 2p indicates the absence of any oxidised $InPO_x$ layer at the interface of core and shell materials.

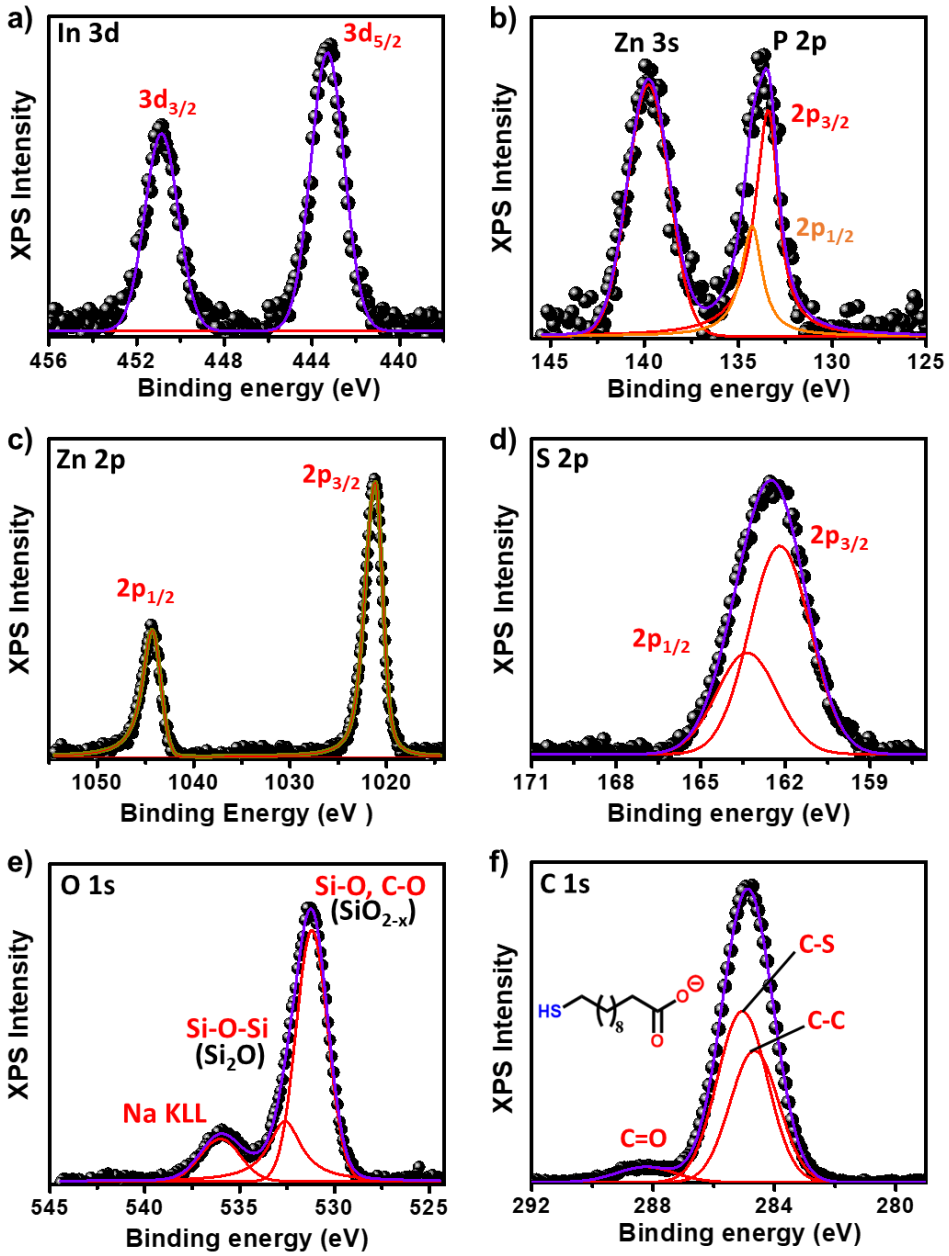

Figure 3.3 Analysis of X-ray photoelectron spectrum of [-] B-QDs: (a) In 3d spectrum; (b) P 2p spectrum, Zn 3s spectrum; (c) Zn 2p spectrum; (d) S 2p spectrum; (e) O 1s spectrum; and (f) C 1s spectrum.

Further, the analysis of O 1s spectrum confirms the absence of oxide layer, instead, there was a presence of Na KLL Auger peak at 536.04 eV, justifying the presences of deprotonated MUA ligand on the QD surface. The Zn 2p XPS exhibit two peaks located at 1021.14 eV ($2p_{3/2}$) and 1044.34 eV ($2p_{1/2}$) (spin-orbit splitting of 23.2 eV between $2p_{3/2}$ and $2p_{1/2}$), assigned to the ZnS shell. A single Zn 3s peak was also observed at 139.74 eV. The S 2p spectrum showed one doublet located at 162.24 eV ($2p_{3/2}$) and 163.34 eV ($2p_{1/2}$) (spin-orbit splitting of 1.1 eV between $2p_{3/2}$ and $2p_{1/2}$). This decrease in spin-orbit splitting can be attributed to the combined

effect of ionic metal-sulphur and covalent C-S bond present in the system. Finally, the characteristic peaks for the surface MUA ligands were analysed with C1s spectrum. The C 1s spectrum showed three peak corresponds to C-C (284.64 eV), C-S (285.04 eV) and C=O (288.24 eV) bond for the MUA ligand.

EDAX Analysis:

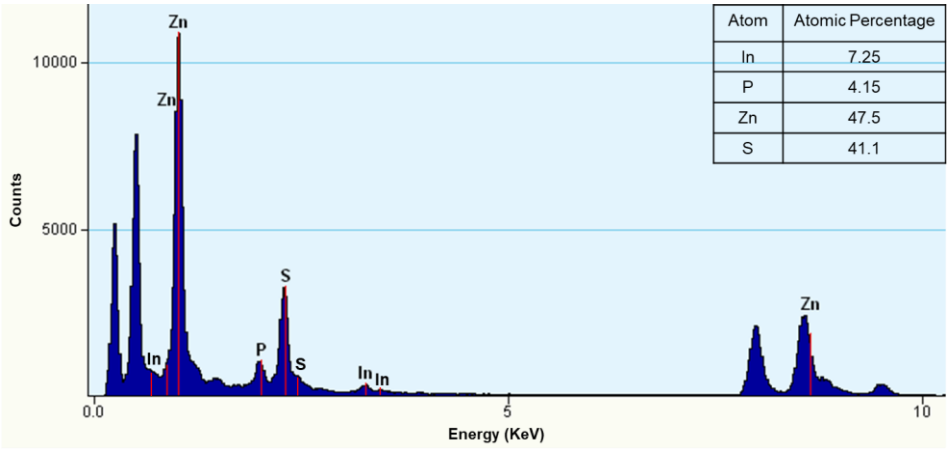

Figure A3.4 EDAX spectrum of [-] InP/ZnS QDs, taken during the HRTEM measurement. The inset shows the atomic percentages of all the major components in [-] InP/ZnS QDs: In, P, Zn and S.

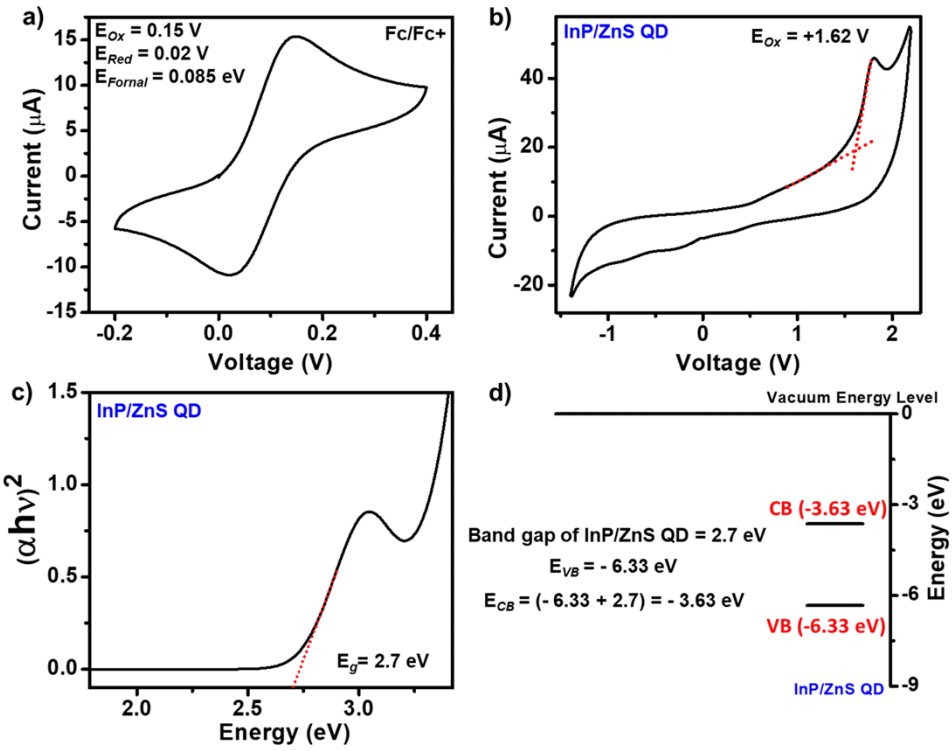

Figure 3.5 Determination of band positions for the pure-blue emitting InP/ZnS QD. Cyclic voltammograms for (a) ferrocene/ferrocenium couple, as internal standard and (b) InP/ZnS QD in

acetonitrile solvent, at a scan rate of 30 mV/s. The measurements for QDs were performed via dip-coating of QDs over the glassy carbon, followed by drying under vacuum to remove the solvent. The measured relative reference electrode potential, E_{ref}, is 4.71 eV. (c) The Tauc plot for InP/ZnS QD. (d) Relative band positions for InP/ZnS QD, with respect to vacuum.

Determination of Molar-Extinction Coefficient of InP/ZnS QDs:

The particle concentration of InP/ZnS QDs and the corresponding molar extinction co-efficient (0.2519 x 10^5 $M^{-1}cm^{-1}$ at 410 nm) were estimated using ICP-MS analysis combined with PXRD, TEM and UV-vis absorption spectrum. Details are provided below:

Size of the particle, *d* (from PXRD analysis) = 17.8 Å

Lattice constant of InP, *a* = 5.83 Å

Note: InP crystallizes in cubic zinc blende structure with a lattice constant (*a*) of 5.83 Å with 8 atoms in unit cell (4 In and 4P)

Volume of the unit cell, $V_{unit\ cell}$ $= a^3$

Total number of atoms in a nanocrystal, A $$= \frac{4}{3}\pi\left(\frac{d}{2}\right)^3 * \frac{8}{V_{unit\ cell}} = 119$$

Let's consider that the mass % of In and P is C_{In} and C_P, respectively.

Concentration of InP/ZnS nanocrystals[21], $C_{InP/ZnS}$ $$= \frac{1}{A}\left(\frac{C_{In}}{M_{In}} + \frac{C_P}{M_P}\right) \quad \ldots (29)$$

M is the molar mass.

N.B. From EDAX analysis, the obtained ratio of In to P was 1:0.56.

Based on the ICP-MS and absorption study, the molar extinction co-efficient was estimated to be 0.2519 x 10^5 $M^{-1}cm^{-1}$.

Cellular Bioimaging Study:

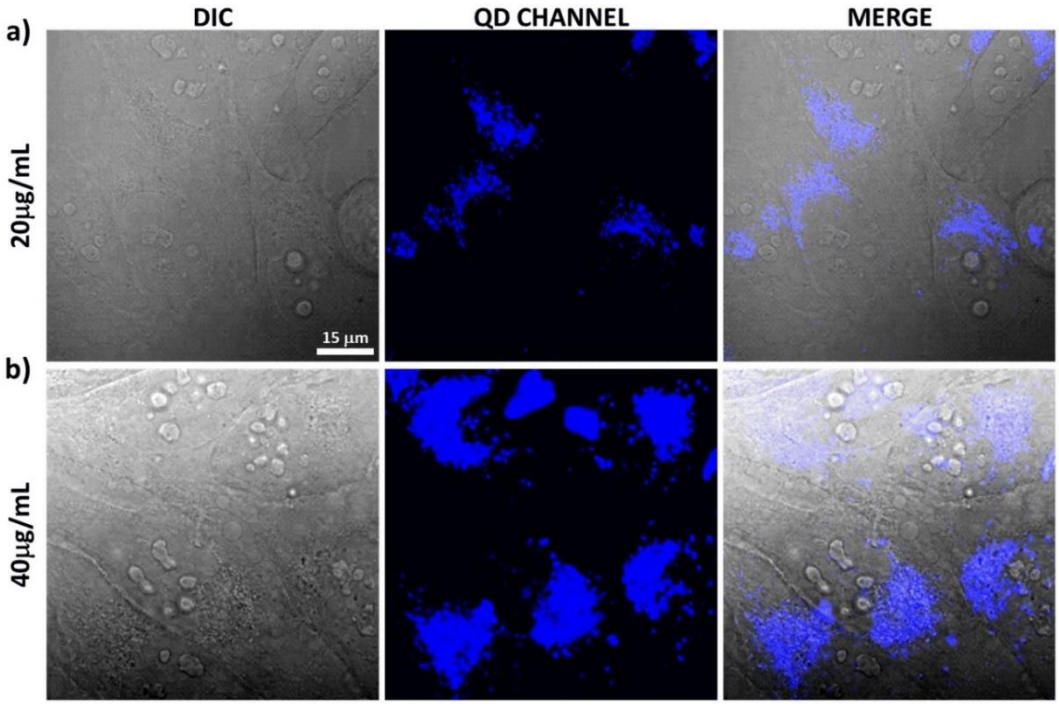

Figure A3.6 Concentration optimization for bio-imaging study. Luminescent confocal images of HeLa cells internalized with (a) 20 µg/mL [-] B-QDs (0.35 µM), and (a) 40 µg/mL [-] B-QDs (0.70 µM) for ~7 h. The first and second column corresponds to phase contrast (DIC) image and the fluorescence image upon excitation with 405 nm laser source, respectively. The third column corresponds to the fluorescence image merged with DIC image.

Light induced resonance energy transfer studies:

Steady-State Measurements

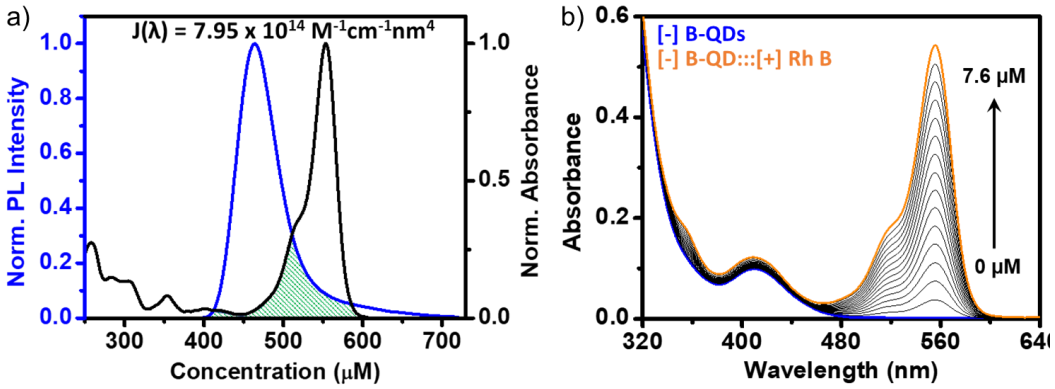

Figure A3.7 FRET study between oppositely charged pure-blue emitting [-] B-QD and Rh B dye in water. (a) The spectral overlap integral between the PL of donor [-] B-QD and the absorption of acceptor Rh B dye. (b) Absorption spectral changes in pure-blue emitting [-] B-QD upon addition of increasing concentration of Rh B dye.

Radius of Quenching Sphere and Perrin Formalism: A detailed Stern-Volmer analyses for [-] B-QD:::Rh B complex in aqueous medium reveal a non-linear variation of relative PL intensity of [-] B-QDs as a function of varying concertation of Rh B dye. In general, the steady-state non-linear Stern-Volmer (I_0/I *vs* [Q]) indicates the presence of both static and dynamic components in the PL quenching. The exponential variation observed in relative PL can be treated within the framework of Perrin formalism, as shown below.

$$\frac{I_0}{I} = e^{\alpha[Q]} = e^{\lambda} \quad \ldots (30)$$

Where, the α represents the quenching constant, [Q] is concentration of acceptor and λ is the number of acceptors in the quenching sphere. Therefore, the plot of "ln (I_0/I) *vs* [Q]" will show a linear relationship and from the slope the quenching constant (α) can be determined. In the Perrin formalism, the quenching constant vary proportionally with the quenching volume (V) of the D-A system, as described below.

$$\alpha = \frac{N_A V}{1000} \quad \ldots (31)$$

Where,

$$V = \frac{4}{3} r_q^3 \quad \ldots (32)$$

r_q is quenching radius for the donor-acceptor system and N_A is the Avogadro number (6.023 x 10^{23} mol^{-1}).

The quenching constant (α) for [-] B-QD:::Rh B donor-acceptor system was estimated to be ~4 x 10^5 M^{-1}. Thus, from the α value obtained, the calculated quenching volume and radius was estimated to be ~6.62 x 10^{-16} cm^3 and ~54.1 nm, respectively. Here, the idea of quenching volume suggests an active volume or "sphere of action" surrounding the excited state QDs. Instantaneous quenching will occur in a randomly distributed system when a quencher happens to be resided within the sphere of action of volume "V".

Proof of electrostatically driven FRET process.

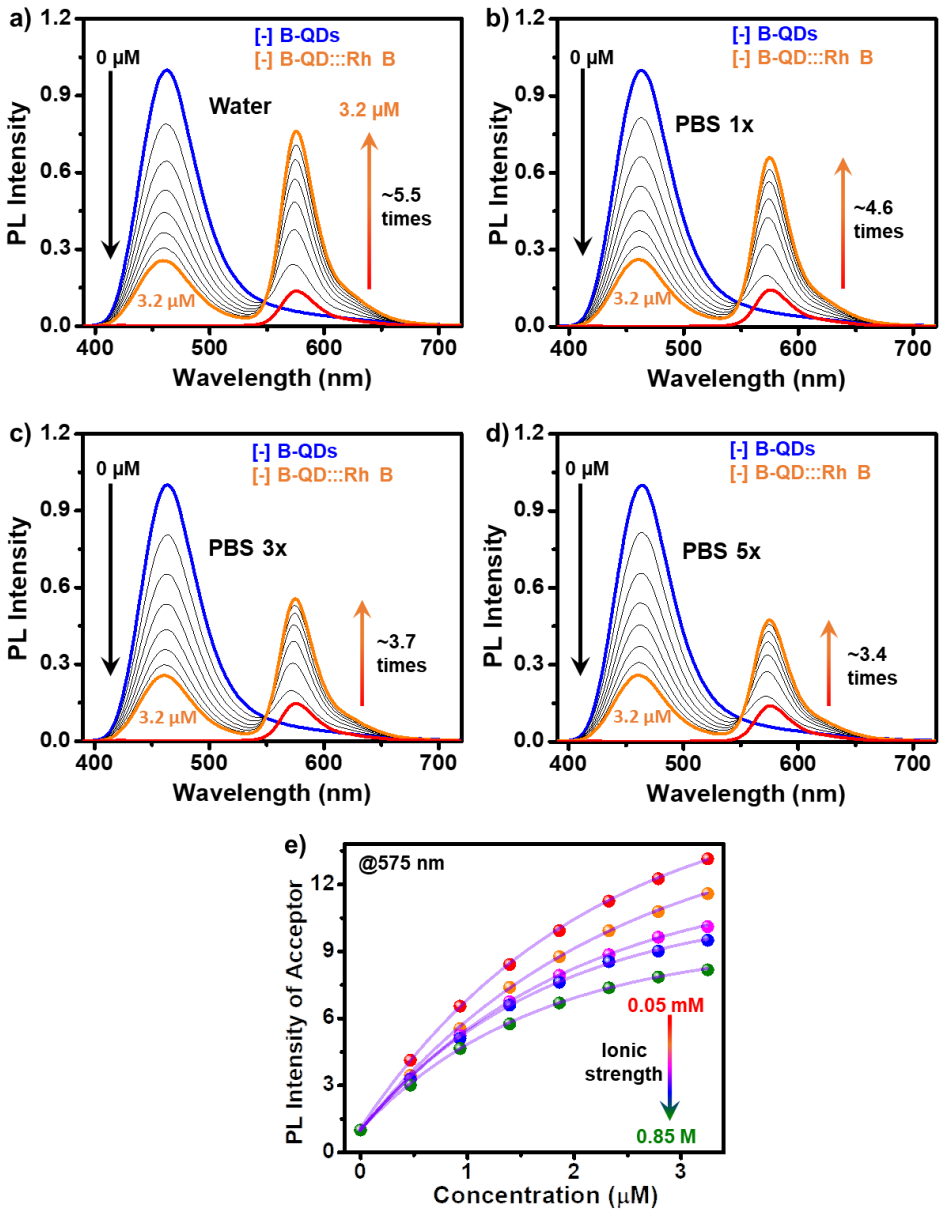

Figure A3.8 Proof of electrostatically driven FRET process. PL spectral changes in [-] B-QDs upon successive addition of Rh B dye (up to concentration of 3.2 µM) in (a) milli-Q water, (b) 1X PBS, (c) 3X PBS and (d) 5X PBS. (e) The PL enhancement in the acceptor dye decreases with increasing the concentration of PBS solution.

Time-Resolved Analysis

Table A3.1 PL decay analysis of [-] B-QD:::Rh B dye complex, upon successive addition of acceptor Rh B dye, in a time window of 3.2 µs.

System	τ_1 (ns)	α_1	τ_2 (ns)	α_2	τ_3 (ns)	α_3	τ_4 (ns)	α_4	$\tau_{avg.}$ (ns)	χ^2
[-] B-QDs	**8.98**	**0.46**	**58.42**	**0.37**	**167.1**	**0.15**	**629.7**	**0.02**	**211.63**	**1.12**
[-] B-QD:::Rh B Dye (0.50 µM)	7.44	0.42	50.71	0.38	153.9	0.18	604.7	0.02	202.20	1.13
[-] B-QD:::Rh B Dye (0.98 µM)	5.33	0.47	38.13	0.33	130.6	0.18	527	0.02	185.56	1.20
[-] B-QD:::Rh B Dye (1.47 µM)	5.72	0.55	35.39	0.28	121.7	0.15	487.4	0.02	178.78	1.14
[-] B-QD:::Rh B Dye (1.95 µM)	5.16	0.8	30.81	0.13	115.5	0.06	482.4	0.01	164.52	1.21
[-] B-QD:::Rh B Dye (2.44 µM)	4.36	0.6	28.29	0.27	116.5	0.12	510.6	0.01	152.11	1.28
[-] B-QD:::Rh B Dye (2.93 µM)	4.65	0.79	26.2	0.14	103.6	0.06	421.3	0.01	142.51	1.13
[-] B-QD:::Rh B Dye (3.41 µM)	3.73	0.75	19.92	0.18	93.14	0.06	390.7	0.01	134.06	1.16
[-] B-QD:::Rh B Dye (3.90 µM)	3.38	0.69	19.44	0.23	90.02	0.07	375.7	0.01	122.98	1.15
[-] B-QD:::Rh B Dye (4.38 µM)	2.94	0.66	15.3	0.26	78.56	0.07	329.6	0.01	107.71	1.29
[-] B-QD:::Rh B Dye (4.87 µM)	2.85	0.77	14.18	0.18	69.93	0.04	279.8	0.01	98.74	1.23
[-] B-QD:::Rh B Dye (5.35 µM)	2.58	0.7	13.45	0.24	67.92	0.05	258.7	0.01	86.02	1.12
[-] B-QD:::Rh B Dye (5.83 µM)	2.64	0.79	11.48	0.17	54.52	0.03	219.5	0.01	76.10	1.17
[-] B-QD:::Rh B Dye (6.31 µM)	1.97	0.71	10.56	0.24	51.81	0.04	199.6	0.01	66.92	1.29
[-] B-QD:::Rh B Dye (6.79 µM)	**2.13**	**0.74**	**10.4**	**0.21**	**47.55**	**0.04**	**184.3**	**0.01**	**60.80**	**1.24**

Distance-Dependent Quenching (DDQ) Model: To obtain mechanistic insights into the nature of collisional quenching, a time-resolved SV plot was generated (relative lifetime *vs* acceptor concertation plot). Interestingly, a non-linear behaviour was recorded for time-resolved Stern-Volmer plot as well, which is not a common observation in FRET study. In general, a linear Stern-Volmer is expected from a time-resolved kinetics, where the dynamic component is responsible for the PL quenching process. However, a non-linear Stern-Volmer plot, with a positive curvature, can be attributed to the involvement of more than one quenching mechanism.

To understand further about the mechanism of lifetime quenching process, the model of distance-dependent quenching (DDQ) was taken into consideration, which indicates the

involvement of through-space interaction. The DDQ model assumes that the rate of quenching k(r) has an exponential dependence on the distance between donor and acceptor, given by the equation.

$$\boldsymbol{k(r) = k_a e^{\left[-\frac{(r-a)}{r_e}\right]}} \quad \ldots (33)$$

Where, k_a is the value of k(r) at encounter distance r = a, a is the distance of closest approach, and r_e is the characteristic parameter of the interaction that defines the decrease of k(r) with distance.

Therefore, the rate of collisional quenching will contain a distance component k(r), as shown below.

$$\boldsymbol{\frac{\tau_0}{\tau} = 1 + k(r)\,\tau_0[Q]} \quad \ldots (34)$$

By substituting the equation (28) in (29), we get

$$\boldsymbol{\left(\frac{\tau_0}{\tau} - 1\right)\frac{1}{[Q]} = k_a\,\tau_0 e^{\left[-\frac{(r-a)}{r_e}\right]} = k'_a e^{\left[-\frac{(r-a)}{r_e}\right]}} \quad \ldots (35)$$

Now, the plot of "$(\tau_0/\tau\text{-}1)/[Q]$ *vs* r" will be exponential, and will provide the bimolecular quenching (k_a) constant value and the possible closet distance (a) of quenching for the system (**Figure A3.9**). Accordingly, the bimolecular quenching constant was estimated to be ~1.24 x 10^{12} $M^{-1}s^{-1}$ using the DDQ model. A higher value of bimolecular quenching constant in comparison with diffusion control quenching rate (typically in order of 10^{10} $M^{-1}s^{-1}$) indicates the presence of strong ground state complexation between donor [-] InP/ZnS QD and acceptor Rh B dye.

Furthermore, the best fit of lifetime quenching process with DDQ model suggest the presence of more than one acceptor inside the quenching volume, surrounding the donor InP/ZnS QD at diffident distances.

Poisson Statistics: To visualize the probability distribution of Rh B dye surrounding the QD, the Poisson distribution probability was calculated using the following equation.

$$\boldsymbol{P(X = n) = \frac{\Lambda^n e^{-\Lambda}}{n!}} \quad \ldots (36)$$

Where, Λ represent the concentration ratio of dye to QD, and n is the number of acceptors in closest to QD.

The estimation of Poisson function at different Λ, and fitting of τ_0/τ *vs* Λ plots provides the distribution of acceptor dyes around QDs. The probability of finding average number of acceptors in closet approach to QD is n = 1, at Λ= 1 and remain n=1 even at Λ >> 1. This again confirms the distance-dependent nature of collisional quenching, and existence of more than one layer of Rh B dye around [-] QD (**Figure A3.9**). The presence of dual charges on Rh B dye might helped in formation of multi-layer arrangement through electrostatic interaction. Accordingly, the acceptor distribution was drawn using the value of n and different ratio of dye to QD (**Figure A3.9c**). A negligible change in the zeta potential value was observed for [-] B-QD:::Rh B dye complex upon increasing the concentration of Rh B dye, which further proves a multi-layer arrangement of the acceptor molecules (see the **Figure A3.10**).

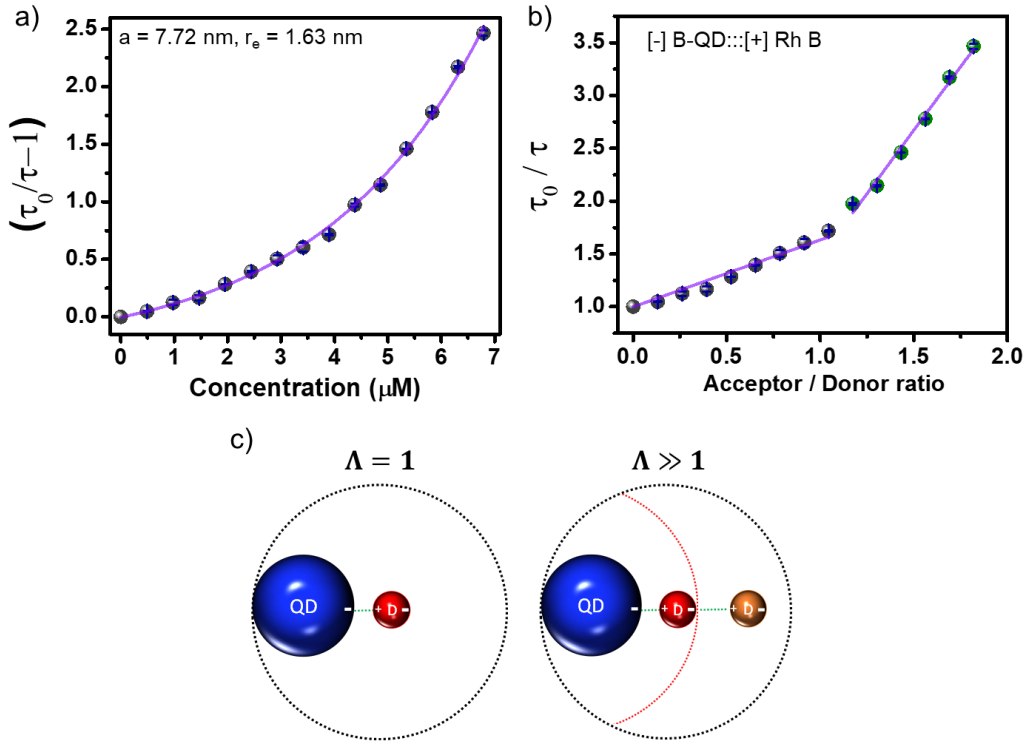

Figure 3.9 The DDQ model analysis. (a) The exponential (τ_0/τ-1) *vs* concentration plot proved the best fitting of DDQ model to with a = 7.72 nm and r_e = 1.63 nm, for [-] B-QD:::Rh B donor-acceptor system. Perrin's analysis of quenching sphere through the combination DDQ model and Poisson distribution at various number acceptor. (b) The relative lifetime decay of donor [-] B-QD as a function of average number of acceptor dye per donor QD. (c) Schematic illustration of interaction between [-] B-QD and Rh B dye when Λ = 1 and Λ>>1.

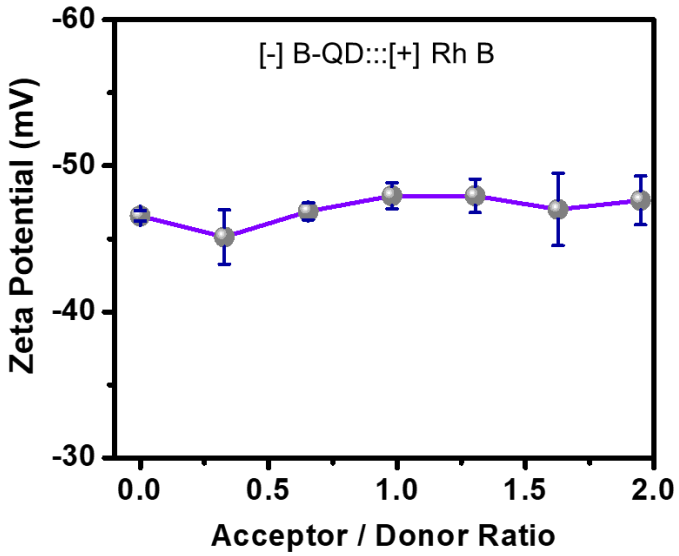

Figure A3.10 Zeta potential of **[-]** B-QD:::Rh B dye complex as a function of increasing concentration of Rh B dye.

Temperature Dependent Lifetime Analysis

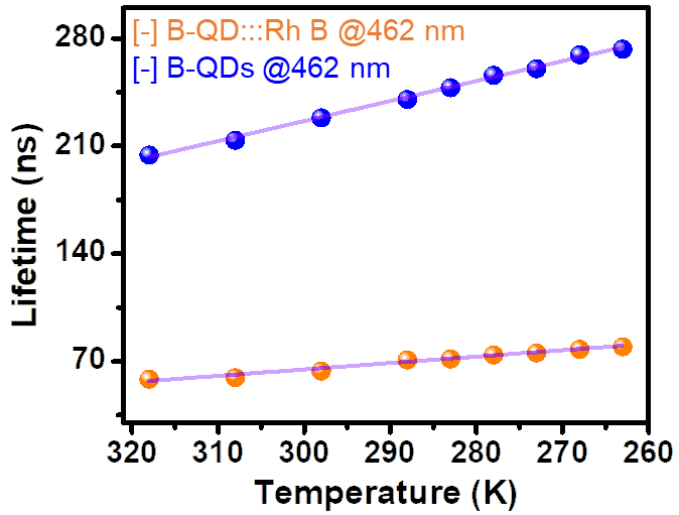

Figure A3.11 Temperature dependent lifetime analysis. Variation in the PL lifetime of [-] B-QDs in presence (orange) and absence (blue) of Rh B dye in water, as a function of temperature.

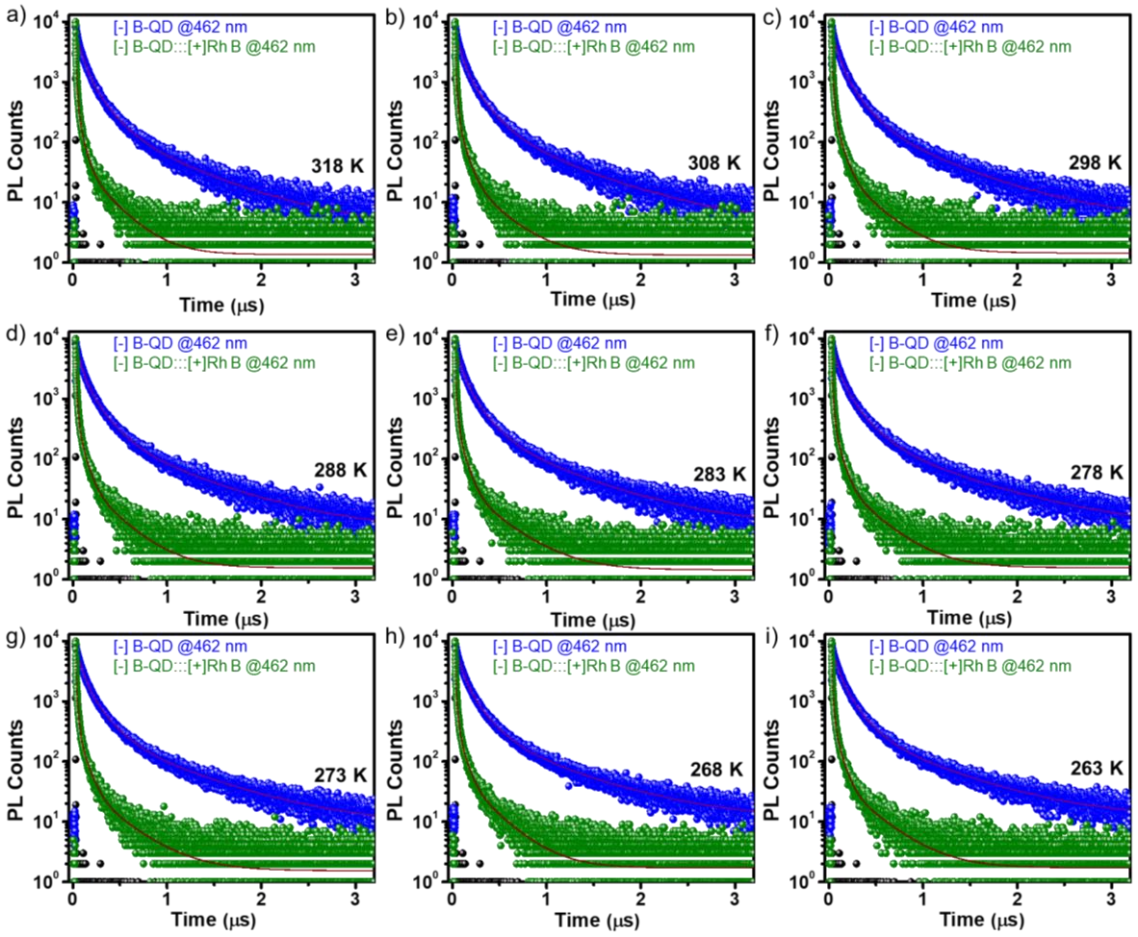

Figure A3.12 Temperature dependent lifetime analysis. PL decay profiles of [-] B-QD (blue) and [-] B-QD:::Rh B dye complex (olive) at different temperatures in water**:** (a) 318 K, (b) 308 K, (c) 298 K, (d) 288 K, (e) 283 K, (f) 278 K, (g) 273 K (h) 268 K and (i) 263 K.

Table A3.2 PL decay analysis of [-] B-QD (blue) and [-] B-QD:::Rh B dye complex (orange) at different temperatures, in a time window of 3.2 µs.

Temperature (K)	System	τ_1 (ns)	α_1	τ_2 (ns)	α_2	τ_3 (ns)	α_3	τ_4 (ns)	α_4	$\tau_{avg.}$ (ns)	χ^2
318 K	[-] B-QDs	9.48	0.35	58.22	0.45	167.89	0.18	639.45	0.02	204.17	1.12
	[-] B-QD:::Rh B	1.95	0.71	8.42	0.24	37.18	0.04	177.04	0.01	58.27	1.27
308 K	[-] B-QDs	11.36	0.37	61.45	0.45	176.02	0.16	670.52	0.02	213.76	1.13
	[-] B-QD:::Rh B	2.23	0.72	9.92	0.23	42.61	0.04	185.32	0.01	59.40	1.31
298 K	[-] B-QDs	7.88	0.28	55.68	0.47	160.21	0.22	623.82	0.03	228.28	1.06
	[-] B-QD:::Rh B	2.21	0.69	9.42	0.26	42.69	0.04	196.88	0.01	63.66	1.28
288 K	[-] B-QDs	8.04	0.26	58.08	0.49	167.84	0.22	661.19	0.03	240.32	1.08
	[-] B-QD:::Rh B	2.22	0.69	10.07	0.26	46.87	0.04	214.82	0.01	70.84	1.20
283 K	[-] B-QDs	9.69	0.28	62.70	0.49	176.65	0.2	681.10	0.03	247.88	1.09
	[-] B-QD:::Rh B	2.00	0.69	9.67	0.26	44.76	0.04	212.32	0.01	71.41	1.34
278 K	[-] B-QDs	9.38	0.25	62.21	0.51	178.01	0.21	709.19	0.03	255.99	1.02
	[-] B-QD:::Rh B	2.49	0.69	11.09	0.26	48.84	0.04	228.95	0.01	74.14	1.38
273 K	[-] B-QDs	10.62	0.25	65.59	0.52	186.39	0.2	724.50	0.03	260.62	1.07
	[-] B-QD:::Rh B	2.51	0.71	11.91	0.24	53.17	0.04	230.92	0.01	75.44	1.21
268 K	[-] B-QDs	10.51	0.25	65.22	0.51	184.92	0.21	748.11	0.03	269.32	1.06
	[-] B-QD:::Rh B	2.45	0.69	11.25	0.26	50.83	0.04	236.93	0.01	77.80	1.32
263 K	[-] B-QDs	6.66	0.23	56.69	0.46	158.89	0.27	677.05	0.04	272.98	1.08
	[-] B-QD:::Rh B	2.28	0.67	10.56	0.27	49.60	0.05	240.62	0.01	79.38	1.25

Chapter – 4

Electrostatics Enable Photoinduced Electron Transfer Process in QD–Dye Model System based on Blue-Emitting InP QDs

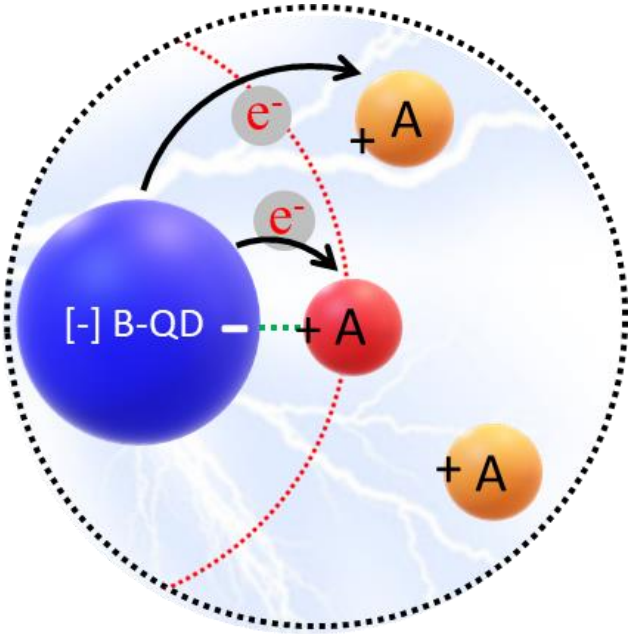

4.1 Abstract

Generation and subsequent extraction of photoexcited delocalised electrons by appropriate acceptors is an active area of research in the context of improving the performance of electronic devices. We accomplish here an efficient electron transfer process between wide-band gap, pure-blue emitting InP/ZnS quantum dot (QD) and methylene blue (MB) dye. The quasi-type-II band structure of B-QD satisfy the thermodynamic criteria of negative Gibbs free energy ($\Delta G = -80$ kJ/mol) as well as the necessity of delocalized photoexcited electron. The dynamics of photoinduced electron transfer (PET) process was monitored with detailed steady-state and time-resolved spectroscopic techniques. The efficiency and rate of the PET process were estimated to be ~60 % and 6.50 μs^{-1}, respectively. Following, the underlying mechanism of the electron transfer process was investigated with polarity- and temperature-dependent PL quenching study. Here, the surface of QD was appropriately functionalized with charged ligand to ensure close-proximity between donor and acceptor for strong electronic interactions. The prominent role of electrostatics in achieving an efficient charge transfer process in [-] B-QD:::MB dye donor:::acceptor system was verified via regulating the ionic strength of the medium. Finally, the charge transfer process in [-] B-QD:::MB dye donor:::acceptor system was confirmed with the transient absorption (TA) spectroscopic studies. Microsecond TA spectral evolution revealed the emergence of characteristic excited state absorbance (ESA) features of $MB^{+\bullet}$ semiquinone. The charge separated state is long-lived, with an average lifetime of 1.8 μs. In short, the pure-blue emitting InP QDs participates in an efficient light-induced electron transfer process in the electrostatically assembled [-] B-QD:::MB dye donor:::acceptor system in water.

4.2 Introduction

The covalency of colloidal semiconductor quantum dot (QD) has a striking influence on the Bohr exciton radius and quantum confinement effect, which further can modulate the optoelectronic properties beyond the finite size effect.[1-4] For instance, flat energy band and localized electron wavefunctions are the characteristics of strong ionic solids, while covalent solids manifest broad, highly curved energy bands and delocalized electron wavefunctions.[2,5] A measure of Phillips ionicity (*f*) determines the degree of covalency in chemical bond between the constituent elements in binary QD.[4,6] Among various binary QDs, the III-V category of semiconductors have smaller Phillips ionicity ($f = 0.3–0.4$) in comparisons with II-VI and IV-

VI QDs ($f > 0.6$), and thus have larger lattice covalency.[6] These finding was accentuated with lighter charge carriers and larger dielectric constant for III-V QDs, suggesting a more delocalized electron wavefunction across the lattice (**Figure 4.1**).[2] This essentially means that the degree of covalency governs both the onset (curvature of energy band) and magnitude of quantum confinement effect, which is more prominent in III-V QDs. Further, the robust structural integrity of covalent III-V semiconductor lattice under electrical and environmental stress offers additional advantages for widespread optoelectronic applications.[7-13]

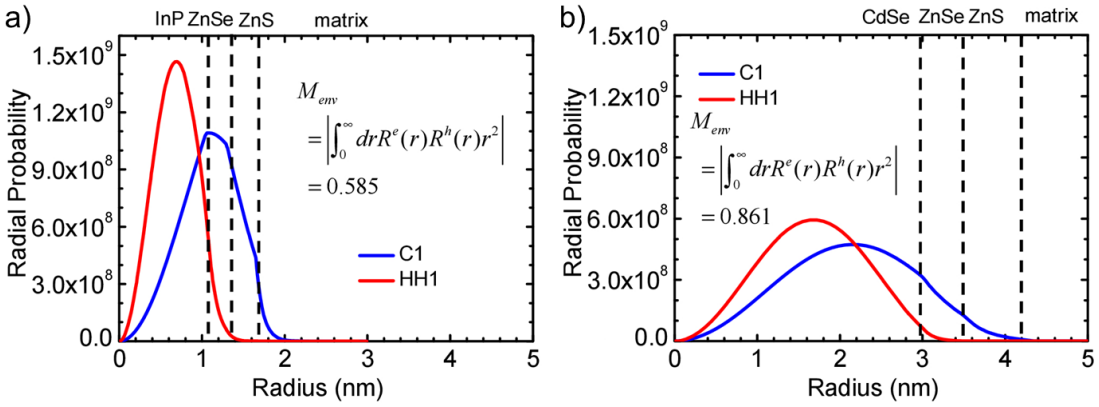

Figure 4.1 Radial probability of electron and hole wave functions in the ground state in (a) InP/ZnSe/ZnS QD and (b) CdSe/ZnSe/ZnS QD. The wavefunction of electron and heavy hole (HH) states is more localised in the CdSe core, in comparison to the InP core. The degree of overlap between two wavefunctions determines the extent of confinement of the charge carrier in the interior of QD. Thus, a large overlap integral between electron and HH wavefunctions will lead to a strong confinement and less scattering of carriers in the II-VI crystal. Reproduced with permission from reference 5. Copyright 2019 Optica Publishing group.

Within the family of III-V semiconductors, indium phosphide (InP) QDs have emerged as a promising candidate for optoelectronic studies due to its (i) tunable band gap spanning from blue to near-infrared (NIR) region, (ii) intrinsically non-toxic nature owing to its constituent elements (In and P atom), (iii) prolonged exciton lifetime, and (iv) multiexciton generation (MEG) possibility.[12-22] Likewise, InP QD has Philips ionicity (*f*) of 0.421 and Bohr excitonic radius of 9.6 nm.[4,6] Therefore, the size effect will be more prominent in the case of InP QD. Alongside, the superior covalency of environmentally friendly InP QDs is reported to produce deep surface traps beneath the conduction band (CB).[23-25] Notably, in a comparison study with similarly sized QD (~3 nm), InP revealed a surface trap at 6.3 kJ/mol below the CB, which is 25 times deeper than the shallow trap in CdSe QD (0.25 kJ/mol).[2,19] The discrepancy in surface traps can be attributed to the weak coupling of bulk and surface state electronic wavefunctions for III-V InP QDs. Consequently, the depth of the traps continues to increase below the CB energy level as the size of InP QD decreases (**Figure 4.2**).[2,4,14] Thus, studying the dynamics of

excited-state charge carriers in InP QDs is fundamentally intriguing and will provide deeper insights into the exciton relaxation processes and the electronic framework. In an early report by Mićić, Nozik and co-workers, the first ever photosensitization of the band gap of TiO_2 nanocrystalline film by 4.5 nm sized InP QDs was demonstrated (**Figure 4.3a**).[26] Visible light-mediated charge transfer process from InP QD to TiO_2 film resulted in an increase in the photocurrent density of the InP/TiO_2 electrodes. Later, the groups of Lian and Thomas, in separate studies, have performed detailed transient absorption study to investigate the exciton relaxation and dissociation dynamics of 2.6 nm and 3.6 nm sized InP QDs with the viologen (V^{2+}) family of electron acceptors (**Figure 4.3b,c**).[19,27] The delocalized 1S electron wavefunction outside the surface showed ultrafast charge separation (~7–14 ps) and a slow charge recombination process (ns–µs) in the InP QD:::dye donor:::acceptor system. The amplitude-average lifetime of the charge-separated state increases from ~45 ns to ~760 µs, with the InP QD size increasing from 2.6 nm to 3.6 nm. These studies showed that the prolonged trapping of charge carriers is characteristic of the environmentally benign InP QD-based electron transfer system.

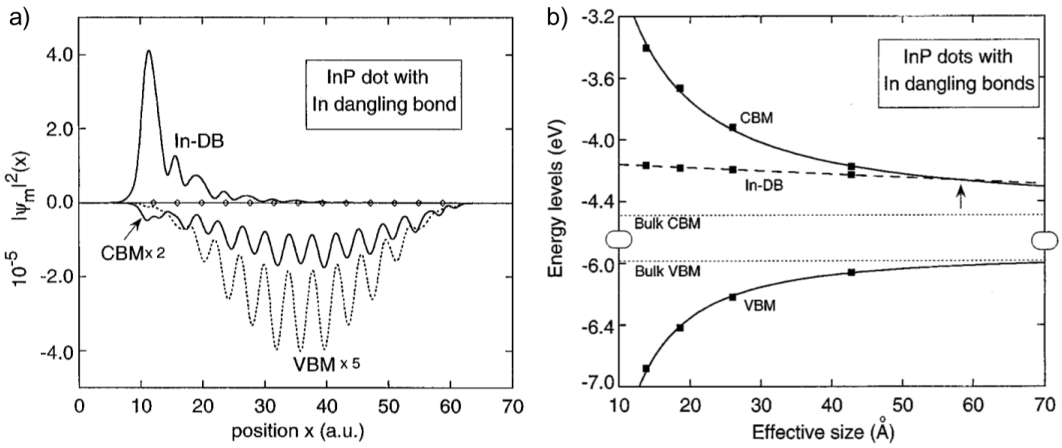

Figure 4.2 (a) Probability density of valence band maxima (VBM), conduction band minima (CBM) and surface states (indium dangling bond) for 2.6 nm sized InP QD along (110) direction. The VB and CB is more delocalized in the interior of QD, whereas the surface site is strongly localized. (b) Size-dependent variation in VB, CB, and surface trap state energies (related to In dangling bond). In contrast to the interior VB and CB energy level, the trap state energy level changes very little with decrease in size, causing an increase in the depth of traps from CB level. Reproduced with permission from references 15. Copyright 1997 American Physical Society.

Moreover, the size-dependent wave function engineering provides the concept of controlling the charge separation dynamics in QDs. Thus, it would be beneficial to explore the exciton dissociation dynamics with various sizes of InP nanocrystals (NCs) for optimizing the light-harvesting process for solar-energy conversion applications. Nevertheless, the photoinduced

electron transfer (PET) studies based on InP QDs are only limited to larger size region (~2.6–8.0 nm), as smaller InP QDs are difficult to synthesize.[19,23-28] Hence, investigating the charge transfer dynamics with smaller InP QD is becoming essential for both fundamental and applied perspective. Our recent development of stable and highly luminescent smaller InP QDs (<2 nm) paved the way for exploring the electron transfer dynamics with smaller InP QDs.[13,29] Furthermore, to the best of our knowledge, the use of electrostatic interactions to regulate the PET process with smaller InP QDs is not reported so far.

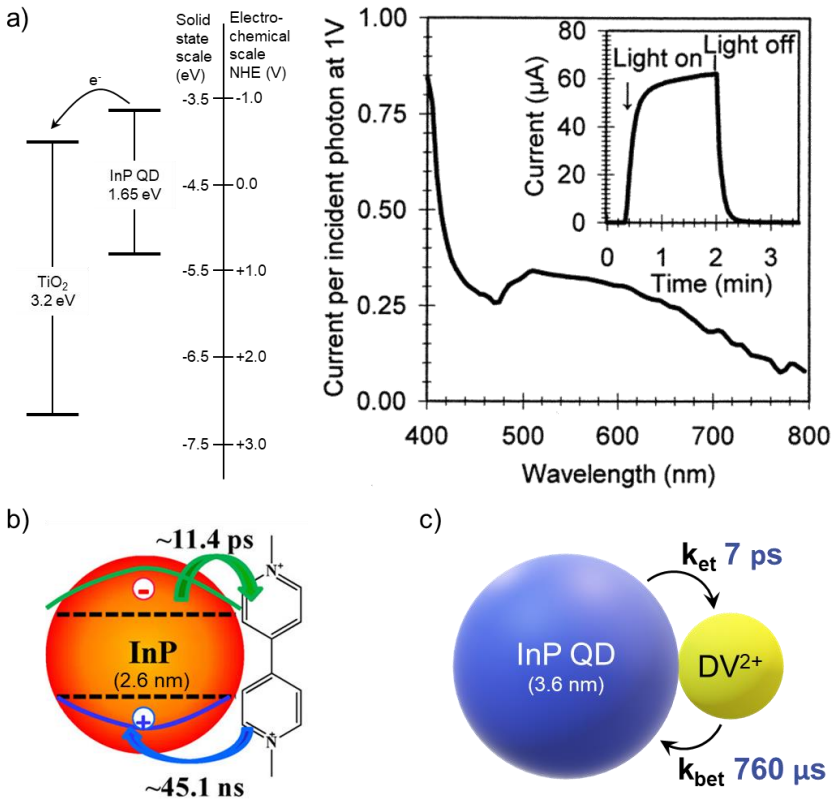

Figure 4.3 (a) Schematic band diagram of InP/TiO_2 heterostructure for charge transfer study. The band gap of InP QD was 1.65 eV and the electron affinity of TiO_2 particle was -4.05 eV. Photoconductivity action spectra of 8 μm thick 4.5 nm InP/TiO_2 film, at +1.0 V bias. Inset shows current ON-OFF cycle under 500 nm irradiation wavelength. Reproduced with permission from references 26. Copyright 1997 American Chemical Society. Charge transfer dynamics from (b) 2.6 nm and (c) 3.6 nm sized InP QD to viologen derivative. Reproduced with permission from references 27 and 19. Copyright 2013 and 2018 American Chemical Society.

Herein, we report the photoinduced electron transfer process from a wide band gap InP/ZnS QDs, emitting in pure-blue region, to methylene blue (MB) dye. A fine control over the nucleation and growth process achieved via the rational choice of zinc and sulphur precursor ratio, which enabled us to stabilize the InP QD below 2 nm size region with a strong band edge emission in the blue region. In general, the core/shell structure of InP/ZnS QD has the type-I

band alignment architecture. However, in our case, the blue InP core and the ZnS shell are believed to follow a quasi-type II band structure.[30] For instance, the photoexcited charge carriers will be delocalized throughout the QDs in the case of core only InP QDs. On the contrary, the presence of ZnS shell will confine the valence band (VB) hole within the InP-core, however, the low conduction band (CB) offset (<0.2 eV) will create the possibility of delocalization of the electron wavefunction into the ZnS shell. This gives rise to partial quasi type-II band alignment architecture.[30] Owing to the quasi type-II band structure of blue-InP core and ZnS shell materials, the current Chapter focuses on investigating the excited state charge transfer dynamics in blue-emitting InP/ZnS QDs. Here, an electrostatically assembled donor:::acceptor system between blue-emitting InP/ZnS QD and MB dye was chosen as a model system to study the excited state electron transfer dynamics. The negative surface of blue InP/ZnS QD ensures a strong electrostatic interaction with permanent positively charged MB dye. The surface-driven electrostatic aggregation was monitored through the UV-vis absorption spectroscopy. The band position calculation supports the thermodynamic feasibility of negative Gibbs free energy for the PET process ($\Delta G = -80$ kJ mol^{-1}). Systematic steady-state and time-resolved photoluminescence (PL) studies revealed the presence of PET process from QD to MB dye in [-] B-QD:::MB donor:::acceptor system. Further, solvent- and temperature-dependent PL investigations support the PET mechanism, that follows the Arrhenius equation of temperature variation. Control experiments prove the decisive role of electrostatic attraction in achieving an efficient PET in [-] B-QD:::MB donor:::acceptor system. Finally, the transient absorption (TA) studies were performed by examining the excited state absorption decay kinetics of [-] B-QDs and exciton depletion dynamics of $MB^{+\bullet}$ semiquinone and MB dye. In short, the developed [-] B-QD:::MB dye donor:::acceptor system participated in an efficient electron transfer process in water. The study is fundamentally intriguing with respect to the quasi type-II [-] B-QD, and, in principle, can find potential application in other light-harvesting applications including photocatalysis and photovoltaics.

4.3 Experimental Section

Details of synthesis procedures for B-QDs, their ligand exchange process, additional experimental methods, instrumental techniques, and formalism for the photoinduced electron transfer (PET) process were already discussed in **Chapter -2**. Water dispersed [-] B-InP/ZnS QDs is abbreviated as [-] B-QDs throughout this Chapter.

4.3.1 Photoinduced Electron Transfer Studies between Pure-Blue Emitting InP/ZnS QD and MB Dye:

The photoinduced electron transfer (PET) experiments were performed with negatively charged blue emitting [-] B-QD and MB dye in water. In a typical electron transfer experiment, a 2.6 mL aqueous solution of donor [-] B-QDs was prepared with an absorbance of ~0.05 at the first excitonic peak (~410 nm), corresponding to ~2 μM of QD concentration. Next, different aliquots of acceptor MB dye (1.5 μL of ~1 mM) were sequentially added to the solution of [-] B-QD, and the subsequent spectral changes were monitored using Shimadzu UV-3600 Plus absorption spectrophotometer and Fluorolog-3 spectrofluorometer (HORIBA Scientific) under 370 nm excitation. The corresponding PL lifetime experiments were carried out in a HORIBA DeltaFlex Time-Correlated Single Photon Counting system using a 370 nm Delta-Diode source. The fluorescence decay was deconvoluted using EZ software, and fit with exponential decay, minimizing the χ^2 values. Later, detailed transient absorption experiments were carried out in femtosecond to nanosecond (fs-ns) and nanosecond to microsecond (ns-μs) time windows to investigate the radical cation characteristics from electron acceptor MB dye.

4.3.2 Ultrafast Transient Absorption Spectroscopy:

Femtosecond laser pulses with a bandwidth of ~100 nm at an 80 MHz repetition rate were generated in the oscillator (Coherent Micra-5 Mode-locked Ti: sapphire Laser system) for the fs-ns transient absorption studies. The laser pulses were further amplified in the Coherent Legend Elite Ultrafast Amplifier Laser system to get ~30 fs/4 mJ with a repetition rate of 1 kHz and bandwidth of ~65 nm. The amplifier output was then directed to a BBO doubling crystal to generate 400 nm pump pulse. The white-light probe continuum (420–750 nm) was generated by focusing amplified output on a 2-mm-thick sapphire, which was then directed to a multichannel detector procured from Ultrafast Systems. The pump and probe pulses were temporally and spatially overlapped within the sample. This transient absorption setup has temporal resolution of close to 90 fs.

The transient absorption data in ns-μs time windows were collected using a commercial pump-probe system (Ultrafast system, EOS) using a 400 nm femtosecond pump pulse. The white light supercontinuum probe (360–1600 nm) was generated by focusing a Nd:YAG laser pulse into a photonic crystal fiber. The probe pulses were electronically synchronized with the femtosecond regenerative amplifier, and the pump-probe delay time was controlled by a digital

delay generator. The temporal resolution obtained in this transient set-up was 800 ps. All the TA measurements were performed in a 1 mm flow cuvette to minimise the chances of photodegradation of samples during measurements. Kinetics traces have been fitted using IGOR pro 5 software with programs for deconvoluting the time constant from IRF.

4.4 Results and Discussion

4.4.1 Synthesis and Characterization of B-InP/ZnS QD:

The current Chapter focuses on investigating the excited state electron transfer dynamics in blue-emitting InP/ZnS QDs. Owing to the quasi type-II band structure of core/shell InP/ZnS QDs, the photoexcited electrons are delocalized throughout the QD lattice.[30]Thus, the objective of the present work was to accomplish an efficient photoinduced electron transfer process in an electrostatically assembled donor:::acceptor system in water. To achieve the desired goal, a model QD-dye nanohybrid system was chosen as the case study. This demands a successful generation of water dispersed blue-emitting InP/ZnS QD, while maintaining their outstanding optoelectronic characteristics. Accordingly, the blue-emitting InP/ZnS QDs was synthesized, and ligand exchanged with 11-mercaptoundecanoic acid (MUA) ligands to yield water dispersed blue QDs ([-] B-QD). Details on the synthesis, place exchange process, characterization of QD are given in **Chapter – 3**. The [-] B-QDs showed negligible change in their photophysical properties after dispersing them in water. The developed highly luminescent, pure-blue emitting [-] B-QDs were used for further photoinduced electron transfer (PET) studies.

4.4.2 Light-Induced Electron Transfer Studies:

The successful generation of water-dispersed [-] B-QDs thrives on examining their ability in light harvesting studies as an efficient electron donor. As is widely accepted, the presence of strong interactions is essential to realize efficient light harvesting properties in donor–acceptor systems. Additionally, the photoinduced charge transfer process is governed by the energetics of donor and acceptor and must satisfy the thermodynamic criteria of negative Gibbs free energy ($-\Delta G$).[31-36] Thus, a rightful selection of a PET acceptor requires careful consideration of both surface-specific strong electrostatic interactions, and thermodynamically feasible energy level alignment. In the present study, methylene blue (MB) dye was chosen as the PET acceptor based on the thermodynamic feasibility criteria. Energy level calculations showed that

the electron transfer process was thermodynamically feasible from the CB of [-] B-QDs to the MB dye (ΔG = –80 kJ mol^{-1}) (**Figure 4.4** and **A4.1**). Furthermore, electrostatic forces were chosen as the tool to regulate the interaction between the donor and acceptor components in the QD-dye based PET system. The cationic MB dye exhibits two major absorption bands at 288 nm ($\pi \rightarrow \pi^*$) and 660 nm ($n \rightarrow \pi^*$) in dilute aqueous solution, along with a shoulder peak at 610 nm, corresponding to 0→1 vibronic transition (**Figure 4.4a**).[37,38] The absorption band position of MB dye at 660 nm is well within the "therapeutic window" of the skin (600–900 nm).[38-40] Following the photoexcitation process, the MB dye can effectively produce triplet species through intersystem crossing (ISC) (Φ_{ISC} = 0.52), which can further sensitize singlet oxygen species ($^1O_2$).[41] This spectroscopic aspect of MB dye is very advantageous for a range of biomedical applications notable in photodynamic therapy (PDT), which include treatment of tumors and cancerous tissue, as well as viruses, fungi, and bacteria.[38-41] One of the PDT mechanisms involves the reduced form of MB dye (MB radical), which directly oxidizes biological targets (DNA, proteins, lipids, and mitochondria).[39-41] Thus, studying the dynamics of the charge transfer process with the MB dye acceptor is fundamentally intriguing and believed to have direct implications from an applied perspective (PDT application). This justifies the model study's use of the [-] B-QD::::MB dye donor:::acceptor system. Accordingly, detailed photophysical studies based on both steady-state and time-resolved spectroscopic techniques were performed on the carrier dynamics of the [-] B-QD::::MB dye donor:::acceptor system.

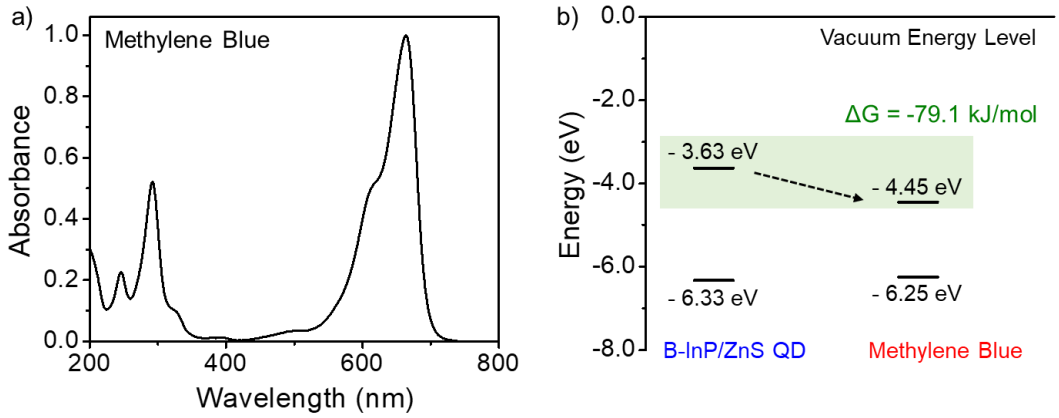

Figure 4.4 (a) UV-vis absorption spectra of MB dye in water. (b) Energy level alignment of [-] B-QDs and MB dye obtained from the cyclic voltammetry and absorption study, showing thermodynamically feasibility of the electron transfer process from QD to the dye (ΔG = –80 kJ mol^{-1}).

4.4.2.1. Steady-State and Time-Resolved Measurements

Analogous to the experimental discussion, systematic photophysical studies were conducted by titrating a 2.6 mL aqueous solution of ~2 µM [-] B-QDs with small aliquots of MB dye (1.5 µL of ~1 mM) (**Scheme 4.1**). The UV-vis absorption study showed the development of a scattering component at 800 nm with increasing the concentration of the MB dye, suggesting a strong complexation between oppositely charged [-] B-QD and MB dye (**Figure 4.5a**). Besides, a clear change in absorption structural features was observed for MB dye in the presence of QDs, with the lower-wavelength shoulder peak being more prominent (~610 nm) (**Figure 4.5a** and **A4.2a**). This indicates the aggregation of MB dyes on the surface of QDs. The electrostatic attraction emanating from the negative surface of QDs likely served as the driving force for this aggregation. Additionally, a hypsochromic shift of ~6 nm in the first excitonic peak of QD was observed (~410→404 nm), implying the localization of holes in QDs (*vide infra*).

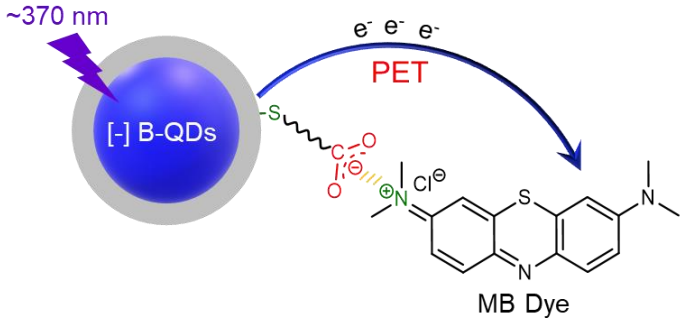

Scheme 4.1 Schematic representation of photoinduced electron transfer process from [-] B-QDs to electrostatically assembled MB organic dye.

The steady-state PL studies were performed by exciting the [+] B-QD:::MB dye donor:::acceptor system at 370 nm to acquire the wide-spectral range for analysis. PL kinetic studies revealed a steady and gradual decrease in the PL intensity for [-] B-QD with increasing the concentration of MB dye (**Figure 4.5b**). Interestingly, no noticeable fluorescence was acquired from MB dye in the [+] B-QD:::MB dye donor:::acceptor system. The relative PL of [-] B-QD, as well as the PL quenching efficiency, were saturated after the addition of ~5 µM of MB dye (**Figure A4.2b**). The PL quenching efficiency was estimated to be ~96 % ($E = 1 - I/I_0$, where I_0 and I are the PL intensities of donor [-] B-QD in the absence and presence of MB dye).[34] A mechanistic investigation of the PL quenching revealed a non-linear variation in the Stern-Vomer (SV) plot as a function of increasing concentration of MB dye (**Figure 4.5c**). This

suggests that the process of PL quenching involves both static and dynamic components. To get further insights into the quenching mechanism, the relative PL of [-] B-QD as a function of the concentration of MB dye was fitted with the standard quadratic Stern-Volmer equation and Perrin's formalism.[34] The result shows a strong deviation from conventional quenching formalism (**Figure A4.3**). This phenomenon is often encountered with micellar systems, which involve a complex combination of static and dynamic components, leading to a strong deviation from conventional SV analysis.[34,42-43] In particular, if either static or dynamic quenching efficiency is sufficiently low (i.e., $K_S[Q]<<1$ or $K_D[Q]<<1$), the modified SV equation exhibits an excellent fit with the relative PL of [-] B-QD in the [-] B-QD:::MB dye donor:::acceptor system ($I_0/\{I_0-I\}$ *vs* $1/[Q]$). According to the findings, the dynamic quenching constant was found to be ~8.6 times higher than the static quenching constant (**Figure A4.4**), (*vide infra*).

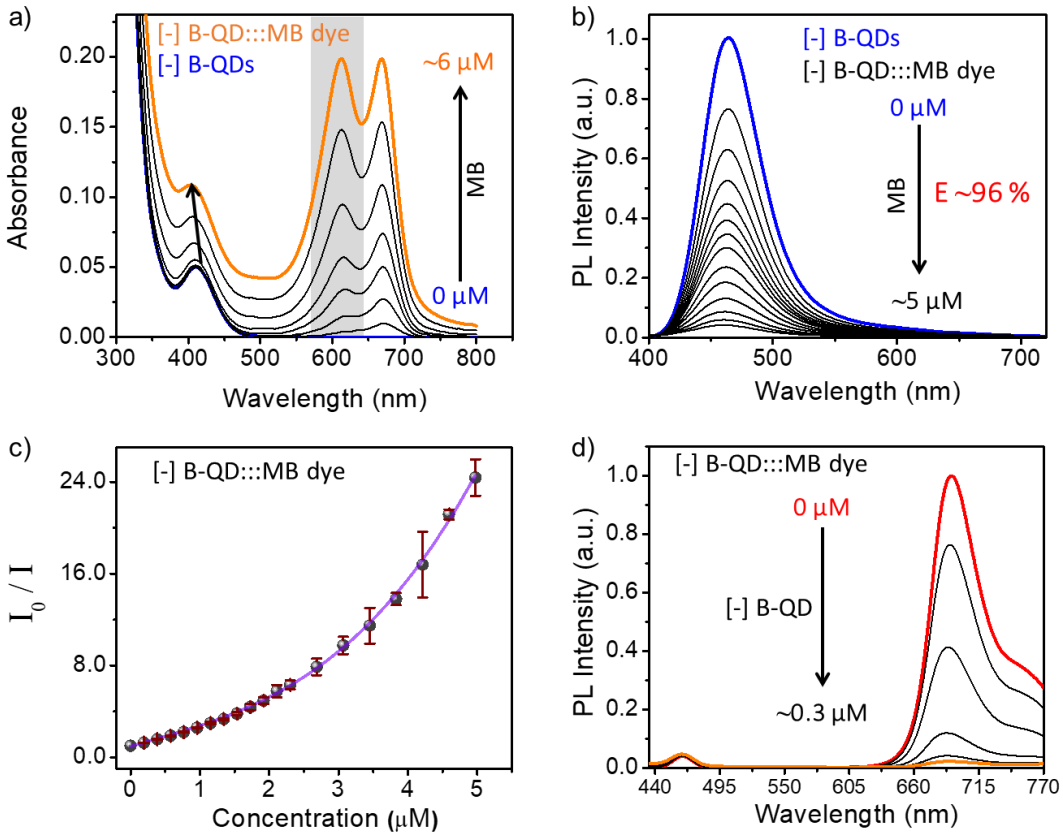

Figure. 4.5 Photoinduced electron transfer (PET) studies in [-] B-QD:::MB dye donor:::acceptor system. (a) UV-vis absorption and (b) PL spectral changes of donor [-] B-QDs upon successive addition of MB dye. The PL quenching efficiency was calculated to be ~96 %. (c) Corresponding Stern-Volmer plot showing the variation in relative PL of [-] B-QD as a function of increasing concentration of MB dye. PL studies were carried out with the excitation wavelength of 370 nm. (d) In an opposite addition experiment, a steady decrease in the PL intensity of ~6 µM of MB dye was observed upon addition of [-] B-QD (0.3 µM), suggesting the involvement of electron transfer process. Excitation wavelength was 400 nm.

Next, in a reverse addition experiment, PL spectra of acceptor MB dye (~6 µM) was monitored upon successive addition of [-] B-QDs (0.5 µL each of ~320 µM QD). A clear quenching in the PL intensity of MB dye was examined in the presence of [-] B-QDs (**Figure 4.5d**). This provided additional evidence of a possible excited state electron transfer process. In brief, the decrease in PL intensity of both [-] B-QD and MB dye, and the hypsochromic shift in the QD absorption peak indicate the presence of an electron transfer process from [-] B-QD to MB dye. Photoconductivity study under ON-OFF irradiation cycle also support the steady-state observation of charge separation process (**Figure 4.6**).

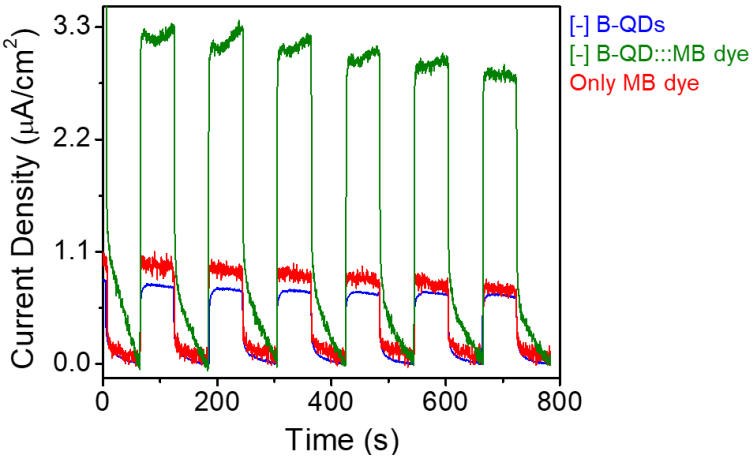

Figure 4.6 Photocurrent measurement of [-] B-QD, [-] B-QD:::MB dye donor:::acceptor system, and MB dye under light ON-OFF condition, with ~365 nm irradiation. The enhanced photocurrent in donor:::acceptor assembly shows a clear indication of the charge separation.

The dynamics of the PET process in the [-] B-QD:::MB dye donor:::acceptor system was further monitored with detailed photoluminescence excitation (PLE) studies and time-resolved PL measurements. Interestingly, the PLE spectra collected at the emission position of MB dye (~780 nm) exhibit two important features (**Figure 4.7a**). A gradual decrease in PLE intensity corresponding to the QD absorption band, indicate the dissociation of excitons after photoexcitation of [-] B-QD. Alongside, a concomitant growth in the electronic absorption band position for MB dye was observed with each addition of MB dye to the solution of [-] B-QD. Hence, the photoexcitation of MB dye does not drive any charge separation process, proving that the photoexcited [-] B-QD is the electron donor and MB is the electron acceptor. This was further supported by the time-resolved PL decay kinetics, where a clear quenching in the PL lifetime of donor [-] B-QD was observed in the presence of acceptor MB dye (**Figure 4.7b**). The average lifetime of [-] B-QD quenched from 216 ns to 90 ns, with a corresponding PET efficiency of ~60 % (**Table 4.1**). Likewise, PLE spectra collected at the emission maxima

of [-] B-QD (~462 nm) showed a close agreement with steady-state and time-resolved measurements (**Figure A4.5a**). One point to be emphasized here is that, in contrast to the [-] B-QD:::MB dye donor:::acceptor system, only MB dye exhibited higher PLE intensity. This can be attributed to the strong aggregation effect of MB dye, as evidenced in absorption studies as well (orange and red trace in **Figure 4.7a**). As the aggregation of MB causes a decrease in the PL intensity, the counterintuitive changes in PLE and absorption studies clearly suggest the existence of two separate forms of MB dye in [-] B-QD:::MB dye complex assembly. The overall observation can be visualized with a basic model of partitioning of quenchers at the surface of QDs following the Poisson statistics (**Figure A4.5c**). To illustrate further, the acceptor MB dye will get distributed between the fixed layer (at surface) and diffuse layer (in bulk), thus contributing to the static and dynamic quenching events, respectively.[43] This was supported by the Stern-Volmer (SV) plot constructed from the PL lifetime quenching experiment, where a negligible change in relative PL lifetime of [-] B-QD was observed at low concentration of MB dye (up to 1:1 ratio of donor: acceptor).

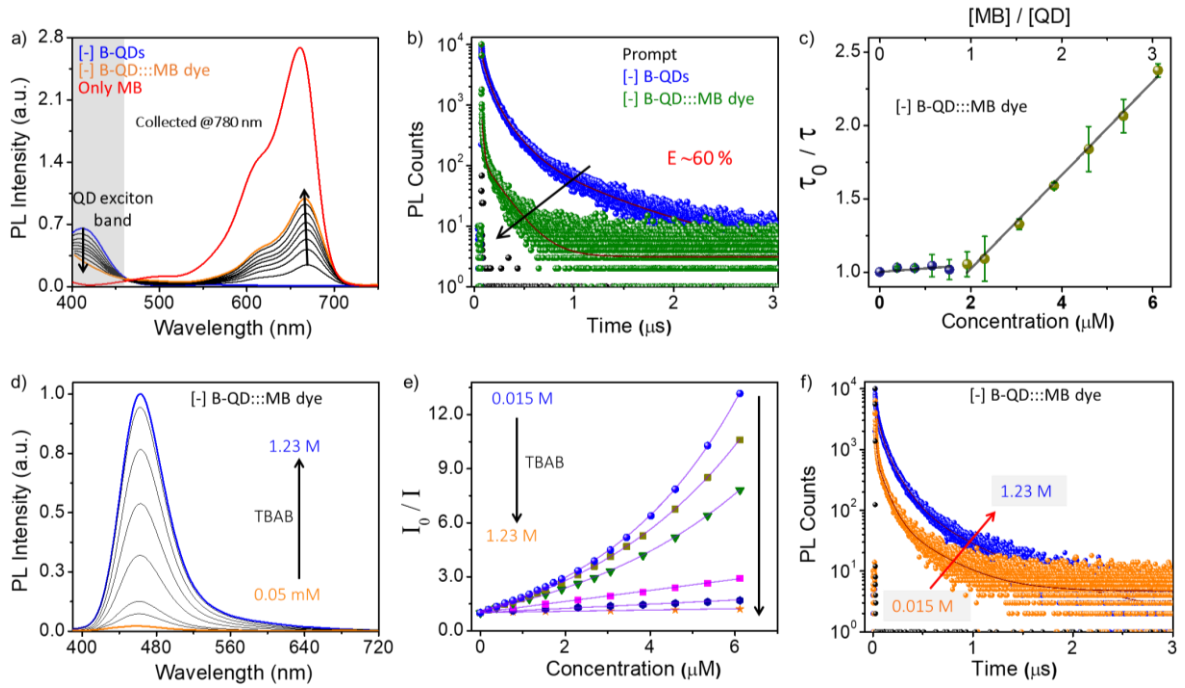

Figure. 4.7 Steady-state and time-resolved PET studies in [-] B-QD:::MB dye donor:::acceptor system. (a) Photoluminescence excitation (PLE) spectra of [-] B-QD:::MB dye donor:::acceptor system, with increasing concentration of MB dye, collected at the emission maxima of MB dye (~780 nm). The red trace is corresponding to PLE spectrum for only MB dye. (b) PL decay kinetics of [-] B-QD in absence (blue) and presence (olive) of MB dye. The PET efficiency was calculated to be ~60 %. (c) Stern-Volmer plot constructed from PL lifetime indicate the layered arrangement of acceptor-MB dye molecules in fixed and diffuse layer surrounding the [-] B-QDs. (d-f) Proof of electrostatically driven PET process in [-] B-QD:::MB dye donor:::acceptor system. (d) The revival of PL intensity of [-] B-QD:::MB dye donor:::acceptor system upon successive addition of TBAB molecules. (e) The

corresponding Stern-Volmer plot at different ionic strengths. (f) PL lifetime decay of [-] B-QD:::MB dye donor:::acceptor system as function of ionic strengths.

Conversely, at higher concentration of MB dye (from 1:1 to 1:3 of donor: acceptor), a linear decrease in the PL lifetime of [-] B-QD was observed with a quenching efficiency of ~60 % (**Figure 4.7c** and **Table A4.1**). Zeta potential study with varying concentrations of MB dye further supports the formation of bilayers of acceptor MB dyes over [-] B-QDs (**Figure A4.6b**). The negative zeta potential of [-] B-QDs gradually decreases up to 1:1 ratio of QD:MB dye, beyond which there were no noticeable changes. Thus, a fixed layer is formed with initial addition of MB dye (up to 1:1 ratio) and subsequent additions remain in the diffuse layer. The prominent role of electrostatics in achieving such strong complexation and multilayer assembly in [-] B-QD:::MB dye donor:::acceptor system was verified with varying electrostatic potential at the interface of QD and water.[44] Here, the tetrabutylammonium bromide (TBAB) molecule was added to regulate the surface potential of QDs. The ionic strength of the medium rises as the concentration of TBA^+ and Br^- ions increase. Additionally, the aliphatic functional ground of the TBA^+ ion screens the negative surface charges of [-] B-QD and reduces the access of MB dyes towards the QD surface. Thus, increasing the concertation of TBAB molecules is expected to weaken the electrostatics and reduce the electron transfer process. Accordingly, PL quenching experiments were performed with increasing concertation of TBA ions in the [-] B-QD:::MB dye donor:::acceptor system. As predicted, the PL intensity and PL lifetime revived with the addition of the TBA ion in the [-] B-QD:::MB dye donor:::acceptor assembly (ionic strength increased from 0.05 mM to 1.23 M) (**Figure 4.7d-f**). Here, the dissociation of the [-] B-QD:::MB dye donor:::acceptor complex was accompanied by the reduction in PET process, and spectral changes were recovered. The PL lifetime increased to 175 ns (**Table A4.2**). The corresponding SV plot became more linear as the ionic strength increased from 0.05 mM to 1.23 M (**Figure 4.6e**). Thus, all the steady-state and time-resolved measurements confirm the photoinduced electron transfer process from [-] B-QD to MB dye in the electrostatically bounded [-] B-QD:::MB dye donor:::acceptor system.

Table 4.1 PL decay analysis of [-] B-QD and [-] B-QD:::MB dye donor:::acceptor assembly, in a time window of 3.2 μs, collected at 462 nm.

System	τ_1 (ns)	α_1	τ_2 (ns)	α_2	τ_3 (ns)	α_3	τ_4 (ns)	α_4	$\tau_{avg.}$ (ns)	χ^2
[-] B-QDs	8.47	0.28	52.61	0.38	148.04	0.30	534.91	0.04	216.53	1.03
[-] B-QD:::MB dye	0.49	0.96	4.08	0.02	19.78	0.01	136.13	0.01	89.90	1.04

4.4.2.2. Polarity- and Temperature-Dependent Studies

In accordance with the Eyring formalism, the PET process involves the transfer of electron from the donor to the acceptor moiety via the formation of a transient charge transfer complex $[D^+:::A^-]^*$ in a photoexcited donor:::acceptor assembly (see the details in **Chapter–2**).[31-34] This essentially means that the process of PET will be influenced by the dielectric constant and temperature of the medium. The formed charge transfer complex $[D^+:::A^-]^*$ will be more stabilized in a higher dielectric medium, whereas, a higher temperature will aid in crossing the activation barrier of the transition-state. Specifically, the PET process will be more efficient in the polar medium and at higher temperatures. Accordingly, PL kinetic studies were carried out with varying solvent polarity and temperature to study the underlying mechanism of the PET process in the [-] B-QD:::MB dye donor:::acceptor system.

A varying ratio (v/v) of water and N,N-dimethylformamide (DMF) mixture was used to tune the dielectric constant of the medium (ε_m) for the polarity-dependent study (ε of water and DMF = 78 and 40 at 298 K, respectively).[45] The PET efficiency was higher in higher dielectric medium (water), which gradually decreased with lowering of the solvent polarity. PL quenching efficiency drops from ~95% to 20 % on lowering the dielectric from ~80 (water) to ~42 (0.5:0.95 v/v water: DMF). Accordingly, the slope of SV plot was higher for the PET process in water compared to that in 0.5:0.95 v/v water:DMF mixture (**Figure 4.8a**). A similar trend was observed in PL lifetime studies as well. For instance, both the efficiency and rate of electron transfer were higher in water (E ~60 % and k_{PET} ~ 6.50 μs^{-1} in water) compared to water: DMF mixture (E ~1 % and k_{PET} ~0.02 μs^{-1} in 0.5:0.95 v/v water: DMF) (**Figures 4.8b** and **A4.6** and **Table A4.3**).

An increase in the temperature of the medium resulted in an enhancement in the PET efficiency in the [-] B-QD:::MB dye donor:::acceptor system. For instance, the dynamic quenching constant K_D obtained from the intercept-to-slope ratio in the modified SV plot decreases from 1.29 μM^{-1} to 1.06 μM^{-1}, as the reaction temperature was lowered from 318 K to 278 K (**Figure 4.8c**). Further, the temperature-dependent modified SV analysis helped to deconvolute the static (K_S) and dynamic (K_D) components in the PL quenching: K_D and K_S ~1.26 x 10^6 M^{-1} and ~1.47 x 10^5 M^{-1}, respectively. Alongside, the rate of the PET process (k_{PET}) increased from 6.35 μs^{-1} to 6.68 μs^{-1}, as the temperature was increased from 278 K to 318 K. The logarithm of the PET rate constant obtained from lifetime PL quenching studies shows a linear variation with the temperature, validating the Arrhenius dependence of k_{PET} on temperature for the electron

transfer process (**Figure 4.8d**).[31-34] The activation energy for the PET process in the [-] B-QD:::MB dye donor:::acceptor system was estimated to be ~3 kJ/mol. Thus, both the solvent polarity and temperature-dependent PL quenching studies confirm the involvement of PET process in the [-] B-QD:::MB dye donor:::acceptor system. Various photoinduced electron transfer parameters associated with the [-] B-QD:::MB dye donor:::acceptor system are summarised in **Table 4.2**.

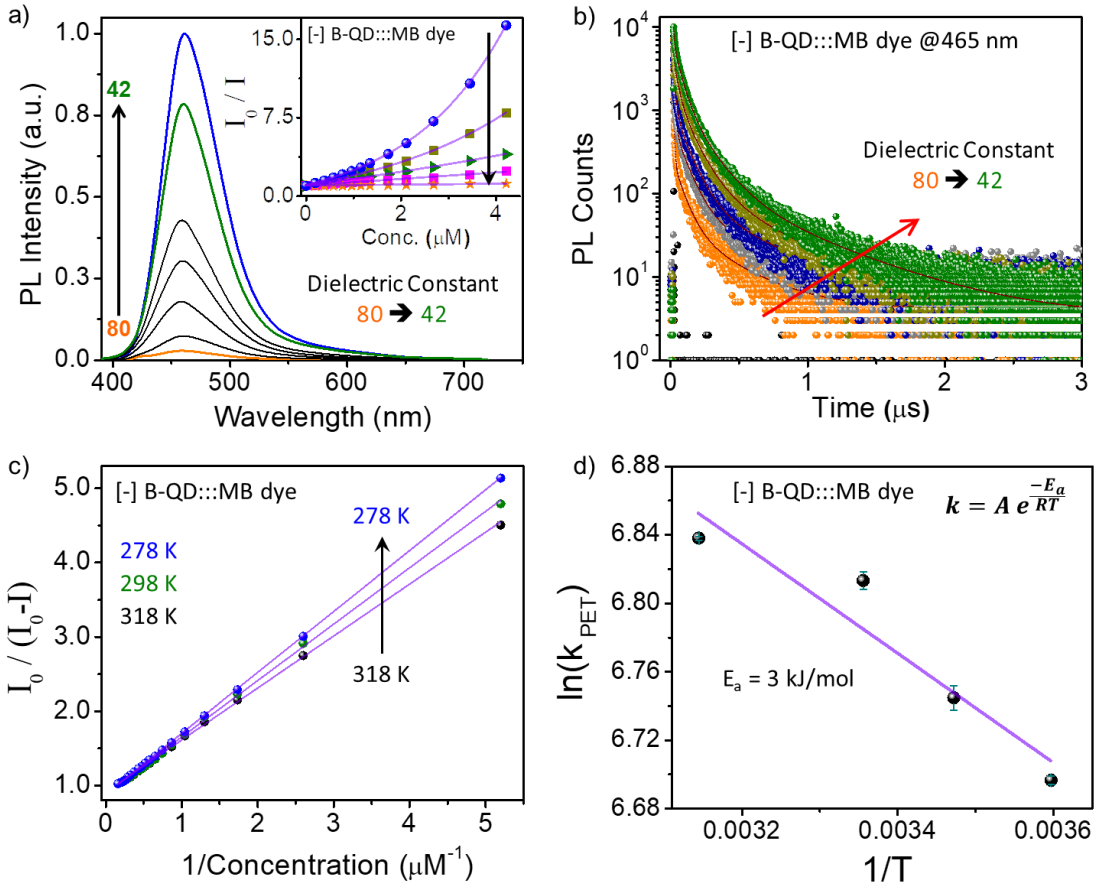

Figure. 4.8 Polarity- and temperature-dependent PL quenching studies in [-] B-QD:::MB dye donor:::acceptor system. (a) PL spectral changes and (b) PL decay profiles of [-] B-QD:::MB dye donor:::acceptor system with increasing the concentration of DMF in water. The dielectric constant of the medium decreases with increase in the DMF percentage in water. The inset of (a) shows the SV plot at different DMF: water mixture. A larger slope in the SV plot and higher PL quenching at higher dielectric constant indicate the role of PET process in the quenching process. (c) Modified SV plot of the [-] B-QD:::MB dye donor:::acceptor system at various temperatures ranging from 318 K to 278 K. The slope of the SV plot ($1/(K_D+K_S)$) increases as the temperature decreases. (d) The plot of $\ln(k_{PET})$ *vs* 1/T validates the Arrhenius dependence of k_{PET} on temperature. The activation energy for the PET process was calculated to be ~3 kJ/mol.

Table 4.2 Photoinduced electron transfer parameter for [-] B-QD:::MB dye donor:::acceptor system.

System	E (%)	K_D (M^{-1})	K_S (M^{-1})	k_{PET} (s^{-1})	E_a (kJ/mol)
[-] B-QD:::MB dye	60	1.26×10^6	$\sim 1.47 \times 10^5$	6.50×10^6	~3

4.4.2.3. Transient-Absorption Studies

The ultimate proof for light-induced electron transfer in electrostatically assembled [-] B-QD:::MB dye donor:::acceptor system was obtained from ultrafast absorption studies (TA studies were done in collaboration with Mr. Kishan K. Yadav and Prof. Jyotishman Dasgupta at TIFR Mumbai). The dynamics of the PET process was monitored in two-time windows, ps-ns and ns-µs, using the pump-probe transient absorption (TA) spectroscopy, with a 400 nm pump excitation. The TA spectrum for only [-] B-QD is dominated by the stimulated emission (~400–480 nm) and excited state absorption (~480–800 nm) features at all time delays (fs-µs) (**Figure 4.9a** and **A4.7**). In contrast, in the presence of MB dye, the stimulated emission (SM) of [-] B-QD was decreased, along with a concomitant formation of a new excited state absorption (ESA) feature in the range of 420–550 nm (**Figure 4.9a,c**). It is to be noted that this ESA in the range of 420–550 nm was absent for only [-] B-QD as well as only MB dye. Further, a long-lived ground state blech (GSB) of MB dye was observed in the presence of [-] B-QD. On contrary, the GSB in only MB depleted within a time delay of 2 ns (**Figure 4.9b,c**). This implies the presence of long-lived electrons in the excited state of MB dye in the [-] B-QD:::MB dye donor:::acceptor system. At lower time delay (200 fs – 30 ps), the GSB of MB dye was less prominent in the [-] B-QD:::MB dye donor:::acceptor system because they overlapped with the much stronger excited state absorption of the [-] B-QD. Later, at longer time delay (1 ns – 5 µs) time delay, the GSB of MB was distinguishable and had minimal interference from the ESA of [-] B-QDs.

In short, two important features were observed in the TA spectroscopy of the [-] B-QD:::MB dye donor:::acceptor system: (i) a growth in the range of 420–550 nm within a time scale of ~5 µs and (ii) a long-lived GSB signal corresponding to MB dye in 550-720 nm region. In accordance with the literature, the ESA features observed in the range of 420–550 nm can be attributed to the reduced form of MB dye ($MB^{+\bullet}$ semiquinone, 430-490 nm).[46-48] **Figure 4.10a,b** compares the single point TA decay kinetics in fs-ns time window at two different wavelengths: (i) at the ESA of QD (525 nm) in only [-] B-QDs and [-] B-QD:::MB dye

donor:::acceptor system and (ii) at the GSB of MB dye (595 nm) in only MB dye and [-] B-QD:::MB dye donor:::acceptor system.

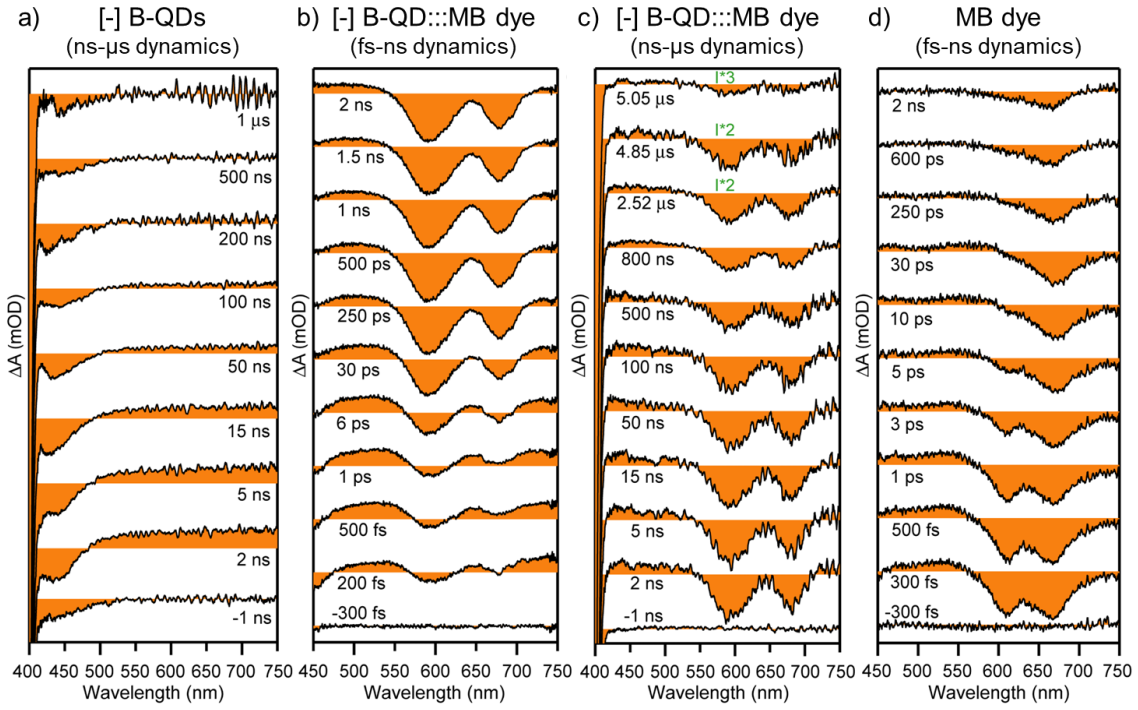

Figure. 4.9 Pump-probe transient absorption spectroscopy studies. Spectral evolution for (a) only [-] B-QDs (ns-µs time scale), (b and c) [-] B-QD:::MB dye donor:::acceptor system in (b) fs-ns and (c) ns-µs time scale), and (d) only MB dye (fs-ns time scale). Appearance of a new EAS feature in the range of 420–550 nm region in [-] B-QD:::MB dye assembly confirms the formation of $MB^{+\cdot}$ semiquinone.

A fast decay in ESA was observed in the [-] B-QD:::MB dye donor:::acceptor system compared to only [-] B-QD (**Figure 4.10a**). On the other hand, GSB of MB dye sustained for a longer time in the presence of [-] B-QD (**Figure 4.10b**). As mentioned before, both [-] B-QD and MB+• semiquinone contributes to the ESA signal observed in the range of 420–550 nm. Hence, it will be difficult to find the lifetime component MB+• semiquinone from **Figure 4.10a**. Consequently, the single point TA decay kinetic analysis was done on the ESA observed in the longer time window (ns-µs) to evaluate the time constant for the PET process. The logic being that the contribution from the only the [-] B-QD in the ESA band observed between 420–550 nm will be negligible in the longer time window (the ESA signal from only the [-] B-QD will decay completely within ~100 ns. **Figure 4.9a**). The best fit for the ESA decay kinetics for [-] B-QD and [-] B-QD:::MB dye donor:::acceptor systems is shown in **Figure 4.10c,d**; from where the average lifetime for $MB^{+\bullet}$ semiquinone was estimated to be ~1.8 µs. Thus, the spectral signatures of $MB^{+\bullet}$ semiquinone re-confirm the presence of a photoinduced electron

transfer process from [-] B-QD to MB dye in the electrostatically bound [-] B-QD:::MB dye donor:::acceptor system.

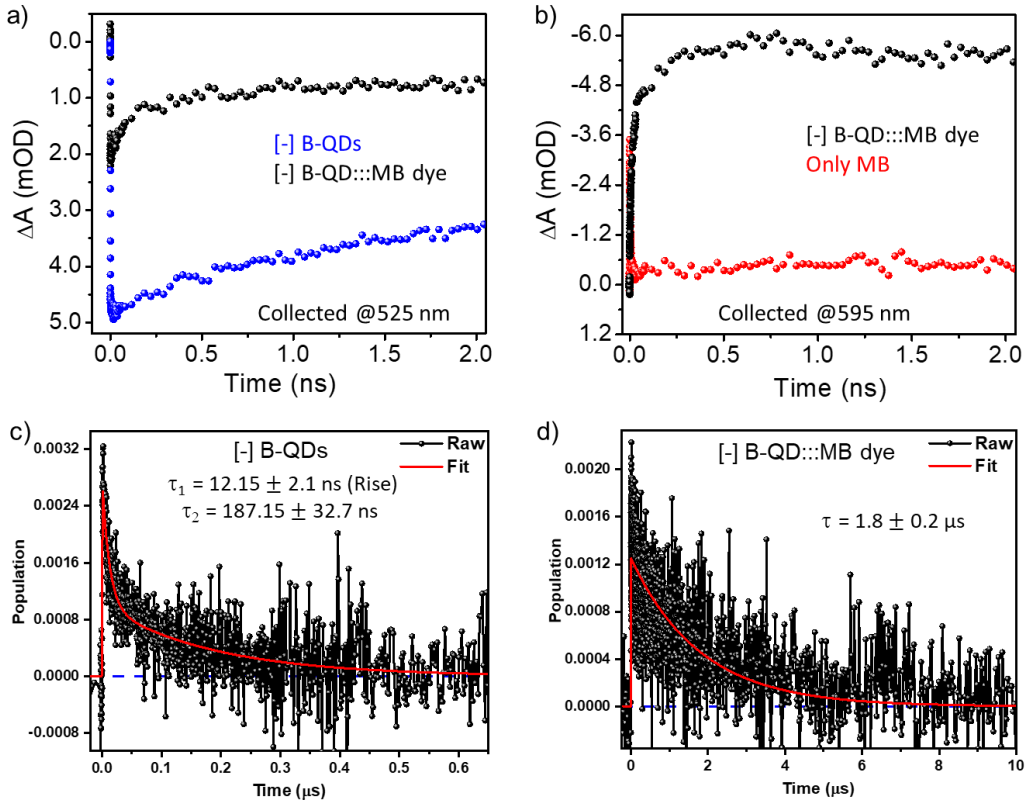

Figure. 4.10 Single point TA decay kinetic study. (a) The excited state absorption (ESA) of [-] B-QD in absence (blue) and presence (red) MB dye, collected at 525 nm. (b) Ground state blech (GSB) of MB dye in absence (black) and presence (red) of [-] B-QD, collected at 595 nm. A clear decrease in the ESA signal of [-] B-QD and delay in the GSB of MB dye was observed in [-] B-QD:::MB dye donor:::acceptor system. Single point decay kinetics of (c) [-] B-QDs and (d) [-] B-QD:::MB dye donor:::acceptor system at 450 nm (ESA position for $MB^{+\cdot}$ semiquinone), generated from the microsecond TA kinetics spectra. The average lifetime of the charge separated state was calculated to be ~1.8 μs.

4.5. Conclusions

The current study prove the ability of the pure-blue emitting InP/ZnS QDs to participate in an efficient PET process, and that too in water. The surface of QD was appropriately functionalized with charge ligands to ensure aqueous dispersion to form an electrostatically assembled [-] B-QD:::MB dye donor:::acceptor system. Using both steady-state and time-resolved spectroscopic measurements, the exciton dynamics in [-] B-QD:::MB dye donor:::acceptor system was monitored, revealing the involvement of an electron transfer process from [-] B-QD to [+] MB dye. Solvent polarity and temperature-dependent PL quenching studies further indicated the process of PET mechanism. The logarithm of the PET

rate constant varies inversely with temperature, thus following the Arrhenius dependence of rate constant on temperature for the electron transfer process. The efficiency of the PET process was estimated to be ~60 %. The mode of interaction responsible for the efficient electron transfer process was confirmed to be electrostatic attraction by performing adequate control experiments in the presence of surfactants. Here, the screening of the negative surface charge on QDs and a rise in the ionic strength of the medium weaken the donor:::acceptor complexation and turn off the PET process. Finally, TA studies confirm the formation of $MB^{+\bullet}$ semiquinone in the photoexcited [-] B-QD:::MB dye donor:::acceptor system. Further, the single point TA decay kinetic analysis revealed (i) a fast decay kinetics for the ESA of [-] B-QDs, and (ii) a long-lived GSB of MB dye in the donor:::acceptor system. Despite being a core-shell geometry, the quasi type-II band structure of B-InP/ZnS QDs paved the way for an efficient PET process in the present study.

In conclusion, **Chapters 3** and **4** conclusively prove the ability of newly synthesised pure-blue emitting InP/ZnS QDs to participate in efficient energy and electron transfer processes, which could find applications in other light harvesting studies such as sensing, photocatalysis, photovoltaics, etc.

4.6 References

(1) Brus, L. E. Electron–Electron and Electron-Hole Interactions in Small Semiconductor Crystallites: The Size Dependence of the Lowest Excited Electronic State. *J. Chem. Phys.* **1984**, *80*, 4403–4409.

(2) Heath, J. R. Covalency in Semiconductor Quantum Dots. *Chem. Soc. Rev.* **1998**, *27*, 65–71.

(3) Tamang, S.; Lincheneau, C.; Hermans, Y.; Jeong, S.; Reiss, P. Chemistry of InP Nanocrystal Syntheses. *Chem. Mater.* **2016**, *28*, 2491–2506.

(4) Kim, Y.; Chang, J. H.; Choi, H.; Kim, Y.-H.; Bae, W. K.; Jeong, S. III–V Colloidal Nanocrystals: Control of Covalent Surfaces. *Chem. Sci.* **2020**, *11*, 913–922.

(5) Jang, D.; Han, Y.; Baek, S.; Kim, J. Theoretical Comparison of the Energies and Wave Functions of the Electron and Hole States Between CdSe- and InP-Based Core/Shell/Shell Quantum Dots: Effect of the Bandgap Energy of the Core Material on the Emission Spectrum. *Opt. Mater. Express* **2019**, *9*, 1257–1270.

(6) Pelatt, B. D.; Ravichandran, R.; Wager, J. F.; Keszler, D. A. Atomic Solid State Energy Scale. *J. Am. Chem. Soc.* **2011**, *133*, 16852–16860.

(7) Schaller, R. D.; Pietryga, J, M.; Klimov, V. I. Carrier Multiplication in InAs Nanocrystal Quantum Dots with an Onset Defined by the Energy Conservation Limit. *Nano Lett.* **2007**, *7*, 3469–3476.

(8) Chang, A. Y.; Liu, W.; Talapin, D. V.; Schaller, R. D. Carrier Dynamics in Highly Quantum-Confined, Colloidal Indium Antimonide Nanocrystals. *ACS Nano* **2014**, *8*, 8513–8519.

(9) Reiss, P.; Carrière, M.; Lincheneau, C.; Vaure, L.; Tamang, S. Synthesis of Semiconductor Nanocrystals, Focusing on Nontoxic and Earth-Abundant Materials. *Chem. Rev.* **2016**, *116*, 10731–10819.

(10) Devatha, D.; Roy, P.; Rao, A.; Roy, A.; Pillai, P. P. Multicolor Luminescent Patterning via Photoregulation of Electron and Energy Transfer Processes in Quantum Dots. *J. Phys. Chem. Lett.* **2020**, *11*, 4099–4106.

(11) Jalali, H. B.; Trizio, L. D.; Manna, L.; Stasio, F. D. Indium Arsenide Quantum Dots: An Alternative to Lead-Based Infrared Emitting Nanomaterials. *Chem. Soc. Rev.* **2022**, *51*, 9861–9881.

(12) Saeboe, A. M.; Nikiforov, A. Y.; Toufanian, R.; Kays, J. C.; Chern, M.; Casas, J. P.; Han, K.; Piryatinski, A.; Jones, D.; Dennis, A. M. Extending the Near-Infrared Emission Range of Indium Phosphide Quantum Dots for Multiplexed in Vivo Imaging. *Nano Lett.* **2021**, *21*, 3271–3279.

(13) Roy, P.; Virmania, M.; Pillai, P. P. Blue-emitting InP Quantum Dots Participate in an Efficient Resonance Energy Transfer Process in Water. *Chem. Sci.* **2023**, *14*, 5167–5176.

(14) Kim, S.-H.; Wolters, R. H.; Heath, J. R. Photophysics of Size-Selected InP Nanocrystals: Exciton Recombination Kinetics. *J. Chem. Phys.* **1996**, *105*, 7957–7963.

(15) Fu, H.; Zunger, A. InP quantum dots: Electronic Structure, Surface Effects, and the Redshifted Emission. *Phys. Rev. B* **1997**, *56*, 1496–1508.

(16) Xie, R.; Battaglia, D.; Peng, X. Colloidal InP Nanocrystals as Efficient Emitters Covering Blue to Near-Infrared. *J. Am. Chem. Soc.* **2007**, *129*, 15432–15433.

(17) Tessier, M. D.; Dupont, D.; De Nolf, K.; De Roo, J.; Hens, Z. Economic and Size-Tunable Synthesis of InP/ZnE (E = S, Se) Colloidal Quantum Dots. *Chem. Mater.* **2015**, *27*, 4893–4898.

(18) Devatha, G.; Roy, S.; Rao, A.; Mallick, A.; Basu, S.; Pillai, P. P. Electrostatically Driven Resonance Energy Transfer in “Cationic” Biocompatible Indium Phosphide Quantum

Dots. *Chem. Sci.* **2017**, *8*, 3879–3884.

(19) Thomas, A.; Sandeep, K.; Somasundaran, S. M.; Thomas, K. G. How Trap States Affect Charge Carrier Dynamics of CdSe and InP Quantum Dots: Visualization through Complexation with Viologen. *ACS Energy Lett.* **2018**, *3*, 2368–2375.

(20) Won, Y.-H.; Cho, O.; Kim, T.; Chung, D.-Y.; Kim, T.; Chung, H.; Jang, H.; Lee, J.; Kim, D.; Jang, E. Highly Efficient and Stable InP/ZnSe/ZnS Quantum Dot Light-Emitting Diodes. *Nature* **2019**, *575*, 634–638.

(21) Lasheen, D.; Fathy, M.; Othman, H. A.; Elkholy, M. M. Kashyout, A. E. H. B. Synthesis and Characterization of InP Quantum Dots for Photovoltaics Applications. *J. Mater. Sci.: Mater. Electron. 2023*, *34*, 843.

(22) Click, S. M.; Rosenthal, S. J. Synthesis, Surface Chemistry, and Fluorescent Properties of InP Quantum Dots. *Chem. Mater.* **2023**, *35*, 822–836.

(23) Chung, H.; Cho, K.-S.; Koh, W.-K.; Kim, D.; Kim, J. Composition-Dependent Trap Distributions in CdSe and InP Quantum Dots Probed Using Photoluminescence Blinking Dynamics. *Nanoscale* **2016**, *8*, 14109–14116.

(24) Rodosthenous, P.; Gómez-Campos, F. M.; Califano, M. Tuning the Radiative Lifetime in InP Colloidal Quantum Dots by Controlling the Surface Stoichiometry. *J. Phys. Chem. Lett.* **2020**, *11*, 10124–10130.

(25) Vishnu, E. K.; Thomas, E. M.; Prasad, L.; Thomas, K. G. Trap States in Semiconductor Quantum Dots: Friends or Foes. *J. Phys. Chem. C* **2024**, *128*, 4373–4382.

(26) Zaban, A.; Mićić, O. I.; Gregg, B. A.; Nozik, A. J. Photosensitization of Nanoporous TiO2 Electrodes with InP Quantum Dots. *Langmuir* **1998**, *14*, 3153–3156.

(27) Wu, K.; Song, N.; Liu, Z.; Zhu, H.; Rodríguez-Córdoba, W.; Lian, T. Interfacial Charge Separation and Recombination in InP and Quasi-Type II InP/CdS Core/Shell Quantum Dot-Molecular Acceptor Complexes. *J. Phys. Chem. A* **2013**, *117*, 7561–7570.

(28) Blackburn, J. L.; Ellingson, R. J.; Mićić, O. I.; Nozik, A. J. Electron Relaxation in Colloidal InP Quantum Dots with Photogenerated Excitons or Chemically Injected Electrons. *J. Phys. Chem. B* **2003**, *107*, 102–109.

(29) Zhang, W.; Ding, S.; Zhuang, W.; Wu, D.; Liu, P.; Qu, X.; Liu, H.; Yang, H.; Wu, Z.; Wang, K.; Sun, X. W. InP/ZnS/ZnS Core/Shell Blue Quantum Dots for Efficient Light-Emitting Diodes. *Adv. Funct. Mater.* **2020**, *30*, 2005303.

(30) Rakshit, S.; Cohen, B.; Gutiérrez, M.; El-Ballouli, A. O. Douhal, A. Deep Blue and Highly Emissive ZnS-Passivated InP QDs: Facile Synthesis, Characterization, and Deciphering of Their Ultrafast-to-Slow Photodynamics. *ACS Appl. Mater. Interfaces*

2023, *15*, 3099–3111.

(31) Marcus, R. A. On the Theory of Oxidation-Reduction Reactions Involving Electron Transfer. I. *J. Chem. Phys.* **1956**, *24*, 966–978.

(32) Huber. R. A Structural Basis of Light Energy and Electron Transfer in Biology (Nobel Lecture). *Angew. Chem. Int. Ed. Engl.* **1989,** *28*, 848–869**.**

(33) Marcus, R. A. Electron Transfer Reactions in Chemistry: Theory and Experiment (Nobel Lecture). *Angew. Chem. Int. Ed. Engl.* **1993**, *32*, 1111–1121.

(34) Lakowicz, J. R. *Principles of Fluorescence Spectroscopy*, 3rd ed.; Springer: New York, 1999.

(35) Huang, J.; Huang, Z.; Yang, Y.; Zhu, H.; Lian, T. Multiple Exciton Dissociation in CdSe Quantum Dots by Ultrafast Electron Transfer to Adsorbed Methylene Blue. *J. Am. Chem. Soc.* **2010**, *132*, 4858–4864.

(36) Sekhar M. C.; Samanta, A. Ultrafast Transient Absorption Study of the Nature of Interaction between Oppositely Charged Photoexcited CdTe Quantum Dots and Cresyl Violet. *J. Phys. Chem. C* **2015**, *119*, 15661–15668.

(37) Heger, D.; Jirkovský, J.; Klán, P. Aggregation of Methylene Blue in Frozen Aqueous Solutions Studied by Absorption Spectroscopy. *J. Phys. Chem. A* **2005**, *109*, 6702–6709.

(38) Dean, J. C.; Oblinsky, D. G.; Rather, S. R.; Scholes, G. D. Methylene Blue Exciton States Steer Nonradiative Relaxation: Ultrafast Spectroscopy of Methylene Blue Dimer. *J. Phys. Chem. B* **2016**, *120*, 440–454.

(39) Tardivo, J. P.; Giglio, A. D.; de Oliveira, C. S.; Gabrielli, D. S.; Junqueira, H. C.; Tada, D. B.; Severino, D.; Turchiello, R. D. F.; Baptista, M. S. Methylene Blue in Photodynamic Therapy: From Basic Mechanisms to Clinical Applications. *Photodiagn. Photodyn. Ther*. **2005**, *2*, 175–191.

(40) Chen, J.; Cesario, T. C.; Rentzepis, P. M. Effect of pH on Methylene Blue Transient States and Kinetics and Bacteria Photoinactivation. *J. Phys. Chem. A* **2011**, *115*, 2702–2707.

(41) Redmond, R. W.; Gamlin, J. N. A Compilation of Singlet Oxygen Yields from Biologically Relevant Molecules. *Photochem. Photobiol.* **1999**, *70*, 391– 475.

(42) Itoh, Y.; Abe, K.; Senoh, S.; Polyelectrolytes Containing Dihydronicotinamide. III. Fluorescence Quenching by Nicotinamide-Containing Polymers in Aqueous Solution. *J. Polym. Sci. A Polym. Chem.* **1987**, *25*, 2871–2880.

(43) Waka, Y.; Hamamoto, K.; Mataga, N. Fluorescence Quenching Mechanisms of Aromatic Hydrocarbon-Dicyanobenzene and-N,N-dimethylaniline Systems in Aqueous Micellar

Solutions. *Chem. Phys. Lett.* **1979**, *62*, 364–367.

(44) He, C.; Nguyen, T. D.; Edme, K.; de la Cruz, M. O.; Weiss, E. A. Noncovalent Control of the Electrostatic Potential of Quantum Dots through the Formation of Interfacial Ion Pairs. *J. Am. Chem. Soc.* **2017**, *139*, 10126–10132.

(45) Kumbharkhane, A. C.; Puranik, S. M.; Mehrotra, S. C. Dielectric Relaxation Studies of Aqueous N,N-dimethylformamide using a Picosecond Time Domain Technique. *J. Solution Chem.* **1993**, *22*, 219–229.

(46) Huang, J.; Huang, Z.; Yang, Y.; Zhu, H.; Lian, T. Multiple Exciton Dissociation in CdSe Quantum Dots by Ultrafast Electron Transfer to Adsorbed Methylene Blue. *J. Am. Chem. Soc.* **2010**, *132*, 4858–4864.

(47) Yang, Y.; Rodríguez-Córdoba, W.; Lian, T. Ultrafast Charge Separation and Recombination Dynamics in Lead Sulfide Quantum Dot–Methylene Blue Complexes Probed by Electron and Hole Intraband Transitions. *J. Am. Chem. Soc.* **2011**, *133*, 9246–9249.

(48) Dworak, L.; Roth, S.; Scheffer, M. P.; Frangakis, A. S.; Wachtveitl, J. A thin CdSe shell boosts the electron transfer from CdTe quantum dots to methylene blue. *Nanoscale* **2018**, *10*, 2162–2169.

4.7 Appendix

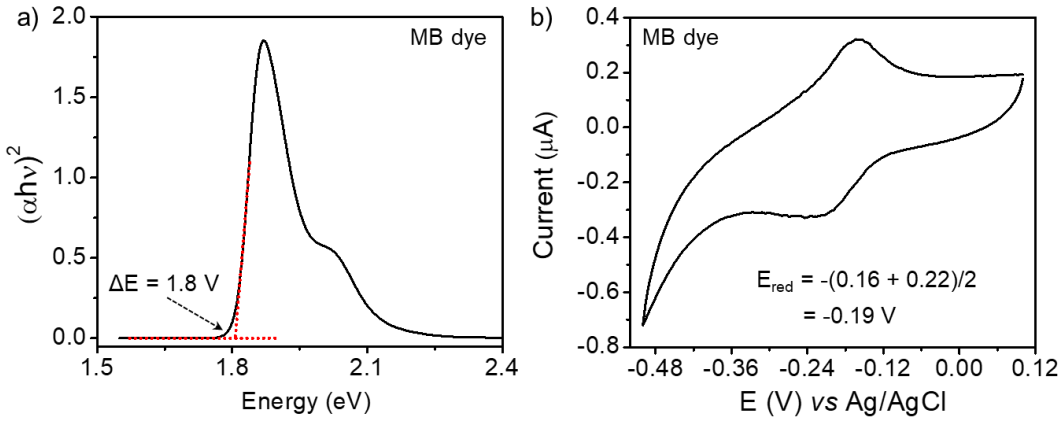

Figure A4.1 Determination of HOMO and LUMO energy level for the MB dye. (a) The Tauc plot for MB dye shows an estimated HOMO-LUMO energy gap of 1.8 eV. (b) Cyclic voltammograms of MB dye at a scan rate of 30 mV/s. The measurement was carried out by dissolving the MB dye in phosphate buffer electrolyte. Electrode system: Glassy carbon as working, Ag/AgCl/Cl^- as reference electrode, and Pt wire as counter electrode. The calculated LUMO energy level was 4.45 eV with respect to vacuum energy level.

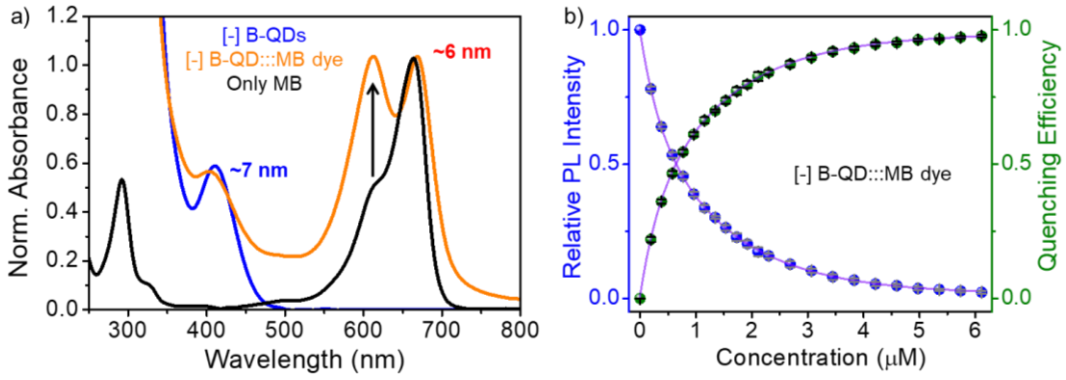

Figure A4.2 (a) Normalised UV-Vis absorption spectra of [-] B-QD, MB dye, and [-] B-QD:::MB dye donor:::acceptor system. There was a hypsochromic shift in QD excitonic band and a hyperchromic shift in MB electronic absorption band, indicating the electronic interactions between QD and MB dye. (b) Plot showing saturation in relative PL of [-] B-QD and PL quenching efficiency after the addition of 5 μM of MB dye.

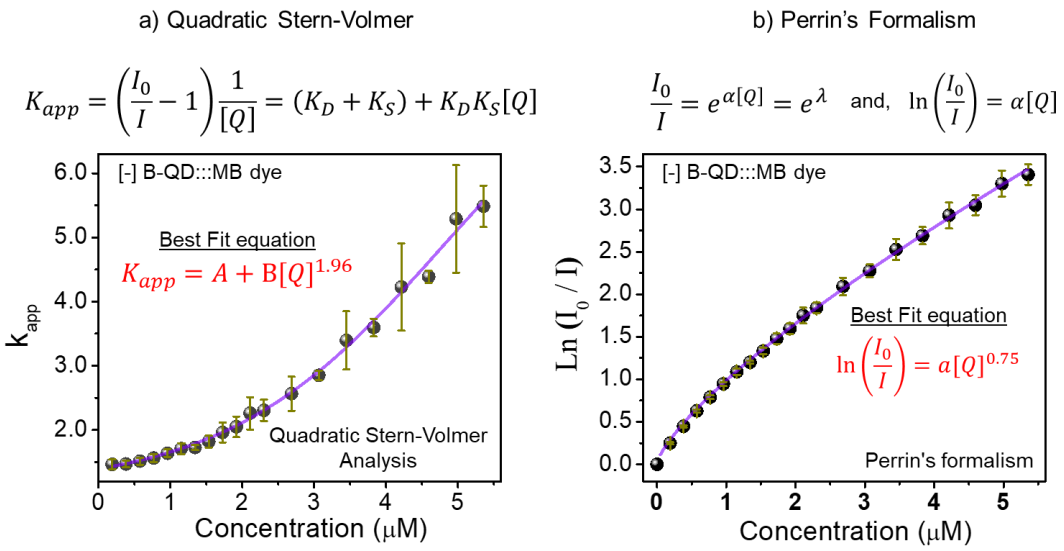

Figure A4.3 Analysis of PL quenching process in [-] B-QD:::MB dye donor:::acceptor system, based on (a) quadratic Stern-Volmer equation, and (b) Perrin's formalism. The deviation of best fit from standard formalism indicates the necessity of further modification in quenching mechanism.

Modification in Stern-Volmer equation:

In general, the non-linear nature of Stern-Volmer plot (I_0/I *vs* [Q]) indicates the presence of both static and dynamic component in quenching event. Thus, I_0/I can be expressed in combination of both static and dynamic quenching constant (K_D and K_S, respectively).

For example, the given quadratic Stern-Volmer equation will be:

$$\frac{\boldsymbol{I_0}}{\boldsymbol{I}} = (\mathbf{1} + \boldsymbol{K_S}[\boldsymbol{Q}])(\mathbf{1} + \boldsymbol{K_D}[\boldsymbol{Q}]) \qquad \ldots (37)$$

Interestingly, the relative PL of [-] B-QD::::MB dye donor:::acceptor system showed strong deviation from the standard form of quadratic equation (equation 37), as well as Perrin's formalism (**Figure A4.3**). This indicates a complex combination of static and dynamic components in PL quenching mechanism.

Thus, to analyze further, we assume that either static or dynamic quenching constant is sufficiently low, such as: $K_S[Q] \ll 1$ or $K_D[Q] \ll 1$; equation 37 can be approximated by

$$\frac{\boldsymbol{I_0}}{\boldsymbol{I_0 - I}} = \frac{\mathbf{1}}{\boldsymbol{K_S + K_D}}\frac{\mathbf{1}}{[\boldsymbol{Q}]} + \frac{\boldsymbol{K_D}}{\boldsymbol{K_S + K_D}} \qquad \ldots (38)$$

$$\frac{\boldsymbol{I_0}}{\boldsymbol{I_0 - I}} = \frac{\mathbf{1}}{\boldsymbol{K_S + K_D}}\frac{\mathbf{1}}{[\boldsymbol{Q}]} + \frac{\boldsymbol{K_S}}{\boldsymbol{K_S + K_D}} \qquad \ldots (39)$$

Hence, the slope and intercept of (I_0/(I_0-I) vs (1/[Q]) plot can be used to find the static and dynamic quenching constants. However, it is impossible to assign K_S and K_D without any support from independent experiment.

The relative PL of [-] B-QD::::MB dye donor:::acceptor system shows a good fit with modified (equation 38 or 39) with slope of 0.708 and intercept of 0.896 (**Figure A4.4**). Further interpretation revealed that one of the components is ~8.6 times higher than the other one, with their estimated values of ~1.26 x 10^6 M^{-1} and ~1.47 x 10^5 M^{-1}, respectively. Interestingly, in temperature dependent SV analysis, the intercept-to-slope ratio decreases with decreasing the temperature of the medium. For temperatures of 318 K, 298 K, and 278 K, the two quenching constants are (1.29 μM^{-1}, 0.135 μM^{-1}); (1.26 μM^{-1}, 0.147 μM^{-1}); and (1.06 μM^{-1}, 0.154 μM^{-1}) (**Figure 4.8c**). Lowering the temperature will reduce the diffusional or collisional quenching, and will favour weak complexation process. Therefore, dynamic quenching constant will decrease, and static quenching constant will increase, as the temperature drops. Thus, the static and dynamic quenching constant for the PL quenching of [-] B-QD::::MB dye donor:::acceptor system can be found to be ~1.47 x 10^5 M^{-1} and, ~1.26 x 10^6 M^{-1} respectively.

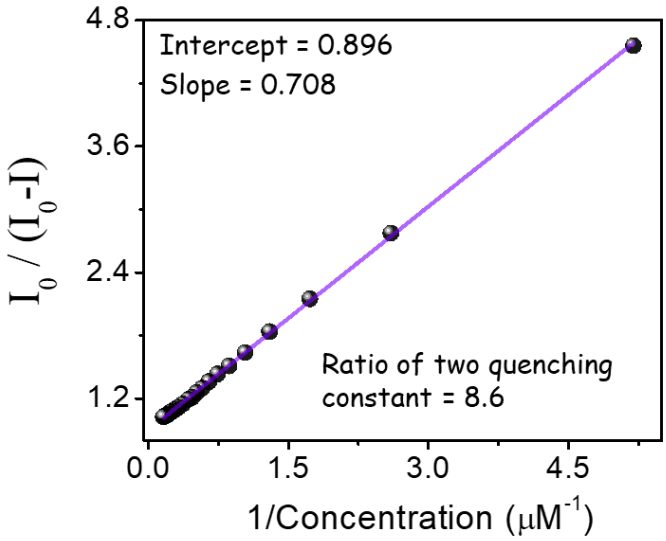

Figure A4.4 Modified Stern-Volmer plot for [-] B-QD:::MB dye donor:::acceptor system. From the slope and intercept of the plot, it was found that the dynamic quenching constants is ~9 times higher than that of static quenching constant.

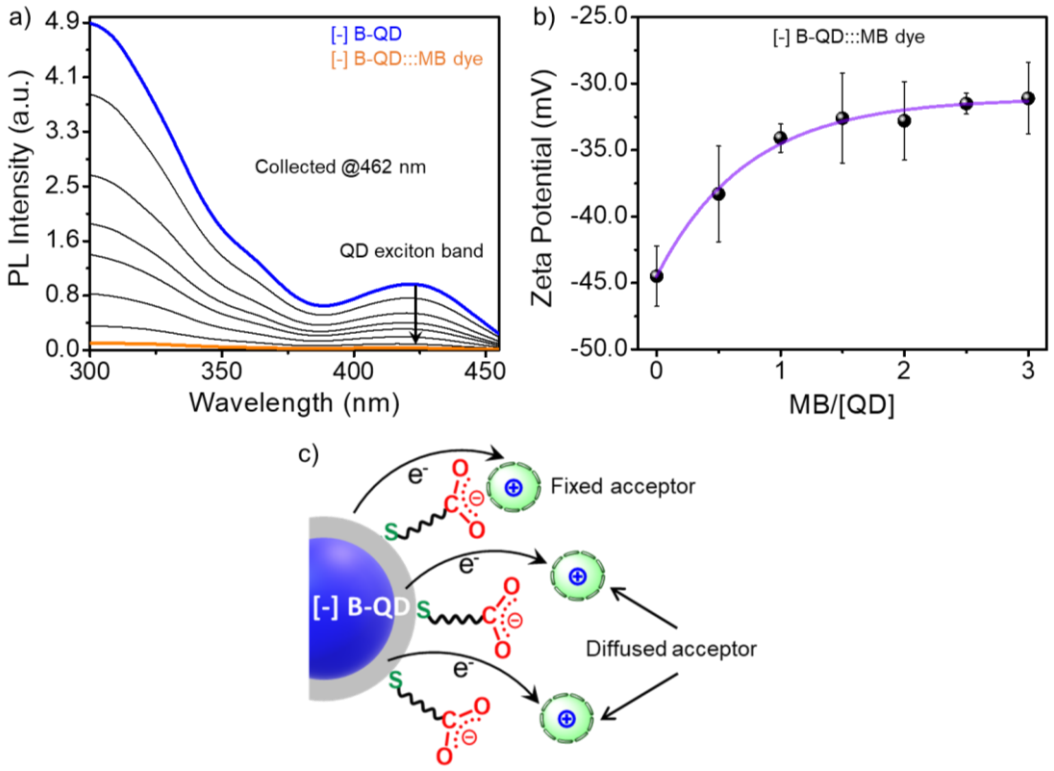

Figure A4.5 (a) PLE spectra and (b) zeta potential study of [-] B-QDs upon successive addition of MB dye. PLE was collected at the emission maxima of [-] B-QDs (~462 nm). The PLE intensity of [-] B-QDs, collected at ~462 nm showed a gradual decrease in the QD excitonic band positions (~410 nm and higher energy bands), indicating the possibility of excited state charge transfer process. Negligible change in the zeta potential value after 1:1 molar ratio of MB:QD, indicate a layered arrangement of acceptor-MB dye molecules around [-] B-QDs. (c) Schematics for the layered arrangement of acceptor-MB dye molecules around [-] B-QDs. MB dye surrounds the [-] B-QDs in fixed and diffused layers, thereby contributing to static and dynamic quenching process, respectively.

Table A4.1 PL decay analysis of [-] B-QD:::MB dye donor:::acceptor system upon successive addition of acceptor MB dye, collected at 462 nm, in time window of 3.2 µs.

System	τ_1 (ns)	α_1	τ_2 (ns)	α_2	τ_3 (ns)	α_3	τ_4 (ns)	α_4	$\tau_{avg.}$ (ns)	χ^2
[-] B-QDs	8.47	0.28	52.61	0.38	148.04	0.3	534.91	0.04	216.53	1.03
[-] B-QD:::MB dye (0.38 µM)	3.29	0.42	35.34	0.27	125.68	0.27	465.88	0.04	209.29	1.10
[-] B-QD:::MB dye (0.77 µM)	3.28	0.44	30.36	0.26	121.07	0.26	458.6	0.04	210.75	1.11
[-] B-QD:::MB dye (1.15 µM)	2.29	0.7	25.79	0.14	109.93	0.13	404.07	0.03	207.61	1.11
[-] B-QD:::MB dye (1.54 µM)	1.42	0.82	18.61	0.09	101.07	0.07	385.74	0.02	211.23	1.18
[-] B-QD:::MB dye (1.92 µM)	1.09	0.94	14.66	0.03	92.34	0.02	344.191	0.01	201.80	1.19
[-] B-QD:::MB dye (2.30 µM)	0.78	0.96	12.11	0.02	83.84	0.01	294.96	0.01	197.49	1.14
[-] B-QD:::MB dye (3.07 µM)	0.76	0.96	10.96	0.02	72.82	0.01	260.06	0.01	171.19	1.19
[-] B-QD:::MB dye (3.83 µM)	0.62	0.96	7.06	0.02	54.99	0.01	205.49	0.01	135.84	1.24
[-] B-QD:::MB dye (4.59 µM)	0.53	0.97	5.98	0.01	42.09	0.01	174.05	0.01	117.46	1.26
[-] B-QD:::MB dye (5.35 µM)	0.57	0.97	4.81	0.01	34.90	0.01	160.64	0.01	105.92	1.15
[-] B-QD:::MB dye (6.10 µM)	0.49	0.96	4.08	0.02	19.78	0.01	136.13	0.01	89.90	1.04

Table A4.2 PL decay analysis of [-] B-QD:::MB dye assembly at lower and higher ionic strengths (0.015 M and 1.23 M), collected at 462 nm, in a time window of 3.2 µs.

System (Ionic strength)	τ_1 (ns)	α_1	τ_2 (ns)	α_2	τ_3 (ns)	α_3	τ_4 (ns)	α_4	$\tau_{avg.}$ (ns)	χ^2
[-] B-QD:::MB Dye (0.015 M)	1.10	0.89	9.47	0.07	68.01	0.03	268.78	0.01	136.35	1.30
[-] B-QD:::MB Dye (1.23 M)	3.72	0.73	41.49	0.18	131.07	0.08	536.39	0.01	175.60	1.19

Polarity-Dependent PL Quenching Study

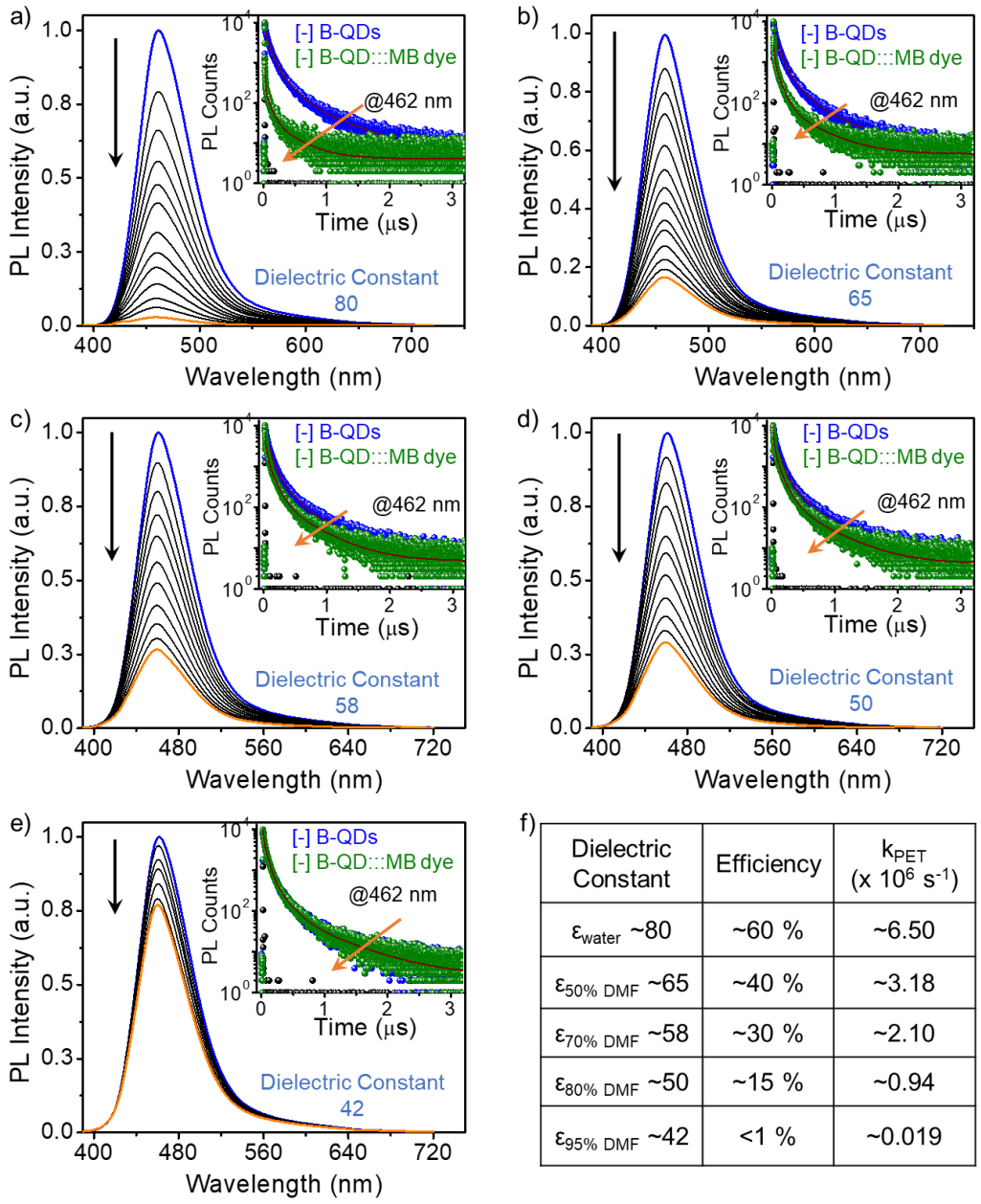

f)

Dielectric Constant	Efficiency	k_{PET} (x 10^6 s^{-1})
ε_{water} ~80	~60 %	~6.50
$\varepsilon_{50\%\ DMF}$ ~65	~40 %	~3.18
$\varepsilon_{70\%\ DMF}$ ~58	~30 %	~2.10
$\varepsilon_{80\%\ DMF}$ ~50	~15 %	~0.94
$\varepsilon_{95\%\ DMF}$ ~42	<1 %	~0.019

Figure A4.6 Polarity-dependent PL analysis. Steady-state and time-resolved PL quenching study at different dielectric strengths (ε) in water: DMF mixture. ε = (a) 80, (b) 65, (c) 58, (d) 50, and (e) 42. (f) Table summarises efficiency and rate of the PET process obtained from the PL lifetime quenching studies ($E = 1–\tau/\tau_0$, and $k_{PET} = 1/\tau–1/\tau_0$, where τ_0 and τ are the PL lifetime of [-] B-QD in absence and presence of MB dye, respectively).

Table A4.3 PL decay analysis of [-] B-QDs and [-] B-QD:::MB dye donor:::acceptor assembly at different dielectric strength of the medium ranging from 80 to 42, collected at 462 nm, in a time window of 3.2 μs.

Dielectric constant	System	τ_1 (ns)	α_1	τ_2 (ns)	α_2	τ_3 (ns)	α_3	τ_4 (ns)	α_4	$\tau_{avg.}$ (ns)	χ^2
ε_{water} ~80	[-] B-QDs	8.47	0.28	52.61	0.38	148.04	0.30	534.91	0.04	216.53	1.03
	[-] B-QD:::MB Dye	0.49	0.96	4.08	0.02	19.78	0.01	136.13	0.01	89.90	1.04
$\varepsilon_{50\% DMF}$ ~65	[-] B-QDs	6.83	0.32	50.53	0.45	140.38	0.20	541.59	0.03	200.80	1.13
	[-] B-QD:::MB Dye	0.98	0.89	9.13	0.07	62.54	0.03	242.44	0.01	122.47	1.33
$\varepsilon_{70\% DMF}$ ~58	[-] B-QDs	6.81	0.30	49.35	0.45	140.33	0.22	530.34	0.03	195.40	1.13
	[-] B-QD:::MB Dye	1.24	0.77	13.40	0.13	81.32	0.09	355.08	0.01	138.61	1.31
$\varepsilon_{80\% DMF}$ ~50	[-] B-QDs	5.89	0.41	47.52	0.39	136.05	0.18	539.73	0.02	178.78	1.19
	[-] B-QD:::MB Dye	2.28	0.71	28.08	0.18	104.69	0.10	455.87	0.01	152.98	1.29
$\varepsilon_{95\% DMF}$ ~42	[-] B-QDs	5.78	0.45	44.51	0.38	129.55	0.15	522.75	0.02	177.13	1.20
	[-] B-QD:::MB Dye	5.41	0.42	44.82	0.39	133.40	0.17	525.59	0.02	176.53	1.18

Transient Absorption (TA) Study

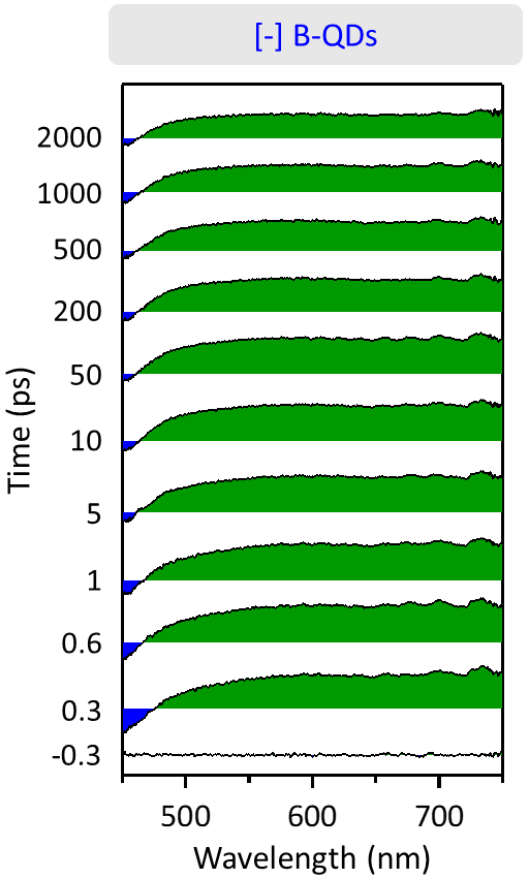

Figure A4.7 Picosecond TA spectral evolution for [-] B-QDs. The pump wavelength was 400 nm.

Chapter – 5

Electrostatically Driven Resonance Energy Transfer in an All-Quantum Dot Based Donor–Acceptor System

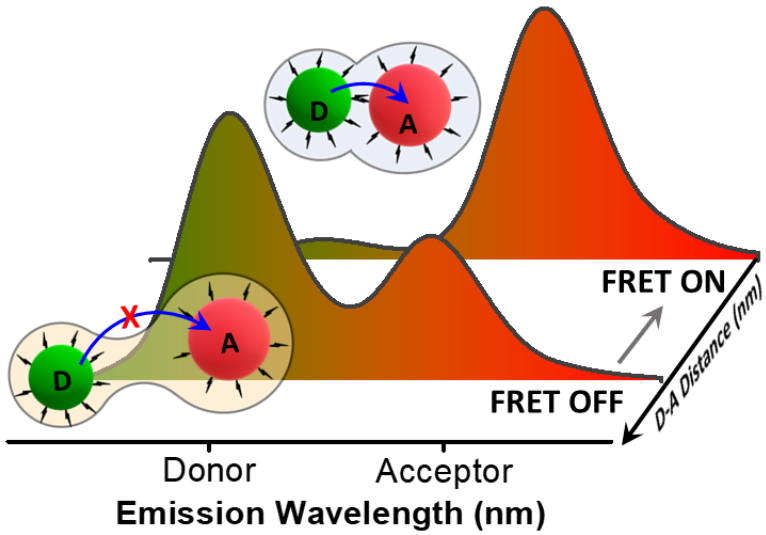

This Chapter has been adapted from the following papers with permission. Copyright 2020 American Chemical Society, Copyright 2023 Elsevier B.V., and Copyright 2024 AIP Publishing.

Roy, P.; Devatha, G.; Roy, S.; Rao, A.; Pillai, P. P. Electrostatically Driven Resonance Energy Transfer in an All-Quantum Dot Based Donor–Acceptor System. *J. Phys. Chem. Lett.* **2020**, *11*, 5354–5360.

Roy, P.; Sury, A. S.; Pillai, P. P. Resonance energy transfer in electrostatically assembled donor-acceptor system based on blue-emitting InP quantum dots. *Chem. Phys. Impact* **2023**, *7*, 100334.

Roy, P.; Sury, A. S.; Pillai, P. P. Electrostatics Enable Resonance Energy Transfer in InP Based All-Quantum Dot Donor-Acceptor Assembly. *Appl. Phys. Lett.* **2024**, *124*, 222104.

5.1 Abstract

Demonstration of fundamental photophysical properties in all-quantum dot (QD) based donor-acceptor systems containing environmentally friendly materials are essential to realise the full potential of QDs in energy and medical research. We accomplish here an efficient light induced resonance energy transfer process in all-QD based donor-acceptor system in water, at a dyad level, deprived of any commonly used organic dye component. Our nanohybrid system comprises of surface engineered (i) indium phosphide/zinc sulfide (InP/ZnS) QD as the donor and acceptor, and (ii) InP/ZnS QD as the donor and copper indium sulfide/zinc sulfide (CIS/ZnS) QD as the acceptor. The fine-control over the reaction kinetics and appropriate surface functionalisation with oppositely charged ligands enabled the formation of electrostatically bound all-QD donor-acceptor dyad assemblies composed of blue, green, and red emitting InP/ZnS QDs and red emitting CIS/ZnS QDs. These dyad assemblies are referred as: such as blue-green, green-red, and blue-red all-InP QD donor-acceptor dyad assemblies and green-red [-] InP/ZnS:::[+] CIS/ZnS QD nanohybrid dyad assembly. The electrostatic attraction between oppositely charged QDs is vital in achieving such a strong ground state complexation in all-QD nanohybrid assemblies. Detailed steady-state and time-resolved spectroscopic studies were conducted to establish the process of the Förster resonance energy transfer (FRET) in all-QD based dyad systems. Accordingly, a road-map for investigating the FRET process in all-QD based dyad systems is developed. Further, a temporal evolution of resonance energy transfer is realized in the solid state as well, which can improve the potential of such 'all-green QD' based nanohybrid systems for device level studies. Control experiments conclusively prove the necessity of appropriately functionalised QDs and electrostatic attraction for achieving an efficient FRET process. In short, our work proves the ability of environmentally friendly InP and CIS QDs to participate in an efficient FRET process at the dyad level, which can accelerate the development of all-QD based multicomponent light harvesting systems for various optoelectronic applications, including photovoltaics and photocatalysis.

5.2 Introduction

Understanding and mimicking of natural light driven processes are crucial to develop efficient energy harvesting systems based on artificial materials.[1-2] Light induced energy and electron transfer are the two key photophysical processes that predominantly govern the efficiency of both natural and artificial light harvesting systems.[3-5] Förster resonance energy transfer (FRET) is one such light driven process which has been extensively used as an optical ruler to monitor various physical processes in science, ranging from biomolecule dynamics to energy harvesting devices.[6-9] The process of FRET involves a nonradiative transfer of excitonic energy from an excited state donor to an energetically coupled ground state acceptor, via long range dipole-dipole interaction.[6-7] Traditionally, diverse sets of fluorophores such as organic dyes, organic-inorganic hybrid metal complexes, polymers, organic/inorganic nanomaterials, etc. have been used to develop model donor-acceptor based energy transfer systems.[8-13] Among them, semiconductor nanoparticles or quantum dots (QDs) have gained a special place in light-harvesting studies because of their unique size- and shape-dependent optoelectronic properties, arising from the quantum confinement effect.[13-15] Along with this, the large absorption cross-section, high color purity, and enhanced photostability of QDs are added advantages over conventional fluorophores.[11-18] Moreover, the unique size tunable absorption and emission of QDs allows a fine control over the spectral overlap integral:[8,13] an important prerequisite for achieving efficient energy transfer process. In that direction, Mattoussi and co-workers, in their pioneering work, first ever investigated an efficient energy transfer process between functionalized CdSe/ZnS QDs and cyanine dye (Cy3) immobilized on the QD surface via maltose binding protein (MBP) (**Figure 5.1a**).[19] Detailed spectroscopic and microscopic measurements evidenced the process of FRET. Under epifluorescence microscopic study (coupled to a spectrometer), QD-MBP-dye nanohybrid assembly (top row of **Figure 5.1b**) showed an enhancement in PL intensity and lifetime of the dye molecule in comparison with only Cy3 dye molecule (bottom row of **Figure 5.1b**), along with a substantial quenching in the QD emission (bottom row of **Figure 5.1b**). Here, the efficiency of the FRET process was monitored both as a function of the spectral overlap integral (by varying the QD size) and the number of dye molecules per donor QD. This finding demonstrated a strong dependence of FRET efficiency on the spectral overlap integral between the emission of QDs and the absorption of dye. Along this path, substantial progress has been achieved in developing a number of efficient QD based energy transfer systems.[8,19-26] Majority of these studies rely on designing QD-dye nanohybrid systems, where QDs were essentially used as FRET donors, and

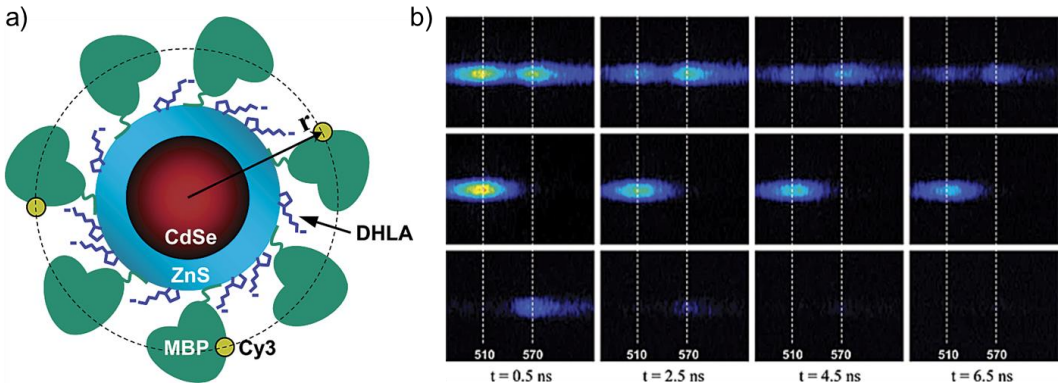

Figure 5.1 (a) Schematic representation of a FRET based donor-acceptor system comprised of CdSe/ZnS QD-MBP-Cy3 dye. Here, the Cy3 dye serving as the FRET acceptor, is covalently linked with MBP, which further immobilizes on the QD surface. (b) the resonance energy transfer process substantially alters the exciton lifetime properties of QDs (at 510 nm) and Cy3 dye (at 570 nm) in QD-MBP-dye nanohybrid assembly. Luminescence images showing the intensity and lifetime of only QDs (middle row), only Cy3 dye (bottom row), and QD-MBP-dye nanohybrid assembly (top row), as recorded by the time-gated intensified charge-coupled device (CCD) camera at 2 ns intervals. Reproduced with permission from references 19. Copyright 2004 American Chemical Society.

dye molecules as acceptors.[19-26] However, the poor photostability of dye molecules often limits the use of such nanohybrid systems in applications requiring long exposure of light like display devices and bioimaging.[16,26] These appealing properties of QDs have inspired the development of all-QD based donor-acceptor systems, where efficient FRET has been demonstrated between QDs.[27-43] In an early report, Klimov and co-workers investigated the dynamics of resonance energy transfer process in close packed film of monodispersed (~7 % size distribution) CdSe/ZnS QDs (**Figure 5.2a,b**).[28] Time resolved photoluminescence (PL) and lifetime studies revealed energy, size, and time-dependent dynamics of interdot energy transfer process. Where, the high energy side of PL spectrum (smaller QD) showed a rapid decay (1.9 ns), followed by a steady increase in the PL lifetime for lower energy side (22 ns) (**Figure 5.2a**). Alongside, the PL spectrum showed 35 meV red shift after 10-20 ns of excitation (**Figure 5.2b**). In another study, Bawendi and co-workers evidenced a dipole-dipole interaction driven interdot energy transfer in close-packed QD solid, causing a red shift in PL spectrum.[28] Later, Kolle and co-workers further examined the homonuclear interdot interaction by covalently cross linking CdTe QDs with dithiol ligand (**Figure 5.2c**).[29] The degree of electronic coupling depends on the extension of wave function outside of QDs, which is larger for smaller QDs.

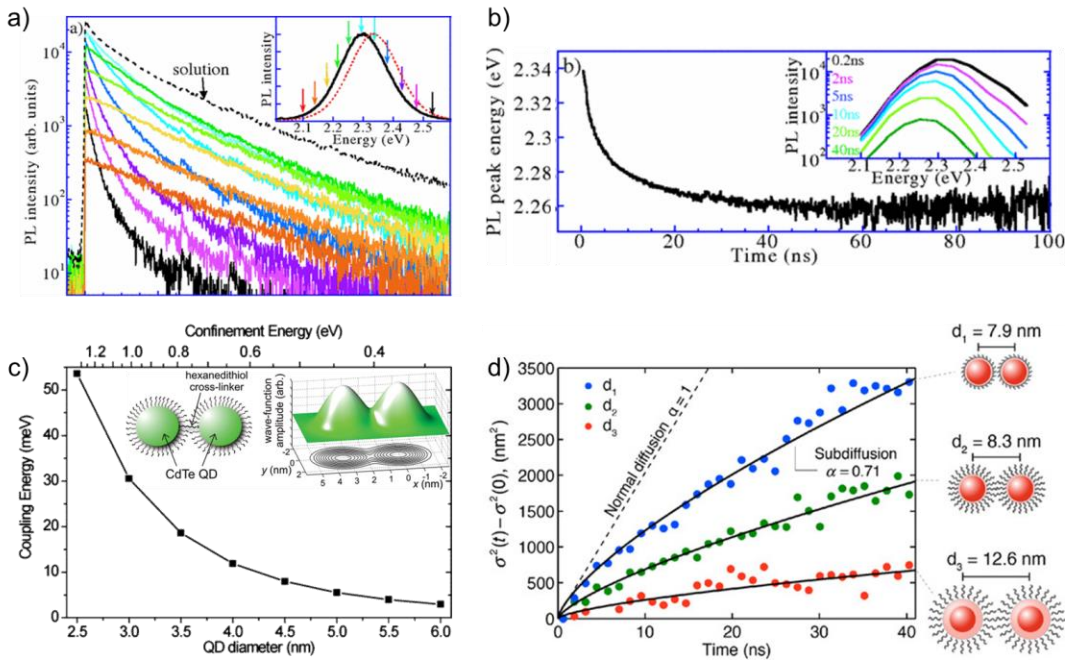

Figure 5.2 Homonuclear interdot electronic interaction in all-QD assemblies. (a) Photoluminescence decay profile of a close-packed film of monodispersed CdSe/ZnS QDs (mean radii 12.4 Å). Inset shows collection energy for lifetime study. (b) Time-dependent PL peak position of close-packed QD film. The inset shows the corresponding time-resolved emission spectra. A clear red shift in the PL peak position and a complementary change in lifetime for high and low energy positions confirm the presence of a resonance energy transfer process. Reproduced with permission from references 28. Copyright 2002 American Physical Society. (c) Couling energy *vs.* diameter of QD (bottom x-axis) and confinement energy (top x-axis) plot. The inset shows a schematic representation of a contour-plot for the interdot coupling process, described as the amplitude of electron wave functions in two covalently coupled QDs (interdot separation of 0.4 nm) with diameter of QD. (d) Exciton diffusivity as a function of time and with variance of center-to-center distance ($d_1<d_2<d_3$). Reproduced in parts with permission from references 29 and 30. Copyright 2006 and 2014 American Chemical Society.

Hence, the interdot coupling energy is dominated for smaller sized QDs (**Figure 5.2c**). This further supports the energetically downhill diffusion nature of excitons. Likewise, Tisdale and co-workers have shown a direct visualization of exciton transport in space, time, and energy.[30] Here, a smaller interdot spacing was shown to cause a faster and more noticeable broadening of the exciton distribution (**Figure 5.2d**).[30] Following the accomplishment of investigating the dynamics of homonuclear interdot resonance within the inhomogeneous size distribution of QDs. The next effort ought to involve assembling multisized QDs to broaden the energy landscape. In that direction, Achermann and co-workers investigated the Förster resonance energy transfer dynamics in two-dimensional (2D) bilayer assembly of multisized CdSe/ZnS QDs using Langmuir–Blodgett (LB) techniques (upper panel of **Figure 5.3a**).[33] The LB assembly of two different sizes of CdSe/ZnS QDs (2.6 nm and 4.1 nm), provided strong coupling because of resonance between the emission transition of smaller QDs and the

absorption transition of larger QDs (good spectral overlap; **Figure 5.3a**). This resulted in faster interlayer transfer of exciton (vertical energy relay) from smaller QDs to larger QDs (energy transfer time constant 120 ps) (lower panel of **Figure 5.3a**). Afterward, Pullerits and co-workers investigated the energy transfer dynamics in an ordered multilayer QD film composed of different sizes of CdSe QDs (2.3 nm and 3.7 nm, respectively) (**Figure 5.3b**).[40] The finding suggests that the densely packed layered architecture can funnel up to 80 % of exciton energy. It was accomplished because of ordered QD film with notably different sizes of CdSe QDs. The lifetime of energy transfer was estimated to be ~1.5 ns (lower panel of **Figure 5.3b**). Now, in comparison with the vast literature of FRET, the number of examples available for all-QD based FRET systems are scarce.[27-43] Moreover, majority of these studies have been reported with QDs containing toxic metals likes Cd, Pb, Se, Te, etc.[33-43] The growing restriction on the use of devices containing toxic metal-ions demands the need for all-QD based donor-acceptor systems containing environmentally friendly QDs.[44-50] Thus, both from fundamental and applied perspectives, it is essential to realize efficient FRET in wider sets of all-QD based donor-acceptor systems, especially with more environmentally friendly QDs. Furthermore, to the best of our knowledge, the use of electrostatic interactions to regulate FRET process between environmentally friendly QDs is not yet reported.

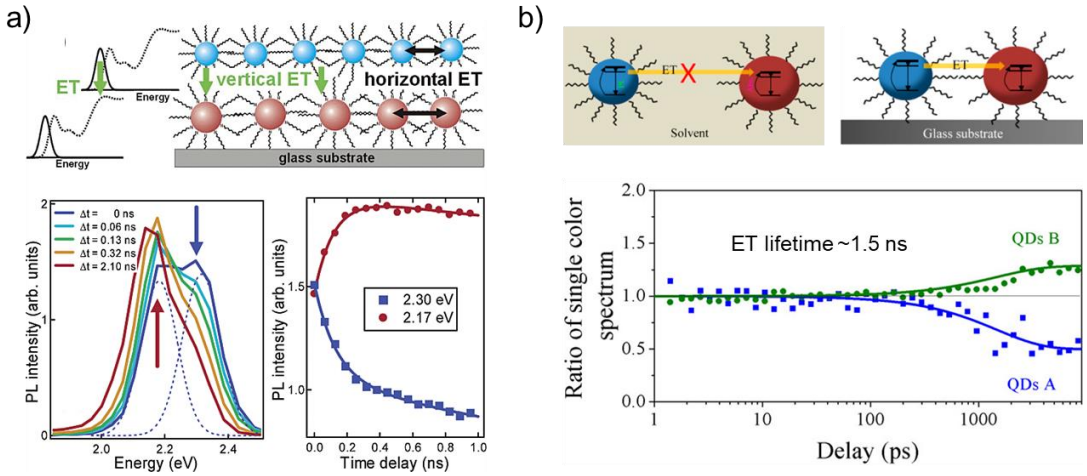

Figure 5.3 Interdot energy transfer studies with multisized QDs. (a) Schematics of a bilayer structure fabricated with two different sizes of CdSe/ZnS QD, allowing interlayer (vertical) transfer of resonance energy in a strong coupling regime (good spectral overlap integral). Time-resolved emission spectra show the energy relay in the energy gradient architecture. The high energy emission for donor QD (2.30 eV) shows rapid decay with increasing delay time, whereas, the low energy emission for acceptor QD (2.17 eV) exhibits growth, with a time constant of 120 ps. Thus, confirming the interlayer energy migration process. (b) Schematic representation of the energy transfer process between two differently sized CdSe QDs (A: 2.3 nm; B: 3.7 nm) in solution state and in thin film. Lower panel: single point decay kinetics from transient absorption (TA) study show a fast decay (donor A QD) and growth factor (acceptor B QD) in Δ abs. value with a time constant of 1.5 ns in thin film of (A+B) QD. Reproduced

in parts with permission from references 33 and 40. Copyright 2003 and 2014 American Chemical Society.

In this Chapter, we report light-induced resonance energy transfer studies in all-QD systems (at the dyad level) comprising of environmentally friendly blue, green, and red emitting InP/ZnS QDs, and red emitting CIS/ZnS QDs, and that too in water. Stable dispersion of QDs in water was achieved by the appropriate surface functionalisation with oppositely charged ligands, which also ensured a strong electrostatic attraction between donor and acceptor QDs. There are four electrostatically bound all-QD based dyad systems developed in this Chapter for light-harvesting studies: (i) blue-green all-InP QD donor-acceptor assembly, (ii) green-red all-InP QD donor-acceptor assembly, (iii) blue-red all-InP QD donor-acceptor assembly, and (iii) green-red [-] InP/ZnS:::[+] CIS/ZnS QD donor-acceptor assembly (**Scheme 5.1**). Systematic steady-state and time-resolved spectroscopic studies confirmed an efficient Förster resonance energy transfer (FRET) process in these electrostatically bound all-QD based dyad assemblies. Detailed Stern-Volmer analysis elucidate the involvement of various components (static and dynamic components) associated with the PL quenching process of donor QDs. Finally, the solid-state studies enabled the distance-dependent temporal visualisation of the FRET process at a fixed donor-acceptor ratio, which ascertains the suitability of all-QD based assemblies for device level light-harvesting studies as well. In short, our work demonstrated that the greener InP and CIS based QDs could practically be alternative to traditional state-of-the-art Cd and Pb based QDs, for energy transfer investigation in all-QD based donor-acceptor assemblies. The finding could pave the way forward to the creation of all-QD based multicomponent light harvesting systems for various optoelectronic applications, including photovoltaics and photocatalysis.

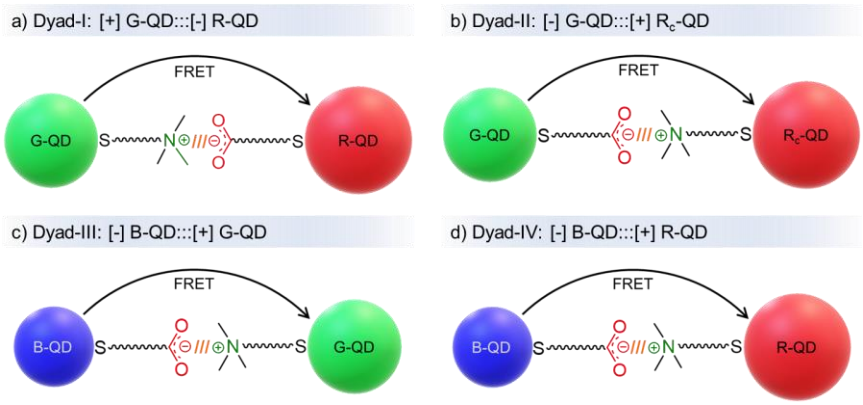

Scheme 5.1 Schematics of electrostatically driven FRET process in dyad assemblies comprising of environmentally friendly blue, green, and red emitting InP/ZnS QDs and, red emitting CIS/ZnS QDs in water. (a) Dyad-I: [+] G-QD:::[+] R-QD; (b) dyad-II: [-] G-QD:::[+] R_{CIS}-QD; (c) dyad-III: [-] B-QD:::[+] G-QD; and (d) dyad-IV: [-] B-QD::: [+] R-QD donor:::acceptor systems.

5.3 Experimental Section

Details of all synthesis procedures for blue, green, and red-emitting InP/ZnS QDs and red-emitting CIS/ZnS QDs, the ligand exchange process of QDs, additional experimental methods, instrumental techniques, and formalism for the Förster resonance energy transfer (FRET) process were already discussed in **Chapter 2**. Water dispersed [-] B-InP/ZnS QDs, [-]/[+] G-InP/ZnS QDs, [-]/[+] R-InP/ZnS QDs, and [-]/[+] R-CIS/ZnS QDs are termed as [-] B-QDs, [-]/[+] G-QDs, [-]/[+] R-QDs, and [-]/[+] R_{CIS}-QDs respectively, throughout the Chapter.

5.3.1 Green-Red All-InP/ZnS QD based Donor-Acceptor Assembly:

The energy transfer experiments were performed with positively charged green-emitting donor [+] G-InP/ZnS QD ([+] G-QD) and negatively charged red-emitting acceptor [-] R-InP/ZnS QD ([-] R-QD). In a typical energy transfer experiment, a 2.5 mL aqueous solution of donor [+] G-QDs was prepared such that the absorbance was ~0.025 at 452 nm (first excitonic peak), corresponding to a QD concentration of ~0.2 μM. Next, different aliquots of acceptor [-] R-QDs were sequentially added (4 μL of ~25 μM) to the donor QD solution, and the spectral changes were monitored using Shimadzu UV-3600 Plus absorption spectrophotometer and Fluorolog-3 spectrofluorometer (HORIBA Scientific). The spectral information were collected by exciting the [+] G-QDs, [-] R-QDs, and [+] G-QD:::[-] R-QD donor:::acceptor assembly at 400 nm. The corresponding lifetime experiments were carried out in a HORIBA Delta Flex Time-Correlated Single Photon Counting system using a 405 nm laser source. The photoluminescence decay was deconvoluted by using EZ software, and fitted with exponential decay, minimizing the χ^2 values.

5.3.2 Green-Red All-QDs Assembly based on G-QD Donor and R_{CIS}-QD Acceptor:

Here, the donor-acceptor energy transfer system was comprised of negatively charged green emitting donor [-] G-InP/ZnS QD ([-] G-QD) and positively charged red emitting acceptor [+] R-CIS/ZnS QD ([+] R_{CIS}-QD). In a typical energy transfer experiment, different aliquots of acceptor [+] R_{CIS}-QD were sequentially added (50 μL of ~ 80 μM) to donor [-] G-QD solution, and the spectral changes were monitored using Shimadzu UV-3600 Plus absorption spectrophotometer and Fluorolog-3 spectrofluorometer (HORIBA Scientific). The spectral information were collected by exciting the [-] G-QDs, [+] R_{CIS}-QDs, and [-] G-QD:::[+] R_{CIS}-

QD donor:::acceptor assembly at 400 nm. The corresponding lifetime experiments were carried out in a HORIBA Delta Flex Time-Correlated Single Photon Counting system using a 405 nm laser source. The fluorescence decay was deconvoluted by using EZ software, and fitted with exponential decay, minimizing the χ^2 values.

5.3.3 Blue-Green All-InP/ZnS QD based Donor-Acceptor Assembly:

Light-induced energy transfer experiments were performed with [-] B-InP/ZnS QD ([-] B-QD) donors and [+] G-InP/ZnS QD ([+] G-QD) acceptors. In a typical energy transfer experiment, a 2.5 mL aqueous solution of [-] B-QDs was prepared such that the absorbance was ~0.05 at 410 nm (first excitonic peak), which corresponds to a QD concentration of ~2 μM. Next, aliquots of acceptor [+] G-QD (15 μL of ~10 μM) were sequentially added to donor QD solution. The spectral changes were monitored using Shimadzu UV-3600 Plus absorption spectrophotometer and Fluorolog-3 spectrofluorometer (HORIBA Scientific). The photophysical studies were performed by exciting the [-] B-QDs, [+] G-QDs and [-] B-QD:::[+] G-QD nanohybrid assembly at 370 nm. The corresponding photoluminescence (PL) lifetime experiments were carried out in a HORIBA Delta Flex Time-Correlated Single Photon Counting system using a 370 nm laser source. The PL decay was analysed using EZ software, and fit with multiexponential kinetics, minimizing the χ^2 values.

5.3.4 Blue-Red All-InP/ZnS QD based Donor-Acceptor Assembly:

A similar procedure was adapted for blue-red all-InP/ZnS QD based donor-acceptor assembly, to investigate the energy transfer process. All the photophysical changes were monitored using Shimadzu UV-3600 Plus absorption spectrophotometer and Fluorolog-3 spectrofluorometer (HORIBA Scientific), and HORIBA Delta Flex Time-Correlated Single Photon Counting system with 370 nm excitation source.

5.4 Results and Discussion

5.4.1 Synthesis and Characterization of InP/ZnS QD:

Our main objective was to demonstrate an efficient light-induced energy transfer process in all-QD assembly at dyad level, comprising of environmentally friendly QDs. This requires the synthesis of different sizes of InP/ZnS QDs with desired band gaps and energy-level alignment,

along with the suitable surface functionalisation.[24,26,48-52] Appropriate choice of indium (In) and phosphorous (P) precursors, along with optimised reaction conditions, allowed us to control the kinetics of nucleation and growth processes in InP/ZnS QDs synthesis.[48-50] This led to the formation of stable and luminescent QDs with the desired size and color: the higher band gap blue emitting, moderate band gap green-emitting, and the lower band gap red-emitting InP/ZnS QDs, respectively (B-QDs, G-QDs, and R-QDs). Details on the synthesis were given in **Chapter 2** and characterizations for blue emitting InP/ZnS QDs were already discussed in **Chapter 3**. Thus, in current Chapter, focus was given to the characterization of G-InP/ZnS QDs and R-InP/ZnS QDs. The green- and red-emitting InP/ZnS QDs exhibited first excitonic peaks at ~452 nm and ~570 nm, with their corresponding PL maxima at ~505 nm and ~600 nm, respectively (**Figure 5.4a,b**). The emission linewidth (FWHM) was calculated to be 50 nm and 49 nm for G-QD and R-QD, respectively. A detailed steady-state excitation energy, excitation power and temperature-dependent emission measurements were carried out to elucidate the underlying mechanism responsible for the evolution of the emission peak (**Figures A5.2-A5.3**). The absolute quantum yield (PL QY_A) was estimated to be ~55 % and ~12 % in $CHCl_3$ for G-QDs and R-QDs, respectively (**Figure A5.1a,b**). Time-resolved emission studies showed multi-exponential PL lifetime decay kinetics for both the G-QDs and R-QDs, with an average lifetime of ~55 ns and ~40 ns, respectively (**Figure A5.1c,d** and **Table A5.1**). The band gaps and energy-level positions were estimated from a combination of cyclic voltammetry and absorption studies, which proves that the green- and red-emitting InP/ZnS QDs satisfy the required energy-level alignment for an efficient energy transfer process (**Figures 5.5a** and **A5.4**). The surfaces of G-QDs and R-QDs were functionalised with oppositely charged thiolated-ligands, to make electrostatically bound donor-acceptor assemblies in water (**Figure 5.5c,d** and **Scheme A5.1**). For this, the hydrophobic ligand shell of as-synthesized QDs was replaced with charged thiolated-ligands. Specifically, myristic acid ligands on G-QDs were place exchanged with cationic N,N,N-trimethyl(11-mercaptoundecyl)ammonium chloride (TMA, [+]) ligands, while olylamine ligands on R-QDs were functionalised with anionic 6-mercaptohexanoic acid (MHA, [−]) ligands (**Figure 5.5c,d**). The transfer of PL from the organic phase (chloroform) to the aqueous phase was the visual proof of the successful ligand exchange process and dispersion of QDs in water (**Figure 5.4e**). Zeta potential (ζ) values of +37.7 ± 2.0 mV and −38.0 ± 1.6 mV for [+] G-QDs and [-] R-QDs, respectively, ascertains the successful functionalization of the respective charged ligands on the surface of QDs (**Figure 5.4f**).

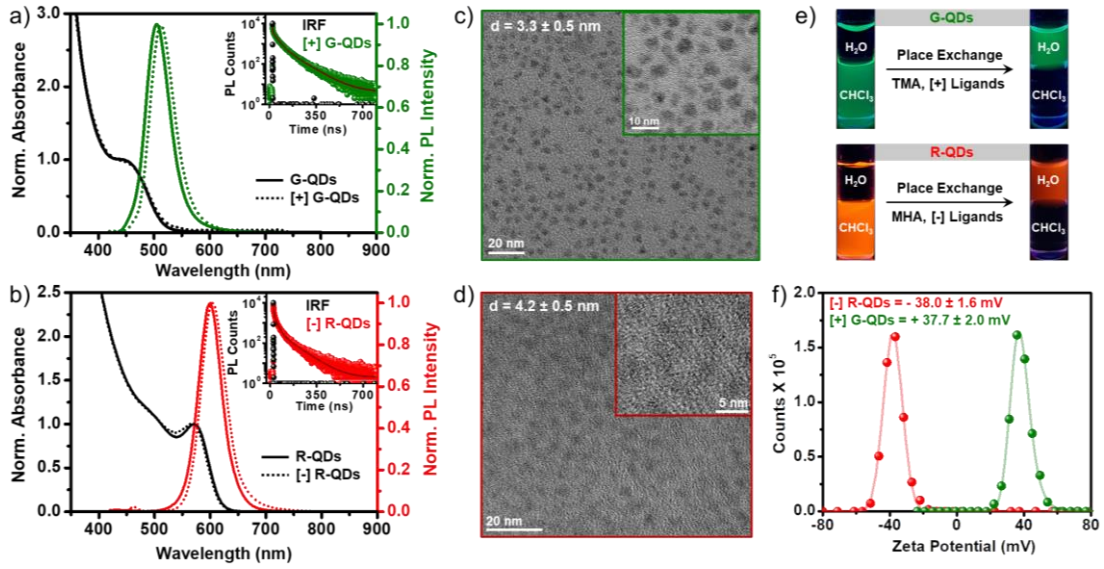

Figure 5.4 Normalized UV-vis absorption and PL spectra of (a) G-QDs and (b) R-QDs, before and after the functionalization with [+] TMA and [-] MHA ligands. Inset shows the corresponding PL decay profiles of [+] G-QDs and [-] R-QDs, collected at 512 nm and 610 nm, respectively. Representative HRTEM images of (c) 3.3 ± 0.5 nm sized [+] G-QDs and (d) 4.2 ± 0.5 nm sized [-] R-QDs. (e) Optical photographs showing the transfer of QD's PL from organic to aqueous phase, confirming the success of ligand-exchange reactions. (f) Representative zeta potential plots of [+] G-QDs and [-] R-QDs.

All the photophysical properties of water-dispersed InP/ZnS QDs were well-preserved after ligand exchange with the charged ligands (**Figure 5.4** and **Table 5.1** and **Tables A5.2**). Notably, the [+] G-QDs and [-] R-QDs retained ~70 % and ~85 % of their PL QY, respectively, after the dispersion in water (**Figure A5.1e,f**). High-resolution transmission electron microscopy (HRTEM) studies confirmed the size and shape uniformity of [+] G-QDs (3.3 ± 0.5) and [-] R-QDs (4.2 ± 0.5 nm) (**Figure 5.4c,d** and **Figure A5.5** in **Appendix Section**). Further, both [+] G-QDs and [-] R-QDs preserved their zinc blend phase in water, as evident from the powder X-ray diffraction (PXRD) studies (**Figure 5.5b**). The diffraction peaks in PXRD shifted towards the ZnS planes, confirming the core-shell structure of [+] G-QDs and [-] R-QDs. Also, the extend of this shift in the diffraction peaks can be directly correlated with the ZnS shell thickness; wherein a comparatively thicker ZnS shell was formed around [+] G-QDs, which is essential for stabilizing small-sized QD nanocrystals.

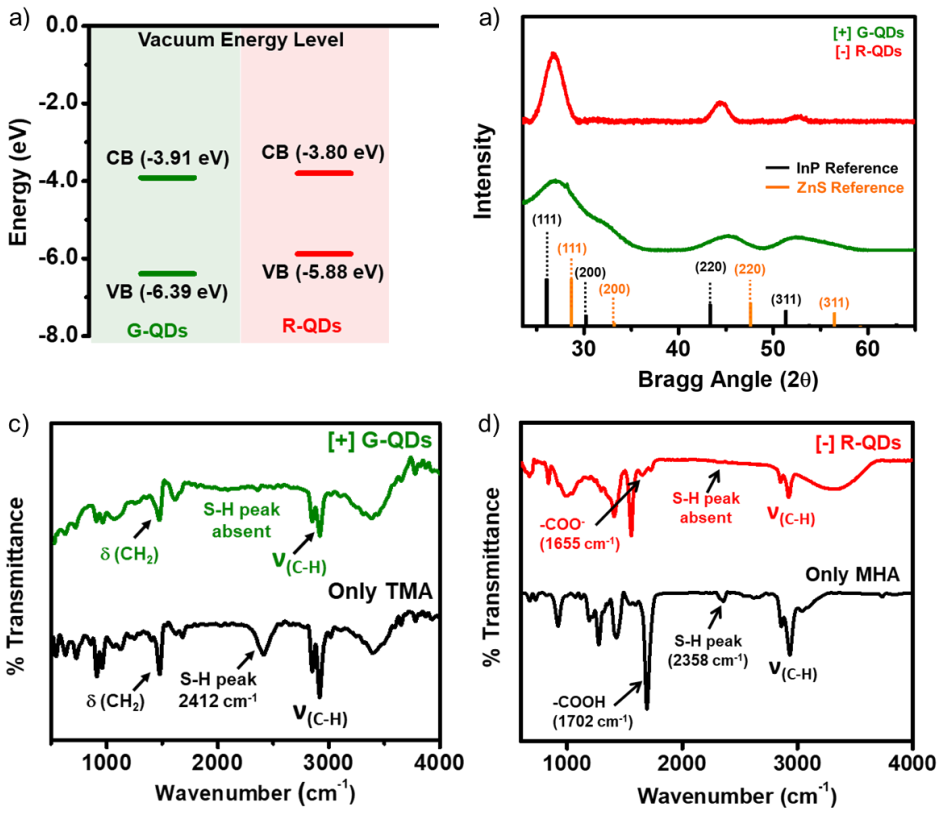

Figure 5.5 Characterization of InP/ZnS QDs. (a) Relative band positions for G-QDs and R-QDs with respect to vacuum energy level, measured from a combination of cyclic voltammetry and absorption studies. (b) Powder X-ray diffraction (PXRD) patterns of [+] G-QDs and [-] R-QDs, respectively. Comparison of PXRD patterns of QDs with bulk InP (black) and bulk ZnS (orange) reference reveals the presence of zinc blend phase in both the QDs. A large shift in diffraction pattern for [+] G-QDs, towards the reference ZnS, indicates the presence of a thicker shell. FTIR spectra of (c) [+] G-QDs, and (d) [-] R-QDs. The presence of characteristics peaks from respective TMA and MHA ligands, confirming the success of ligand-exchange reactions.

Table 5.1 PL decay analysis of [+] G-QDs and [-] R-QDs, in a time window of 800 ns.

System	τ_1 (ns)	α_1	τ_2 (ns)	α_2	τ_3 (ns)	α_3	$\tau_{avg.}$ (ns)	χ^2
[+] G-QDs @512 nm	4.72	0.42	40.22	0.43	115.02	0.15	73.62	1.18
[-] R-QDs @610 nm	3.12	0.63	21.78	0.31	85.84	0.06	42.72	1.25

5.4.2 Synthesis and Characterization of CIS/ZnS QD:

In effort to develop the dyad assembly based on *different core material*, environmentally friendly InP/ZnS QD and CIS/ZnS QD were selected as the donor and acceptor components, respectively. It is well known that the presence of strong interactions is essential to realize efficient light harvesting properties in donor-acceptor systems.[13,24,50,52] Thus, electrostatic

forces were chosen as the tool to control the interaction between the donor-acceptor components in all-QD based FRET system. Accordingly, the organic ligands on the surfaces of QDs were replaced with anionic 11-mercaptoundecanoic acid ([-]) and cationic N,N,N-trimethyl(11-mercaptoundecyl) ammonium chloride ([+]) ligands to yield water stable [-] G-InP/ZnS QD and [+] R_{CIS}-CIS/ZnS QD, respectively (**Scheme A5.1**). Details on the synthesis of QDs were given in the **Chapter-2**. Characterization of green emitting G-InP/ZnS QDs before and after the ligand exchange process have already been discussed **Section-5.4.1** and in **Appendix Section** (**Figures A5.1-A5.6** and **Tables A5.1-A5.2**).

In case of CIS/ZnS QD, the success of place exchange reaction, along with the presence of [+] TMA ligands on CIS/ZnS QDs, were confirmed with standard analytical studies (**Figure 5.6**). The thiol groups of the bifunctional [+] ligands coordinated with the Zn^{2+} ions of the QD shell, and the ionic head groups provided the stability in aqueous medium. The as-synthesized QDs were thoroughly characterized using various spectroscopic and microscopic techniques (**Figure 5.6** and **Table A5.3**). The steady-state and time-resolved spectroscopic experiments revealed negligible changes in the absorption (first excitonic peak) and photoluminescence (PL) properties of QDs upon place exchange reaction (**Figures 5.6a,b**). Remarkably, ~85 % of PL was retained for water stable [+] R_{CIS}-QDs, after the place exchange reaction (inset of **Figure 5.6a**). Likewise, the powder X-ray diffraction studies confirm the retention of chalcopyrite crystal structures for [+] R_{CIS}-QDs (**Figure 5.6d**).[53] Transmission electron microscopy (TEM) studies confirmed the formation of uniform QDs, with an average diameter of 3.7 ± 0.3 nm for [+] R_{CIS}-QD (**Figure 5.6c**). Furthermore, zeta potential studies validated the presence of cationic groups on the surface of [+] R_{CIS}-QDs (+61.8 ± 1.9 mV) (**Figure 5.6f**).

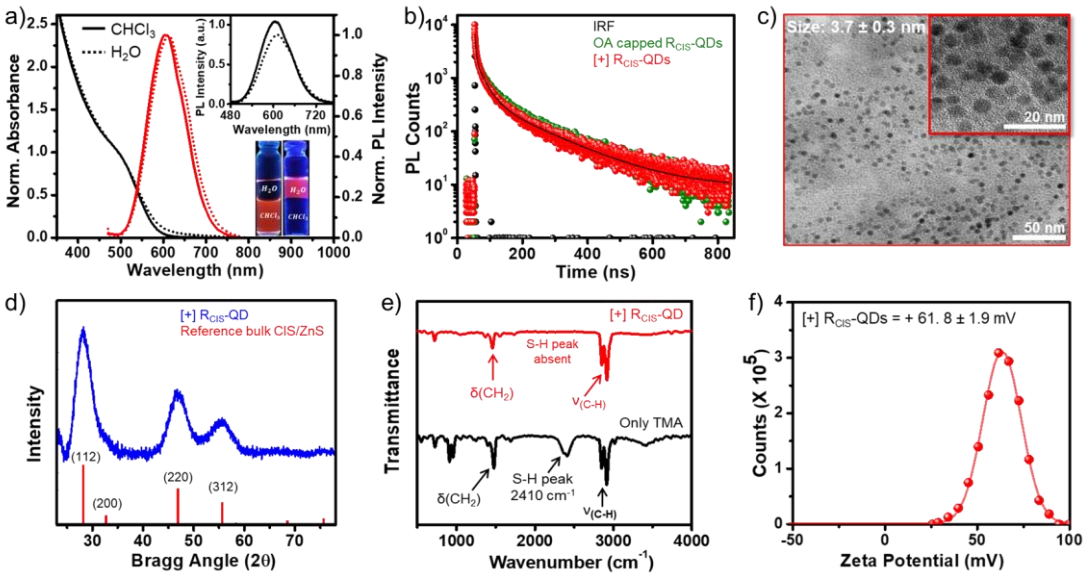

Figure 5.6 Spectroscopic and microscopic characterization of CIS/ZnS QDs. (a) Normalized UV-vis absorption, PL spectra, and (b) PL decay profile of CIS/ZnS QDs, before and after the functionalization with [+] TMA ligands. Inset of (a) shows the corresponding unnormalized PL spectra. Approximately ~85% of the PL QY is retained in [+] CIS/ZnS QDs after place exchange process. (c) Representative HRTEM image and (d) power x-ray diffraction spectrum of 3.7 ± 0.3 nm sized [+] CIS/ZnS QD. (e) FTIR spectra of [+] TMA ligand (black) and [+] TMA capped CIS/ZnS QD (red). The absence of characteristics S-H stretching frequency confirm that sulphur is the binding site to QD. (f) Representative zeta potential plots of [+] R_{CIS}-QDs.

5.4.3 Light Induced Resonance Energy Transfer Studies:

5.4.3.1 Dyad – 1: [+] G-QD:::[-] R-QD Donor:::Acceptor Assembly

Light-induced energy transfer process between [+] G-QDs and [-] R-QDs was investigated using steady-state and time-resolved PL quenching experiments. A large spectral overlap integral ($J(\lambda)$) = (~1.72×10^{15} M^{-1} cm^{-1} nm^4) between the PL of [+] G-QDs and the absorption of [-] R-QDs suggests that the two QDs can form an appropriate donor–acceptor pair for resonance energy transfer studies (**Figure 5.7a**).[6-7] Proximity and strong electronic coupling between donor and acceptor moieties are essential to realise an efficient resonance energy transfer process.[7,13] The favourable electrostatic interaction between the oppositely charged QDs will ensure a strong complexation in [+] G-QD:::[-] R-QD donor:::acceptor system (**Scheme 5.2**).

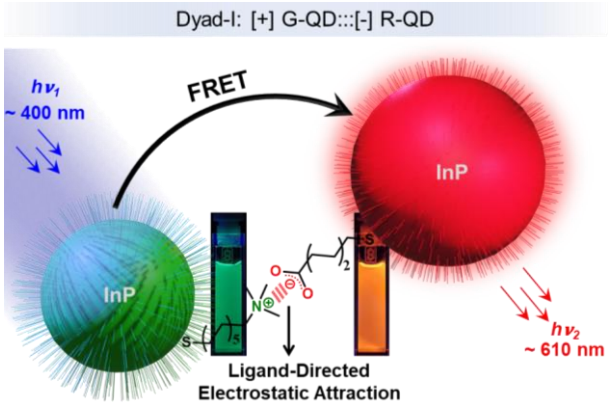

Scheme 5.2 Schematics of electrostatically regulated FRET in all-QD based light-harvesting system containing [+] G-QD and [-] R-QD as donor and acceptor, respectively.

In a typical PL quenching experiment, different aliquots (4 µL of ~25 µM stock solution) of acceptor [-] R-QDs were sequentially added to a solution of [+] G-QDs (~0.2 µM) (**Figure 5.7**). The absorption study shows an increase in the scattering component at higher wavelength region (600-800 nm), with increase in the acceptor QD concentration, indicating a strong aggregation process between the oppositely charged QDs (**Figures 5.7b** and **A5.7**). The electrostatically bonded FRET assemblies (1:2 molar ratio of [+] G-QD:::[-] R-QD donor:::acceptor system) retained their colloidal stability for at least 6 h, without settling down (**Figure A5.7** in **Appendix Section**). This time window was enough to complete all the photophysical experiments. A gradual decrease in the PL corresponding to the donor [+] G-QD was observed, along with a concomitant enhancement in the PL at ~610 nm corresponding to the acceptor [-] R-QD (**Figure 5.7c**). This indicates the involvement of an energy transfer process from [+] G-QD to [-] R-QD. The PL quenching efficiency was estimated to be ~92 % ($E = 1 - I/I_0$, where I_0 and I are the PL intensities of donor QDs in absence and presence of acceptor QDs, respectively).[7] **Figure 5.7d** shows that the relative PL of donor [+] G-QD, and the PL quenching efficiency saturated after the addition of ~0.4 µM of [-] R-QDs. Further, a non-linear Stern-Volmer plot (I_0/I *vs* acceptor QD concentration) confirms the involvement of both static as well as dynamic components in the PL quenching of [+] G-QDs by [-] R-QDs (**Figures 5.7e** and **A5.8**).

One of the biggest challenges in studying the light-induced processes in all QD-based donor-acceptor systems is to achieve a selective excitation of the donor QD in the presence of the acceptor QD. Owing to the broad absorption of QDs, it is inevitable to overcome the direct excitation of acceptor QDs during the energy transfer studies in an all-QD based donor-acceptor system. As a result, there will be interference of the residual PL from the direct excitation of

the acceptor QD in the PL quenching studies. Having said that, there are certain experiments that can be performed to confirm that the PL enhancement seen in the acceptor QD in an all-QD based donor-acceptor system is due to the energy transfer process. One of them is to compare the PL intensities of the acceptor QDs in all-QD based donor-acceptor system *vs* only-acceptor QD solution, under the same excitation wavelength and acceptor concentration. In the present study, the PL intensity of the acceptor QDs in [+] G-QD:::[−] R-QD donor:::acceptor complex was higher than that obtained from the direct excitation of only [-] R-QDs (~0.4 μM) (blue spectrum in **Figure 5.7c**). Another approach is to perform a reverse addition experiment by adding donor QDs to a fixed concentration of acceptor QDs (**Figure 5.7f**). In a typical experiment, the PL of acceptor [-] R-QDs (~0.4 μM) was monitored upon the successive addition of donor [+] G-QDs (0.5 μL of ~20 μM stock solution). A steady increase in the PL intensity of [-] R-QDs was observed in the presence of donor [+] G-QDs, which saturated after ~0.03 μM of donor QDs (~2 times PL enhancement was observed) (**Figure 5.7f**). Along with the above two control experiments, the photoluminescence excitation (PLE) studies also confirm the involvement of a light-induced energy transfer process from [+] G-QDs to [-] R-QDs (**Figure 5.8**).

As in steady-state experiments, the time-resolved studies too revealed a clear quenching in the PL decay kinetics of the donor [+] G-QDs in the presence of acceptor [-] R-QDs (**Figure 5.9a**). The average PL lifetime of donor [+] G-QDs decreased from ~75 ns to ~30 ns (collected at 512 nm) in the presence of ~0.4 μM acceptor [-] R-QDs, corresponding to a quenching efficiency of ~60 % ($E = 1 - \tau/\tau_0$, where τ_0 and τ are the lifetime of donor QDs in absence and presence of acceptor QDs, respectively) (**Table 5.2**). Along with this, a ~50 % enhancement in the PL lifetime of acceptor [-] R-QDs was observed (~40 ns to ~60 ns) (**Figure 5.9b**), which unambiguously confirms the energy transfer process from [+] G-QDs to [-] R-QDs. As per the exciton-exciton interaction model, the energy transfer-mediated exciton generation rate in acceptor QDs will exceed the carrier recombination rate, resulting in an increase in the PL lifetime of acceptor QDs.[52] Further, a linear Stern-Volmer plot was obtained from the time-resolved PL studies proving the involvement of dynamic quenching process in [+] G-QD:::[-] R-QD donor:::acceptor system (**Figures 5.9c** and **A5.9**, and **Table A5.4**).[7] Static and dynamic quenching constants were estimated to be ~1.8 x 10^7 M^{-1} and ~2.8 x 10^6 M^{-1}, respectively. Further, a high bimolecular quenching constant (~3.8 x 10^{13} M^{-1} s^{-1}) confirms a strong ground state interaction between the oppositely charged donor [+] G-QDs and acceptor [-] R-QDs.[7,13]

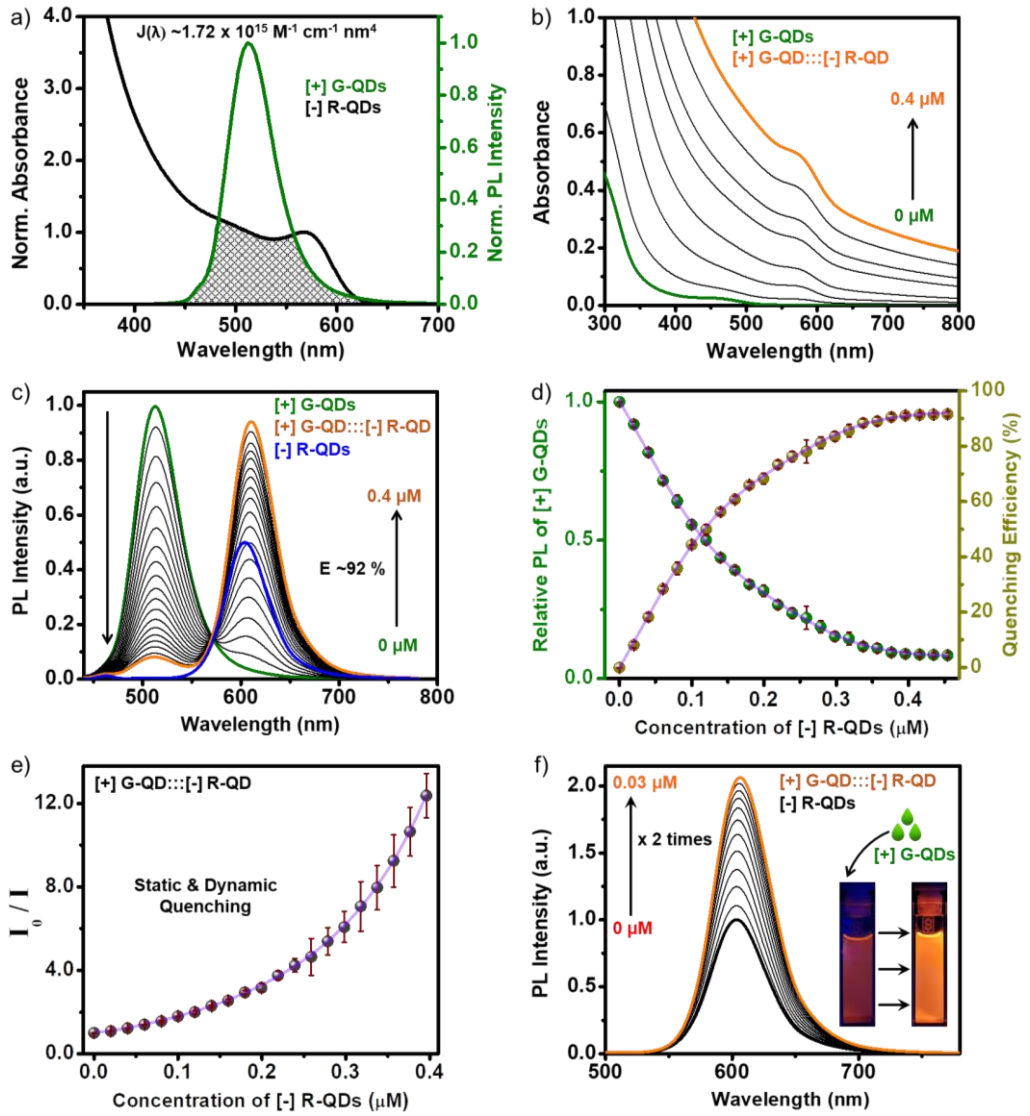

Figure 5.7 Steady-state energy-transfer studies in [+] G-QD:::[-] R-QD donor:::acceptor system. (a) The spectral overlap integral between the PL of [+] G-QDs and absorbance of [-] R-QDs. (b) The steady-state UV-vis absorption and (c) PL spectral changes upon successive addition of acceptor [-] R-QDs to ~0.2 μM of donor [+] G-QDs. The blue trace shows the residual PL from the direct excitation of [-] R-QDs (~0.4 μM). (d) A plot showing the saturation in the relative PL of donor [+] G-QDs and PL quenching efficiency ($1-I/I_0$), after the addition of ~0.4 μM of acceptor [-] R-QDs. (e) A non-linear Stern-Volmer plot was constructed from the relative PL of donor [+] G-QDs vs concentration of acceptor [-] R-QDs. (f) Reverse addition experiment: A gradual enhancement in the PL of acceptor [-] R-QDs was observed, upon increasing the concentration of the donor [+] G-QDs. Inset shows the corresponding enhancement in the PL color of acceptor [-] R-QDs. The excitation wavelength was 400 nm in all these studies.

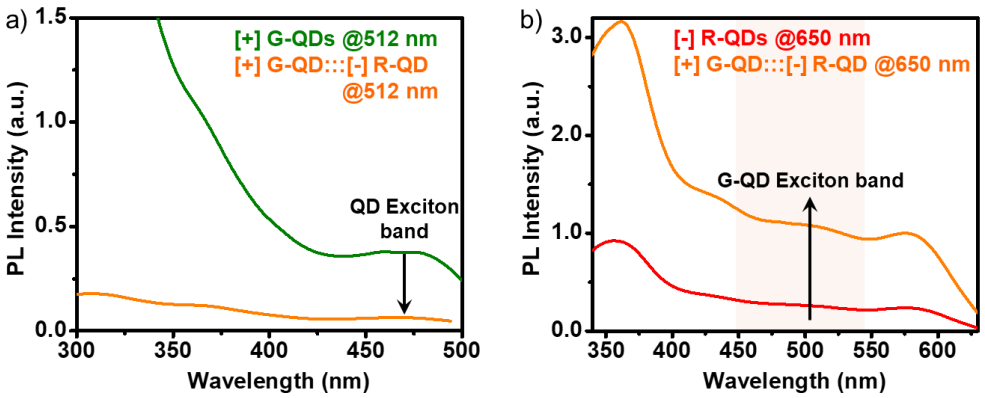

Figure 5.8 Photoluminescence excitation (PLE) study in [+] G-QD:::[-] R-QD donor:::acceptor complex. (a) The PLE spectra of donor [+] G-QDs in absence (olive-green) and presence (orange) of acceptor [-] R-QDs, collected at 512 nm. (b) The PLE spectra of acceptor [-] R-QDs in absence (red) and presence (orange) of [+] G-QDs, collected at 650 nm.

Next, temperature-dependent PL lifetime studies were performed to prove the energy transfer process in [+] G-QD:::[-] R-QD donor:::acceptor assembly. In general, the PL lifetime of fluorophores increases as the temperature is lowered, because of the suppression of the phonon vibrations.[51-52] In contrast, an energy transfer process via the FRET mechanism can be independent of the temperature at a specific donor-acceptor distance, as it is a dipole-dipole mediated non-radiative resonance energy transfer process.[51-52] In our system too, a continuous increase in the PL lifetime of donor [+] G-QDs was observed in absence and presence of acceptor [-] R-QDs, as the temperature was dropped from 318 K to 268 K (**Figure A5.10** and **Table A5.5**). However, there was a negligible change in the efficiency of the PL lifetime quenching as a function of temperature (**Figure 5.9d** and **Table A5.5**), which definitely overrules the involvement of an electron transfer process. Thus, the PL lifetime studies prove that an efficient FRET process is occurring from the donor [+] G-QDs to the acceptor [-] R-QDs. Accordingly, all the energy transfer parameters were estimated using the FRET formalism as summarised in **Figure 5.9e**. The rate of the energy transfer in [+] G-QD:::[-] R-QD donor:::acceptor system was calculated to be ~1.02 x 10^7 s^{-1}, which is comparable to some of the best FRET pairs developed based on QDs (**Table A5.6**).[22] Further, control experiments with similarly charged InP/ZnS QDs ([-] G-QDs and [-] R-QDs) proved the necessity of electrostatic attractions in achieving an efficient FRET in [+] G-QD:::[-] R-QD donor:::acceptor system (**Figures A5.11-A5.12** and **Table A5.7**). Even though the PL quenching could happen because of an electron transfer process, all the steady-state and time-resolved experiments conclusively prove that energy transfer via the FRET mechanism is the main process operating in [+] G-QD:::[-] R-QD donor:::acceptor assembly.

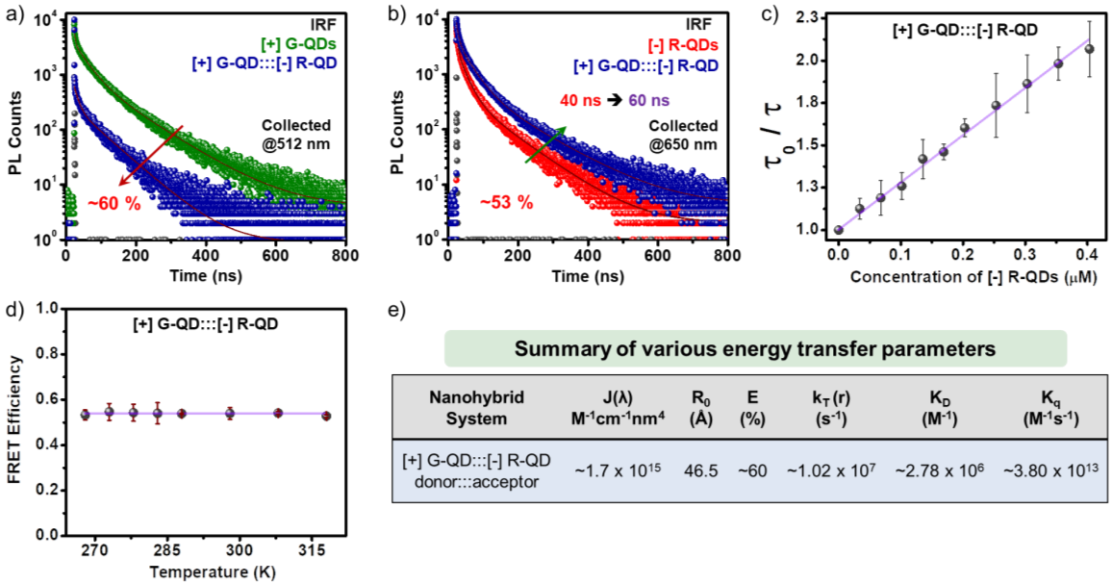

Figure 5.9 Time-resolved FRET studies in [+] G-QD:::[-] R-QD donor:::acceptor system. (a) PL decay profiles of [+] G-QDs in absence and presence of ~0.4 μM of acceptor [-] R-QDs. The excitation wavelength was 405 nm, and the PL was collected at 512 nm corresponding to the emission of donor QDs. (b) Corresponding PL decay profiles of acceptor [-] R-QDs in absence and presence of donor [+] G-QDs. The excitation wavelength was 405 nm, and the PL was collected at 650 nm corresponding to the emission of acceptor QDs. (c) A Stern–Volmer plot constructed from the relative PL lifetime of donor [+] G-QDs vs concentration of acceptor [-] R-QDs. (d) Temperature change had a negligible influence on the PL quenching efficiency, confirming that the energy transfer process follows the FRET mechanism. (e) Summary of various energy transfer parameters calculated based on the FRET formalism: the spectral overlap integral [J(λ)]; Förster radius (R_0); FRET efficiency (E); rate of energy transfer (k_T), dynamic quenching constant (K_D), and bimolecular quenching constant (k_q).

Table 5.2 PL decay analysis of donor [+] G-QDs, acceptor [-] R-QDs and [+] G-QD:::[-] R-QD donor:::acceptor complex, in a time window of 800 ns. The PL decay was collected at 512 nm and 650 nm for donor and acceptor QDs, respectively.

System	τ_1 (ns)	α_1	τ_2 (ns)	α_2	τ_3 (ns)	α_3	$\tau_{avg.}$ (ns)	χ^2
[+] G-QDs @512 nm	4.72	0.42	40.22	0.43	115.02	0.15	73.62	1.18
[+] G-QD:::[-] R-QD @512 nm	0.11	0.98	4.27	0.01	41.45	0.01	30.75	1.19
[-] R-QDs @650 nm	2.07	0.64	16.08	0.29	72.02	0.07	39.97	1.32
[+] G-QD:::[-] R-QD @650 nm	5.58	0.52	34.13	0.40	116.98	0.08	60.85	1.30

It is important to demonstrate the FRET in solid-state as well, to prove the suitability of [+] G-QD:::[-] R-QD donor:::acceptor assembly for device level studies. In one example, FRET studies were performed in thin agarose film of InP/ZnS QD based donor-acceptor complex. Agarose films of only-donor, only-acceptor, and donor-acceptor complex were prepared according to the previously reported procedures.[26,45] PL maxima of [+] G-QDs and [-] R-QDs

were retained in only-donor and only-acceptor agarose films, proving negligible intra-QD interactions. On the other hand, a drastic quenching in the PL of donor [+] G-QDs was observed in the agarose film containing [+] G-QD:::[-] R-QD donor:::acceptor complex (**Figure 5.10a**). The PL lifetime of [+] G-QDs decreased from 53 ns to 14 ns in [+] G-QD:::[-] R-QD donor:::acceptor complex agarose film, confirming an efficient energy transfer process (~75 %) (**Figure 5.10b** and **Table 5.3**). The higher energy transfer efficiency in the agarose film, compared to the aqueous medium, can be attributed to the better dipole-dipole interaction between the closely spaced donor-acceptor pairs in the agarose film.

Finally, the process of FRET in [+] G-QD:::[-] R-QD donor:::acceptor complex was visualized in a temporal fashion at a constant donor-acceptor ratio, using the droplet evaporation method. Droplets of only-donor, only-acceptor, and donor-acceptor complex were placed on Teflon-coated glass slides, and their respective PL colours were monitored as a function of droplet evaporation. The drying had a negligible effect on the PL colour of only-donor and only-acceptor samples, which once again confirms minimal intra-QD interactions in the solid-state (first and last rows in **Figure 5.10c**). On the contrary, the PL colour of the donor-acceptor droplet gradually shifted towards the acceptor PL colour as a function of drying, and the same trend was observed in droplets made with different donor-acceptor ratios (middle rows in **Figure 5.10c)**. This observation can be explained based on the FRET formalism as follows. Initially, the droplet showed a mixed PL color corresponding to the physical mixture of donor and acceptor QDs. As the droplet evaporation proceeds, the distance between donor and acceptor QDs decreases. This will enable a better dipole-dipole interaction between QDs in the dried-state, leading to a significant enhancement in the FRET efficiency ($E \alpha 1/r^6$, where r is the donor-acceptor distance).[40] Similarly, in a separate study, donor-acceptor droplet showed drying assisted enhancement in FRET process, when monitored under confocal microscope (**Figure 5.11**). Thus, along with proving the suitability of InP/ZnS QD based donor-acceptor complex for solid-state applications, the droplet evaporation studies helped in visualising the distance-dependent nature of the FRET process in [+] G-QD:::[-] R-QD nanohybrid system as well.

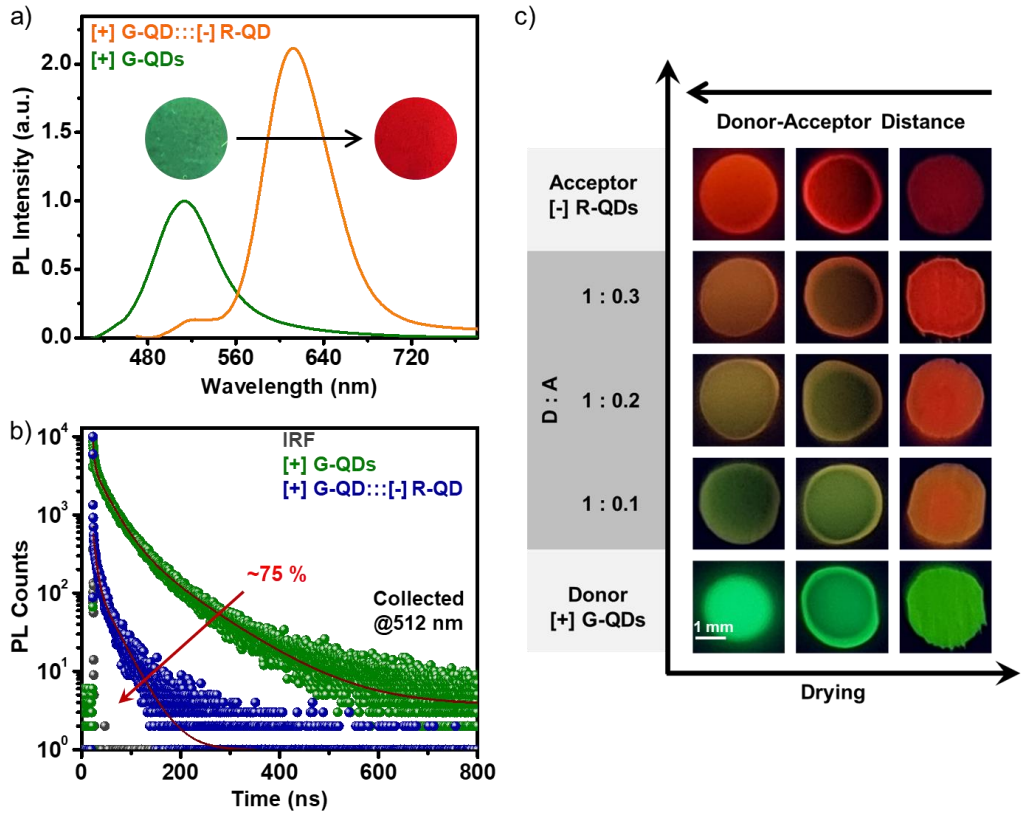

Figure 5.10 FRET process in solid-state. (a) Steady-state and (b) time-resolved PL spectra of donor [+] G-QDs, in agarose film, in absence and presence of [-] R-QDs. (c) Optical photographs showing the temporal variation in the PL as a function of drying: PL images of only-donor [+] G-QDs (bottom row) and only-acceptor [-] R-QDs (top row). Middle rows show the temporal changes in the PL of [+] G-QD:::[-] R-QD mixture, containing different donor: acceptor ratios. First and third columns correspond to QD samples in liquid-state (droplet, at 0 h) and dried-state (film, after ~12 h), respectively.

Table 5.3 PL decay analysis of donor [+] G-QDs and [+] G-QD:::[-] R-QD donor:::acceptor complex in agarose film, collected at 512 nm, in a time window of 800 ns.

System	τ_1 (ns)	α_1	τ_2 (ns)	α_2	τ_3 (ns)	α_3	$\tau_{avg.}$ (ns)	χ^2
[+] G-QDs @512 nm	2.75	0.57	29.97	0.36	99.46	0.07	52.80	1.36
[+] G-QD:::[-] R QD @512 nm	0.21	0.97	5.04	0.02	26.99	0.01	13.64	1.19

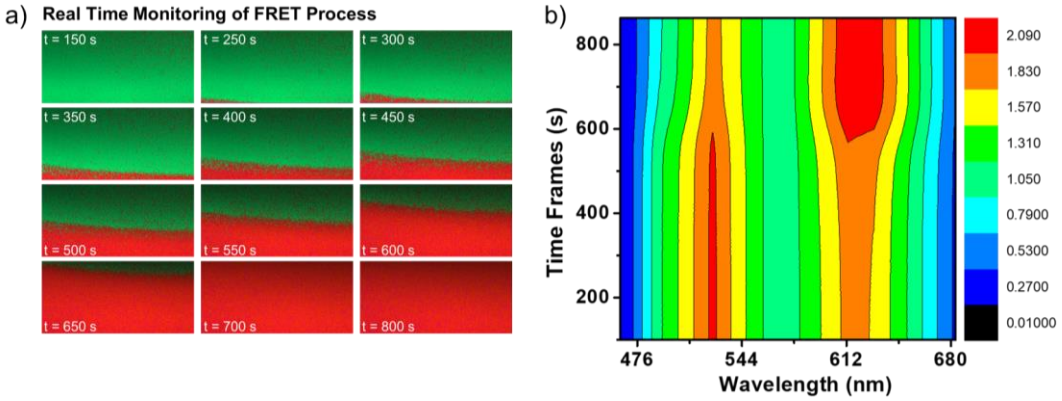

Figure 5.11 Real-time monitoring of the FRET process under a confocal microscope. (a) The confocal luminescence image at different time-frames summarises the influence of the drying event on the energy transfer in [+] G-QD:::[-] R-QD donor::: acceptor complex. The droplet began to solidify after 150 s and dried off within 700 s. Here, the process of drying began at the periphery and moved towards the centre of the droplet, which could be attributed to the coffee-ring effect. The appearance of red emission as a function of evaporation signifies the enhancement in the efficiency of the FRET process in the [+] G-QD:::[-] R-QD donor:::acceptor mixture. (b) The contour plot summarises the real-time PL information as a function of drying event. There was a decrease in the PL intensity of donor [+] G-QD as a function of drying, along with an enhancement in the PL intensity in [-] R-QD.

Thus, a light-induced resonance energy transfer process was demonstrated in an all-InP QD based donor-acceptor assembly ([+] G-QD:::[-] R-QD) in water. The strong electrostatic attraction between the oppositely charged donor [+] G-QDs and acceptor [-] R-QDs turned out to be decisive in achieving an efficient FRET process. Steady-state and time-resolved spectroscopic studies revealed the involvement of both static and dynamic components in the PL quenching of donor [+] G-QD by acceptor [-] R-QDs. The rate of energy transfer in electrostatically bound [+] G-QD:::[-] R-QD donor:::acceptor system was calculated to be ~1.02 x 10^7 s^{-1}, which is comparable to some of the best FRET pairs developed based on QDs. Further, the solid-state studies helped in visualising the distance-dependent nature of the FRET process in the electrostatically bound [+] G-QD:::[-] R-QD donor:::acceptor system. Our study probably would be the first demonstration of an electrostatically-driven light-induced energy transfer process in an all-QD assembly containing environmentally friendly InP QDs, as the donor as well as the acceptor. A future target could be the design of a library of donor-acceptor systems based on environmentally friendly QDs and also expanding the concept among QDs with *different core materials*.

5.4.3.2 Dyad – 2: [-] G-QD:::[+] R_{CIS}-QD Donor:::Acceptor Assembly

For FRET studies in all-QD nanohybrid system based on *different core materials*, ~515 nm emitting negatively charged [-] G-QD was chosen as the energy donor and ~630 nm emitting positively charged [+] R_{CIS}-QD was selected as the acceptor (**Scheme 5.3**).

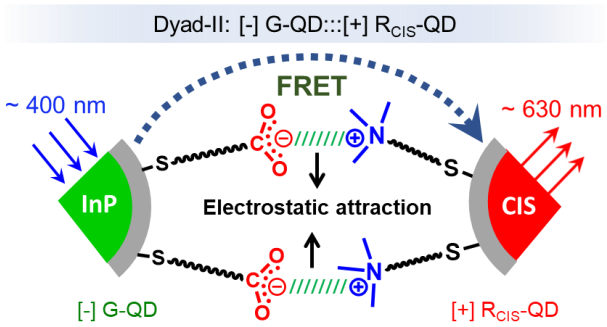

Scheme 5.3 Schematic representation of electrostatically driven FRET from donor [-] G-QD to acceptor [+] R_{CIS}-QD.

A strong spectral overlap between the PL of [-] G-QD and absorption of [+] R_{CIS}-QD suggested that these QDs can form a good donor-acceptor pair for resonance energy transfer process (**Figure A5.13a**). Spectral overlap integral value was estimated to be ~1.46 × 10^{15} $M^{-1}cm^{-1}nm^4$.[7] Systematic energy transfer studies were performed by monitoring the PL of [-] G-QD:::[+] R_{CIS}-QD donor-acceptor complex in water, at the excitation wavelength of 400 nm (**Figure 5.12**). Small aliquots of [+] R_{CIS}-QD (50 µL of ~80 µM) were added to a 3 mL solution of 0.6 µM [-] G-QD, under argon atmosphere. **Figure A5.13b** shows the variation in the absorption spectrum of [-] G-QD in the presence of varying concentrations of acceptor [+] R_{CIS}-QD. A steady decrease in the PL of [-] G-QD was observed in the presence of acceptor [+] R_{CIS}-QD, along with a concomitant appearance of a new band at ~630 nm corresponding to the PL of [+] R_{CIS}-QD (**Figure 5.12a**). A non-linear Stern-Volmer plot confirmed the involvement of both static and dynamic components in the PL quenching of [-] G-QD:::[+] R_{CIS}-QD donor-acceptor complex (inset of **Figure 5.12a** and **Figure A5.13c,d**).[7-8,13] Likewise, a large bimolecular quenching constant of ~1.38 × 10^{12} $M^{-1}s^{-1}$ confirmed a strong ground state interaction between the oppositely charged donor and acceptor QDs.[7-8,13] The PL quenching efficiency from steady-state experiments was estimated to be ~75 % (E = 1- I/I_0; where I and I_0 are the donor PL intensity in presence and absence of acceptor QDs). The relative PL of [-] G-QD and quenching efficiency got saturated upon the addition of ~14 µM of [+] R_{CIS}-QD (**Figure 5.12b**). Owing to the broad absorption of QDs, a selective excitation of donor [-] G-

QD is not possible in an all-QD nanohybrid, and this can strongly interfere with the estimation of the PL quenching process. However, a direct excitation of ~14 μM of [+] R_{CIS}-QDs, at 400 nm, exhibited lower PL intensity compared to that in the [-] InP/ZnS:::[+] R_{CIS}-QD complex (black spectra in **Figure 5.12a**). This indicates that the PL quenching in all-QD complex was predominantly due to an efficient resonance energy transfer from [-] G-QD to [+] R_{CIS}-QDs. A close agreement of excitation spectra with the steady-state PL of [-] G-QD:::[+] R_{CIS}-QD complex further directs towards an efficient energy transfer process (**Figure A5.14**).

Detailed time-resolved spectroscopic studies were performed to ascertain the mechanism of PL quenching in [-] G-QD:::[+] R_{CIS}-QD complex. Time-correlated single photon counting (TCSPC) studies revealed a clear quenching in the PL decay of [-] G-QD (collected at 515 nm) in the presence of [+] R_{CIS}-QDs. The average lifetime of [-] G-QD decreased from ~54 ns to ~23 ns in the presence of ~14 μM of [+] R_{CIS}-QDs (**Figure 5.12c** and **Table 5.4**). The efficiency of PL quenching from lifetime studies was estimated to be ~60 % ($E = 1 - \tau/\tau_0$; where τ and τ_0 are the average lifetimes of the donor in presence and absence of acceptor). Consequently, the rate of PL quenching due to FRET was calculated to be 3.45×10^7 s^{-1}. Interestingly, the average PL lifetime of acceptor [+] R_{CIS}-QD (collected at 631 nm) increased from ~92 ns to ~118 ns in the all-QD donor-acceptor complex (**Figure 5.12d** and **Table 5.4**). The increase in acceptor lifetime is usually considered as a conclusive proof for the resonance energy transfer process, and can be explained based on the exciton-exciton interaction model in QD-QD FRET pair.[51] As per this model, the rate of exciton generation due to nonradiative energy transfer will essentially exceed the carrier recombination rate in acceptor QDs, thereby leading to an increase in its PL lifetime.[51] Thus, the time-resolved spectroscopic studies confirmed an efficient resonance energy transfer process from donor [-] G-QD to acceptor [+] R_{CIS}-QD in the all-QD complex. The various parameters related to the resonance energy transfer process in [-] G-QD:::[+] R_{CIS}-QD donor-acceptor complex are summarized in **Table 5.5**.

Another prominent way to prove the energy transfer process is to perform temperature dependent time-resolved PL studies.[51] As per the literature, a steady decrease in temperature will essentially inhibit the nonradiative recombination channels, because of the suppression of phonon vibrations.[52] Consequently, the lifetime of donor QD will steadily increase with a decrease in the temperature. Whereas, FRET is a nonradiative process and independent of temperature, at a given donor-acceptor distance.[50,51] Accordingly, the PL lifetime of donor [-] G-QD was monitored in the absence and presence of [+] R_{CIS}-QD by systematically varying the temperature from 298 K to 268 K (**Figure 5.12e** and **Table A5.8**). A steady and uniform

increase in the lifetime of [-] G-QD was observed as a function of decrease in temperature (both in the absence and presence of [+] R_{CIS}-QD). However, negligible changes were observed in the PL quenching efficiency in [-] G-QD:::[+] R_{CIS}-QD complex throughout the different temperatures studied (**Figure 5.12f** and **Table A5.8**). Thus, the temperature dependent lifetime experiments conclusively prove the prominent role of a non-radiative energy transfer process in [-] G-QD:::[+] R_{CIS}-QD complex.

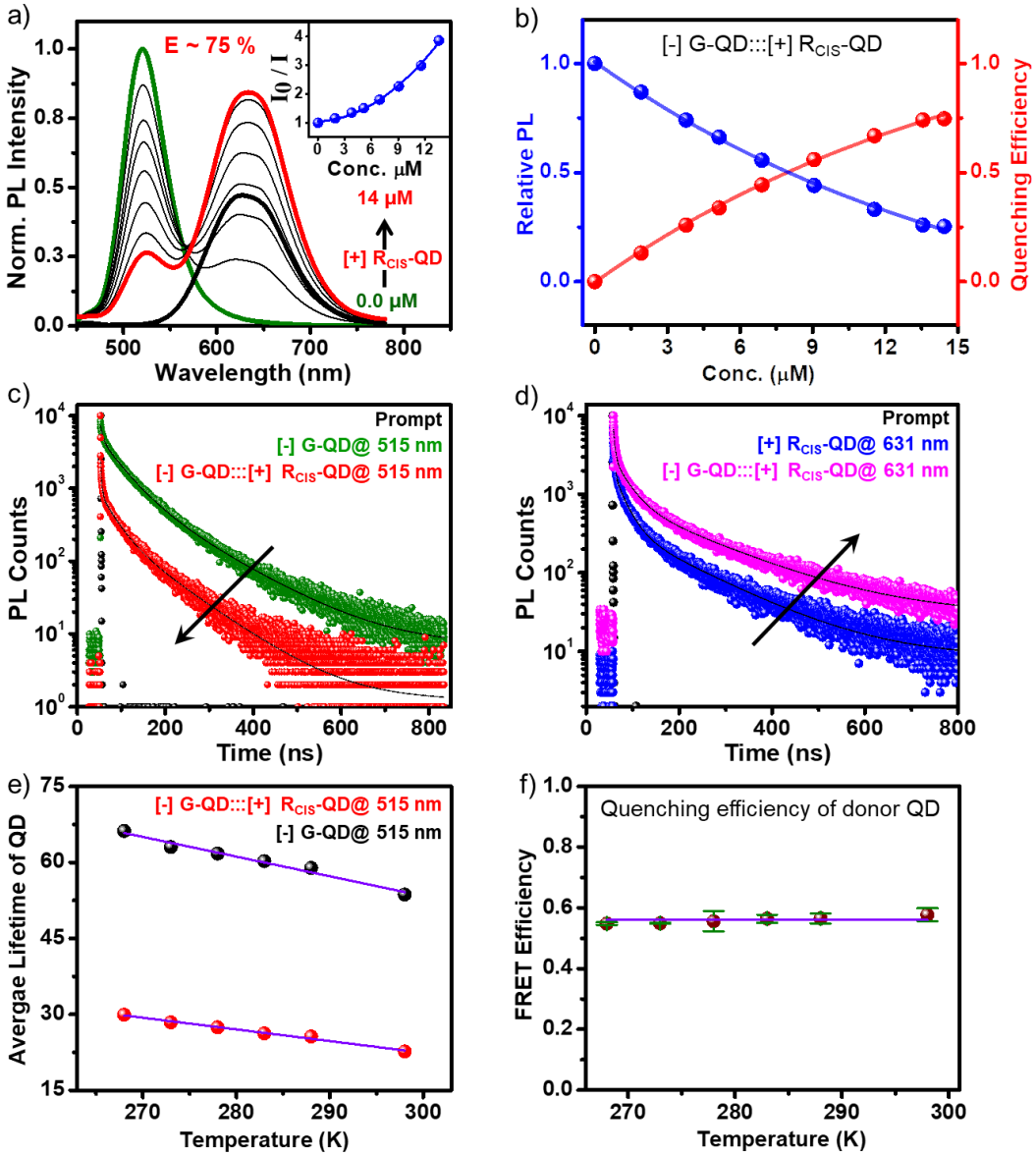

Figure 5.12 Steady-state and time-resolved PL quenching studies in [-] G-QD:::[+] R_{CIS}-QD complex. (a) Spectral changes in the PL of the [-] G-QD upon the addition of varying concentrations of [+] R_{CIS}-QD. The inset shows the corresponding Stern-Volmer plot. (b) A plot showing the saturation in the relative PL of donor [-] G-QD and PL quenching efficiency, as a function of acceptor [+] R_{CIS}-QD concentration. (c) PL decay profiles of donor [-] G-QD in the absence and presence of acceptor [+] R_{CIS}-QD, collected at 515 nm. (d) PL decay profiles of acceptor [+] R_{CIS}-QD in the absence and presence of donor [-] G-QD, collected at 631 nm. (e,f) Temperature dependent PL quenching experiments. (e) Variation in the PL lifetime of [-] G-QD in the absence (black) and presence (red) of [+] R_{CIS}-QD, as a

function of temperature. (f) A plot showing negligible variation in the FRET efficiency in [-] G-QD:::[+] R_{CIS}-QD complex, as a function of temperature.

Next, we investigated the mode of interaction between the donor and the acceptor QDs, which led to an efficient FRET in [-] G-QD:::[+] R_{CIS}-QD complex. Presence of opposite surface charges on donor and acceptor QDs points towards a strong electrostatic interaction between the two QDs. Control experiments were performed with similarly charged QDs to prove the potency of electrostatics in driving an efficient FRET in all-QD based donor-acceptor system (**Figure 5.13**). For instance, systematic energy transfer experiments were performed with [+] G-QD as the donor and [+] R_{CIS}-QD as the acceptor (**Figure 5.13b**). Furthermore, negligible changes in the PL decay of donor and acceptor QDs confirmed weak interaction between [+] G-QD and [+] R_{CIS}-QDs [(Inset of **Figure 5.13b**) and **Figure A5.15c** and **Table A5.9**). A similar result was obtained with [-] G-QD and [-] R_{CIS}-QDs as the donor-acceptor pair (**Figures 5.13a,c** and **A5.15b,d** and **Table A5.10**), thereby proving the necessity of opposite surface charges in achieving an efficient energy transfer in all-QD based donor-acceptor system.

Table 5.4 PL decay analysis of donor [-] G-QDs, acceptor [+] R_{CIS}-QDs and [-] G-QD:::[+] R_{CIS}-QD donor:::acceptor complex, in a time window of 800 ns. The PL decay was collected at 515 nm and 630 nm for donor and acceptor QDs, respectively.

System	τ_1 (ns)	α_1	τ_2 (ns)	α_2	τ_3 (ns)	α_3	$\tau_{avg.}$ (ns)	χ^2
[-] G-QDs @515 nm	5.90	0.47	30.50	0.44	101.95	0.09	53.65	1.29
[-] G-QD:::[+] R_{CIS}-QD @515 nm	2.11	0.69	19.11	0.29	62.50	0.02	22.68	1.20
[+] R_{CIS}-QDs @631 nm	5.08	0.51	33.70	0.37	146.62	0.12	92.27	1.35
[-] G-QD:::[+] R_{CIS}-QD @631 nm	5.33	0.46	39.00	0.37	167.66	0.17	117.98	1.19

Table 5.5 Resonance energy transfer parameters for [-] G-QD:::[+] R_{CIS}-QD complex in water.

System	J(λ) ($M^{-1}cm^{-1}nm^4$)	R_0 (Å)	E (%)	$k_T(r)$ (s^{-1})	k_q ($M^{-1}s^{-1}$)
[-] G-QD:::[-] R_{CIS}-QD	1.46×10^{15}	48	60	1.72×10^{6}	1.38×10^{12}

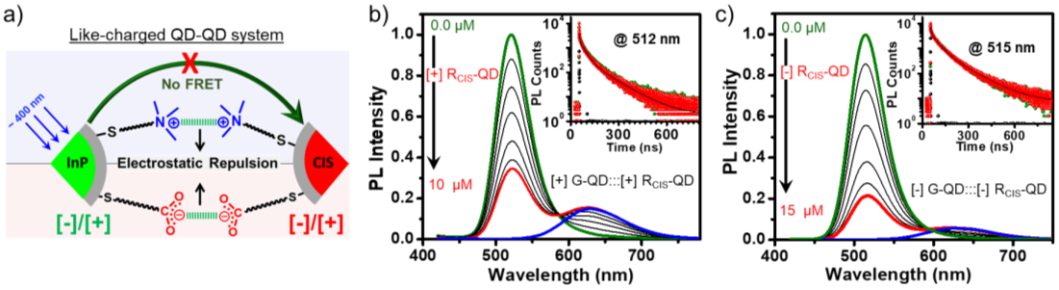

Figure 5.13 Proof of electrostatically driven FRET. (a) Schematic representation of negligible resonance energy transfer between similarly charged [+] G-QD:::[+] R_{CIS}-QD and [-] G-QD:::[-] R_{CIS}-QD assembly. (b) Steady-state PL spectra of [+] G-QD in varying concentrations of [+] R_{CIS}-QD. Inset show the PL decay profiles of [+] G-QDs in absence (olive) and presence (red) of [+] R_{CIS}-QDs, collected at 512 nm. (c) Steady-state PL spectra of [-] G-QD in varying concentrations of [-] R_{CIS}-QD. Inset show the PL decay profiles of [-] G-QDs in absence (olive) and presence (red) of [-] R_{CIS}-QDs, collected at 515 nm.

Finally, the process of FRET in [-] G-QD:::[+] R_{CIS}-QD complex was demonstrated in a temporal fashion in the solid state. For this, a solution of [-] G-QD:::[+] R_{CIS}-QD complex was dropped on a glass slide, followed by monitoring the PL as a function of drying (**Figure 5.14a**). In the initial stages, the PL of the drop was yellow colored due to the mixing of green and red emitting QDs, indicating negligible photophysical interaction between the donor and acceptor QDs ((ii) and (iii) in **Figure 5.14a**). As the drying proceeded, the PL color of the drop changed from yellow (at t = 0 h) to orange (at t~2 h), and finally to deep-red (at t~7 h). The temporal changes in the PL color of the drop as a function of drying can be explained as follows. The process of FRET is extremely sensitive to the variation in the distance between the donor and acceptor components (E_{FRET} α $1/r^6$; r is the donor-acceptor distance).[6,7] With a steady evaporation of the solvent, the distance between the donor and acceptor QDs will gradually decrease leading to an increase in the FRET efficiency.[7] Thus, the temporal shifts in the PL color observed from donor PL (yellow) towards acceptor PL (deep red) once again confirm the involvement of efficient FRET in [-] G-QD:::[+] R_{CIS}-QD complex. Furthermore, the efficiency of energy transfer in the solid state was appreciably higher than that in the solution state. For instance, the ratio of acceptor to donor emission intensity ($I_{[+]\ R\{CIS\}\text{-}QD}$ / $I_{[-]\ G\text{-}QD}$) was ~ 5.5 times higher in the solid state, compared to that in the solution state (**Figure 5.14b**). The effect of drying (and hence aggregation) on the PL color change was overruled by performing control experiments with donor G-QD and acceptor R_{CIS}-QDs, separately [(i) and (iv) in **Figure 5.14a**). After complete drying, the individual thin films of donor and acceptor QDs retained their inherent green and red PL colors, respectively [(i) and (iv) in **Figure 5.14a**). Thus, we were successful in realizing a temporal evolution of an efficient FRET process in [-] G-QD:::[+]

R_{CIS}-QD complex in the solid state as well, which can be a useful information for future device level applications.

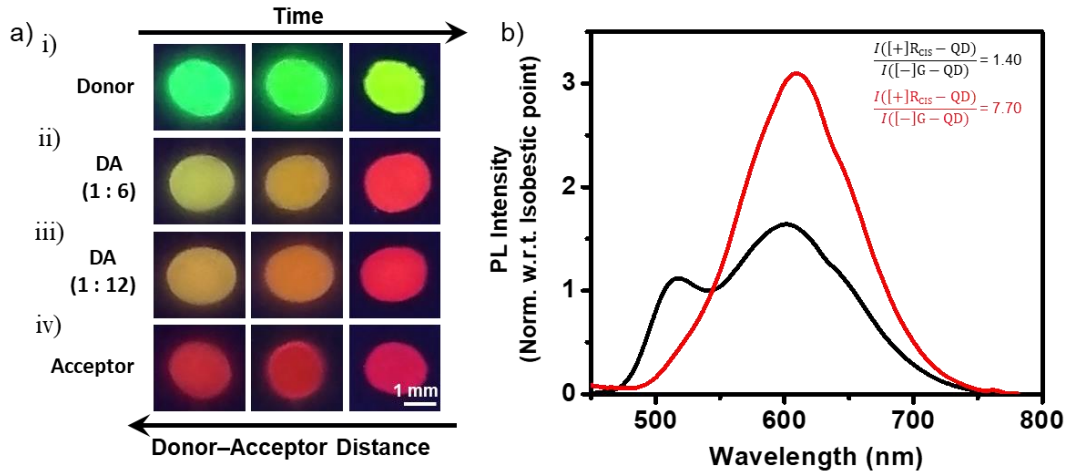

Figure 5.14 a) Temporal FRET studies in the solid state. True-color PL images of (i) [-] G-QD, (ii & iii) [-] G-QD:::[+] R_{CIS}-QD donor-acceptor complex, and (iv) [+] R_{CIS}-QD, as a function of solvent drying. First (at ~0 h) and third columns (at ~7 h) in all panels correspond to liquid drop and thin films, respectively. Kindly note that the solvent completely evaporated to form a stable solid film at the end of ~7 h of drying. The donor-acceptor distance decreases with respect to time, because of solvent evaporation (from left to right). All the PL images were collected under ~364 nm irradiation. (b) The corresponding PL spectra of [-] G-QD:::[+] R_{CIS}-QD complex in solution (black) and solid state (red) normalized with respect to the isobestic point of donor-acceptor transition.

As a conclusion of this section, we have demonstrated an electrostatically regulated resonance energy transfer in an all-QD based donor-acceptor complex in water, comprising of environmentally friendly QDs of *different core materials*. Appropriate surface functionalization resulted in the formation of water-stable G-QD and R_{CIS}-QD, with opposite surface charges. Detailed steady-state and time-resolved PL quenching experiments revealed an efficient nonradiative resonance energy transfer from [-] G-QD to [+] R_{CIS}-QD, in the all-QD based donor-acceptor complex. A non-linear Stern-Volmer plot confirms the involvement of both static and dynamic components in the PL quenching of donor [-] G-QD. The electrostatic attraction between the oppositely charged QDs resulted in a high bimolecular quenching constant (~1.38 x 10^{12} $M^{-1}s^{-1}$), which further confirms a strong ground state interaction between the donor and acceptor QDs. Negligible variations in the PL quenching efficiency in [-] G-QD:::[+] R_{CIS}-QD complex, as a function of temperature, confirmed the process of FRET in the all-QD based donor-acceptor system. Finally, the process of FRET in [-] G-QD:::[+] R_{CIS}-QD complex was successfully translated into solid state, in a temporal fashion. Thus, the demonstration of interaction driven resonance energy transfer between two environmentally friendly QDs is fundamentally intriguing, and such QD-QD based donor-

acceptor systems can have far reaching applications in the areas of biophysics as well as light harvesting devices.

5.4.3.3 Dyad – 3: [-] B-QD:::[+] G-QD Donor:::Acceptor Assembly

The concept of quantum confinement effect can be explored to prepare QDs that can emit in the entire blue-to-red regions of the visible-spectrum, thereby enabling a large color gamut in the energy transfer process.[48-50] However, the lack of availability of stable and luminescent blue-emitting QDs has been a roadblock to expand the energy transfer studies in the blue region with all-QD based donor-acceptor systems. The successful generation of stable and highly luminescent pure-blue emitting InP/ZnS QDs, and further, demonstration an efficient Förster resonance energy transfer (FRET) process in model QD-dye system (in **Chapter – 3**), paved the way for possibility of developing all-QD based donor-acceptor systems containing this new class of pure-blue emitting InP QDs as donor.[50] These pure-blue emitting InP QDs have been used in the present work to develop an all-environmentally friendly QD based donor-acceptor system comprising blue-emitting QDs for efficient energy transfer studies. Thus, the all-environmentally friendly QD based light harvesting system consists of electrostatically assembled [-] B-InP/ZnS:::[+] G-InP/ZnS QD donor:::acceptor system (**Scheme 5.4**).

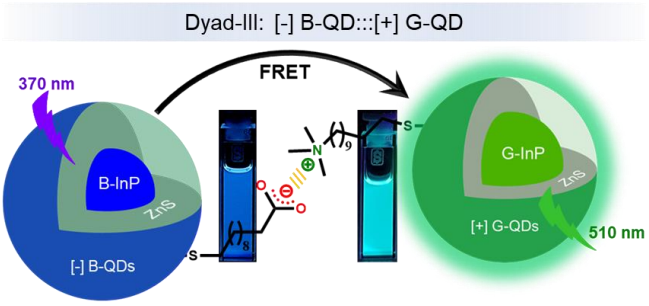

Scheme 5.4 Schematic representation of a FRET process in an electrostatically assembled all-QD based donor-acceptor system containing blue- and green-emitting InP QDs.

A large spectral overlap integral ($J(\lambda) = (\sim 3.16 \times 10^{15}\ M^{-1}\ cm^{-1}\ nm^4)$ between the PL of [-] B-QDs and absorption of [+] G-QDs indicates that [-] B-QD:::[+] G-QD can form a good donor:::acceptor pair for resonance energy transfer studies (**Figure 5.15a**).[6-13] Moreover, the presence of opposite charges on the surface of [-] B-QDs and [+] G-QDs will ensure a strong electrostatic attraction between the two QDs in water, leading to the formation of all-InP/ZnS

QD based nanohybrid assembly (**Scheme 5.4**). As a result, the [-] B-QDs donors and [+] G-QDs acceptors will be closely spaced, which is essential for achieving an efficient resonance energy transfer process. In a typical energy transfer experiment, different aliquots of acceptor [+] G-QDs (15 μL of ~10 μM) were added to a solution of [-] B-QDs (~2 μM) and the subsequent spectral changes were monitored (**Figures 5.15** and **A5.16-A5.17**). UV-vis absorption studies show the development of a scattering component ~800 nm with increase in the addition of acceptor [+] G-QDs, which indicates a strong electrostatic aggregation between the oppositely charged InP/ZnS QDs (**Figure 5.15b**). Also, a visual signature of aggregation was observed in the form of slight turbidity. The size of the electrostatic assembly increased as the concentration of the acceptor [+] G-QD was increased, and thus, the scattering component and the turbidity increased as well (**Figure A5.16b**). The absorption changes were accompanied by a gradual decrease in the PL of [-] B-QDs, with a concomitant increase in the PL signal at ~512 nm corresponding to the acceptor [+] G-QDs (**Figure 5.15c**). The PL intensity obtained by the direct excitation of a solution containing only ~0.52 μM of acceptor [+] G-QDs was lower than its emission in the [-] B-QD:::[+] G-QD donor:::acceptor assembly (~40 % PL enhancement), indicating the energy transfer process (**Figures 5.15c** and **A5.17**). The PL quenching efficiency was estimated to be ~75 % ($E = 1 - I/I_0$, where I_0 and I are the PL intensities of donor [-] B-QDs in the absence and presence of the acceptor [+] G-QDs, respectively). This signifies that ~75 % of the exciton energy of donor QDs was transferred to acceptor QDs.

There is a strong overlap between the emission cross-sections of [-] B-QDs and [+] G-QDs, which can influence the PL quenching efficiency of donor [-] B-QDs and as well as the PL enhancement of acceptor [+] G-QDs calculated from **Figure 5.15c**. Hence, the PL of [-] B-QDs was deconvoluted using Fityk software as shown in **Figures 5.15d** and **A5.17**, which gave a PL quenching efficiency of ~75 %. More insights in the PL quenching process in [-] B-QD:::[+] G-QD donor:::acceptor assembly was obtained by constructing the Stern-Volmer plot (**Figure 5.15e**). The non-linear nature of the Stern-Volmer plot (I_0/I *vs* acceptor concentration) confirms the involvement of both static and dynamic components in the PL quenching of donor [-] B-QDs by acceptor [+] G-QDs (**Figure 5.15e**). This was further confirmed by the linear fit obtained in the quadratic Stern-Volmer plot (K_{app} *vs* acceptor concentration. $K_{app} = (K_S + K_D) + K_S K_D[Q]$) (**Figure 5.15f**). The contribution of static and dynamic components were quantified by combing the Stern-Volmer plots obtained from steady-state and time-resolved PL quenching studies (vide infra). Owing to the broad absorption of QDs, it is inevitable to

overcome the direct excitation of acceptor QDs during the FRET studies in an all-QD based donor-acceptor system. To nullify the contribution from the direct excitation of acceptor QDs, a reverse addition experiment was performed by adding the donor [-] B-QDs to a solution of acceptor [+] G-QDs (**Figure A5.18**). In a typical experiment, the PL of acceptor [+] G-QDs (~0.5 μM) was monitored upon the successive addition of donor [-] B-QDs (aliquots of 1.0 μL of ~0.7 mM was added) (**Figure A5.18a**). A steady increase in the PL intensity of acceptor [+] G-QDs was observed in the presence of ~3.1 μM of donor [-] B-QDs (~1.2 times PL enhancement was obtained after the deconvolution of the PL of acceptor [+] G-QDs) (**Figure A5.18b,c**). Furthermore, the photoluminescence excitation studies (PLE) revealed the strong contribution of the donor QD absorption in the PL enhancement of the acceptor QD (**Figure A5.19**). Both these reverse addition and PLE studies confirm the involvement of an efficient energy transfer process in [-] B-QD:::[+] G-QD donor:::acceptor assembly.

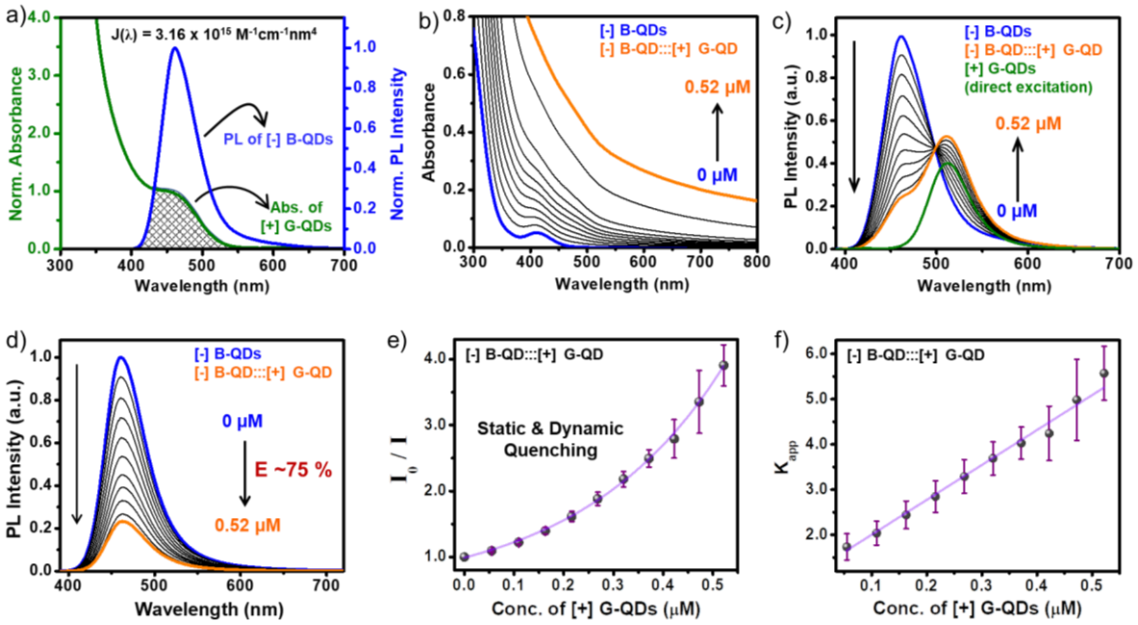

Figure 5.15 Steady-state energy-transfer studies in the [-] B-QD:::[+] G-QD donor:::acceptor assembly. (a) The spectral overlap integral between the PL of [-] B-QDs and absorbance of [+] G-QDs. (b) UV-vis absorption and (c) PL spectral changes of [-] B-QDs upon the successive addition of [+] G QDs in water. (d) Spectral changes in the all-QD assembly obtained after the deconvolution of the PL of [-] B-QD from the total spectral changes shown in **Figure 5.15c.** (e) The corresponding Stern-Volmer (SV) plot constructed from the relative PL intensity of donor [-] B-QDs in the presence of increasing concentrations of acceptor [+] G-QDs, after the deconvolution process. The non-linear nature of SV plot indicates the presence of both static and dynamic components in the PL quenching process. (f) A linear plot was obtained when a quadratic form of the SV plot was constructed, which confirms the involvement of both static and dynamic components in the PL quenching process.

Further, a clear quenching in the PL decay kinetics of donor [-] B-QDs was observed in the presence of acceptor [+] G-QDs (**Figure 5.16a**). Specifically, the average PL lifetime of donor

[-] B-QDs decreased from ~212 ns to ~77 ns, with the quenching efficiency calculated to be ~65 % ($E = 1 - \tau/\tau_0$, where τ_0 and τ are the lifetime of donor QDs in the absence and presence of the acceptor QDs, respectively) (**Table A5.11**).[7] A linear variation was obtained in the Stern-Volmer plot constructed from the lifetime studies (τ_0/τ vs [acceptor QD]), which confirms the involvement of the dynamic component in the PL quenching of donor [-] B-QDs by acceptor [+] G-QDs (**Figure 5.16b** and **Table A5.12**). The dynamic (K_D) and static (K_S) quenching constants were estimated to be ~3.52 x 10^6 M^{-1} and ~2.19 x 10^6 M^{-1}, respectively. A large value of the bimolecular quenching constant (~1.66 x 10^{13} $M^{-1}s^{-1}$) confirms a strong ground-state interaction between the oppositely charged donor and acceptor QDs. The quenching observed in both steady-state and time-resolved PL studies confirm the process of resonance energy transfer operating in [-] B-QD:::[+] G-QD donor:::acceptor assembly. Accordingly, the FRET formalism was used to determine all the energy transfer parameters as summarised in **Figure 5.16e**.[6-7] The rate of the PL quenching process was calculated to be ~8.76 x 10^6 s^{-1} from lifetime studies, which confirms an efficient FRET process in [-] B-QD:::[+] G-QD donor:::acceptor assembly. As in previous dyad systems, a temperature dependent PL lifetime studies were performed to unambiguously confirm the FRET process in [-] B-QD:::[+] G-QD donor:::acceptor assembly. As expected, the PL lifetime of donor [-] B-QDs increased in the absence and presence of acceptor [+] G-QDs as the temperature of the solution was lowered from 318 to 268 K: τ_D = 189 ns and 246 ns, and τ_{DA} = 68 ns and 89 ns at 318 and 268 K, respectively (**Figure 5.16c** and **Table A5.13**). As envisaged, there was a negligible change in the PL lifetime quenching efficiency, as a function of temperature, which proved that a non-radiative dipolar process of FRET was occurring from donor [-] B-QDs to acceptor [+] G-QDs (**Figure 5.16d**).

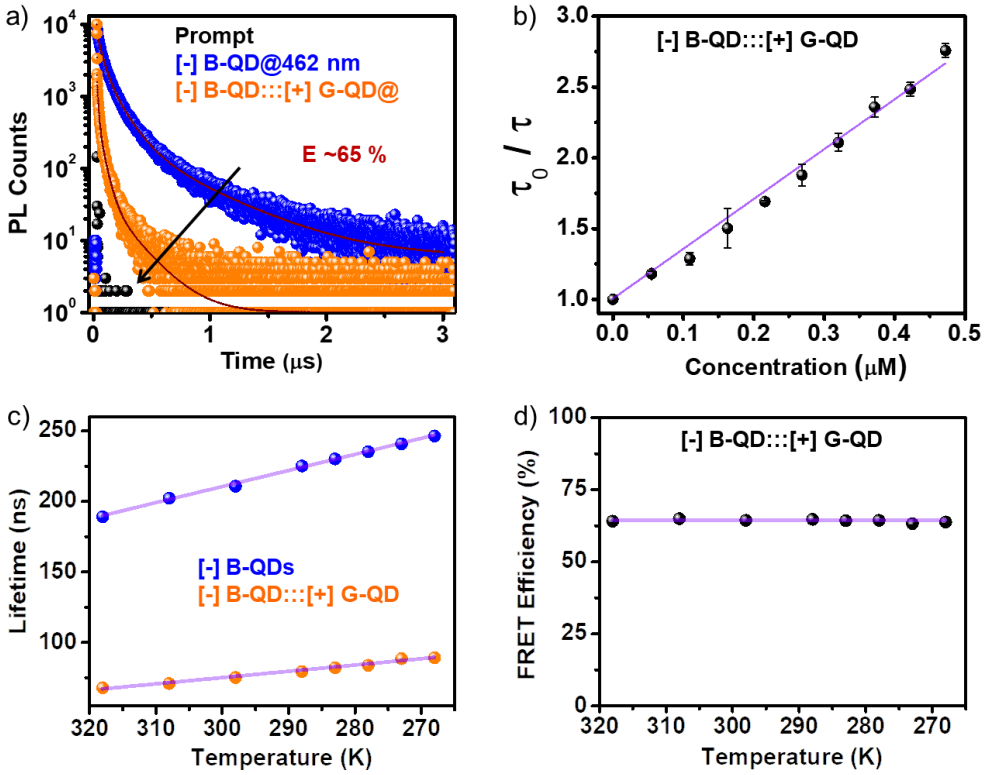

e)

QD-QD System	J(λ) $M^{-1}cm^{-1}nm^4$	R_0 (Å)	E (%)	K_D (M^{-1})	K_S (M^{-1})	k_q ($M^{-1}s^{-1}$)	$k_T(r)$ (s^{-1})
[-] B-QD:::[+] G-QD	~3.16 x 10^{15}	52.7	~65	~3.52 x 10^6	~2.19 x 10^6	~1.66 x 10^{13}	~3.37 x 10^7

Figure 5.16 Time-resolved energy transfer studies in [-] B-QD:::[+] G-QD donor:::acceptor assembly. (a) PL decay profiles of [-] B-QDs in the absence (blue) and presence (orange) of ~0.52 μM [+] G-QDs (the excitation wavelength was 370 nm). (b) The corresponding Stern–Volmer plot showing a linear variation in the relative lifetime of donor [-] B-QDs as a function of increasing concentrations of acceptor [+] G-QDs. Temperature-dependent lifetime quenching experiments: (c) Variation in the PL lifetime of donor [-] B-QDs in absence (blue) and presence (orange) of [+] G-QDs, as a function of varying temperatures from 318 K to 268 K. (d) A negligible change in the FRET efficiency was observed in [-] B-QD:::[+] G-QD donor:::acceptor assembly as a function of temperature, which conclusively prove the non-radiative energy transfer process operating in [-] B-QD:::[+] G-QD donor:::acceptor assembly. (e) Table summarizing various quenching parameters estimated based on FRET Formalism: the spectral overlap integral (J(λ)); Förster radius (R_0); FRET efficiency (E); static and dynamic quenching constants (K_S and K_D, respectively); bimolecular quenching constant (k_q) and rate of energy transfer (k_T).

The presence of oppositely charged ligands on the surface of QDs indicate the involvement of electrostatic interaction in the assembling of [-] B-QD:::[+] G-QD donor:::acceptor system. As a result, donor [-] B-QDs and acceptor [+] G-QDs will be in a close proximity to yield an efficient FRET process. The active role of electrostatic interactions in the FRET process was confirmed by performing the PL quenching studies in similarly charged [-] B-QD:::[-] G-QD donor:::acceptor system (surfaces of both the QDs were functionalised with [-] MUA ligands).

Addition of [-] G-QDs to a solution of [-] B-QDs had no noticeable influence on the absorption and PL properties of [-] B-QDs, confirming a negligible photophysical interaction between the two similarly charged QDs (**Figure 5.17**). An additive absorption and PL spectra were obtained for a mixture of similarly charged [-] B-QDs and [-] G-QDs (**Figure 5.17a,b**). Similarly, negligible changes were observed in the PL decay profile of [-] B-QDs in the presence of [-] G-QDs (**Figure 5.17c** and **Table A5.14**). It is worth mentioning that no signature of aggregation was observed in the absorption studies, which confirms that the strong electrostatic repulsion prevented the similarly charged QDs to participate in any photophysical interaction. Thus, these control experiments conclusively prove the necessity of appropriately functionalised QDs and electrostatic attraction for achieving an efficient FRET process in [-] B-QD:::[+] G-QD donor:::acceptor system.

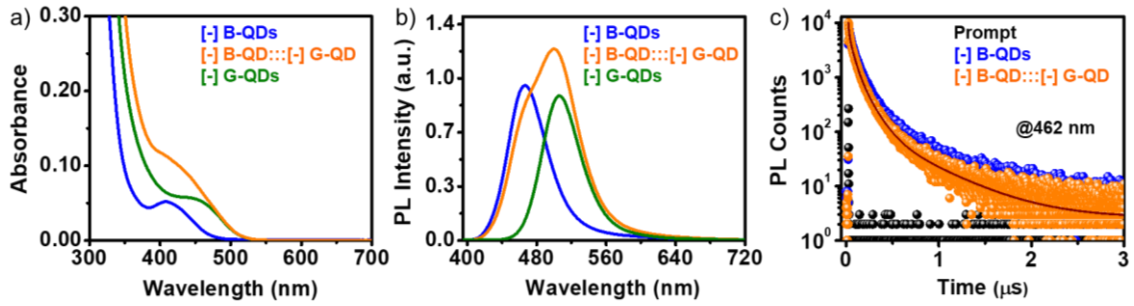

Figure 5.17 Proof of electrostatically driven FRET. (a) UV-vis absorption and (b) steady-state PL spectra of only [-] B-QDs (blue), only [-] G-QDs (olive-green), and [-] B-QD:::[-] G-QD donor:::acceptor assembly (orange). No signature of scattering was observed in the absorption studies, indicating the absence of complexation between similarly charged InP QDs. (c) Negligible changes were observed in the PL decay profile of [-] B-QDs in the presence of [-] G-QDs.

Therefore, an efficient FRET process was achieved in an all-environmentally friendly QD assembly based on blue and green emitting InP/ZnS QDs in water. The surfaces of donor B-QDs and acceptor G-QDs were functionalised with oppositely charged ligands to form electrostatically bounded QD assemblies. Detailed steady-state and time-resolved studies confirmed the involvement of both static as well as dynamic components in the PL quenching of [-] B-QDs by [+] G-QDs. A large value of bimolecular quenching constant (~1.66 x 10^{13} $M^{-1}s^{-1}$) reveals a strong ground-state interaction in electrostatically bounded [-] B-QD:::[+] G-QD donor:::acceptor assemblies. Temperature dependent lifetime studies unambiguously proved that an efficient (~65 %) FRET was operating from donor [-] B-QDs to acceptor [+] G-QDs. The strong electrostatic attraction between the oppositely charged QDs will bring the donor and acceptor QDs close to each other, leading to an efficient FRET process in [-] B-QD:::[+] G-QD donor:::acceptor assemblies. In a broader perspective, our work showcases the potency

of blue-emitting InP QDs in participating in an efficient FRET process in an all-QD based light harvesting system. In future, the colour-gamut of the FRET process can be expanded from the blue to the NIR region by preparing QD assemblies containing appropriate emitters.

5.4.3.4 Dyad – 4: [-] B-QD:::[+] R-QD Donor:::Acceptor Assembly

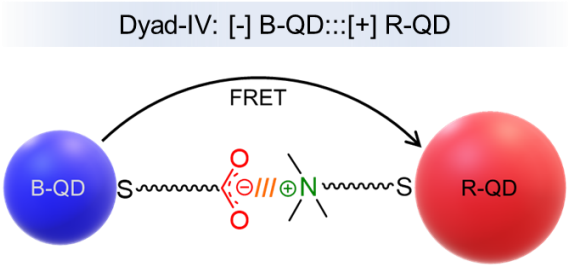

Scheme 5.5 Schematics of electrostatically regulated FRET in all-QD based light-harvesting system containing [-] B-QD and [+] R-QD as donor and acceptor, respectively.

In another attempt to demonstrate the energy transfer process in a wider color gamut (in energy scale), blue- and red-emitting InP/ZnS QDs were chosen as donor and acceptor, respectively (**Scheme 5.5**). An electrostatically regulated efficient long range energy transfer process at an energy scale of 610 meV was demonstrated in the [-] B-QD:::[+] R-QD donor:::acceptor assembly. Details of the FRET studies are given in the **Appendix Section** (**Figures A5.20-A5.21** and **Tables A5.15-A5.16**). Steady-state and time-resolved measurements conclude that electrostatically assembled [-] B-QD:::[+] R-QD donor:::acceptor system participates in the energy transfer process. However, unlike the previously described three dyad assemblies, the blue-red all-InP QD based donor:::acceptor system showed lower efficiency for the energy transfer process. The efficiency and rate of the energy transfer process were estimated to be ~35 % and 1.31 x 10^6 s^{-1}, respectively. Thus, for the creation of multicomponent assemblies with all eco-friendly QDs, the rightful choice of dyad assemblies would be: blue-green all-InP QD, green-red all-InP QD, and green-red InP-CIS QD based dyad assemblies.

5.5 Conclusions

In summary, our work demonstrated the Förster resonance energy transfer (FRET) process in all-QD based donor-acceptor systems based on environmentally friendly materials. Four dyad assemblies were introduced based on InP/ZnS QD and CIS/ZnS QD. A precise control over the synthesis of different sizes of QDs and their surface modifications allows us to develop a library of QDs emitting throughout the visible spectrum of the color gamut with the desired surface chemistry. Appropriate functionalization with charged ligands allows us to install favourable electrostatic interactions between oppositely charged donor and acceptor QDs, which is vital in achieving such a strong ground state complexation in all-QD nanohybrid assemblies. The four dyad studied were: [-] B-QD:::[+] G-QD, [+] G-QD:::[-] R-QD, [-] B-QD:::[+] R-QD, and [-] G-QD:::[+] R_{CIS}-QD donor:::acceptor systems. A good spectral overlap integral (~10^{15}-10^{16} $M^{-1}cm^{-1}nm^4$) for all the dyad systems, and close proximity in electrostatic assembly ensure strong dipolar interaction between donor and acceptor QDs. Detailed steady-state and time-resolved PL quenching experiments revealed an efficient non-radiative energy transfer process in all-QD based dyad systems. The dynamics of the FRET process were assessed with the aid of Stern-Volmer analysis, yielding a large value of the bimolecular quenching constant (~10^{12}-10^{13} $M^{-1}s^{-1}$) in all-QD systems. The calculated rate of the energy transfer process (~10^6-10^7 s^{-1}) was comparable to some of the best FRET pairs developed so far based on QDs. Moreover, temperature-dependent lifetime quenching studies unambiguously proved the non-radiative mechanism of the FRET process, and overruled the charge transfer process. Finally, the solid-state translation of the energy transfer process improves the potential of such 'all-green QD' based nanohybrid systems for device level studies. Further, the prominent role of electrostatics in an efficient energy transfer process was verified with like-charged QD-assembly, where repulsive interactions increase the donor-acceptor separation and hence decrease the probability of the FRET process.

One of the biggest challenges in studying the light-induced processes in all QD-based donor-acceptor systems was to achieve a selective excitation of the donor QD in the presence of the acceptor QD. Owing to the broad absorption of QDs, it is inevitable to overcome the direct excitation of acceptor QDs during the energy transfer studies in an all-QD based donor-acceptor system. As a result, there will be interference of the residual PL from the direct excitation of the acceptor QD in the PL quenching studies. However, our study provides a road-map for investigating the FRET process in all-QD systems. These studies can accelerate the potential

development of a library of all-QD systems based on environmentally benign QDs, which will find application in areas of biophysics as well as energy devices.

Table 5.6 Summary of important FRET parameters for four electrostatically bound all-QD based dyad systems.

Systems	Spectral Overlap Integral [$J(\lambda)$; $M^{-1}cm^{-1}nm^4$]	Efficiency (%)	Bimolecular Quenching Constant (k_q; $M^{-1}s^{-1}$)	Rate of FRET (k_T; s^{-1})
Blue-Green (all-InP QD)	3.16×10^{15}	65	1.66×10^{13}	3.37×10^{7}
Green-Red (all-InP QD)	1.72×10^{15}	60	3.80×10^{13}	1.02×10^{7}
Green-Red (InP-CIS)	1.46×10^{15}	60	1.38×10^{12}	1.72×10^{6}
Blue-Red (all-InP QD)	1.79×10^{16}	35	6.60×10^{12}	1.31×10^{7}

5.6 Future Direction

The focus of the present thesis was to develop donor-acceptor assemblies based on environmentally benign QDs. Accordingly, a roadmap for the FRET investigation was presented for all-QD based dyad assemblies. Additionally, we have introduced a pure-blue emitting InP/ZnS QD in an aqueous medium, which was a missing puzzle in completing the color gamut. Now, a logical extension of the current thesis would be to expand the light harvesting components in donor-acceptor assembly. Thus, the creation of a multicomponent system solely based on QDs will be the closed replication of photosynthesis machinery in terms of long-range processes (both with respect to energy and distance). Thus, a rightful choice of donors and acceptors QD and their control assemblies could be the future for multicomponent donor-acceptor assembly. Looking forward, there are many opportunities ahead for the design of multicomponent systems for the cascade flow of energy to the desired domain of an architecture.

5.7 References

(1) Huber. R. A Structural Basis of Light Energy and Electron Transfer in Biology (Nobel Lecture). *Angew. Chem. Int. Ed. Engl.* **1989,** *28*, 848–869**.**

(2) Deisenhofer, J.; Michel, H. The Photosynthetic Reaction Center from the Purple Bacterium Rhodopseudomonas Viridis (Nobel Lecture). *Angew. Chem. In. Ed. Engl.* **1989**, *28*, 829–847.

(3) Gust, D.; Moore, T. A.; Moore, A. L. Molecular Mimicry of Photosynthetic Energy and Electron Transfer. *Acc. Chem. Res.* **1993**, *26*, 198–205.

(4) Kamat, P. V. Meeting the Clean Energy Demand: Nanostructure Architectures for Solar Energy Conversion. *J. Phys. Chem. C* **2007**, *111*, 2834–2860.

(5) Otsuki, J. Supramolecular Approach Towards Light-Harvesting Materials based on Porphyrins and Chlorophylls. *J. Mater. Chem. A* **2018**, *6*, 6710–6753.

(6) Förster, T. 10th Spiers Memorial Lecture. Transfer Mechanisms of Electronic Excitation. *Discuss. Faraday Soc.* **1959**, *27*, 7–17.

(7) Lakowicz, J. R. *Principles of Fluorescence Spectroscopy*, 3rd ed.; Springer: New York, 1999.

(8) Hildebrandt, N.; Spillmann, C. M.; Algar, W. R.; Pons, T.; Stewart, M. H.; Oh, E.; Susumu, K.; Díaz, S. A.; Delehanty, J. B.; Medintz, I. L. Energy Transfer with Semiconductor Quantum Dot Bioconjugates: A Versatile Platform for Biosensing, Energy Harvesting, and Other Developing Applications. *Chem. Rev.* **2017**, *117*, 536–711.

(9) Qiu, X.; Guo, J.; Xu, J.; Hildebrandt, N. Three-Dimensional FRET Multiplexing for DNA Quantification with Attomolar Detection Limits. *J. Phys. Chem. Lett.* **2018**, *9*, 4379–4384.

(10) Sapsford, K. E.; Berti, L.; Medintz, I. L. Materials for Fluorescence Resonance Energy Transfer Analysis: Beyond Traditional Donor-Acceptor Combinations. *Angew. Chem. Int. Ed.* **2006**, *45*, 4562–4588.

(11) Praveen, V. K.; Ranjith, C.; Bandini, E.; Ajayaghosh, A.; Armaroli, N. Oligo(phenylenevinylene) Hybrids and Self-Assemblies: Versatile Materials for Excitation Energy Transfer. *Chem. Soc. Rev.* **2014**, *43*, 4222–4242.

(12) Cao, S.; Rosławska, A.; Doppagne, B.; Romeo, M.; Féron, M.; Chérioux, F.; Bulou, H.; Scheurer, F.; Schull, G. Energy funnelling within multichromophore architectures monitored with subnanometre resolution. *Nat. Chem.* **2021**, *13*, 766–770.

(13) Chakraborty, I. N.; Roy, P.; Rao, A.; Devatha, G.; Roy, S.; Pillai, P. P. The Unconventional Role of Surface Ligands in Dictating the Light Harvesting Properties of Quantum Dots. *J. Mater. Chem. A* **2021**, *9*, 7422–7457.

(14) Brus, L. E. Electron–Electron and Electron-Hole Interactions in Small Semiconductor Crystallites: The Size Dependence of the Lowest Excited Electronic State. *J. Chem. Phys.* **1984**, *80*, 4403–4409.

(15) Pietryga, J. M.; Park, Y.-S.; Lim, J.; Fidler, A. F.; Bae, W. K.; Brovelli, S.; Klimov, V. I. Spectroscopic and Device Aspects of Nanocrystal Quantum Dots. *Chem. Rev.* **2016**, *116*, 10513–10622.

(16) Resch-Genger, U.; Grabolle, M.; Cavaliere-Jaricot, S.; Nitschke, R.; Nann, T. Quantum Dots Versus Organic Dyes as Fluorescent Labels. *Nat. Methods* **2008**, *5*, 763–775.

(17) Kamat, P. V. Quantum Dot Solar Cells. The Next Big Thing in Photovoltaics. *J. Phys. Chem. Lett.* **2013**, *4*, 908–918.

(18) Yamashita, S.-i.; Hamada, M.; Nakanishi, S.; Saito, H.; Nosaka, Y.; Wakida, S.-i.; Biju, V. Auger Ionization Beats Photo-Oxidation of Semiconductor Quantum Dots: Extended Stability of Single-Molecule Photoluminescence. *Angew. Chem. Int. Ed.* **2015**, *54*, 3892–3896.

(19) Clapp, A. R.; Medintz, I. L.; Mauro, J. M.; Fisher, B. R.; Bawendi, M. G.; Mattoussi, H. Fluorescence Resonance Energy Transfer Between Quantum Dot Donors and Dye-Labeled Protein Acceptors. *J. Am. Chem. Soc.* **2004**, *126*, 301–310.

(20) Ji, X.; Wang, W.; Mattoussi, H. Controlling the Spectroscopic Properties of Quantum Dots via Energy Transfer and Charge Transfer Interactions: Concepts and Applications. *Nano Today* **2016**, *11*, 98–121.

(21) Sarkar, S.; Bose, R.; Jana, S.; Jana, N. R.; Pradhan, N. Doped Semiconductor Nanocrystals and Organic Dyes: An Efficient and Greener FRET System. *J. Phys. Chem. Lett.* **2010**, *1*, 636–640.

(22) Thomas, A.; Nair, P. V.; Thomas, K. G. InP Quantum Dots: An Environmentally Friendly Material with Resonance Energy Transfer Requisites. *J. Phys. Chem. C* **2014**, *118*, 3838–3845.

(23) Wang, C.; Weiss, E. A. Sub-Nanosecond Resonance Energy Transfer in the Near-Infrared within Self-Assembled Conjugates of PbS Quantum Dots and Cyanine Dye J-aggregates. *J. Am. Chem. Soc.* **2016**, *138*, 9557–9564.

(24) Devatha, G.; Roy, S.; Rao, A.; Mallick, A.; Basu, S.; Pillai, P. P. Electrostatically Driven Resonance Energy Transfer in “Cationic” Biocompatible Indium Phosphide Quantum

Dots. *Chem. Sci.* **2017**, *8*, 3879–3884.

(25) Saha, S.; Majhi, D.; Bhattacharyya, K.; Preeyanka, N.; Datta, A.; Sarkar, M. Evidence of Homo-FRET in Quantum Dot-Dye Hetrostructured Assembly. *Phys. Chem. Chem. Phys.* **2018**, *20*, 9523–9535.

(26) Devatha, G.; Rao, A.; Roy S.; Pillai, P. P. Förster Resonance Energy Transfer Regulated Multicolor Photopatterning from Single Quantum Dot Nanohybrid Films. *ACS Energy Lett.* **2019**, *4*, 1710–1716.

(27) Kagan, C. R.; Murray, C. B.; Bawendi, M. G. Long-range resonance transfer of electronic excitations in close-packed CdSe quantum-dot solids. *Phys. Rev. B* **1996**, *54*, 8633–8643.

(28) Crooker, S. A.; Hollingsworth, J. A.; Tretiak, S.; Klimov, V. I. Spectrally Resolved Dynamics of Energy Transfer in Quantum-Dot Assemblies: Towards Engineered Energy Flows in Artificial Materials. *Phys. Rev. Lett.* **2002**, *89*, 186802.

(29) Koole, R.; Liljeroth, P.; de Mello Donegá, C.; Vanmaekelbergh, D.; Meijerink, A. Electronic Coupling and Exciton Energy Transfer in CdTe Quantum-Dot Molecules. *J. Am. Chem. Soc.* **2006**, *128*, 10436–10441.

(30) Akselrod, G. M.; Prins, F.; Poulikakos, L. V.; Lee, E. M. Y.; Weidman, M. C.; Mork, A. J.; Willard, A. P.; Bulović, V.; Tisdale, W. A. Subdiffusive Exciton Transport in Quantum Dot Solids. *Nano Lett.* **2014**, *14*, 3556–3562.

(31) Thuy, U. T. D.; Thuy, P. T.; Liem, N. Q.; Li, L.; Reiss, P. Comparative Photoluminescence Study of Close-Packed and Colloidal InP/ZnS Quantum Dots. *Appl. Phys. Lett.* **2010**, *96,* 073102.

(32) Jalali, H. B.; Melikov, R.; Sadeghi, S.; Nizamoglu, S. Excitonic Energy Transfer within InP/ZnS Quantum Dot Langmuir-Blodgett Assemblies. *J. Phys. Chem. C* **2018***, 122,* 11616-11622.

(33) Achermann, M.; Petruska, M. A.; Crooker, S. A.; Klimov, V. I. Picosecond Energy Transfer in Quantum Dot Langmuir−Blodgett Nanoassemblies. *J. Phys. Chem. B* **2003**, *107*, 13782–13787.

(34) Franzl, T.; Klar, T. A.; Schietinger, S.; Rogach, A. L.; Feldmann, J. Exciton Recycling in Graded Gap Nanocrystal Structures. *Nano Lett.* **2004**, *4,* 1599-1603.

(35) Wargnier, R.; Baranov, A. V.; Maslov, V. G.; Stsiapura, V.; Artemyev, M.; Pluot, M.; Sukhanova, A.; Nabiev, I. Energy Transfer in Aqueous Solutions of Oppositely Charged CdSe/ZnS Core/Shell Quantum Dots and in Quantum Dot−Nanogold Assemblies. *Nano Lett.* **2004**, *4*, 451–457.

(36) Xu, L.; Xu, J.; Ma, Z.; Li, W.; Huang, X.; Chen, K. Direct Observation of Resonant

Energy Transfer between Quantum Dots of two Different Sizes in a Single Water Droplet. *Appl. Phys. Lett.* **2006**, *89*, 033121.

(37) Wang, C.-H.; Chen, C.-W.; Wei, C.-M.; Chen, Y.-F.; Lai, C.-W.; Ho, M.-L.; Chou, P-T. Resonant Energy Transfer between CdSe/ZnS Type I and CdSe/ZnTe Type II Quantum Dots. *J. Phys. Chem. C* **2009**, *113,* 15548-15552.

(38) Wolf, A.; Lesnyak, V.; Gaponik, N.; Eychmüller, A. Quantum-Dot-Based (Aero)gels: Control of the Optical Properties. *J. Phys. Chem. Lett.* **2012**, *3*, 2188–2193.

(39) Sarker, S.; Maity, A. R.; Karan, N. S.; Pradhan, N. Fluorescence Energy Transfer from Doped to Undoped Quantum Dots. *J. Phys. Chem. C* **2013**, *117,* 21988–21994.

(40) Zheng, K.; Zidek, K.; Abdellah, M.; Zhu, N.; Chábera, P.; Lenngren, N.; Chi, Q.; Pullerits, T. Direct Energy Transfer in Films of CdSe Quantum Dots: Beyond the Point Dipole Approximation. *J. Am. Chem. Soc.* **2014**, *136,* 6259–6268.

(41) Chou, K. F.; Dennis, A. M. Forster Resnance Energy Tarnsfer between Quantum Donors and Quantum Dot Accepotrs. *Sensors* **2015**, *15*, 13288–13325.

(42) Hoffman, J. B.; Alam, R.; Kamat, P. V. Why Surface Chemistry Matters for QD–QD Resonance Energy Transfer. *ACS Energy Lett.* **2017**, *2*, 391–396.

(43) Kodaimati, M. S.; Lian, S.; Schatz, G. C.; Weiss, E. A. Energy Transfer-Enhanced Photocatalytic Reduction of Proton within Quantum Dot Light-Harvesting-Catalyst Assemblies. *Proc. Natl. Acad. Sci. U.S.A.* **2018**, *115,* 8290–8295.

(44) Thomas, A.; Sandeep, K.; Somasundaran, S. M.; Thomas, K. G. How Trap States Affect Charge Carrier Dynamics of CdSe and InP Quantum Dots: Visualization through Complexation with Viologen. *ACS Energy Lett.* **2018**, *3*, 2368–2375.

(45) Devatha, D.; Roy, P.; Rao, A.; Roy, A.; Pillai, P. P. Multicolor Luminescent Patterning via Photoregulation of Electron and Energy Transfer Processes in Quantum Dots. *J. Phys. Chem. Lett.* **2020**, *11*, 4099–4106.

(46) Sobhanan, J.; Rival, J. V.; Anas, A.; Shibu, E. S.; Takano, Y.; Biju, V. Luminescent Quantum Dots: Synthesis, Optical Properties, Bioimaging and Toxicity. *Adv. Drug Deliv. Rev.* **2023**, *197*, 114830.

(47) Manoj, B.; Rajan, D.; Thomas, K. G. InP Quantum Dots: Stoichiometry Regulates Carrier Dynamics. *J. Chem. Phys.* **2023**, *158*, 174706.

(48) Li, L.; Reiss, P. One-Pot Synthesis of Highly Luminescent InP/ZnS Nanocrystals without Precursor Injection. *J. Am. Chem. Soc.* **2008**, *130*, 11588–11589.

(49) Tessier, M. D.; Dupont, D.; De Nolf, K.; De Roo, J.; Hens, Z. Economic and Size-Tunable Synthesis of InP/ZnE (E = S, Se) Colloidal Quantum Dots. *Chem. Mater.* **2015**, *27*, 4893–

4898.

(50) Roy, P.; Virmania, M.; Pillai, P. P. Blue-emitting InP quantum dots participate in an efficient resonance energy transfer process in water. *Chem. Sci.* **2023**, *14*, 5167–5176.

(51) Mutlugun, E.; Hernandez-Martinez, P. L.; Eroglu, C.; Coskun, Y.; Erdem, T.; Sharma, V. K.; Unal, E.; Panda, S. K.; Hickey, S. G.; Gaponik, N.; Eychmüller, A.; Demir, H. V. Large-Area (over 50 cm × 50 cm) Freestanding Films of Colloidal InP/ZnS Quantum Dots. *Nano Lett.* **2012**, *12*, 3986–3993.

(52) Jain, V.; Roy, S.; Roy P.; Pillai, P. P. When Design Meets Function: The Prodigious Role of Surface Ligands in Regulating Nanoparticle Chemistry. *Chem. Mater.* **2022**, *34*, 7579–7597.

(53) Zhong, H.; Zhou, Y.; Ye, M.; He, Y.; Ye, J.; He, C.; Yang, C.; Li, Y. Controlled Synthesis and Optical Properties of Colloidal Ternary Chalcogenide CuInS2 Nanocrystals. *Chem. Mater.* **2008**, *20*, 6434–6443.

5.8 Appendix

Characterization of green and red emitting InP/ZnS QDs:

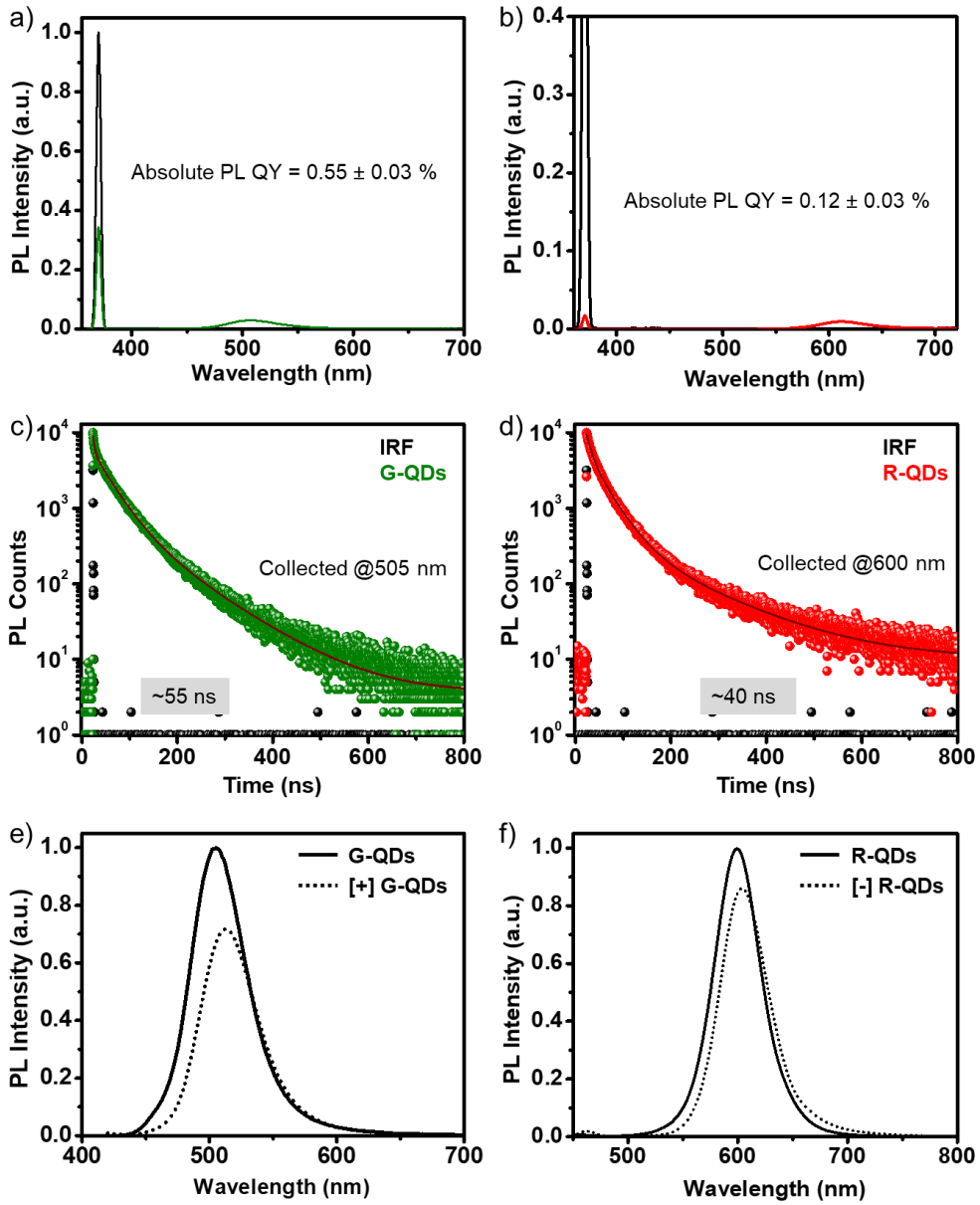

Figure A5.1 Absolute PL quantum yield (QY_A) measurements and time-resolved PL decay profiles of (a,c) MA capped green-emitting (G-QDs) and (b,d) oleylamine capped red-emitting (R-QDs) InP/ZnS QDs, respectively in $CHCl_3$. Steady-state PL of (e) green- and, (f) red-emitting InP/ZnS QD before (solid line) and after (dotted line) place exchange with [+] TMA and [-] MHA ligands, respectively. Approximately 70 % and 85 % of the PL were retained in [+] G-QDs and [-] R-QDs, respectively, after the place exchange process.

Excitation energy and power-dependent PL Analysis: The green- and red-emitting InP/ZnS QDs have their first excitonic peaks at ~452 nm and ~570 nm, along with their PL maxima

centred around ~505 nm and ~600 nm, respectively. The strong absorption band can be assigned to the transitions from the low-lying valence band to the conduction band in QDs, which is caused by the quantum size effect. Excitation emission matrix (EEM) 2D contour plots provided additional information regarding the nature of electronic transitions and origin of emission. On varying the excitation wavelength from the band edge transition to higher energy, we did not observe any change in the PL peak energy (**Figure A5.2a,b**). This evidenced the presence of stable electronic states that contribute to strong band edge emission and independent to excitation wavelength. Hence, the emission in G-QDs and R-QDs are originating from a stable low-lying excited state electron and ground state hole recombination process.

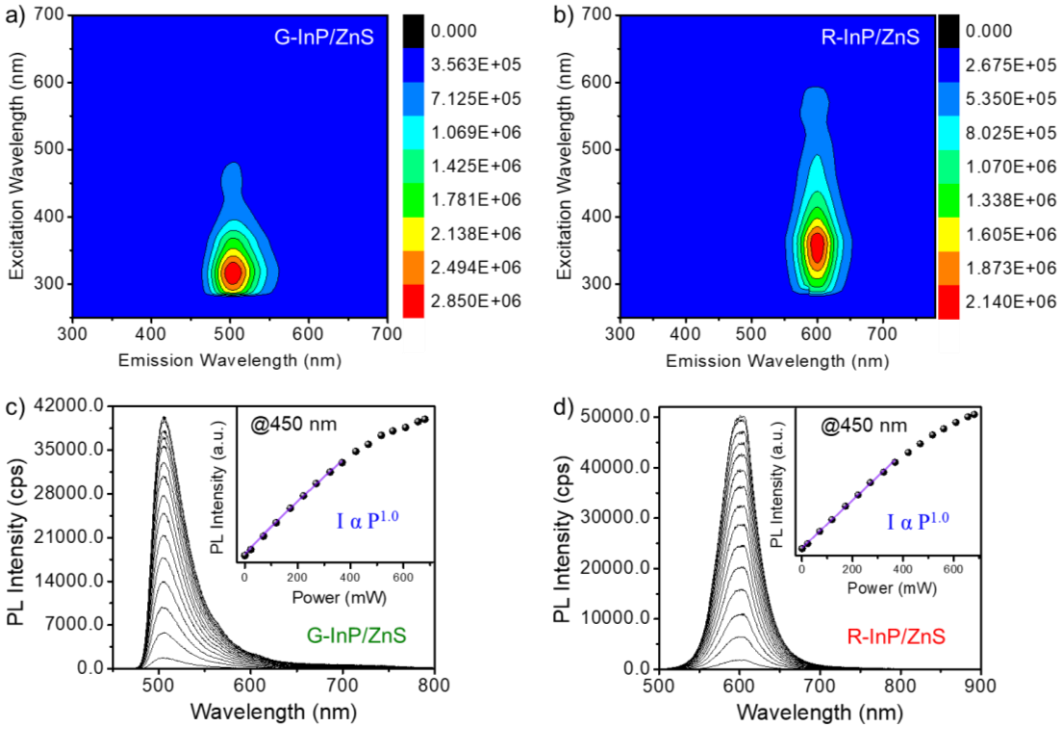

Figure A5.2 2D contour plots of excitation emission matrix (EEM) of (a) G-QDs, and (b) R-QDs, respectively. The band edge emission is 505 nm and 600 nm for G-QDs and R-QDs, respectively. Excitation power dependence emission spectra for (c) G-QDs, and (d) R-QDs, respectively. The inset shows the corresponding fitted data with power law (I α P1.0). All the measurements were carried out with 450 nm cw laser irradiation. The PL emission was detected with portable Ocean FX-UV-VIS spectrometer, with wavelength range of 200-850 nm and CMOS detector with entrance slit of 25 µm.

High PL QY was observed at shorter excitation wavelength, which can be attributed to the broad absorption features of QDs. To further elucidate the underlying mechanism responsible for the evolution of the emission peak, excitation-power dependence PL spectra was recorded for G-QDs and R-QDs, respectively, using 450 nm continuous wave (cw) laser irradiation. The

PL intensity increases linearly with the excitation power, as expected for excitonic emission (**Figure A5.2c,d**). The measurements were fitted with I α P^x power function, where I is the PL intensity, P is the excitation laser power, and x is the power parameter defining the characteristics of emission. When operating in low power regime, the PL peak intensity increases with excitation power by approximately I α $P^{1.0}$, and began to saturate at around 400 mW power for both G-QD and R-QD, respectively, typical features of excitonic emission. On contrary, in the high-power regime, the rise component shows a slight decrease because of the state-filling effect. The discrete energy levels of atomic-like structure in QDs are the reason to state filling effect owing to the Pauli Exclusion Principle. It originates from strong electron–electron interaction in confined geometries, a typical characteristics of QD emission (*J. Phys.: Condens. Matter* **2007**, *19*, 386213).

Temperature-Dependent PL Analysis: Afterwards, the dynamics of photoexcited charge carriers in G-QDs and R-QDs were then investigated using temperature-dependent PL analysis. **Figure A5.3** summaries the PL peak energy, linewidth, and integrated intensity as a function of temperature. The integrated PL intensity gradually increases as the temperature decreases. This could be attributed to the loss of non-radiative recombination channel because of the suppression of phonon vibration (*Physica* **1967**, *34*, 149–154; *Appl. Phys. Lett.* **2000**, *77*, 2837–2839).

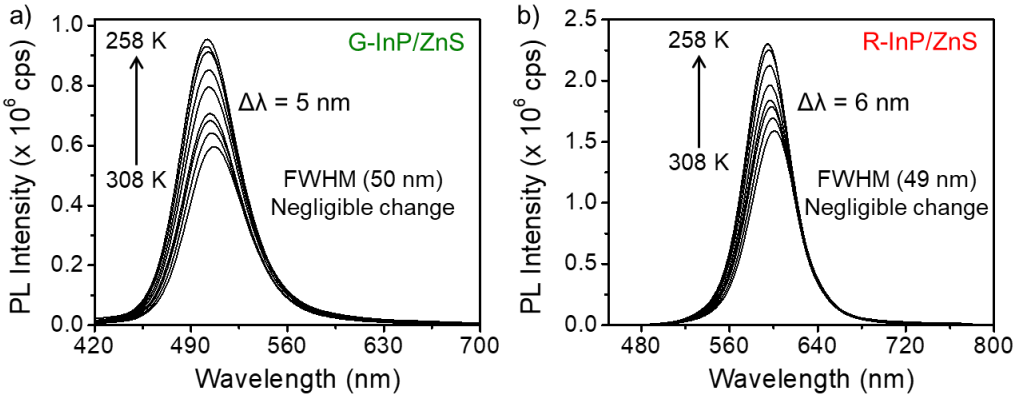

Figure A5.3 Temperature-dependent PL spectra for (a) G-QDs, and (b) R-QDs, respectively. The PL intensity increases with decrease in temperature, while negligible change in FWHM and a hypsochromic shift in PL peak energy was recorded for both G-QD and R-QD, respectively.

Importantly, the PL linewidth (FWHM) shows negligible changes with varying temperatures, indicating that phonon scattering contributes very little to the emission. On contrary, the PL peak energy is found to be blue shifted with decrease in temperature. The hypsochromic shift was calculated to be 5 nm and 6 nm for G-QD and R-QD, respectively. The observed changes

in PL peak energy can be attributed primarily to electron–phonon interaction and partially to thermal expansion, as expected by Varshni's empirical formula describing the temperature dependence of a semiconductor bandgap (*Physica* **1967**, *34*, 149–154). Thus, all the photoluminescence study conclude that the high-quality emission is originating from the band edge recombination of electron-hole pair in InP/ZnS QDs.

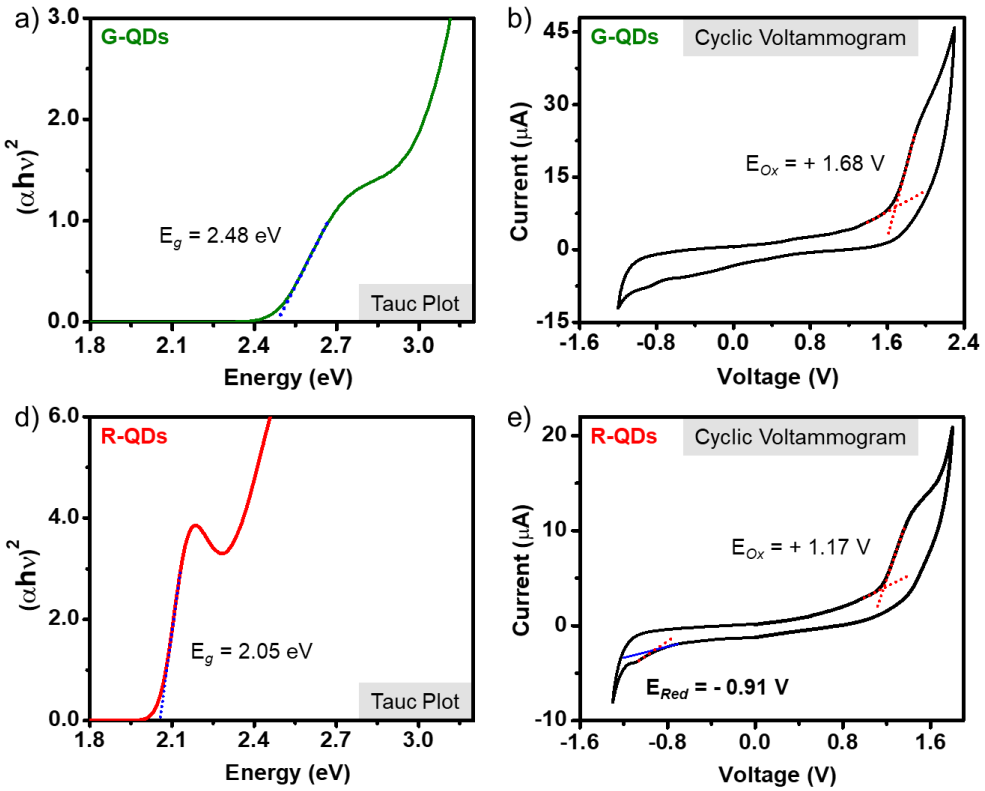

Figure A5.4 Determination of band positions for green- and red-emitting InP/ZnS QDs. (a,b) The Tauc plots, and (c,d) cyclic voltammograms of G-QDs and R-QDs, respectively. Optical band gap was measured to be 2.48 eV and 2.05 eV for G-QDs and R-QDs, respectively. All the cyclic voltammogram experiments for QDs were performed via dip-coating of QDs over the glassy carbon, followed by drying under vacuum to remove the solvent. The scan rate for measurements was 30 mV/s. The optical (2.05 eV) and electrochemical band gap (2.08 eV) for R-QDs are in good agreement with each other.

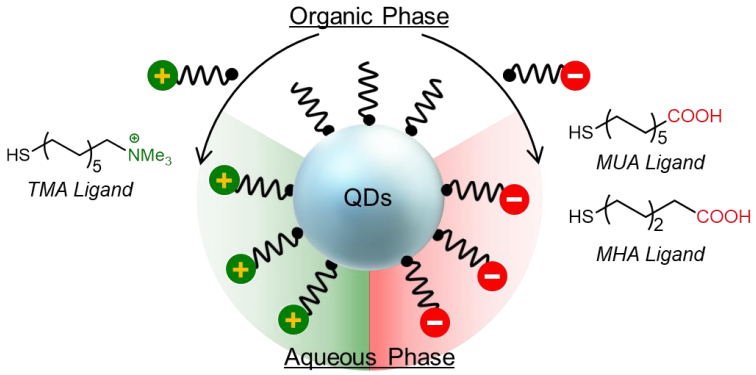

Scheme A5.1 Schematic representation of place exchange reaction of hydrophobic ligand capped QDs (myristic acid, oleylamine, oleic acid, etc.) with charged thiolated ligands (TMA, MUA, and MHA ligands).

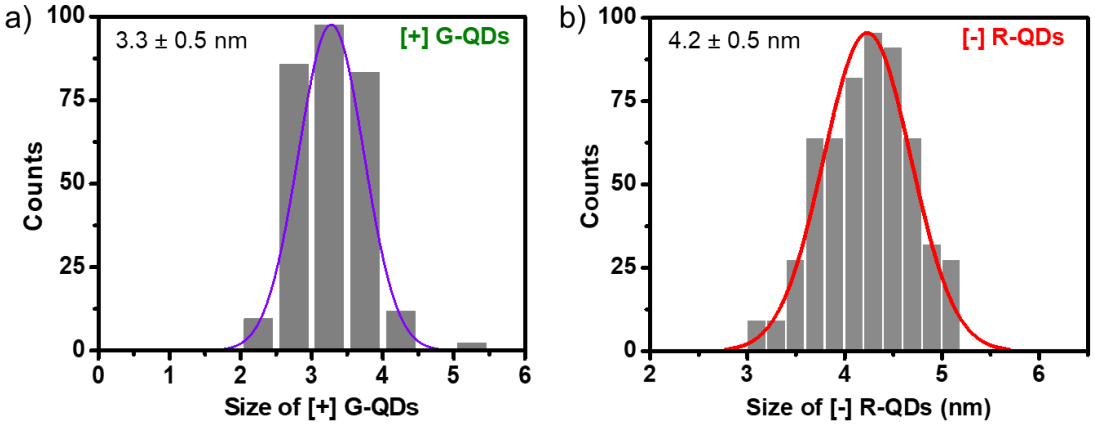

Figure A5.5 The size distribution histograms (from ~300 QDs) for (a) [+] G-QDs and, (b) [-] R-QDs.

Table A5.1 PL decay analysis of G-QDs and R-QDs in $CHCl_3$, in a time window of 800 ns.

System	τ_1 (ns)	α_1	τ_2 (ns)	α_2	τ_3 (ns)	α_3	$\tau_{avg.}$ (ns)	χ^2
G-QDs @505 nm	3.31	0.45	34.94	0.47	104.31	0.08	55.19	1.30
R-QDs @600 nm	10.03	0.45	37.20	0.50	141.03	0.05	39.97	1.21

Characterization of MUA capped [-] G-InP/ZnS QDs:

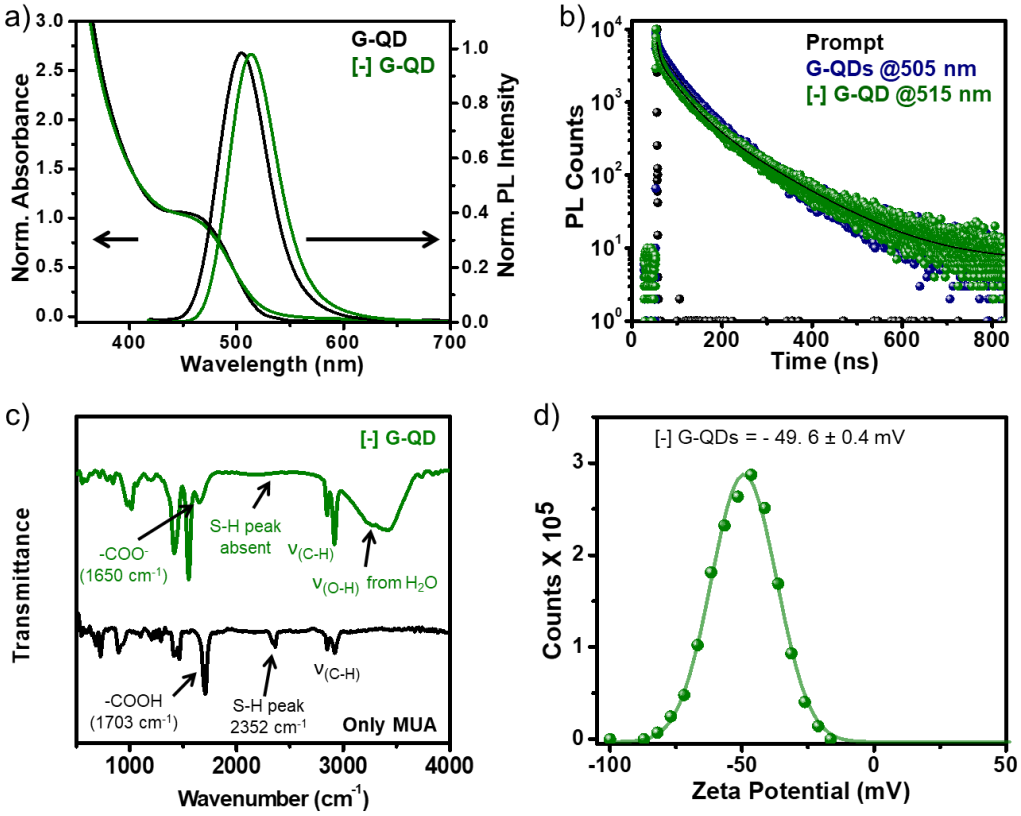

Figure A5.6 Spectroscopic characterization of [-] G-QDs. (a) Normalized UV-vis absorption, PL spectra, and (b) PL decay profile of G-QDs, before and after the functionalization with [-] MUA ligands. (c) FTIR spectra, and (d) representative zeta potential plots of [-] G-QDs.

Table A5.2 PL decay analysis of G-QDs and [-] G-QDs, collected at 505 nm and 515 nm, respectively, in a time window of 800 ns.

System	τ_1 (ns)	α_1	τ_2 (ns)	α_2	τ_3 (ns)	α_3	$\tau_{avg.}$ (ns)	χ^2
G-QDs @505 nm	3.31	0.45	34.94	0.47	104.31	0.08	55.19	1.30
[-] G-QDs @515 nm	5.90	0.47	30.50	0.44	101.95	0.09	53.65	1.29

Characterization of red-emitting CIS/ZnS QDs:

Table A5.3 PL decay analysis of R_{CIS}-QDs before and after the ligand exchange process, in a time window of 800 ns.

System	τ_1 (ns)	α_1	τ_2 (ns)	α_2	τ_3 (ns)	α_3	$\tau_{avg.}$ (ns)	χ^2
R_{CIS}-QDs @631 nm	3.58	0.56	34.02	0.31	138.75	0.13	93.78	1.31
[+] R_{CIS}-QDs @631 nm	5.08	0.51	33.70	0.37	146.62	0.12	92.27	1.35

Light induced resonance energy transfer studies:

Dyad – 1: [+] G-QD:::[-] R-QD Donor:::Acceptor Assembly

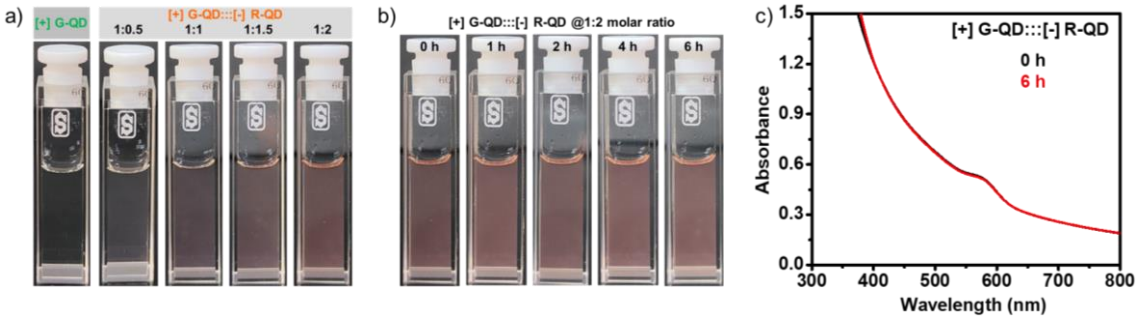

Figure. A5.7 Colloidal stability studies. (a) Optical photographs showing the increase in the QD aggregation, with increase in the concentration of acceptor QDs. (b) Optical photographs showing the colloidal stability of 1:2 molar ratio of [+] G-QD:::[-] R-QD donor:::acceptor FRET system for at least 6 h. (c) Corresponding absorption spectra of 1:2 molar ratio of [+] G-QD:::[-] R-QD donor:::acceptor FRET system at t = 0 and 6 h are shown.

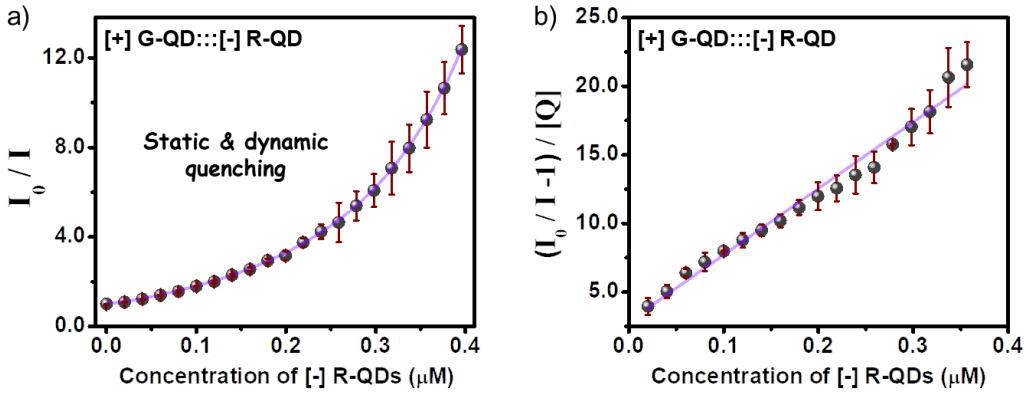

Figure A5.8 (a) Stern-Volmer and (b) modified Stern-Volmer plots, derived from steady-state PL studies, showing the relative changes in PL intensity of [+] G-QDs as function of increasing concentration of [-] R-QDs.

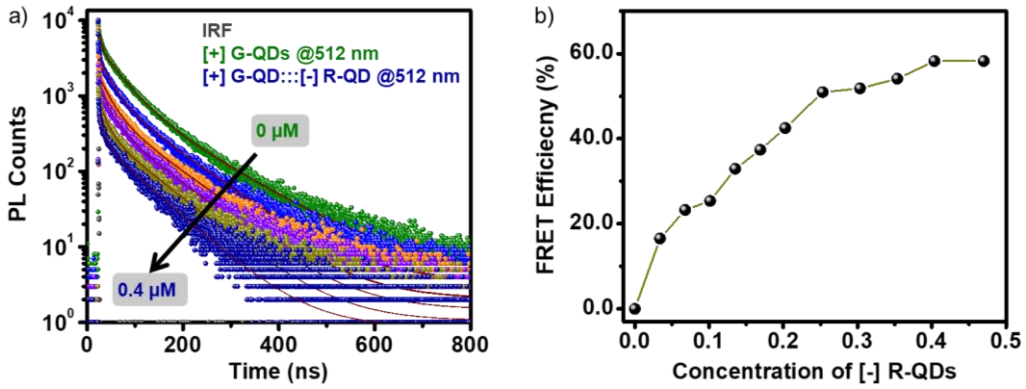

Figure. A5.9 (a) PL decay kinetics of donor [+] G-QDs with increasing concentration of acceptor [-] R-QDs, collected at the PL maxima of [+] G-QDs. (b) Variation in the FRET efficiency ($1-\tau/\tau_0$) with increasing concentration of acceptor [-] R-QDs. The energy transfer efficiency was higher at a donor: acceptor ratio of 1:2 compared to 1:1.

Table A5.4 PL decay analysis of [+] G-QD:::[-] R-QD donor:::acceptor complex, upon successive addition of acceptor [+] R-QDs, in a time window of 800 ns, collected at 512 nm.

System	τ_1 (ns)	α_1	τ_2 (ns)	α_2	τ_3 (ns)	α_3	$\tau_{avg.}$ (ns)	χ^2
[+] G-QDs	**4.72**	**0.42**	**40.22**	**0.43**	**115.02**	**0.15**	**73.62**	**1.18**
[+] G-QD:::[-] R QD (0.03 µM)	0.60	0.66	24.22	0.25	91.67	0.09	61.44	1.20
[+] G-QD:::[-] R QD (0.07 µM)	0.36	0.86	20.49	0.10	83.73	0.04	56.51	1.20
[+] G-QD:::[-] R QD (0.10 µM)	0.31	0.89	20.36	0.08	83.48	0.03	54.96	1.23
[+] G-QD:::[-] R QD (0.13 µM)	0.16	0.93	16.31	0.05	72.92	0.02	49.39	1.27
[+] G-QD:::[-] R QD (0.17 µM)	0.14	0.94	12.29	0.04	63.85	0.02	46.10	1.24
[+] G-QD:::[-] R QD (0.20 µM)	0.13	0.95	9.31	0.03	55.39	0.02	42.35	1.36
[+] G-QD:::[-] R QD (0.25 µM)	0.12	0.97	8.88	0.02	53.11	0.01	36.11	1.15
[+] G-QD:::[-] R QD (0.30 µM)	0.12	0.97	7.54	0.02	51.60	0.01	35.47	1.06
[+] G-QD:::[-] R QD (0.35 µM)	0.11	0.98	6.30	0.01	45.58	0.01	33.81	1.36
[+] G-QD:::[-] R QD (0.40 µM)	**0.11**	**0.98**	**4.27**	**0.01**	**41.45**	**0.01**	**30.75**	**1.19**

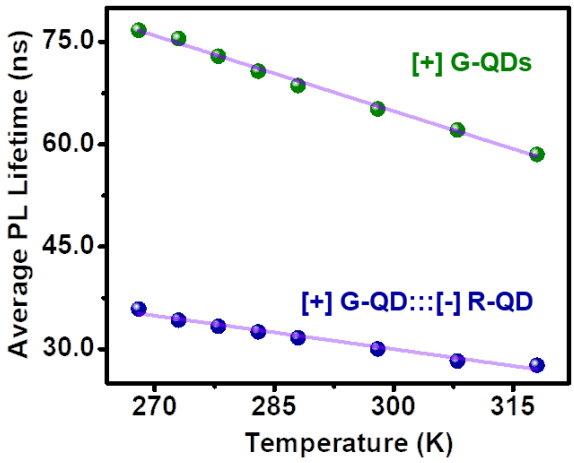

Figure. A5.10 Temperature-dependent PL lifetime study. Variation in the PL lifetime of donor [+] G-QDs in absence and presence of ~0.4 μM of acceptor [-] R-QDs, at different temperatures.

Table A5.5 PL decay analysis of [+] G-QDs and [+] G-QD:::[-] R-QD donor:::acceptor complex at different temperatures ranging from 318 k to 268 K, collected at 512 nm, in a time window of 800 ns.

Temperature (K)	System	τ_1 (ns)	α_1	τ_2 (ns)	α_2	τ_3 (ns)	α_3	$\tau_{avg.}$ (ns)	χ^2
318 K	[+] G-QDs	3.93	0.49	31.79	0.39	95.45	0.12	58.00	1.20
	[+] G-QD:::[-] R-QD	0.11	0.98	4.88	0.01	38.26	0.01	27.61	1.26
308 K	[+] G-QDs	4.24	0.46	34.27	0.41	100.63	0.13	62.10	1.30
	[+] G-QD:::[-] R-QD	0.10	0.98	3.41	0.01	37.78	0.01	28.24	1.30
298 K	[+] G-QDs	4.61	0.45	36.84	0.42	106.09	0.13	65.18	1.16
	[+] G-QD:::[-] R-QD	0.11	0.98	4.10	0.01	40.58	0.01	30.01	1.21
288 K	[+] G-QDs	4.69	0.43	38.30	0.43	109.55	0.14	68.60	1.24
	[+] G-QD:::[-] R-QD	0.11	0.98	4.72	0.01	42.61	0.01	31.65	1.19
283 K	[+] G-QDs	4.47	0.41	38.83	0.44	110.80	0.15	70.72	1.20
	[+] G-QD:::[-] R-QD	0.11	0.98	4.31	0.01	43.36	0.01	32.50	1.22
278 K	[+] G-QDs	4.07	0.40	38.95	0.44	111.75	0.16	72.92	1.21
	[+] G-QD:::[-] R-QD	0.10	0.98	3.79	0.01	43.40	0.01	33.32	1.24
273 K	[+] G-QDs	4.24	0.40	40.76	0.44	115.70	0.16	75.51	1.19
	[+] G-QD:::[-] R-QD	0.10	0.98	3.73	0.01	44.33	0.01	34.22	1.27
268 K	[+] G-QDs	4.13	0.39	41.38	0.45	117.83	0.16	76.72	1.20
	[+] G-QD:::[-] R-QD	0.10	0.98	4.08	0.01	46.25	0.01	35.87	1.28

Table A5.6 FRET parameter calculation with respect to different donor: acceptor ratios using PL lifetime.

Donor: acceptor ratio	FRET efficiency (%)	Average lifetime of donor QD (τ_D, ns)	$\left(\frac{R_0^6}{r^6}\right)$	Rate of FRET (s^{-1})
1:1	43	73.62	0.754	~1.02 x 10^7
1:2	60		0.750	~1.02 x 10^7

Proof for Electrostatically Driven FRET

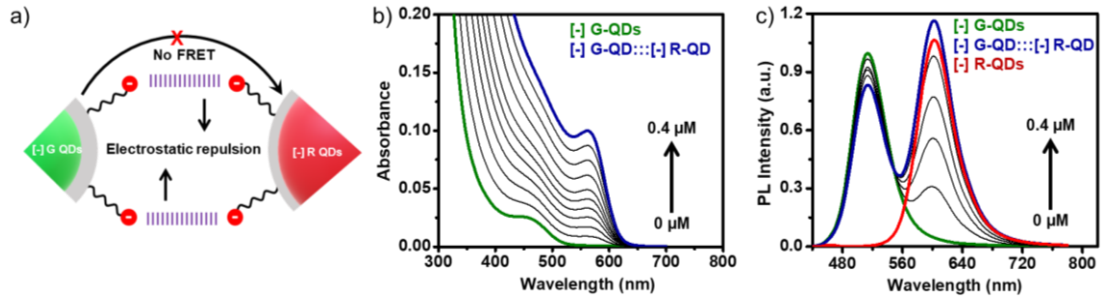

Figure. A5.11 Proof of electrostatically driven FRET process in mention the dyad system all-InP QD based nanohybrid system. (a) A schematic representation of negligible photophysical interaction between similarly charged [-] G-QDs and [-] R-QDs. The steady-state (b) UV-vis absorption and (c) PL changes of [-] G-QDs with increasing concentration of [-] R-QDs. Here, no signature of scattering component was observed at longer wavelengths, indicating that the similarly charged QDs do not participate in a strong aggregation event, which ascertains the need of electrostatic attraction in achieving an efficient FRET process.

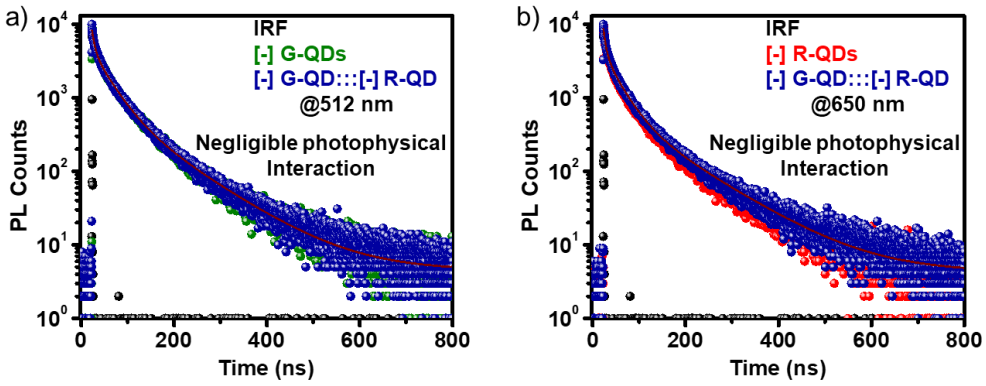

Figure A5.12 Time-resolved measurements in [-] G-QD:::[-] R-QD nanohybrid system. PL decay profiles of (a) [-] G-QDs and, (b) [-] R-QDs in absence (olive-green and red) and presence (royal blue) of [-] R-QDs and, [-] G-QDs, respectively. A negligible change in the PL lifetime of donor [+] G-QDs and acceptor [-] R-QDs was observed in the presence of each other. This conclusively proves that no sign of PL quenching and energy transfer takes place between similarly charged [-] G-QDs and [-] R-QDs.

This above control experiment ascertains the need of electrostatic attraction in achieving an efficient FRET process.

Table A5.7 PL decay analysis of [-] G-QD and [-] G-QD:::[-] R-QD complex, in a time window of 800 ns. The PL decay was collected at 512 nm and 650 nm for donor and acceptor QDs, respectively.

System	τ_1 (ns)	α_1	τ_2 (ns)	α_2	τ_3 (ns)	α_3	$\tau_{avg.}$ (ns)	χ^2
[-] G-QDs @512 nm	5.96	0.48	35.53	0.43	104.63	0.09	56.07	1.23
[-] G-QD:::[-] R QD @512 nm	5.46	0.47	34.47	0.43	103.50	0.10	57.54	1.30
[-] R-QDs @650 nm	2.07	0.64	16.08	0.29	72.02	0.07	39.97	1.32
[-] G-QD:::[-] R-QD @650 nm	3.65	0.59	23.52	0.35	84.50	0.06	40.76	1.25

Dyad – 2: [-] G-QD:::[+] R_{CIS}-QD Donor:::Acceptor Assembly

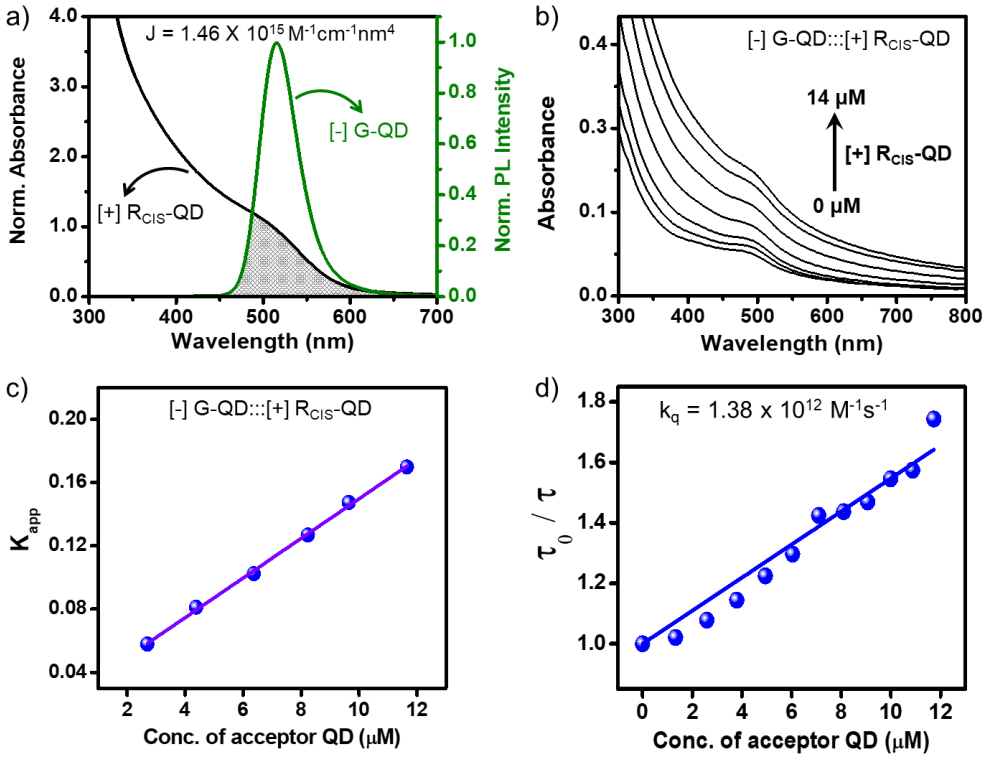

Figure A5.13 (a) The spectral overlap integral between the PL of donor [-] G-QD and the absorption of acceptor [+] R_{CIS}-QD. (b) Variation in the UV-Vis absorption spectra of [-] G-QD with increasing concentration of [+] R_{CIS}-QDs. (c) Modified Stern-Volmer plots derived from steady-state studies, and (d) Stern-Volmer plot derived from PL lifetime studies for [-] G-QD:::[+] R_{CIS}-QD donor:::acceptor assembly. The measured value of bimolecular quenching constant is ~1.38 x 10^{12} $M^{-1}s^{-1}$.

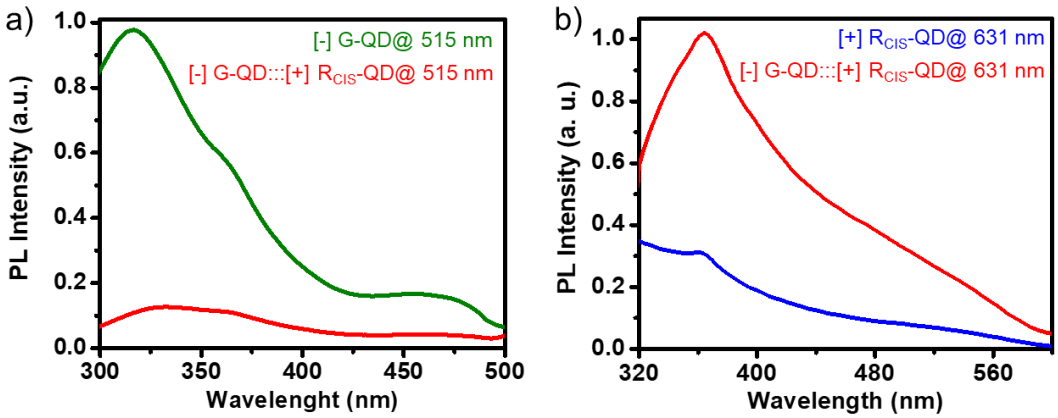

Figure A5.14 Photoluminescence excitation study. (a) The PLE spectra of donor [-] G-QD, and (b) acceptor [+] R_{CIS}-QD in presence (red) and absence (olive and blue) of acceptor and donor QDs, respectively. Collected at 515 nm (a), and 630 nm (b), respectively.

Table A5.8 PL decay analysis of [-] G-QD and [-] G-QD:::[+] R_{CIS}-QD complex at different temperatures ranging from 298 k to 268 K, collected at 515 nm, in a time window of 800 ns.

Temperature (K)	Sample	τ_1 (ns)	α_1	τ_2 (ns)	α_2	τ_3 (ns)	α_3	$\tau_{avg.}$ (ns)	χ^2	E (%)
298 K	[-] G-QD	5.90	0.47	30.50	0.44	101.95	0.09	53.65	1.29	57.73
	[-] G-QD:::[+] R_{CIS}-QD	2.11	0.69	19.11	0.29	62.50	0.02	22.68	1.20	
288 K	[-] G-QD	6.13	0.46	36.70	0.44	106.55	0.10	58.91	1.26	56.50
	[-] G-QD:::[+] R_{CIS}-QD	2.11	0.67	19.37	0.30	62.69	0.03	25.63	1.30	
283 k	[-] G-QD	6.65	0.45	38.14	0.45	109.51	0.10	60.24	1.27	56.44
	[-] G-QD:::[+] R_{CIS}-QD	2.18	0.65	20.63	0.32	63.55	0.03	26.24	1.31	
278 K	[-] G-QD	5.83	0.44	37.40	0.45	108.27	0.11	61.77	1.27	55.60
	[-] G-QD:::[+] R_{CIS}-QD	2.2	0.68	22.32	0.29	64.26	0.03	27.44	1.23	
273 K	[-] G-QD	6.38	0.43	38.80	0.46	111.14	0.11	63.04	1.21	54.91
	[-] G-QD:::[+] R_{CIS}-QD	2.25	0.67	23.40	0.30	66.10	0.03	28.42	1.34	
268 K	[-] G-QD	7.24	0.42	40.43	0.47	117.86	0.11	66.22	1.27	54.81
	[-] G-QD:::[+] R_{CIS}-QD	2.25	0.66	24.93	0.31	68.63	0.03	29.92	1.35	

Proof for Electrostatically Driven FRET

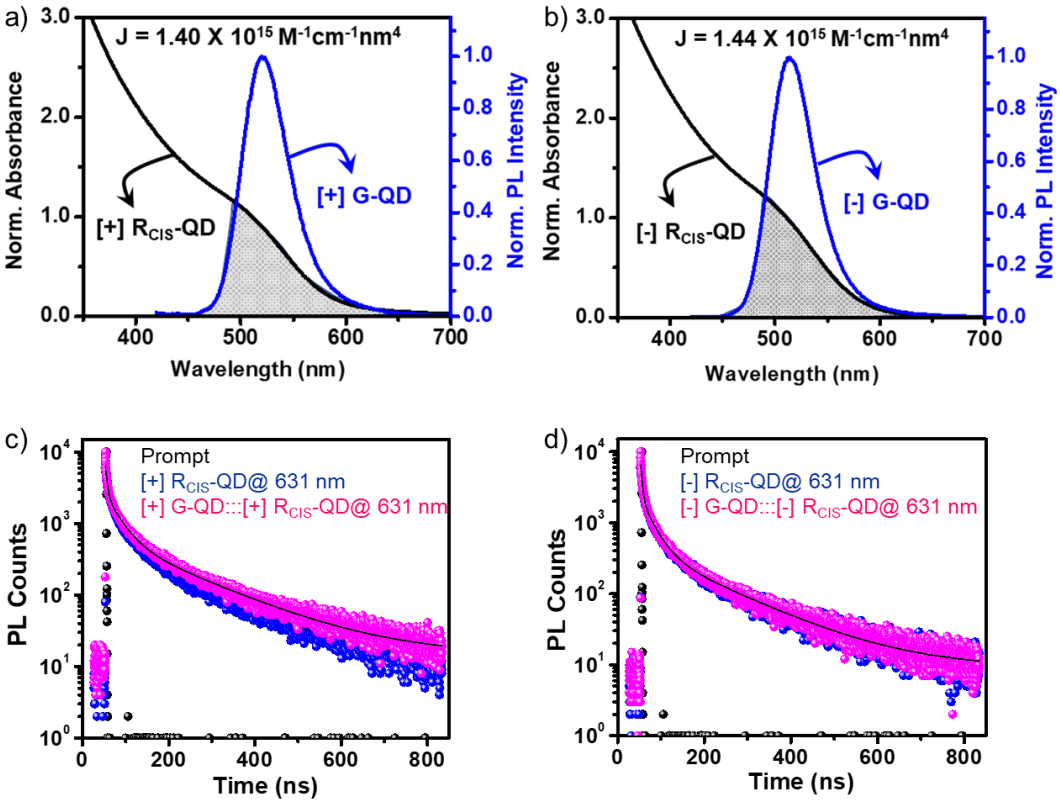

Figure A5.15 Photoluminescence excitation study. (a) The PLE spectra of donor [-] G-QD, and (b) acceptor [+] R_{CIS}-QD in presence (red) and absence (olive and blue) of acceptor and donor QDs, respectively. Collected at 515 nm (a), and 630 nm (b), respectively.

Table A5.9 PL decay analysis of [+] G-QD in absence and presence of [+] R_{CIS}-QD and vice-versa, in a time window of 800 ns.

System	τ_1 (ns)	α_1	τ_2 (ns)	α_2	τ_3 (ns)	α_3	$\tau_{avg.}$ (ns)	χ^2
[+] G-QDs @512 nm	4.72	0.42	40.22	0.43	115.02	0.15	73.62	1.18
[+] G-QD:::[+] R_{CIS}-QD @512 nm	4.48	0.45	32.43	0.40	110.17	0.15	71.41	1.18
[+] R_{CIS}-QDs @631 nm	5.08	0.51	33.70	0.37	146.62	0.12	92.27	1.35
[+] G-QD:::[+] R_{CIS}-QD @631 nm	4.96	0.52	34.81	0.36	145.68	0.12	91.91	1.23

Table A5.10 PL decay analysis of [-] G-QD in absence and presence of [-] R_{CIS}-QD and vice-versa, in a time window of 800 ns.

System	τ_1 (ns)	α_1	τ_2 (ns)	α_2	τ_3 (ns)	α_3	$\tau_{avg.}$ (ns)	χ^2
[+] G-QDs @512 nm	4.72	0.42	40.22	0.43	115.02	0.15	73.62	1.18
[+] G-QD:::[+] R_{CIS}-QD @512 nm	4.48	0.45	32.43	0.40	110.17	0.15	71.41	1.18
[+] R_{CIS}-QDs @631 nm	5.08	0.51	33.70	0.37	146.62	0.12	92.27	1.35
[+] G-QD:::[+] R_{CIS}-QD @631 nm	4.96	0.52	34.81	0.36	145.68	0.12	91.91	1.23

Dyad – 3: [-] B-QD:::[+] G-QD Donor:::Acceptor Assembly

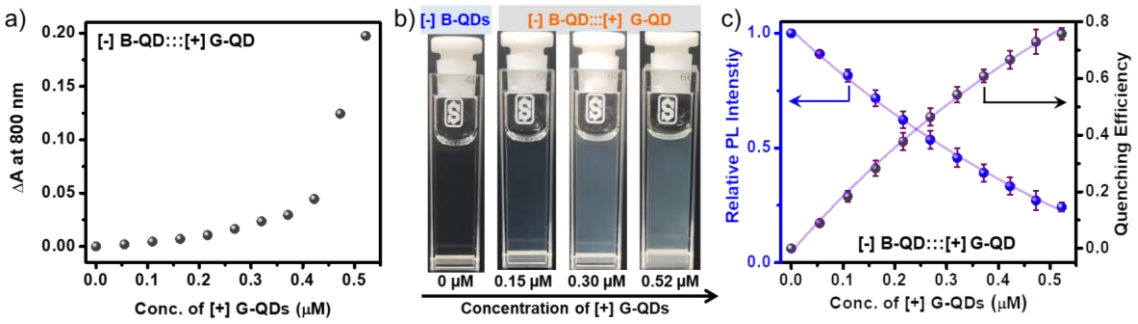

Figure A5.16 Variation in the scattering component (Δ absorbance at 800 nm) of [-] B-QD:::[+] G-QD donor:::acceptor assembly, with increase in the concentration of acceptor [+] G-QDs. (b) Corresponding optical photographs showing the increase in the turbidity. (c) Plot showing variations in the relative PL of donor [-] B-QDs and PL quenching efficiency ($1 - I/I_0$) as a function of increasing concentration of acceptor [+] G-QDs.

Steady-State PL Measurements

There is a strong overlap between the emission cross-sections of [-] B-QDs and [+] G-QDs, which can influence the PL quenching efficiency of donor [-] B-QDs and as well as the PL enhancement of [+] G-QDs calculated from **Figure 5.15c**. Hence, the PL of both [-] B-QDs and [+] G-QDs were deconvoluted using Fityk software, as shown below.

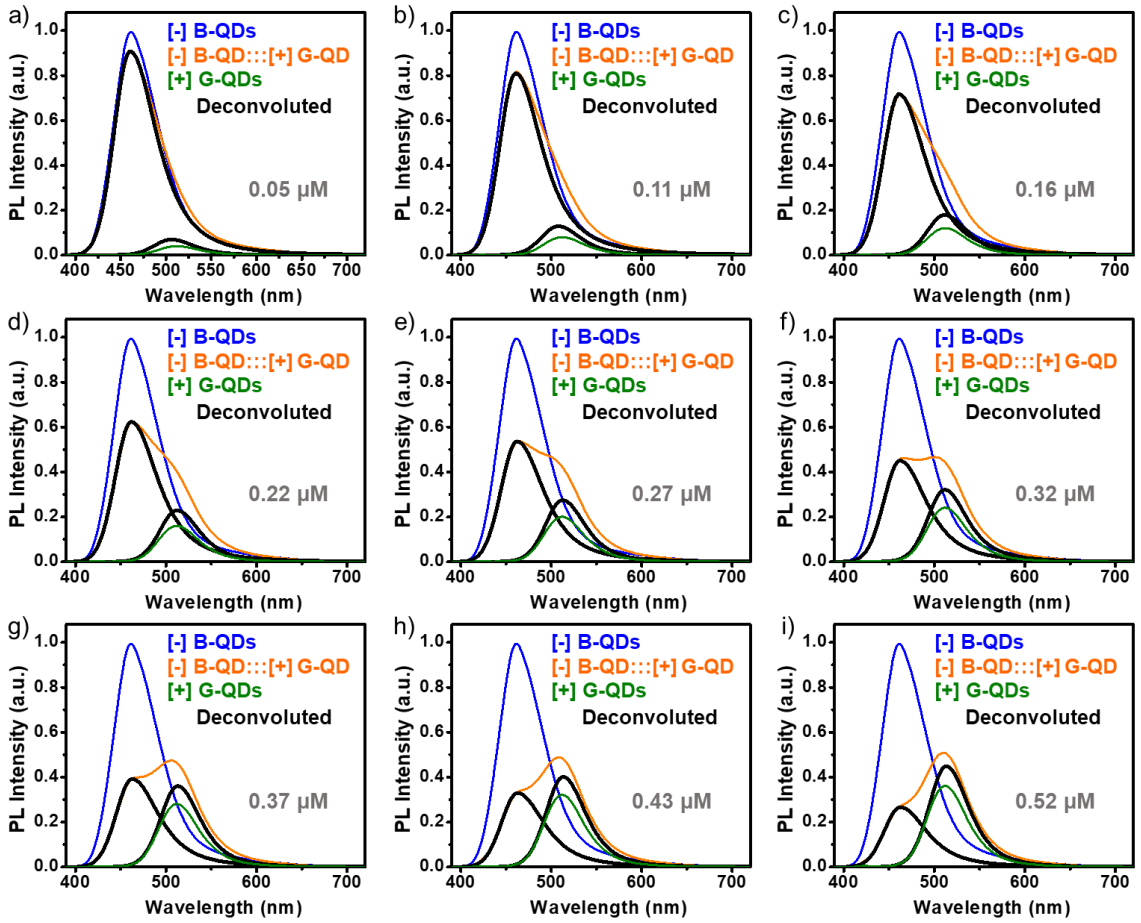

Figure A5.17 Deconvolution of PL spectral changes during the FRET studies in [-] B-QD:::[+] G-QD donor:::acceptor assembly. PL spectra of both QDs in the assembly were deconvoluted at different concentrations of acceptor [+] G-QDs: (a) 0.05 µM, (b) 0.11 µM, (c) 0.16 µM, (d) 0.22 µM, (e) 0.27 µM, (f) 0.32 µM, (g) 0.37 µM, (h) 0.43 µM, and (i) 0.52 µM. The excitation wavelength was 370 nm.

Color coding of spectra

Blue for only ~2 µM donor [-] B-QDs.

Olive-green for only acceptor [+] G-QDs at different concentrations as mentioned inside the figure. Orange for [-] B-QD:::[+] G-QD donor:::acceptor assemblies at different concentrations of acceptor [+] G-QDs as mentioned inside the figure.

Black for deconvoluted spectra of donor [-] B-QD and acceptor [+] G-QD in the assembly at different concentrations of acceptor [+] G-QDs as mentioned inside the figure.

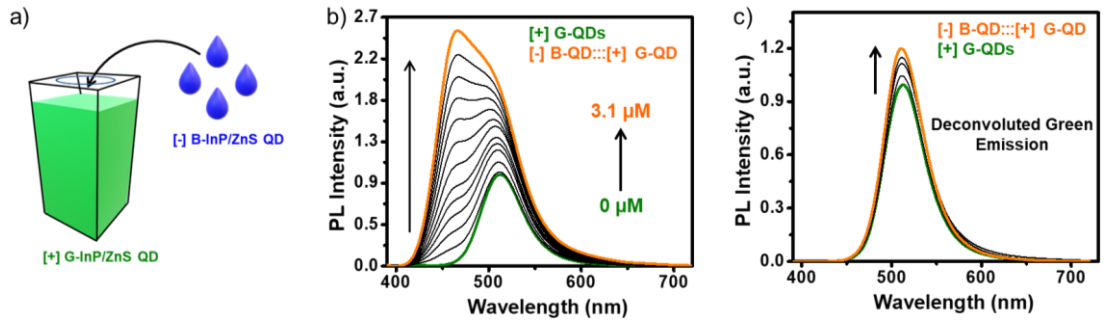

Figure A5.18 Reverse addition experiment. (a) Schematic representation of reverse addition experiments, showing the successive addition of donor [-] B-QDs to a solution of acceptor [+] G-QDs. The corresponding PL spectral changes was monitored under excitation at 370 nm. (b) A steady enhancement in the PL of ~0.5 µM acceptor [+] G-QDs was observed, upon addition of varying concentrations of the [-] B-QDs donor (upto ~3.1 µM). (c) A plot showing the deconvoluted part of the green region, revealing ~1.2 times enhancement in PL of acceptor [+] G-QDs in presence of [-] B-QDs.

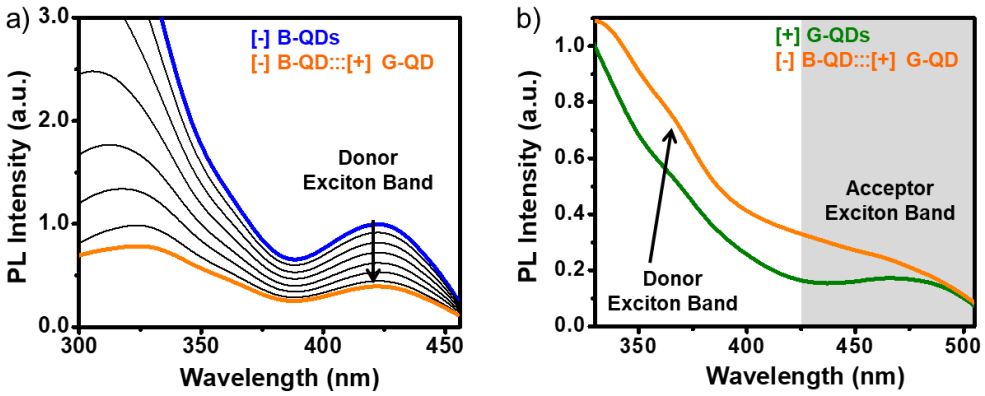

Figure A5.19 PLE studies in [-] B-QD:::[+] G-QD donor:::acceptor assembly. (a) PLE spectra collected at the emission maxima of donor [-] B-QDs in absence (blue) and presence (black followed by orange) of acceptor [+] G-QDs. (b) PLE spectra collected at the emission of acceptor [+] G-QDs in absence (olive-green) and presence (orange) of [-] B-QDs.

There was a decrease in the PL intensity of donor [-] B-QDs, and an increase in the PL intensity of acceptor [+] G-QDs in [-] B-QD:::[+] G-QD donor:::acceptor assembly, when compared to the individual QD solutions. Additionally, the PLE of acceptor [+] G-QDs shows absorbance from higher excitonic peak of [-] B-QDs. This proved that the ground state absorption of donor QD contributes to the acceptor PL in the complex mixture. Hence, there was a transfer of excitation energy from donor to acceptor QD, leading to the higher PL from acceptor QDs.

Table A5.11 PL decay analysis of donor [-] B-QDs in absence and presence of acceptor [+] G-QDs, in a time window of 3.2 μs. The PL decay was collected at 462 nm.

System	τ_1 (ns)	α_1	τ_2 (ns)	α_2	τ_3 (ns)	α_3	τ_4 (ns)	α_4	$\tau_{avg.}$ (ns)	χ^2
[-] B-QDs @462 nm	6.31	0.31	49.15	0.38	147.51	0.28	569.45	0.03	211.98	1.13
[-] B-QD:::[+] G-QD @462 nm	0.60	0.94	7.69	0.03	32.38	0.02	139.71	0.01	76.87	1.06

Table A5.12 PL decay analysis of [-] B-QD:::[+] G-QD donor:::acceptor assembly, upon successive addition of acceptor [+] G-QDs, in a time window of 3.2 μs, collected at 462 nm.

System	τ_1 (ns)	α_1	τ_2 (ns)	α_2	τ_3 (ns)	α_3	τ_4 (ns)	α_4	$\tau_{avg.}$ (ns)	χ^2
[-] B-QDs	6.31	0.31	49.15	0.38	147.51	0.28	569.45	0.03	211.98	1.13
[-] B-QD:::[+] G-QD (0.05 μM)	2.44	0.56	27.42	0.21	108.05	0.20	395.94	0.03	177.27	1.12
[-] B-QD:::[+] G-QD (0.11 μM)	1.17	0.67	19.05	0.17	95.96	0.14	354.96	0.02	157.67	1.15
[-] B-QD:::[+] G-QD (0.16 μM)	0.85	0.79	13.76	0.11	76.49	0.08	268.37	0.02	141.16	1.18
[-] B-QD:::[+] G-QD (0.22 μM)	0.81	0.83	12.39	0.09	62.83	0.06	225.25	0.02	125.81	1.18
[-] B-QD:::[+] G-QD (0.27 μM)	0.79	0.87	13.40	0.08	64.53	0.04	236.40	0.01	110.42	1.07
[-] B-QD:::[+] G-QD (0.32 μM)	0.70	0.90	11.71	0.06	56.11	0.03	200.69	0.01	100.72	1.09
[-] B-QD:::[+] G-QD (0.37 μM)	0.68	0.92	10.77	0.05	46.84	0.02	174.71	0.01	92.34	1.12
[-] B-QD:::[+] G-QD (0.43 μM)	0.64	0.94	9.20	0.03	36.61	0.02	154.21	0.01	84.88	1.01
[-] B-QD:::[+] G-QD (0.52 μM)	0.60	0.94	7.69	0.03	32.38	0.02	139.71	0.01	76.87	1.06

Table A5.13 PL decay analysis of [-] B-QDs and [-] B-QD:::[+] G-QD donor:::acceptor assembly at different temperatures ranging from 318 k to 268 K, collected at 462 nm, in a time window of 3.2 μs.

Temperature (K)	System	τ_1 (ns)	α_1	τ_2 (ns)	α_2	τ_3 (ns)	α_3	τ_4 (ns)	α_4	$\tau_{avg.}$ (ns)	χ^2
318 K	[-] B-QDs	7.87	0.35	47.38	0.40	133.06	0.22	506.68	0.03	189.13	1.12
	[-] B-QD:::[+] G-QD	0.51	0.93	6.49	0.04	28.88	0.02	124.51	0.01	67.92	1.06
308 K	[-] B-QDs	7.56	0.34	49.80	0.41	141.39	0.22	541.43	0.03	202.29	1.12
	[-] B-QD:::[+] G-QD	0.52	0.93	7.11	0.04	29.69	0.02	129.84	0.01	70.85	1.26
298 K	[-] B-QDs	6.93	0.35	51.60	0.42	146.28	0.20	558.74	0.03	210.80	1.07
	[-] B-QD:::[+] G-QD	0.51	0.93	6.80	0.04	29.23	0.02	134.96	0.01	75.11	1.25
288 K	[-] B-QDs	5.97	0.38	51.59	0.39	147.73	0.20	583.47	0.03	225.08	1.11
	[-] B-QD:::[+] G-QD	0.54	0.93	6.70	0.04	29.66	0.02	141.9	0.01	79.43	1.15
283 K	[-] B-QDs	4.52	0.40	45.82	0.36	138.98	0.21	580.84	0.03	230.17	1.12
	[-] B-QD:::[+] G-QD	0.53	0.92	7.74	0.05	34.71	0.02	149.97	0.01	82.21	1.19
278 K	[-] B-QDs	4.60	0.40	48.57	0.36	145.18	0.21	595.36	0.03	235.21	1.12
	[-] B-QD:::[+] G-QD	0.54	0.92	8.34	0.05	34.17	0.02	153.34	0.01	83.76	1.11
273 K	[-] B-QDs	4.25	0.41	46.28	0.33	140.07	0.23	605.54	0.03	240.77	1.14
	[-] B-QD:::[+] G-QD	0.49	0.92	7.12	0.05	32.61	0.02	155.99	0.01	88.56	1.19
268 K	[-] B-QDs	3.14	0.46	45.80	0.30	138.50	0.21	595.68	0.03	246.33	1.12
	[-] B-QD:::[+] G-QD	0.53	0.92	8.25	0.05	34.67	0.02	160.53	0.01	89.22	1.23

Proof for Electrostatically Driven FRET

Table A5.14 PL decay analysis of [-] B-QDs and [-] B-QD:::[-] G-QD assembly, in a time window of 3.2 μs. The PL decay was collected at 462 nm.

System	τ_1 (ns)	α_1	τ_2 (ns)	α_2	τ_3 (ns)	α_3	τ_4 (ns)	α_4	$\tau_{avg.}$ (ns)	χ^2
[-] B-QDs @462 nm	6.31	0.31	49.15	0.38	147.51	0.28	569.45	0.03	211.98	1.13
[-] B-QD:::[-] G-QD @462 nm	6.67	0.35	47.5	0.42	126.95	0.20	512.08	0.03	191.21	1.14

Dyad – 4: [-] B-QD:::[+] R-QD Donor:::Acceptor Assembly

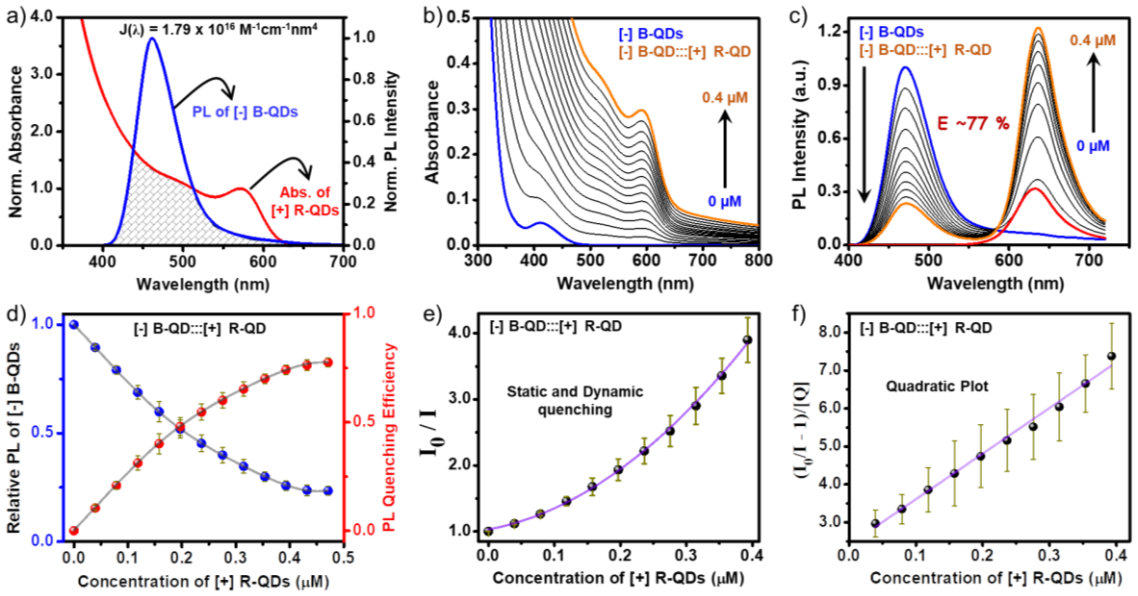

Figure A5.20 Steady-state energy transfer studies in [-] B-QD:::[+] R-QD donor:::acceptor assembly. (a) Spectral overlap integral between absorption of [+] R-QD and emission of [-] B-QD. (b) UV-vis absorption and (c) PL spectral changes of [-] B-QDs upon the successive addition of [+] R-QDs in water. (c) A plot showing saturation in relative PL of [-] B-QDs and PL quenching efficiency, as a function of increasing concentration of [+] R-QDs. (e) A non-liner Stern-Volmer (SV) plot, and (f) liner quadratic SV plot was constructed from the relative PL of [-] B-QD vs concentration of [+] R-QDs.

The nanohybrid system composed of negatively charged [-] B-QDs (MUA capped) and positively charged [+] R-QDs (TMA capped) was chosen for long range energy transfer investigation (long range in terms of energy scale). As seen with previous dyad assemblies, a strong spectral overlap integral (~1.79 x 10^{16} $M^{-1}cm^{-1}nm^4$) was observed between the absorption of [+] R-QDs and emission [-] B-QDs, indicating the possibility of making good donor-acceptor FRET pair (**Figure A5.20a**). In a typical FRET study, small aliquots of [+] R-QD solution (1.5 μL of 66 μM) were sequentially added to a solution of [-] B-QD (2.5 mL of (~2 μM) and subsequent spectral changes were recorded. Steady-state absorption and PL study shows that complexation leading to an energy transfer process in [-] B-QD:::[+] R-QD donor:::acceptor assembly (**Figure A5.20b,c**). A steady decrease in the PL intensity of donor [-] B-QD was observed, followed by enhancement in PL intensity of [+] R-QDs. The direct excitation-based PL intensity of only [+] R-QD was lower than the PL intensity from [-] B-QD:::[+] R-QD donor:::acceptor system (red and orange spectrum in **Figure A5.20c**, respectively). The quenching efficiency was estimated to be ~77 %, which saturated after the addition of ~0.4 μM of [+] R-QDs (**Figure A5.20c,d**). A non-linear Stern-Volmer plot confirm

the presence of both static and dynamic components in PL quenching process (**Figure A5.20e**). A quadratic SV plot was constructed to further analyse the PL quenching event in [-] B-QD:::[+] R-QD donor:::acceptor system (**Figure A5.20f**). Next, in an opposite addition experiment, a steady growth of acceptor [+] R-QD PL was observed in presence of 0.2 μM of [-] B-QD, nullify the inevitable direct excitation issue associated with all-QD system (**Figure A5.21a**). Furthermore, the photoluminescence excitation studies (PLE) revealed the strong contribution of the donor QD absorption in the PL enhancement of the acceptor QD (**Figure A5.21b,c**). Thus, both steady-state PL and PLE studies confirm the involvement of an efficient energy transfer process in [-] B-QD:::[+] R-QD donor:::acceptor assembly.

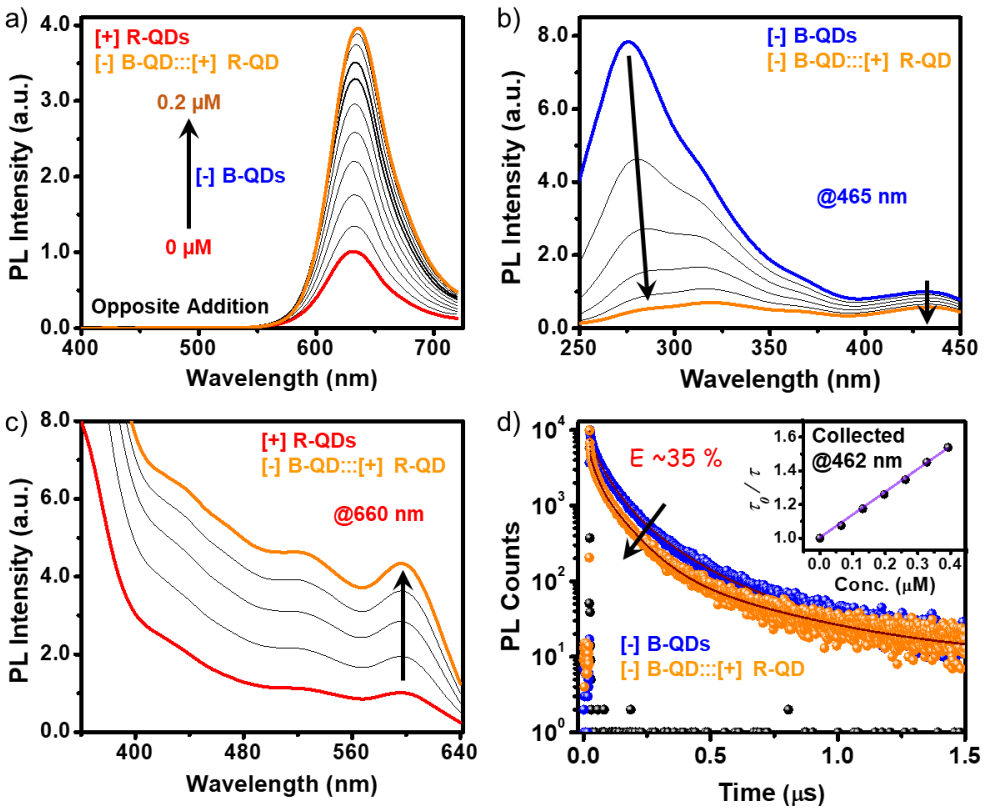

Figure A5.21 (a) Reverse addition experiment shows a gradual enhancement in the PL of acceptor [+] R-QDs upon successive additions of donor [-] B-QDs. (b) PLE spectra collected at the emission maxima of donor [-] B-QDs in absence (blue) and presence (black followed by orange) of acceptor [+] R-QDs. (c) PLE spectra collected at the emission of acceptor [+] R-QDs in absence (red) and presence (orange) of [-] B-QDs. (d) PL decay kinetics of [-] B-QDs in absence and presence of [+] R-QD. Inset shows the corresponding lifetime SV plot.

As in steady-state experiments, the time-resolved PL decay kinetics too revealed a clear quenching in average PL lifetime of [-] B-QD in presence of [+] R-QDs. The average lifetime decreases from ~205 ns to ~133 ns, corresponding to ~35 % FRET efficiency ($E = 1 - \tau/\tau_0$, where τ_0 and τ are the lifetime of donor QDs in absence and presence of acceptor QDs,

respectively) (**Figure A5.19d** and **Table A5.19**). The rate of energy transfer process was estimated to be ~1.31 x 10^7 s^{-1}. The measured values of the static and dynamic quenching constants were ~8.90 x 10^6 M^{-1} and ~1.35 x 10^6 M^{-1}, respectively. Further, a large bimolecular quenching constant (~6.60 x 10^{12} M^{-1} s^{-1}) from lifetime SV plot confirm a strong ground state interaction in [-] B-QD:::[+] R-QD donor:::acceptor assembly (**Table A5.20**). **Table A5.20** summaries all the energy transfer parameters associated with [-] B-QD:::[+] R-QD donor:::acceptor assembly. In conclusion, the present study demonstrated an long range energy transfer process at energy scale of 610 meV in [-] B-QD:::[+] R-QD donor:::acceptor assembly. Details steady-state and time-resolved analysis were performed to conclusively prove the existence of FRET process in electrostatically assembled donor-acceptor QDs. In future, the long-range FRET studies in all-QD systems could further be expanded to NIR region as well.

Table A5.15 PL decay analysis of [-] B-QDs and [-] B-QD:::[+] R-QD assembly, in a time window of 3.2 µs. The PL decay was collected at 462 nm.

System	τ_1 (ns)	α_1	τ_2 (ns)	α_2	τ_3 (ns)	α_3	τ_4 (ns)	α_4	$\tau_{avg.}$ (ns)	χ^2
[-] B-QDs @465 nm	8.31	0.36	50.26	0.42	139.88	0.19	546.46	0.03	205.18	1.09
[-] B-QD:::[+] R-QD @462 nm	1.17	0.65	17.98	0.17	80.15	0.16	314.11	0.02	133.36	1.13

Table A5.16 Resonance energy transfer parameters for [-] B-QD:::[+] R-QD complex.

System	J(λ) ($M^{-1}cm^{-1}nm^4$)	R_0 (Å)	E (%)	$k_T(r)$ (s^{-1})	k_q ($M^{-1}s^{-1}$)
[-] B-QD:::[+] R-QD	1.79 x 10^{16}	72	35	1.31 x 10^7	6.60 x 10^{12}

Chapter – 6

Thesis Summary and Future Direction

6.1 Thesis Summary

In conclusion, different Chapters of the present Thesis summarise the journey of developing design strategy to mimic nature's favourite photosynthetic machinery solely based on environmentally friendly semiconductor QDs, notably with InP/ZnS QDs and CIS/ZnS QDs, respectively. To recall, nature's masterpiece, the photosynthetic machinery functions on the principles of multicomponent assembly, where various light harvesting components are tied together through non-covalent interaction. In this direction, a library of light harvesting components were produced by tuning the phenomena of quantum confinement effect (**Figure 6.1a**). Furthermore, a careful choregraphing of surface chemistry of InP and CIS QDs allow us to regulate interparticle interactions at nanoscale to create precise assemblies with QD based light-harvesters. In our first attempt, we have completed the color gamut in the visible region of environmentally friendly InP QD family by introducing a water stable pure-blue emitter.[1] Here, a fine control over the nucleation and growth process, followed by rational choice of reactive precursors allow us to stabilize band edge blue emission from smaller InP core (<2 nm). Following this, the capabilities of blue-emitting InP/ZnS QDs was explored in energy transfer and bioimaging studies (**Figure 6.1b**). Next, a comprehensive investigation of the exciton dynamics of newly-developed QDs was conducted, following the framework of the excited state electron transfer process (**Figure 6.1b**). Once, the optoelectronic characteristics of InP-based blue emitter was discovered, a significant effort was made to develop electrostatically driven all-QD based donor-acceptor system for FRET study. The combinations of all-primary colors such as blue-green-and red-emitting InP/ZnS QDs, and red-emitting CIS/ZnS QDs, produces four dyad assemblies, as illustrated in **Figure 6c**.[2-4] The four dyad assembles are blue-green, green-red, and blue-red al-InP/ZnS QD donor-acceptor assemblies, and green-red [-] InP/ZnS:::[+] CIS/ZnS QD nanohybrid assembly. Optimization of all dyad assemblies significantly improves our FRET database, and established a roadmap for FRET investigation between inter-QD donor-acceptor system.

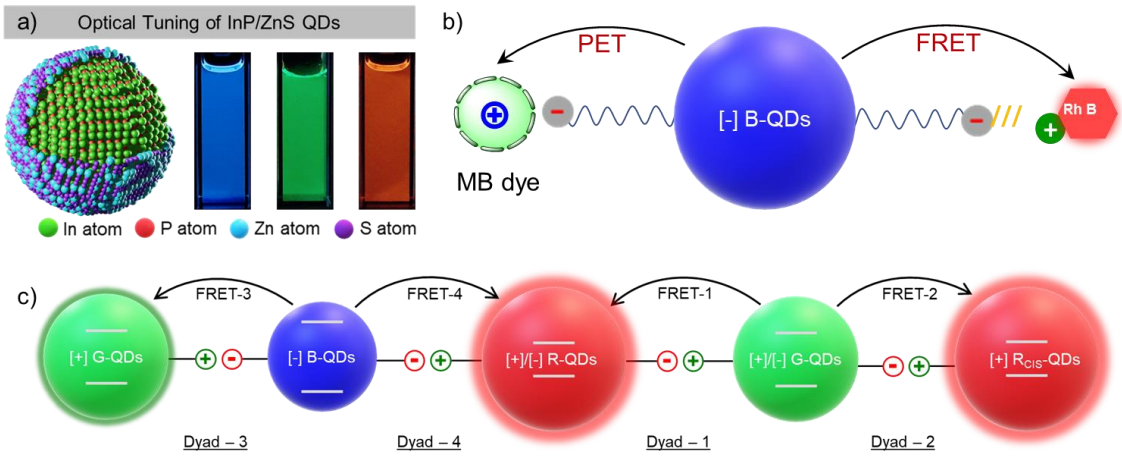

Figure 6.1 (a) Tuning the optical band gap of core/shell InP/ZnS QDs leads to the creation of blue, green, and red-emissions. (b) Schematics showing the suitability of pure-blue emitting InP/ZnS QDs in participating in efficient light induced energy and electron transfer processes with appropriate organic dyes. (c) Four FRET dyads developed in the Thesis: All-QD dyad assemblies based on blue, green, and red-emitting InP/ZnS QDs, and red-emitting CIS/ZnS QDs.

6.2 Future Directions

All the primary colors for the environmentally benign InP QD family is readily accessible, and a roadmap for FRET investigation has been established in this Thesis. Therefore, a logical extension of the present Thesis would be the development of multicomponent donor-acceptor systems based on three or more different sizes of QDs. Subsequently, multicomponent all-QD based light harvesting antenna systems could further be coupled with electron transfer complexes and catalytic centers to accomplish artificial photosynthesis (**Figure 6.2a**). Furthermore, QD-QD FRET construct can be employed to enhance the performances of solar cells and solid-state lighting devices. As reported by Grimes and co-workers, incident photon to current conversion efficiency (IPCE) of a dye sensitized solar cells (DSSCs) can be improved to ~25 %, by the assistance of FRET process (**Figure 6.2b**).[5] Additionally, the multicomponent assembly of environmentally benign QDs can be utilized to study various other fundamental photophysical processes as well, such as photoinduced electron transfer (PET) and dexter energy transfer (DET) processes. Thus, we believe that all-QD based multicomponent donor-acceptor systems will have a far-reaching contribution to a wide-variety of fields, including solar-light-harvesting, electronic, solid-state devices and so on.

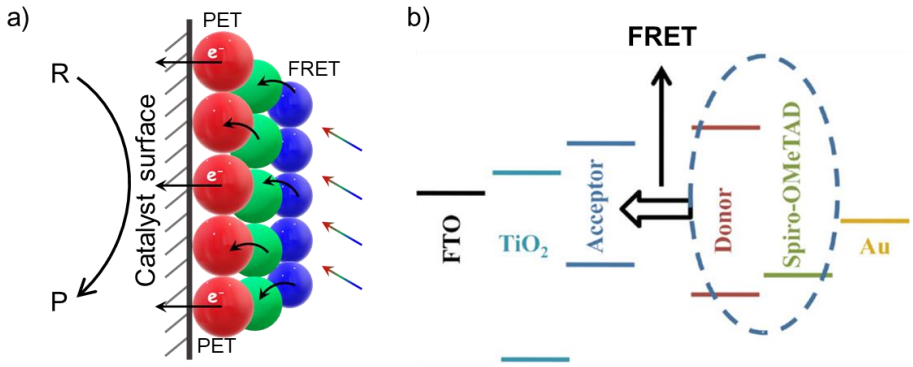

Figure 6.2 (a) Integrating energy transfer, electron transfer, and catalytic center to mimic photosynthesis in all-QD based donor-acceptor assembly. (b) Diagram showing the relative energy levels of the components in a FRET-assisted dye-sensitized solar cell (DSSC). Reproduced with permission from reference 5. Copyright 2010, American Chemical Society.

6.3 References

(1) Roy, P.; Virmani, M.; Pillai, P. P. Blue-emitting InP quantum dots participate in an efficient resonance energy transfer process in water. *Chem. Sci.* **2023**, *14*, 5167–5176.

(2) Roy, P.; Devatha, G.; Roy, S.; Rao, A.; Pillai, P. P. Electrostatically Driven Resonance Energy Transfer in an All-Quantum Dot Based Donor–Acceptor System. *J. Phys. Chem. Lett.* **2020**, *11*, 5354–5360.

(3) Roy, P.; Sury, A. S.; Pillai, P. P. Resonance energy transfer in electrostatically assembled donor-acceptor system based on blue-emitting InP quantum dots. *Chem. Phys. Impact* **2023**, *7*, 100334.

(4) Roy, P.; Sury, A. S.; Pillai, P. P. Electrostatics Enable Resonance Energy Transfer in InP Based All-Quantum Dot Donor-Acceptor Assembly. *Appl. Phys. Lett.* **2024**, *124*, 222104.

(5) Mor, G. K.; Basham, J.; Paulose, M.; Kim, S.; Varghese, O. K.; Vaish, A.; Yoriya, S.; Grimes, C. A. High-Efficiency Förster Resonance Energy Transfer in Solid-State Dye Sensitized Solar Cells. *Nano Lett.* **2010**, *10*, 2387–2394.

List of Publications

Included in the Thesis

(1) **Pradyut Roy**, Gayathri Devatha, Soumendu Roy, Anish Rao, Pramod P. Pillai* "Electrostatically Driven Resonance Energy Transfer in an All-Quantum Dot Based Donor–Acceptor System" *J. Phys. Chem. Lett.* **2020**, *11*, 5354–5360.

(2) Indra Narayan Chakraborty,‡ **Pradyut Roy**,‡ Anish Rao, Gayathri Devatha, Soumendu Roy, Pramod P. Pillai* "The Unconventional Role of Surface Ligands in Dictating the Light Harvesting Properties of Quantum Dots" *J. Mater. Chem. A* **2021**, *9*, 7422–7457. (‡equal contribution)

(3) **Pradyut Roy**, Mishika Virmani, Pramod P. Pillai* "Blue-Emitting InP Quantum Dots Participate in an Efficient Resonance Energy Transfer Process in Water" *Chem. Sci.* **2023**, *14*, 5167–5176.

(4) **Pradyut Roy**, Adhra S. Sury, Pramod P. Pillai* "Resonance Energy Transfer in Electrostatically Assembled Donor-Acceptor System based on Blue-Emitting InP Quantum Dots" *Chem. Phys. Impact* **2023**, *7*, 100334.

(5) **Pradyut Roy**, Adhra S. Sury, Pramod P. Pillai* "Electrostatics Enable Resonance Energy Transfer in InP Based All-Quantum Dot Donor-Acceptor Assembly" *Appl. Phys. Lett.* **2024**, *124*, 222104.

(6) **Pradyut Roy**, Kishan K Yadav, Jyotishman Dasgupta*, Pramod P. Pillai* "Electrostatics Enable Photoinduced Electron Transfer Process in QD-Dye Model System based on Blue InP QDs" *Manuscript Submitted.*

Not Included in the Thesis

(7) Gayathri Devatha, **Pradyut Roy**, Anish Rao, Soumendu Roy, Pramod P Pillai* "Multicolor Luminescent Patterning via Photoregulation of Electron and Energy Transfer Processes in Quantum Dots". *J. Phys. Chem. Lett.* **2020**, *11*, 4099–4106.

(8) Vanshika Jain, Sumit Roy,‡ **Pradyut Roy**,‡ Pramod P Pillai* "When Design Meets Function: The Prodigious Role of Surface Ligands in Regulating Nanoparticle Chemistry" *Chem. Mater.* **2022**, *34*, 7579–7597. (‡equal contribution)

(9) Indra Narayan Chakraborty, **Pradyut Roy**, Pramod P Pillai* "Visible Light-Mediated Quantum Dot Photocatalysis Enables Olefination Reactions at Room Temperature" *ACS Catal.* **2023**, *13*, 7331–7338.

(10) Indra Narayan Chakraborty, Vanshika Jain, **Pradyut Roy**, Pawan Kumar, Chathakudath P Vinod, Pramod P Pillai* "Photocatalytic Regeneration of Reactive Cofactors with InP Quantum Dots for the Continuous Chemical Synthesis" *ACS Catal.* **2024**, *14*, 6740–6748.

(11) Vanshika Jain, Shreya Tyagi, **Pradyut Roy**, Pramod P Pillai* "Ammonia Synthesis with Visible Light and Quantum Dots" *Manuscript Under Review.*

List of Conferences Attended

(1) Presented a poster titled "*Light-Harvesting Studies on the Surface Engineered Green Quantum Dots*" at **Center for Energy Science (CES)** one-day symposium, held at **Indian Institute of Science Education and Research (IISER) Pune** on October 18, 2019.

(2) Presented a poster titled "*Light-Harvesting and Photopatterning with Surface Engineered Quantum Dots*" at **Low Dimensional Materials (LDM-2020)** conference, held at **IISER Pune** on March 11, 2020.

(3) Presented a poster titled "*Light-Harvesting and Photopatterning with Surface Engineered Quantum Dots*" at the inauguration of Cipla Foundation at **IISER Pune**, scheduled on January 29, 2020.

(4) Presented a poster titled "*Electrostatically Driven Resonance Energy Transfer in an All-Quantum Dot based Donor-Acceptor System*" at **CHEMSCI2021: Leaders in the field symposium**, held at **Jawaharlal Nehru Centre for Advanced Scientific Research (JNCASR)**, scheduled in December 2021.

(5) Gave a talk titled "Electrostatically Driven Resonance Energy Transfer in an All–Quantum Dot Based Donor–Acceptor System" in **11th Asian Photochemistry Conference (APC) 2021**, in November 2021.

(6) Presented a poster titled "*Blue-Emititng InP Quantum Dots: Towards Expanding the Scope for FRET and Photopatterning Studies*" at **Low Dimensional Materials (LDM-2022)** conference, held at **IISER Pune** in May 2022.

(7) Gave a talk titled "*Light-Harvesting with Environmentally Friendly Quantum Dots*" in **Chemsymphoria** (in-house symposium) at **IISER Pune** in December 2022.

(8) Presented a poster titled "*Light Harvesting Studies with 'Blue' InP QDs in Water*" in **Emerging Materials Conference**, held at **IISER Pune** in July 2023.

(9) Gave a talk titled "*Light-Harvesting Studies with Indium Phosphide Quantum Dots*" in **12th Asian Photochemistry Conference (APC) 2021**, held at Melbourne Convention and Exhibition Centre (MCEC) in **Australia**, on November 27 –December 1, 2023.

(10) Presented a poster titled "*Light Harvesting Studies with 'Blue' InP QDs in Water*" in **International Conference on Quantum Energy (ICQE)**, held at Melbourne in **Australia** in December 2023

Permissions and Copyrights

Figures adapted from open access papers –

1. Figure 1.1
2. Figure 1.3

The unconventional role of surface ligands in dictating the light harvesting properties of quantum dots

I. N. Chakraborty, P. Roy, A. Rao, G. Devatha, S. Roy and P. P. Pillai, *J. Mater. Chem. A*, 2021, **9**, 7422 **DOI:** 10.1039/D0TA12623C

Blue-emitting InP quantum dots participate in an efficient resonance energy transfer process in water

P. Roy, M. Virmani and P. P. Pillai, *Chem. Sci.*, 2023, **14**, 5167 **DOI:** 10.1039/D3SC00164D

RightsLink

PR

Electrostatically Driven Resonance Energy Transfer in an All-Quantum Dot Based Donor–Acceptor System

Author: Pradyut Roy, Gayathri Devatha, Soumendu Roy, et al
Publication: Journal of Physical Chemistry Letters
Publisher: American Chemical Society
Date: Jul 1, 2020

PERMISSION/LICENSE IS GRANTED FOR YOUR ORDER AT NO CHARGE

This type of permission/license, instead of the standard Terms and Conditions, is sent to you because no fee is being charged for your order. Please note the following:

- Permission is granted for your request in both print and electronic formats, and translations.
- If figures and/or tables were requested, they may be adapted or used in part.
- Please print this page for your records and send a copy of it to your publisher/graduate school.
- Appropriate credit for the requested material should be given as follows: "Reprinted (adapted) with permission from {COMPLETE REFERENCE CITATION}. Copyright {YEAR} American Chemical Society." Insert appropriate information in place of the capitalized words.
- One-time permission is granted only for the use specified in your RightsLink request. No additional uses are granted (such as derivative works or other editions). For any uses, please submit a new request.

If credit is given to another source for the material you requested from RightsLink, permission must be obtained from that source.

BACK CLOSE WINDOW

IISER PUNE

Roy Pradyut <roy.pradyut@students.iiserpune.ac.in>

RE: Copyright Permission

1 message

AIPRights Permissions <Rights@aip.org> Mon, Jul 15, 2024 at 7:16 PM
To: Roy Pradyut <roy.pradyut@students.iiserpune.ac.in>

Dear Dr. Pradyut,

Thank you for reaching out to AIP Publishing with your reproduction request. We are delighted to be able to assist!

You are permitted to include all or part of your published article in your thesis, provided you also include a credit line referencing the original publication.

Our preferred format is (please fill in the citation information):

“Reproduced from [FULL CITATION], with the permission of AIP Publishing.”

If the thesis will be available electronically, please include a link to the version of record on AIP Publishing’s site.

Please let us know if you have any questions. Congratulations on the completion of your thesis and your degree!

Sincerely,

Suzanne Inge

From: Roy Pradyut <roy.pradyut@students.iiserpune.ac.in>
Sent: Sunday, July 14, 2024 4:30 PM
To: AIPRights Permissions <rights@aip.org>
Subject: Copyright Permission

Dear APL,

I would like to take the copyright permission for my published article (DOI: 10.1063/5.0206273), to reuse in my PhD thesis. Please prove the permission for so.

Reason: Reuse in Thesis

Requester Type: I am an Author (Pradyut Roy)

Format: Print & Electronic

Portion: Full Article

Will be translating: No

Regards,

Pradyut

Thanking you,

Pradyut Roy

Prime Minister's Research Fellow, PhD Student, Department of Chemistry, IISER Pune

Main Building;C214, NanoAlchemy Lab

Dr. Pramod P. Pillai's Group

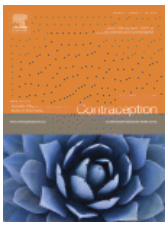

Resonance energy transfer in electrostatically assembled donor-acceptor system based on blue-emitting InP quantum dots

Author: Pradyut Roy,Adhra S. Sury,Pramod P. Pillai

Publication: Chemical Physics Impact

Publisher: Elsevier

Date: December 2023

Journal Author Rights

Please note that, as the author of this Elsevier article, you retain the right to include it in a thesis or dissertation, provided it is not published commercially. Permission is not required, but please ensure that you reference the journal as the original source. For more information on this and on your other retained rights, please visit: https://www.elsevier.com/about/our-business/policies/copyright#Author-rights

BACK CLOSE WINDOW

Figure 1.4

SPRINGER NATURE LICENSE
TERMS AND CONDITIONS

Jul 01, 2024

This Agreement between Pradyut Roy ("You") and Springer Nature ("Springer Nature") consists of your license details and the terms and conditions provided by Springer Nature and Copyright Clearance Center.

License Number	5820390139452
License date	Jul 01, 2024
Licensed Content Publisher	Springer Nature
Licensed Content Publication	Nature Chemistry
Licensed Content Title	Energy funnelling within multichromophore architectures monitored with subnanometre resolution
Licensed Content Author	Shuiyan Cao et al
Licensed Content Date	May 24, 2021
Type of Use	Thesis/Dissertation
Requestor type	non-commercial (non-profit)
Format	electronic
Portion	figures/tables/illustrations
Number of figures/tables/illustrations	1
Would you like a high resolution image with your order?	no

Will you be translating?	no
Circulation/distribution	1 - 29
Author of this Springer Nature content	no
Title of new work	Light-Harvesting Studies in Electrostatically Bonded All-Quantum Dot Assemblies
Institution name	Indian Institute of Science Education and Research Pune
Expected presentation date	Oct 2024
Order reference number	1
Portions	Figure 3
The Requesting Person / Organization to Appear on the License	Pradyut Roy
Requestor Location	Mr. Pradyut Roy IISER Pune Dr Homi Bhabha Road Pashan Pune, Pashan 411008 India Attn: Mr. Pradyut Roy
Billing Type	Invoice
Billing Address	Mr. Pradyut Roy IISER Pune Dr Homi Bhabha Road Pashan Pune, India 411008 Attn: Pradyut Roy
Total	0.00 USD
Terms and Conditions	

Springer Nature Customer Service Centre GmbH Terms and Conditions

The following terms and conditions ("Terms and Conditions") together with the terms specified in your [RightsLink] constitute the License ("License") between you as Licensee and Springer Nature Customer Service Centre GmbH as Licensor. By clicking 'accept' and completing the transaction for your use of the material ("Licensed Material"), you confirm your acceptance of and obligation to be bound by these Terms and Conditions.

1. Grant and Scope of License

1. 1. The Licensor grants you a personal, non-exclusive, non-transferable, non-sublicensable, revocable, world-wide License to reproduce, distribute, communicate to the public, make available, broadcast, electronically transmit or create derivative works using the Licensed Material for the purpose(s) specified in your RightsLink Licence Details only. Licenses are granted for the specific use requested in the order and for no other use, subject to these Terms and Conditions. You acknowledge and agree that the rights granted to you under this License do not include the right to modify, edit, translate, include in collective works, or create derivative works of the Licensed Material in whole or in part unless expressly stated in your RightsLink Licence Details. You may use the Licensed Material only as permitted under this Agreement and will not reproduce, distribute, display, perform, or otherwise use or exploit any Licensed Material in any way, in whole or in part, except as expressly permitted by this License.

1. 2. You may only use the Licensed Content in the manner and to the extent permitted by these Terms and Conditions, by your RightsLink Licence Details and by any applicable laws.

1. 3. A separate license may be required for any additional use of the Licensed Material, e.g. where a license has been purchased for print use only, separate permission must be obtained for electronic re-use. Similarly, a License is only valid in the language selected and does not apply for editions in other languages unless additional translation rights have been granted separately in the License.

1. 4. Any content within the Licensed Material that is owned by third parties is expressly excluded from the License.

1. 5. Rights for additional reuses such as custom editions, computer/mobile applications, film or TV reuses and/or any other derivative rights requests require additional permission and may be subject to an additional fee. Please apply to journalpermissions@springernature.com or bookpermissions@springernature.com for these rights.

2. Reservation of Rights

Licensor reserves all rights not expressly granted to you under this License. You acknowledge and agree that nothing in this License limits or restricts Licensor's rights in or use of the Licensed Material in any way. Neither this License, nor any act, omission, or statement by Licensor or you, conveys any ownership right to you in any Licensed Material, or to any element or portion thereof. As between Licensor and you, Licensor owns and retains all right, title, and interest in and to the Licensed Material subject to the license granted in Section 1.1. Your permission to use the Licensed Material is expressly conditioned on you not impairing Licensor's or the applicable copyright owner's rights in the Licensed Material in any way.

3. Restrictions on use

3. 1. Minor editing privileges are allowed for adaptations for stylistic purposes or formatting purposes provided such alterations do not alter the original meaning or

intention of the Licensed Material and the new figure(s) are still accurate and representative of the Licensed Material. Any other changes including but not limited to, cropping, adapting, and/or omitting material that affect the meaning, intention or moral rights of the author(s) are strictly prohibited.

3. 2. You must not use any Licensed Material as part of any design or trademark.

3. 3. Licensed Material may be used in Open Access Publications (OAP), but any such reuse must include a clear acknowledgment of this permission visible at the same time as the figures/tables/illustration or abstract and which must indicate that the Licensed Material is not part of the governing OA license but has been reproduced with permission. This may be indicated according to any standard referencing system but must include at a minimum 'Book/Journal title, Author, Journal Name (if applicable), Volume (if applicable), Publisher, Year, reproduced with permission from SNCSC'.

4. STM Permission Guidelines

4. 1. An alternative scope of license may apply to signatories of the STM Permissions Guidelines ("STM PG") as amended from time to time and made available at https://www.stm-assoc.org/intellectual-property/permissions/permissions-guidelines/.

4. 2. For content reuse requests that qualify for permission under the STM PG, and which may be updated from time to time, the STM PG supersede the terms and conditions contained in this License.

4. 3. If a License has been granted under the STM PG, but the STM PG no longer apply at the time of publication, further permission must be sought from the Rightsholder. Contact journalpermissions@springernature.com or bookpermissions@springernature.com for these rights.

5. Duration of License

5. 1. Unless otherwise indicated on your License, a License is valid from the date of purchase ("License Date") until the end of the relevant period in the below table:

Reuse in a medical communications project	Reuse up to distribution or time period indicated in License
Reuse in a dissertation/thesis	Lifetime of thesis
Reuse in a journal/magazine	Lifetime of journal/magazine
Reuse in a book/textbook	Lifetime of edition
Reuse on a website	1 year unless otherwise specified in the License
Reuse in a presentation/slide kit/poster	Lifetime of presentation/slide kit/poster. Note: publication whether electronic or in print of presentation/slide kit/poster may require further permission.
Reuse in conference proceedings	Lifetime of conference proceedings
Reuse in an annual report	Lifetime of annual report
Reuse in training/CME materials	Reuse up to distribution or time period indicated in License
Reuse in newsmedia	Lifetime of newsmedia

Reuse in coursepack/classroom materials	Reuse up to distribution and/or time period indicated in license

6. Acknowledgement

6. 1. The Licensor's permission must be acknowledged next to the Licensed Material in print. In electronic form, this acknowledgement must be visible at the same time as the figures/tables/illustrations or abstract and must be hyperlinked to the journal/book's homepage.

6. 2. Acknowledgement may be provided according to any standard referencing system and at a minimum should include "Author, Article/Book Title, Journal name/Book imprint, volume, page number, year, Springer Nature".

7. Reuse in a dissertation or thesis

7. 1. Where 'reuse in a dissertation/thesis' has been selected, the following terms apply: Print rights of the Version of Record are provided for; electronic rights for use only on institutional repository as defined by the Sherpa guideline (www.sherpa.ac.uk/romeo/) and only up to what is required by the awarding institution.

7. 2. For theses published under an ISBN or ISSN, separate permission is required. Please contact journalpermissions@springernature.com or bookpermissions@springernature.com for these rights.

7. 3. Authors must properly cite the published manuscript in their thesis according to current citation standards and include the following acknowledgement: '*Reproduced with permission from Springer Nature*'.

8. License Fee

You must pay the fee set forth in the License Agreement (the "License Fees"). All amounts payable by you under this License are exclusive of any sales, use, withholding, value added or similar taxes, government fees or levies or other assessments. Collection and/or remittance of such taxes to the relevant tax authority shall be the responsibility of the party who has the legal obligation to do so.

9. Warranty

9. 1. The Licensor warrants that it has, to the best of its knowledge, the rights to license reuse of the Licensed Material. **You are solely responsible for ensuring that the material you wish to license is original to the Licensor and does not carry the copyright of another entity or third party (as credited in the published version).** If the credit line on any part of the Licensed Material indicates that it was reprinted or adapted with permission from another source, then you should seek additional permission from that source to reuse the material.

9. 2. EXCEPT FOR THE EXPRESS WARRANTY STATED HEREIN AND TO THE EXTENT PERMITTED BY APPLICABLE LAW, LICENSOR PROVIDES THE LICENSED MATERIAL "AS IS" AND MAKES NO OTHER REPRESENTATION OR WARRANTY. LICENSOR EXPRESSLY DISCLAIMS ANY LIABILITY FOR ANY CLAIM ARISING FROM OR OUT OF THE CONTENT, INCLUDING BUT NOT LIMITED TO ANY ERRORS, INACCURACIES, OMISSIONS, OR DEFECTS CONTAINED THEREIN, AND ANY IMPLIED OR EXPRESS WARRANTY AS TO MERCHANTABILITY OR FITNESS FOR A PARTICULAR PURPOSE. IN NO EVENT SHALL LICENSOR

BE LIABLE TO YOU OR ANY OTHER PARTY OR ANY OTHER PERSON OR FOR ANY SPECIAL, CONSEQUENTIAL, INCIDENTAL, INDIRECT, PUNITIVE, OR EXEMPLARY DAMAGES, HOWEVER CAUSED, ARISING OUT OF OR IN CONNECTION WITH THE DOWNLOADING, VIEWING OR USE OF THE LICENSED MATERIAL REGARDLESS OF THE FORM OF ACTION, WHETHER FOR BREACH OF CONTRACT, BREACH OF WARRANTY, TORT, NEGLIGENCE, INFRINGEMENT OR OTHERWISE (INCLUDING, WITHOUT LIMITATION, DAMAGES BASED ON LOSS OF PROFITS, DATA, FILES, USE, BUSINESS OPPORTUNITY OR CLAIMS OF THIRD PARTIES), AND WHETHER OR NOT THE PARTY HAS BEEN ADVISED OF THE POSSIBILITY OF SUCH DAMAGES. THIS LIMITATION APPLIES NOTWITHSTANDING ANY FAILURE OF ESSENTIAL PURPOSE OF ANY LIMITED REMEDY PROVIDED HEREIN.

10. Termination and Cancellation

10. 1. The License and all rights granted hereunder will continue until the end of the applicable period shown in Clause 5.1 above. Thereafter, this license will be terminated and all rights granted hereunder will cease.

10. 2. Licensor reserves the right to terminate the License in the event that payment is not received in full or if you breach the terms of this License.

11. General

11. 1. The License and the rights and obligations of the parties hereto shall be construed, interpreted and determined in accordance with the laws of the Federal Republic of Germany without reference to the stipulations of the CISG (United Nations Convention on Contracts for the International Sale of Goods) or to Germany´s choice-of-law principle.

11. 2. The parties acknowledge and agree that any controversies and disputes arising out of this License shall be decided exclusively by the courts of or having jurisdiction for Heidelberg, Germany, as far as legally permissible.

11. 3. This License is solely for Licensor's and Licensee's benefit. It is not for the benefit of any other person or entity.

Questions? For questions on Copyright Clearance Center accounts or website issues please contact springernaturesupport@copyright.com or +1-855-239-3415 (toll free in the US) or +1-978-646-2777. For questions on Springer Nature licensing please visit https://www.springernature.com/gp/partners/rights-permissions-third-party-distribution

Other Conditions:

Version 1.4 - Dec 2022

Questions? customercare@copyright.com.

Figure 1.5

RightsLink

Combining Light-Harvesting and Charge Separation in a Self-Assembled Artificial Photosynthetic System Based on Perylenediimide Chromophores

Author: Boris Rybtchinski, Louise E. Sinks, Michael R. Wasielewski

Publication: Journal of the American Chemical Society
Publisher: American Chemical Society
Date: Oct 1, 2004

PERMISSION/LICENSE IS GRANTED FOR YOUR ORDER AT NO CHARGE

This type of permission/license, instead of the standard Terms and Conditions, is sent to you because no fee is being charged for your order. Please note the following:

- Permission is granted for your request in both print and electronic formats, and translations.
- If figures and/or tables were requested, they may be adapted or used in part.
- Please print this page for your records and send a copy of it to your publisher/graduate school.
- Appropriate credit for the requested material should be given as follows: "Reprinted (adapted) with permission from {COMPLETE REFERENCE CITATION}. Copyright {YEAR} American Chemical Society." Insert appropriate information in place of the capitalized words.
- One-time permission is granted only for the use specified in your RightsLink request. No additional uses are granted (such as derivative works or other editions). For any uses, please submit a new request.

If credit is given to another source for the material you requested from RightsLink, permission must be obtained from that source.

BACK CLOSE WINDOW

RightsLink

Chemical Approaches to Artificial Photosynthesis. 2

Author: James H. Alstrum-Acevedo, M. Kyle Brennaman, Thomas J. Meyer
Publication: Inorganic Chemistry
Publisher: American Chemical Society
Date: Oct 1, 2005

PERMISSION/LICENSE IS GRANTED FOR YOUR ORDER AT NO CHARGE

This type of permission/license, instead of the standard Terms and Conditions, is sent to you because no fee is being charged for your order. Please note the following:

- Permission is granted for your request in both print and electronic formats, and translations.
- If figures and/or tables were requested, they may be adapted or used in part.
- Please print this page for your records and send a copy of it to your publisher/graduate school.
- Appropriate credit for the requested material should be given as follows: "Reprinted (adapted) with permission from {COMPLETE REFERENCE CITATION}. Copyright {YEAR} American Chemical Society." Insert appropriate information in place of the capitalized words.
- One-time permission is granted only for the use specified in your RightsLink request. No additional uses are granted (such as derivative works or other editions). For any uses, please submit a new request.

If credit is given to another source for the material you requested from RightsLink, permission must be obtained from that source.

BACK CLOSE WINDOW

RightsLink

A Supramolecular Artificial Light-Harvesting System with Excitation Energy and Electron Transfer

Author: Kun-Xu Teng, Zhi-Peng An, Li-Ya Niu, et al
Publication: ACS Materials Letters
Publisher: American Chemical Society
Date: Jan 1, 2024

PERMISSION/LICENSE IS GRANTED FOR YOUR ORDER AT NO CHARGE

This type of permission/license, instead of the standard Terms and Conditions, is sent to you because no fee is being charged for your order. Please note the following:

- Permission is granted for your request in both print and electronic formats, and translations.
- If figures and/or tables were requested, they may be adapted or used in part.
- Please print this page for your records and send a copy of it to your publisher/graduate school.
- Appropriate credit for the requested material should be given as follows: "Reprinted (adapted) with permission from {COMPLETE REFERENCE CITATION}. Copyright {YEAR} American Chemical Society." Insert appropriate information in place of the capitalized words.
- One-time permission is granted only for the use specified in your RightsLink request. No additional uses are granted (such as derivative works or other editions). For any uses, please submit a new request.

If credit is given to another source for the material you requested from RightsLink, permission must be obtained from that source.

BACK CLOSE WINDOW

Marketplace

FIgure 1.6

Order Confirmation

Thank you, your order has been placed. An email confirmation has been sent to you. Your order license details and printable licenses will be available within 24 hours. Please access Manage Account for final order details.

This is not an invoice. Please go to manage account to access your order history and invoices.

CUSTOMER INFORMATION

Payment by invoice: You can cancel your order until the invoice is generated by contacting customer service.

Billing Address

Mr. Pradyut Roy
IISER Pune
Dr Homi Bhabha Road
Pashan
Pune, Pashan 411008
India

+91 2025908678
roy.pradyut@students.iiserpune.ac.in

Customer Location

Mr. Pradyut Roy
IISER Pune
Dr Homi Bhabha Road
Pashan
Pune, Pashan 411008
India

PO Number (optional)

N/A

Payment options

Invoice

PENDING ORDER CONFIRMATION

Confirmation Number: Pending

Order Date: 15-Jul-2024

1. Chemical Society reviews

0.00 USD

Article: Synthesis and properties of colloidal heteronanocrystals.

Order License ID	Pending	**Publisher**	ROYAL SOCIETY OF CHEMISTRY
ISSN	1460-4744		
Type of Use	Republish in a thesis/dissertation	**Portion**	Chart/graph/table/figure

LICENSED CONTENT

Publication Title	Chemical Society reviews	**Publication Type**	e-Journal
Article Title	Synthesis and properties of colloidal heteronanocrystals.	**Start Page**	1512
		End Page	1546
Author / Editor	Royal Society of Chemistry (Great Britain)	**Issue**	3
		Volume	40
Date	01/01/1972	**URL**	http://www.rsc.org/csr
Language	English		
Country	United Kingdom of Great Britain and Northern Ireland		
Rightsholder	Royal Society of Chemistry		

REQUEST DETAILS

Portion Type	Chart/graph/table/figure	**Distribution**	Worldwide

Number of Charts / Graphs / Tables / Figures Requested	1	Translation	Original language of publication
Format (select all that apply)	Print, Electronic	Copies for the Disabled?	No
Who Will Republish the Content?	Academic institution	Minor Editing Privileges?	Yes
Duration of Use	Life of current edition	Incidental Promotional Use?	No
Lifetime Unit Quantity	Up to 499	Currency	USD
Rights Requested	Main product		

NEW WORK DETAILS

Title	Light-Harvesting Studies in Electrostatically Bonded All-Quantum Dot Assemblies	Institution Name	Indian Institute Of Science Education And Research Pune
Instructor Name	Pradyut Roy	Expected Presentation Date	2024-09-01

ADDITIONAL DETAILS

Order Reference Number	N/A	The Requesting Person / Organization to Appear on the License	Pradyut Roy

REQUESTED CONTENT DETAILS

Title, Description or Numeric Reference of the Portion(s)	Figure 1.6	Title of the Article / Chapter the Portion Is From	Synthesis and properties of colloidal heteronanocrystals.
Editor of Portion(s)	DonegÃ¡, Celso de Mello	Author of Portion(s)	DonegÃ¡, Celso de Mello
Volume / Edition	40 / ONLINE	Issue, if Republishing an Article From a Serial	3
Page or Page Range of Portion	1512-1546	Publication Date of Portion	2011-03-01

Total Items: 1

Total Due: 0.00 USD

Accepted: Marketplace Permissions General Terms and Conditions and any applicable Publisher Terms and Conditions

Figure 1.9

Influence of Thiol Capping on the Exciton Luminescence and Decay Kinetics of CdTe and CdSe Quantum Dots

Author: Sander F. Wuister, Celso de Mello Donegá, Andries Meijerink
Publication: The Journal of Physical Chemistry B
Publisher: American Chemical Society
Date: Nov 1, 2004

PERMISSION/LICENSE IS GRANTED FOR YOUR ORDER AT NO CHARGE

This type of permission/license, instead of the standard Terms and Conditions, is sent to you because no fee is being charged for your order. Please note the following:

- Permission is granted for your request in both print and electronic formats, and translations.
- If figures and/or tables were requested, they may be adapted or used in part.
- Please print this page for your records and send a copy of it to your publisher/graduate school.
- Appropriate credit for the requested material should be given as follows: "Reprinted (adapted) with permission from {COMPLETE REFERENCE CITATION}. Copyright {YEAR} American Chemical Society." Insert appropriate information in place of the capitalized words.
- One-time permission is granted only for the use specified in your RightsLink request. No additional uses are granted (such as derivative works or other editions). For any uses, please submit a new request.

If credit is given to another source for the material you requested from RightsLink, permission must be obtained from that source.

BACK CLOSE WINDOW

Quantum Dot Surface Chemistry: Ligand Effects and Electron Transfer Reactions

Author: Douglas A. Hines, Prashant V. Kamat
Publication: The Journal of Physical Chemistry C
Publisher: American Chemical Society
Date: Jul 1, 2013

PERMISSION/LICENSE IS GRANTED FOR YOUR ORDER AT NO CHARGE

This type of permission/license, instead of the standard Terms and Conditions, is sent to you because no fee is being charged for your order. Please note the following:

- Permission is granted for your request in both print and electronic formats, and translations.
- If figures and/or tables were requested, they may be adapted or used in part.
- Please print this page for your records and send a copy of it to your publisher/graduate school.
- Appropriate credit for the requested material should be given as follows: "Reprinted (adapted) with permission from {COMPLETE REFERENCE CITATION}. Copyright {YEAR} American Chemical Society." Insert appropriate information in place of the capitalized words.
- One-time permission is granted only for the use specified in your RightsLink request. No additional uses are granted (such as derivative works or other editions). For any uses, please submit a new request.

If credit is given to another source for the material you requested from RightsLink, permission must be obtained from that source.

BACK CLOSE WINDOW

Ligand Binding to Distinct Sites on Nanocrystals Affecting Energy and Charge Transfer

Author: Xin Li, Lydia W. Slyker, Valerie M. Nichols, et al

Publication: Journal of Physical Chemistry Letters

Publisher: American Chemical Society

Date: May 1, 2015

PERMISSION/LICENSE IS GRANTED FOR YOUR ORDER AT NO CHARGE

This type of permission/license, instead of the standard Terms and Conditions, is sent to you because no fee is being charged for your order. Please note the following:

- Permission is granted for your request in both print and electronic formats, and translations.
- If figures and/or tables were requested, they may be adapted or used in part.
- Please print this page for your records and send a copy of it to your publisher/graduate school.
- Appropriate credit for the requested material should be given as follows: "Reprinted (adapted) with permission from {COMPLETE REFERENCE CITATION}. Copyright {YEAR} American Chemical Society." Insert appropriate information in place of the capitalized words.
- One-time permission is granted only for the use specified in your RightsLink request. No additional uses are granted (such as derivative works or other editions). For any uses, please submit a new request.

If credit is given to another source for the material you requested from RightsLink, permission must be obtained from that source.

BACK CLOSE WINDOW

Figure 1.10

Predicting the Rate Constant of Electron Tunneling Reactions at the CdSe–TiO2 Interface

Author: Douglas A. Hines, Ryan P. Forrest, Steven A. Corcelli, et al
Publication: The Journal of Physical Chemistry B
Publisher: American Chemical Society
Date: Jun 1, 2015

PERMISSION/LICENSE IS GRANTED FOR YOUR ORDER AT NO CHARGE

This type of permission/license, instead of the standard Terms and Conditions, is sent to you because no fee is being charged for your order. Please note the following:

- Permission is granted for your request in both print and electronic formats, and translations.
- If figures and/or tables were requested, they may be adapted or used in part.
- Please print this page for your records and send a copy of it to your publisher/graduate school.
- Appropriate credit for the requested material should be given as follows: "Reprinted (adapted) with permission from {COMPLETE REFERENCE CITATION}. Copyright {YEAR} American Chemical Society." Insert appropriate information in place of the capitalized words.
- One-time permission is granted only for the use specified in your RightsLink request. No additional uses are granted (such as derivative works or other editions). For any uses, please submit a new request.

If credit is given to another source for the material you requested from RightsLink, permission must be obtained from that source.

BACK CLOSE WINDOW

Tuning Electron Transfer Rates through Molecular Bridges in Quantum Dot Sensitized Oxides

Author: Hai Wang, Erik R. McNellis, Sachin Kinge, et al

Publication: Nano Letters

Publisher: American Chemical Society

Date: Nov 1, 2013

PERMISSION/LICENSE IS GRANTED FOR YOUR ORDER AT NO CHARGE

This type of permission/license, instead of the standard Terms and Conditions, is sent to you because no fee is being charged for your order. Please note the following:

- Permission is granted for your request in both print and electronic formats, and translations.
- If figures and/or tables were requested, they may be adapted or used in part.
- Please print this page for your records and send a copy of it to your publisher/graduate school.
- Appropriate credit for the requested material should be given as follows: "Reprinted (adapted) with permission from {COMPLETE REFERENCE CITATION}. Copyright {YEAR} American Chemical Society." Insert appropriate information in place of the capitalized words.
- One-time permission is granted only for the use specified in your RightsLink request. No additional uses are granted (such as derivative works or other editions). For any uses, please submit a new request.

If credit is given to another source for the material you requested from RightsLink, permission must be obtained from that source.

BACK CLOSE WINDOW

Figure 1.12

RightsLink

Sign in/Register

Energy Transfer in Aqueous Solutions of Oppositely Charged CdSe/ZnS Core/Shell Quantum Dots and in Quantum Dot−Nanogold Assemblies

Author: Richard Wargnier, Alexandre V. Baranov, Vladimir G. Maslov, et al
Publication: Nano Letters
Publisher: American Chemical Society
Date: Mar 1, 2004

PERMISSION/LICENSE IS GRANTED FOR YOUR ORDER AT NO CHARGE

This type of permission/license, instead of the standard Terms and Conditions, is sent to you because no fee is being charged for your order. Please note the following:

- Permission is granted for your request in both print and electronic formats, and translations.
- If figures and/or tables were requested, they may be adapted or used in part.
- Please print this page for your records and send a copy of it to your publisher/graduate school.
- Appropriate credit for the requested material should be given as follows: "Reprinted (adapted) with permission from {COMPLETE REFERENCE CITATION}. Copyright {YEAR} American Chemical Society." Insert appropriate information in place of the capitalized words.
- One-time permission is granted only for the use specified in your RightsLink request. No additional uses are granted (such as derivative works or other editions). For any uses, please submit a new request.

If credit is given to another source for the material you requested from RightsLink, permission must be obtained from that source.

BACK CLOSE WINDOW

Marketplace

Order Confirmation

Thank you, your order has been placed. An email confirmation has been sent to you. Your order license details and printable licenses will be available within 24 hours. Please access Manage Account for final order details.

This is not an invoice. Please go to manage account to access your order history and invoices.

CUSTOMER INFORMATION

Payment by invoice: You can cancel your order until the invoice is generated by contacting customer service.

Billing Address

Mr. Pradyut Roy
IISER Pune
Dr Homi Bhabha Road
Pashan
Pune, Pashan 411008
India

+91 2025908678
roy.pradyut@students.iiserpune.ac.in

Customer Location

Mr. Pradyut Roy
IISER Pune
Dr Homi Bhabha Road
Pashan
Pune, Pashan 411008
India

PO Number (optional)

N/A

Payment options

Invoice

PENDING ORDER CONFIRMATION

Confirmation Number: Pending

Order Date: 15-Jul-2024

1. Chemical communications

0.00 USD

Article: The photoluminescence spectral profiles of water-soluble aggregates of PbS quantum dots assembled through reversible metal coordination.

Order License ID	Pending	**Publisher**	ROYAL SOCIETY OF CHEMISTRY
ISSN	1364-548X		
Type of Use	Republish in a thesis/dissertation	**Portion**	Chart/graph/table/figure

LICENSED CONTENT

Publication Title	Chemical communications	**Rightsholder**	Royal Society of Chemistry
Article Title	The photoluminescence spectral profiles of water-soluble aggregates of PbS quantum dots assembled through reversible metal coordination.	**Publication Type**	e-Journal
		Start Page	1981
		End Page	1984
		Issue	12
		Volume	53
Author / Editor	Royal Society of Chemistry (Great Britain)		
Date	01/01/1996		
Language	English		
Country	United Kingdom of Great Britain and Northern Ireland		

REQUEST DETAILS

Portion Type	Chart/graph/table/figure	Distribution	Worldwide
Number of Charts / Graphs / Tables / Figures Requested	1	Translation	Original language of publication
Format (select all that apply)	Print, Electronic	Copies for the Disabled?	No
Who Will Republish the Content?	Academic institution	Minor Editing Privileges?	Yes
Duration of Use	Life of current edition	Incidental Promotional Use?	No
Lifetime Unit Quantity	Up to 499	Currency	USD
Rights Requested	Main product		

NEW WORK DETAILS

Title	Light-Harvesting Studies in Electrostatically Bonded All-Quantum Dot Assemblies	Institution Name	Indian Institute of Science Education and Research Pune
Instructor Name	Pradyut Roy	Expected Presentation Date	2024-09-01

ADDITIONAL DETAILS

Order Reference Number	N/A	The Requesting Person / Organization to Appear on the License	Pradyut Roy

REQUESTED CONTENT DETAILS

Title, Description or Numeric Reference of the Portion(s)	Figure 2b	Title of the Article / Chapter the Portion Is From	The photoluminescence spectral profiles of water-soluble aggregates of PbS quantum dots assembled through reversible metal coordination.
Editor of Portion(s)	Wang, Chen; Kodaimati, Mohamad Saeed; Schatz, George C.; Weiss, Emily A.	Author of Portion(s)	Wang, Chen; Kodaimati, Mohamad Saeed; Schatz, George C.; Weiss, Emily A.
Volume / Edition	53	Issue, if Republishing an Article From a Serial	12
Page or Page Range of Portion	1981-1984	Publication Date of Portion	2017-02-11

Total Items: 1

Total Due: 0.00 USD

Accepted: Marketplace Permissions General Terms and Conditions and any applicable Publisher Terms and Conditions

Figure 1.13

JOHN WILEY AND SONS LICENSE
TERMS AND CONDITIONS

Jul 14, 2024

This Agreement between Pradyut Roy ("You") and John Wiley and Sons ("John Wiley and Sons") consists of your license details and the terms and conditions provided by John Wiley and Sons and Copyright Clearance Center.

License Number	5827790262781
License date	Jul 14, 2024
Licensed Content Publisher	John Wiley and Sons
Licensed Content Publication	Small
Licensed Content Title	Functional Quantum-Dot/Dendrimer Nanotubes for Sensitive Detection of DNA Hybridization
Licensed Content Author	Wolfgang Knoll, Jean Pierre Majoral, Anne-Marie Caminade, et al
Licensed Content Date	May 19, 2008
Licensed Content Volume	4
Licensed Content Issue	5
Licensed Content Pages	6
Type of use	Dissertation/Thesis
Requestor type	University/Academic
Format	Print and electronic

Portion	Figure/table
Number of figures/tables	1
Will you be translating?	No
Title of new work	Light-Harvesting Studies in Electrostatically Bonded All-Quantum Dot Assemblies
Institution name	Indian Institute of Science Education and Research Pune
Expected presentation date	Oct 2024
Portions	Figures 3a,c
The Requesting Person / Organization to Appear on the License	Pradyut Roy
Requestor Location	Mr. Pradyut Roy IISER Pune Dr Homi Bhabha Road Pashan Pune, Pashan 411008 India Attn: Mr. Pradyut Roy
Publisher Tax ID	EU826007151
Total	0.00 USD

Terms and Conditions

TERMS AND CONDITIONS

This copyrighted material is owned by or exclusively licensed to John Wiley & Sons, Inc. or one of its group companies (each a"Wiley Company") or handled on behalf of a society with which a Wiley Company has exclusive publishing rights in relation to a particular work (collectively "WILEY"). By clicking "accept" in connection with completing this licensing transaction, you agree that the following terms and conditions apply to this transaction (along with the billing and payment terms and conditions established by the Copyright Clearance Center Inc., ("CCC's Billing and Payment terms and conditions"), at the time that you opened your RightsLink account (these are available at any time at http://myaccount.copyright.com).

Terms and Conditions

- The materials you have requested permission to reproduce or reuse (the "Wiley Materials") are protected by copyright.

- You are hereby granted a personal, non-exclusive, non-sub licensable (on a stand-alone basis), non-transferable, worldwide, limited license to reproduce the Wiley Materials for the purpose specified in the licensing process. This license, **and any CONTENT (PDF or image file) purchased as part of your order,** is for a one-time use only and limited to any maximum distribution number specified in the license. The first instance of republication or reuse granted by this license must be completed within two years of the date of the grant of this license (although copies prepared before the end date may be distributed thereafter). The Wiley Materials shall not be used in any other manner or for any other purpose, beyond what is granted in the license. Permission is granted subject to an appropriate acknowledgement given to the author, title of the material/book/journal and the publisher. You shall also duplicate the copyright notice that appears in the Wiley publication in your use of the Wiley Material. Permission is also granted on the understanding that nowhere in the text is a previously published source acknowledged for all or part of this Wiley Material. Any third party content is expressly excluded from this permission.

- With respect to the Wiley Materials, all rights are reserved. Except as expressly granted by the terms of the license, no part of the Wiley Materials may be copied, modified, adapted (except for minor reformatting required by the new Publication), translated, reproduced, transferred or distributed, in any form or by any means, and no derivative works may be made based on the Wiley Materials without the prior permission of the respective copyright owner.**For STM Signatory Publishers clearing permission under the terms of the STM Permissions Guidelines only, the terms of the license are extended to include subsequent editions and for editions in other languages, provided such editions are for the work as a whole in situ and does not involve the separate exploitation of the permitted figures or extracts,** You may not alter, remove or suppress in any manner any copyright, trademark or other notices displayed by the Wiley Materials. You may not license, rent, sell, loan, lease, pledge, offer as security, transfer or assign the Wiley Materials on a stand-alone basis, or any of the rights granted to you hereunder to any other person.

- The Wiley Materials and all of the intellectual property rights therein shall at all times remain the exclusive property of John Wiley & Sons Inc, the Wiley Companies, or their respective licensors, and your interest therein is only that of having possession of and the right to reproduce the Wiley Materials pursuant to Section 2 herein during the continuance of this Agreement. You agree that you own no right, title or interest in or to the Wiley Materials or any of the intellectual property rights therein. You shall have no rights hereunder other than the license as provided for above in Section 2. No right, license or interest to any trademark, trade name, service mark or other branding ("Marks") of WILEY or its licensors is granted hereunder, and you agree that you shall not assert any such right, license or interest with respect thereto

- NEITHER WILEY NOR ITS LICENSORS MAKES ANY WARRANTY OR REPRESENTATION OF ANY KIND TO YOU OR ANY THIRD PARTY, EXPRESS, IMPLIED OR STATUTORY, WITH RESPECT TO THE MATERIALS OR THE ACCURACY OF ANY INFORMATION CONTAINED IN THE MATERIALS, INCLUDING, WITHOUT LIMITATION, ANY IMPLIED WARRANTY OF MERCHANTABILITY, ACCURACY, SATISFACTORY QUALITY, FITNESS FOR A PARTICULAR PURPOSE, USABILITY,

INTEGRATION OR NON-INFRINGEMENT AND ALL SUCH WARRANTIES ARE HEREBY EXCLUDED BY WILEY AND ITS LICENSORS AND WAIVED BY YOU.

- WILEY shall have the right to terminate this Agreement immediately upon breach of this Agreement by you.

- You shall indemnify, defend and hold harmless WILEY, its Licensors and their respective directors, officers, agents and employees, from and against any actual or threatened claims, demands, causes of action or proceedings arising from any breach of this Agreement by you.

- IN NO EVENT SHALL WILEY OR ITS LICENSORS BE LIABLE TO YOU OR ANY OTHER PARTY OR ANY OTHER PERSON OR ENTITY FOR ANY SPECIAL, CONSEQUENTIAL, INCIDENTAL, INDIRECT, EXEMPLARY OR PUNITIVE DAMAGES, HOWEVER CAUSED, ARISING OUT OF OR IN CONNECTION WITH THE DOWNLOADING, PROVISIONING, VIEWING OR USE OF THE MATERIALS REGARDLESS OF THE FORM OF ACTION, WHETHER FOR BREACH OF CONTRACT, BREACH OF WARRANTY, TORT, NEGLIGENCE, INFRINGEMENT OR OTHERWISE (INCLUDING, WITHOUT LIMITATION, DAMAGES BASED ON LOSS OF PROFITS, DATA, FILES, USE, BUSINESS OPPORTUNITY OR CLAIMS OF THIRD PARTIES), AND WHETHER OR NOT THE PARTY HAS BEEN ADVISED OF THE POSSIBILITY OF SUCH DAMAGES. THIS LIMITATION SHALL APPLY NOTWITHSTANDING ANY FAILURE OF ESSENTIAL PURPOSE OF ANY LIMITED REMEDY PROVIDED HEREIN.

- Should any provision of this Agreement be held by a court of competent jurisdiction to be illegal, invalid, or unenforceable, that provision shall be deemed amended to achieve as nearly as possible the same economic effect as the original provision, and the legality, validity and enforceability of the remaining provisions of this Agreement shall not be affected or impaired thereby.

- The failure of either party to enforce any term or condition of this Agreement shall not constitute a waiver of either party's right to enforce each and every term and condition of this Agreement. No breach under this agreement shall be deemed waived or excused by either party unless such waiver or consent is in writing signed by the party granting such waiver or consent. The waiver by or consent of a party to a breach of any provision of this Agreement shall not operate or be construed as a waiver of or consent to any other or subsequent breach by such other party.

- This Agreement may not be assigned (including by operation of law or otherwise) by you without WILEY's prior written consent.

- Any fee required for this permission shall be non-refundable after thirty (30) days from receipt by the CCC.

- These terms and conditions together with CCC's Billing and Payment terms and conditions (which are incorporated herein) form the entire agreement between you and WILEY concerning this licensing transaction and (in the absence of fraud) supersedes all prior agreements and representations of the parties, oral or written. This Agreement may not be amended except in writing signed by both parties. This Agreement shall be binding upon and inure to the benefit of the parties' successors, legal representatives, and authorized assigns.

- In the event of any conflict between your obligations established by these terms and conditions and those established by CCC's Billing and Payment terms and

conditions, these terms and conditions shall prevail.

- WILEY expressly reserves all rights not specifically granted in the combination of (i) the license details provided by you and accepted in the course of this licensing transaction, (ii) these terms and conditions and (iii) CCC's Billing and Payment terms and conditions.

- This Agreement will be void if the Type of Use, Format, Circulation, or Requestor Type was misrepresented during the licensing process.

- This Agreement shall be governed by and construed in accordance with the laws of the State of New York, USA, without regards to such state's conflict of law rules. Any legal action, suit or proceeding arising out of or relating to these Terms and Conditions or the breach thereof shall be instituted in a court of competent jurisdiction in New York County in the State of New York in the United States of America and each party hereby consents and submits to the personal jurisdiction of such court, waives any objection to venue in such court and consents to service of process by registered or certified mail, return receipt requested, at the last known address of such party.

WILEY OPEN ACCESS TERMS AND CONDITIONS

Wiley Publishes Open Access Articles in fully Open Access Journals and in Subscription journals offering Online Open. Although most of the fully Open Access journals publish open access articles under the terms of the Creative Commons Attribution (CC BY) License only, the subscription journals and a few of the Open Access Journals offer a choice of Creative Commons Licenses. The license type is clearly identified on the article.

The Creative Commons Attribution License

The Creative Commons Attribution License (CC-BY) allows users to copy, distribute and transmit an article, adapt the article and make commercial use of the article. The CC-BY license permits commercial and non-

Creative Commons Attribution Non-Commercial License

The Creative Commons Attribution Non-Commercial (CC-BY-NC)License permits use, distribution and reproduction in any medium, provided the original work is properly cited and is not used for commercial purposes.(see below)

Creative Commons Attribution-Non-Commercial-NoDerivs License

The Creative Commons Attribution Non-Commercial-NoDerivs License (CC-BY-NC-ND) permits use, distribution and reproduction in any medium, provided the original work is properly cited, is not used for commercial purposes and no modifications or adaptations are made. (see below)

Use by commercial "for-profit" organizations

Use of Wiley Open Access articles for commercial, promotional, or marketing purposes requires further explicit permission from Wiley and will be subject to a fee.

Further details can be found on Wiley Online Library
http://olabout.wiley.com/WileyCDA/Section/id-410895.html

Other Terms and Conditions:

v1.10 Last updated September 2015

Questions? customercare@copyright.com.

Quantum-Dot-Based (Aero)gels: Control of the Optical Properties

Author: André Wolf, Vladimir Lesnyak, Nikolai Gaponik, et al
Publication: Journal of Physical Chemistry Letters
Publisher: American Chemical Society
Date: Aug 1, 2012

PERMISSION/LICENSE IS GRANTED FOR YOUR ORDER AT NO CHARGE

This type of permission/license, instead of the standard Terms and Conditions, is sent to you because no fee is being charged for your order. Please note the following:

- Permission is granted for your request in both print and electronic formats, and translations.
- If figures and/or tables were requested, they may be adapted or used in part.
- Please print this page for your records and send a copy of it to your publisher/graduate school.
- Appropriate credit for the requested material should be given as follows: "Reprinted (adapted) with permission from {COMPLETE REFERENCE CITATION}. Copyright {YEAR} American Chemical Society." Insert appropriate information in place of the capitalized words.
- One-time permission is granted only for the use specified in your RightsLink request. No additional uses are granted (such as derivative works or other editions). For any uses, please submit a new request.

If credit is given to another source for the material you requested from RightsLink, permission must be obtained from that source.

BACK CLOSE WINDOW

FRET-Activated Delayed Fluorescence in Densely Packed PbS Quantum-Dot Ensembles

Author: Aleksandr P. Litvin, Peter S. Parfenov, Elena V. Ushakova, et al
Publication: The Journal of Physical Chemistry C
Publisher: American Chemical Society
Date: Jul 1, 2015

PERMISSION/LICENSE IS GRANTED FOR YOUR ORDER AT NO CHARGE

This type of permission/license, instead of the standard Terms and Conditions, is sent to you because no fee is being charged for your order. Please note the following:

- Permission is granted for your request in both print and electronic formats, and translations.
- If figures and/or tables were requested, they may be adapted or used in part.
- Please print this page for your records and send a copy of it to your publisher/graduate school.
- Appropriate credit for the requested material should be given as follows: "Reprinted (adapted) with permission from {COMPLETE REFERENCE CITATION}. Copyright {YEAR} American Chemical Society." Insert appropriate information in place of the capitalized words.
- One-time permission is granted only for the use specified in your RightsLink request. No additional uses are granted (such as derivative works or other editions). For any uses, please submit a new request.

If credit is given to another source for the material you requested from RightsLink, permission must be obtained from that source.

BACK CLOSE WINDOW

Efficient Exciton Funneling in Cascaded PbS Quantum Dot Superstructures

Author: Fan Xu, Xin Ma, Chelsea R. Haughn, et al

Publication: ACS Nano

Publisher: American Chemical Society

Date: Dec 1, 2011

PERMISSION/LICENSE IS GRANTED FOR YOUR ORDER AT NO CHARGE

This type of permission/license, instead of the standard Terms and Conditions, is sent to you because no fee is being charged for your order. Please note the following:

- Permission is granted for your request in both print and electronic formats, and translations.
- If figures and/or tables were requested, they may be adapted or used in part.
- Please print this page for your records and send a copy of it to your publisher/graduate school.
- Appropriate credit for the requested material should be given as follows: "Reprinted (adapted) with permission from {COMPLETE REFERENCE CITATION}. Copyright {YEAR} American Chemical Society." Insert appropriate information in place of the capitalized words.
- One-time permission is granted only for the use specified in your RightsLink request. No additional uses are granted (such as derivative works or other editions). For any uses, please submit a new request.

If credit is given to another source for the material you requested from RightsLink, permission must be obtained from that source.

BACK CLOSE WINDOW

Figure 1.14

IISER PUNE

Roy Pradyut <roy.pradyut@students.iiserpune.ac.in>

Re: Copyright Request Permission

1 message

Dr Syed Ali Raza Naqvi <draliraza@gcuf.edu.pk> Mon, Jul 15, 2024 at 10:46 AM
To: Roy Pradyut <roy.pradyut@students.iiserpune.ac.in>

Dear Roy

Thanks for your mail. I am pleased to allow you to use Figure 1 in your MS/PhD thesis.

Stay blessed.

Prof. Ali

On Mon, 15 Jul 2024, 1:13 am Roy Pradyut, <roy.pradyut@students.iiserpune.ac.in> wrote:

> Dear Syed Ali Raza-Naqvi,
>
> I am Pradyut Roy, from Indian Institute of Science Education and Research (IISER) Pune, India. IISER Pune is a non-profit academic institute. I would like to take the copyright permission for Figure 1 from your published article (DOI: 10.4067/S0717-97072022000305615), to reuse in my PhD thesis. Could you please provide the permission for this?
>
> Title of the article: Toxicology of Heavy Metals Used in Cosmetics
>
> DOI: 10.4067/S0717-97072022000305615
>
> Figure Details: Figure 1
>
> Regards,
>
> Pradyut
>
> N.B. I am unable to take the copyright permission directly from the journal.
>
> ***Thanking you,***
> ***Pradyut Roy***
> ***Prime Minister's Research Fellow, PhD Student, Department of Chemistry, IISER Pune***
> ***Main Building;C214, NanoAlchemy Lab***
> ***Dr. Pramod P. Pillai's Group***

Figure 3.1

RightsLink

Chemistry of InP Nanocrystal Syntheses

Author: Sudarsan Tamang, Christophe Lincheneau, Yannick Hermans, et al
Publication: Chemistry of Materials
Publisher: American Chemical Society
Date: Apr 1, 2016

PERMISSION/LICENSE IS GRANTED FOR YOUR ORDER AT NO CHARGE

This type of permission/license, instead of the standard Terms and Conditions, is sent to you because no fee is being charged for your order. Please note the following:

- Permission is granted for your request in both print and electronic formats, and translations.
- If figures and/or tables were requested, they may be adapted or used in part.
- Please print this page for your records and send a copy of it to your publisher/graduate school.
- Appropriate credit for the requested material should be given as follows: "Reprinted (adapted) with permission from {COMPLETE REFERENCE CITATION}. Copyright {YEAR} American Chemical Society." Insert appropriate information in place of the capitalized words.
- One-time permission is granted only for the use specified in your RightsLink request. No additional uses are granted (such as derivative works or other editions). For any uses, please submit a new request.

If credit is given to another source for the material you requested from RightsLink, permission must be obtained from that source.

BACK CLOSE WINDOW

Figure 3.2

RightsLink

Synthesis of Colloidal Blue-Emitting InP/ZnS Core/Shell Quantum Dots with the Assistance of Copper Cations

Author: Fan Huang, Chenghao Bi, Ruiqi Guo, et al
Publication: Journal of Physical Chemistry Letters
Publisher: American Chemical Society
Date: Nov 1, 2019

PERMISSION/LICENSE IS GRANTED FOR YOUR ORDER AT NO CHARGE

This type of permission/license, instead of the standard Terms and Conditions, is sent to you because no fee is being charged for your order. Please note the following:

- Permission is granted for your request in both print and electronic formats, and translations.
- If figures and/or tables were requested, they may be adapted or used in part.
- Please print this page for your records and send a copy of it to your publisher/graduate school.
- Appropriate credit for the requested material should be given as follows: "Reprinted (adapted) with permission from {COMPLETE REFERENCE CITATION}. Copyright {YEAR} American Chemical Society." Insert appropriate information in place of the capitalized words.
- One-time permission is granted only for the use specified in your RightsLink request. No additional uses are granted (such as derivative works or other editions). For any uses, please submit a new request.

If credit is given to another source for the material you requested from RightsLink, permission must be obtained from that source.

BACK CLOSE WINDOW

Marketplace

All types | 10.3390/nano10112171 | Advanced Search | Search Tips

Filter your results:

No filters are available

0 publications and 1 articles/chapters matched your search term(s)

Hide filters

Article/Chapter Results

Sort by Relevance

Synthesis of Blue-Emissive InP/GaP/ZnS Quantum Dots via Controlling the Reaction Kinetics of Shell Growth and Length of Capping Ligands

Lee, Woosuk; Lee, Changmin; Kim, Boram; Choi, Yonghyeok; Chae, ...More

Nanomaterials, 01 Nov 2020, Vol. 10, Issue 11, pages 2171 - ...

ISSN: 20794991
DOI: 10.3390/nano10112171
PMID: 33143226
PMCID: PMC7692729

Publisher: MDPI; MDPI AG
Language: English
Country: Switzerland
URL: https://www.mdpi.com/2079-4991/10/11/2171

Details >

Request Reprints/ePrints | Request Single Copy | Request Permission | Open Access - Creative Commons CC BY 4.0

Marketplace

Order Confirmation

Thank you, your order has been placed. An email confirmation has been sent to you. Your order license details and printable licenses will be available within 24 hours. Please access Manage Account for final order details.

This is not an invoice. Please go to manage account to access your order history and invoices.

CUSTOMER INFORMATION

Payment by invoice: You can cancel your order until the invoice is generated by contacting customer service.

Billing Address

Mr. Pradyut Roy
IISER Pune
Dr Homi Bhabha Road
Pashan
Pune, Pashan 411008
India

+91 2025908678
roy.pradyut@students.iiserpune.ac.in

Customer Location

Mr. Pradyut Roy
IISER Pune
Dr Homi Bhabha Road
Pashan
Pune, Pashan 411008
India

PO Number (optional)

N/A

Payment options

Invoice

PENDING ORDER CONFIRMATION

Confirmation Number: Pending

Order Date: 15-Jul-2024

1. Nanotechnology

0.00 USD

Article: Synthesis of blue emitting InP/ZnS quantum dots through control of competition between etching and growth.

Order License ID	Pending	**Publisher**	IOP Publishing
ISSN	1361-6528	**Portion**	Chart/graph/table/figure
Type of Use	Republish in a thesis/dissertation		

LICENSED CONTENT

Publication Title	Nanotechnology	**Rightsholder**	IOP Publishing, Ltd
Article Title	Synthesis of blue emitting InP/ZnS quantum dots through control of competition between etching and growth.	**Publication Type**	e-Journal
		Start Page	485609
		Issue	48
		Volume	23
Author / Editor	Institute of Physics (Great Britain)	**URL**	http://www.iop.org/Journals/na
Date	01/01/1996		
Language	English		
Country	United Kingdom of Great Britain and Northern Ireland		

REQUEST DETAILS

Portion Type	Chart/graph/table/figure	**Distribution**	Worldwide
Number of Charts / Graphs / Tables / Figures Requested	1	**Translation**	Original language of publication
Format (select all that apply)	Print, Electronic	**Copies for the Disabled?**	No
Who Will Republish the Content?	Academic institution	**Minor Editing Privileges?**	Yes
		Incidental Promotional Use?	No
Duration of Use	Life of current edition	**Currency**	USD
Lifetime Unit Quantity	Up to 499		
Rights Requested	Main product		

NEW WORK DETAILS

Title	Light-Harvesting Studies in Electrostatically Bonded All-Quantum Dot Assemblies	**Institution Name**	Indian Institute of Science Education and Research (IISER) Pune
Instructor Name	Pradyut Roy	**Expected Presentation Date**	2024-09-01

ADDITIONAL DETAILS

Order Reference Number	N/A	**The Requesting Person / Organization to Appear on the License**	Pradyut Roy

REQUESTED CONTENT DETAILS

Title, Description or Numeric Reference of the Portion(s)	Figures 1d,f	**Title of the Article / Chapter the Portion Is From**	Synthesis of blue emitting InP/ZnS quantum dots through control of competition between etching and growth.
Editor of Portion(s)	Lim, Kipil; Jang, Ho Seong; Woo, Kyoungja	**Author of Portion(s)**	Lim, Kipil; Jang, Ho Seong; Woo, Kyoungja
Volume / Edition	23	**Issue, if Republishing an Article From a Serial**	48
Page or Page Range of Portion	485609	**Publication Date of Portion**	2012-12-07

RIGHTSHOLDER TERMS AND CONDITIONS

These special terms and conditions are in addition to the standard terms and conditions for CCC's Republication Service and, together with those standard terms and conditions, govern the use of the Works. As the User you will make all reasonable efforts to contact the author(s) of the article which the Work is to be reused from, to seek consent for your intended use. Contacting one author who is acting expressly as authorised agent for their co-author(s) is acceptable. User will reproduce the following wording prominently alongside the Work: the source of the Work, including author, article title, title of journal, volume number, issue number (if relevant), page range (or first page if this is the only information available) and date of first publication; and a link back to the article (via DOI); and if practicable, and IN ALL CASES for new works published under any of the Creative Commons licences, the words "© IOP Publishing. Reproduced with permission. All rights reserved" Without the express permission of the author(s) and the Rightsholder of the article from which the Work is to be reused, User shall not use it in any way which, in the opinion of the Rightsholder, could: (i) distort or alter the author(s)' original intention(s) and meaning; (ii) be prejudicial to the honour or reputation of the author(s); and/or (iii) imply endorsement by the author(s) and/or the Rightsholder. This licence does not apply to any article which is credited to another source and which does not have the copyright line '© IOP Publishing Ltd'. User must check the copyright line of the article from which the Work is to be reused to check that IOP Publishing Ltd has all the necessary rights to be able to grant permission. User is solely responsible for identifying and obtaining separate licences and permissions from the copyright owner for reuse of any such third party material/figures which the Rightsholder is not the copyright owner of. The Rightsholder shall not reimburse any fees which User pays for a republication license for such third party content. This licence does not apply to any material/figure which is credited to another source in the Rightsholder's publication or has been obtained from a third party. User must check the Version of Record of the article from which the Work is to be reused, to check whether any of the material in the Work is third party material. Third party citations and/or copyright notices and/or permissions statements may not be included in any other version of the article from which the Work is to be reused and so cannot be relied upon by the User. User is solely responsible for identifying and obtaining separate licences and permissions from the copyright owner for reuse of any such third party material/figures where the Rightsholder is not the copyright owner. The Rightsholder shall not reimburse any fees which User pays for a republication license for such third party content. User and CCC acknowledge that the Rightsholder may, from time to time, make changes or additions to these special terms and conditions without express notification, provided that these shall not apply to permissions already secured and paid for by User prior to such change or addition. User acknowledges that the Rightsholder (which includes companies within its group and third parties for whom it publishes its titles) may make use of personal data collected through the service in the course of their business. If User is the author of the Work, User may automatically have the right to reuse it under the rights granted back when User transferred the copyright in the article to the Rightsholder. User should check the copyright form and the relevant author rights policy to check whether permission is required. If User is the author of the Work and does require permission for proposed reuse of the Work, User should select 'Author of requested content' as the Requestor Type. The Rightsholder shall not reimburse any fees which User pays for a republication license. If User is the author of the article which User wishes to reuse in User's thesis or dissertation, the republication licence covers the right to include the Version of Record of the article, provided it is not then shared or deposited online. User must include citation details. Where User wishes to share their thesis or dissertation online, they

Total Items: 1

Total Due: 0.00 USD

Accepted: Marketplace Permissions General Terms and Conditions and any applicable Publisher Terms and Conditions

Figure 3.3

RightsLink

Economic and Size-Tunable Synthesis of InP/ZnE (E = S, Se) Colloidal Quantum Dots.

Author: Mickael D. Tessier, Dorian Dupont, Kim De Nolf, et al

Publication: Chemistry of Materials

Publisher: American Chemical Society

Date: Jul 1, 2015

PERMISSION/LICENSE IS GRANTED FOR YOUR ORDER AT NO CHARGE

This type of permission/license, instead of the standard Terms and Conditions, is sent to you because no fee is being charged for your order. Please note the following:

- Permission is granted for your request in both print and electronic formats, and translations.
- If figures and/or tables were requested, they may be adapted or used in part.
- Please print this page for your records and send a copy of it to your publisher/graduate school.
- Appropriate credit for the requested material should be given as follows: "Reprinted (adapted) with permission from {COMPLETE REFERENCE CITATION}. Copyright {YEAR} American Chemical Society." Insert appropriate information in place of the capitalized words.
- One-time permission is granted only for the use specified in your RightsLink request. No additional uses are granted (such as derivative works or other editions). For any uses, please submit a new request.

If credit is given to another source for the material you requested from RightsLink, permission must be obtained from that source.

BACK CLOSE WINDOW

Figure 4.1

IISER PUNE

Roy Pradyut <roy.pradyut@students.iiserpune.ac.in>

RE: Copyright Permission {2471}

1 message

Optica Publishing Group Copyright <copyright@optica.org> Thu, Jul 18, 2024 at 12:30 AM
Reply-To: copyright@optica.org
To: roy.pradyut@students.iiserpune.ac.in

--reply above this line--

Dear Pradyut Roy,

Thank you for contacting Optica Publishing Group.

For the use of figure 5 from Deokho Jang, Younho Han, Seungin Baek, and Jungho Kim, "Theoretical comparison of the energies and wave functions of the electron and hole states between CdSe- and InP-based core/shell/shell quantum dots: effect of the bandgap energy of the core material on the emission spectrum," Opt. Mater. Express 9, 1257-1270 (2019):

> Optica Publishing Group considers your requested use of its copyrighted material to be Fair Use under United States Copyright Law. We request that a complete citation of the original material be included in any publication.
>
> As this article is published under the terms of the Optica Publishing Group Open Access Publishing Agreement (OAPA), when adapting or otherwise creating a derivative version of the article, users must maintain attribution to the author(s) and the published article's title, journal citation, and DOI. Users should also indicate if changes were made and avoid any implication that the author or Optica Publishing Group endorses the use.

While your publisher should be able to provide additional guidance, we prefer the below citation formats:

> For citations in figure captions:
>
> [Reprinted/Adapted] with permission from [ref #] © Optical Society of America [or Optica Publishing Group, as applicable]. (Please include the full citation in your reference list)
>
> For images without captions:
>
> Journal Vol. #, first page (year published) An example: Opt. Express 27, 1164 (2019)

Please let me know if you have any questions.

Kind Regards,

Cassie Travers

Cassie Travers
17 July 2024
Authorized Agent, Optica Publishing Group

Dear Optica Publishing Group,
I am Pradyut Roy, from Indian Institute of Science Education and Research (IISER) Pune, India. IISER Pune is an non-profit academic institute. I would like to take the copyright permission for Figure 5 from an article (DOI: 10.1364/OME.9.001257) to reuse in my PhD thesis. Could you please provide the permission for this?

Title of the article: Theoretical comparison of the energies and wave functions of the electron and hole states between CdSe- and InP-based core/shell/shell quantum dots: effect of the bandgap energy of the core material on the emission spectrum
DOI: 10.1364/OME.9.001257
Figure Details: Figure 5

Thanking you,

Pradyut Roy
Prime Minister's Research Fellow, PhD Student, Department of Chemistry, IISER Pune
Main Building;C214, NanoAlchemy Lab
Dr. Pramod P. Pillai's Group

Permission requests / Unsorted | In progress | Normal priority

NOTE: When replying to this email please leave the subject-line intact.

Figure 4.2

American Physical Society
Reuse and Permissions License

17-Jul-2024

This license agreement between the American Physical Society ("APS") and Pradyut Roy ("You") consists of your license details and the terms and conditions provided by the American Physical Society and SciPris.

Licensed Content Information

License Number:	**RNP/24/JUL/081381**
License date:	17-Jul-2024
DOI:	10.1103/PhysRevB.56.1496
Title:	InP quantum dots: Electronic structure, surface effects, and the redshifted emission
Author:	Huaxiang Fu and Alex Zunger
Publication:	Physical Review B
Publisher:	American Physical Society
Cost:	USD $ 0.00

Request Details

Does your reuse require significant modifications: No

Specify intended distribution locations:	Worldwide
Reuse Category:	Reuse in a thesis/dissertation
Requestor Type:	Academic Institution
Items for Reuse:	Figures/Tables
Number of Figure/Tables:	2
Figure/Tables Details:	Figure 7 and Figure 8
Format for Reuse:	Print and Electronic
Total number of print copies:	Up to 1000

Information about New Publication:

University/Publisher:	Indian Institute Of Science Education And Research Pune
Title of dissertation/thesis:	Light-Harvesting Studies in Electrostatically Bonded All-Quantum Dot Assemblies
Author(s):	Pradyut Roy
Expected completion date:	Sep. 2024

License Requestor Information

Name:	Pradyut Roy
Affiliation:	Individual
Email Id:	roy.pradyut@students.iiserpune.ac.in
Country:	India

American Physical Society
Reuse and Permissions License

TERMS AND CONDITIONS

The American Physical Society (APS) is pleased to grant the Requestor of this license a non-exclusive, non-transferable permission, limited to Print and Electronic format, provided all criteria outlined below are followed.

1. You must also obtain permission from at least one of the lead authors for each separate work, if you haven't done so already. The author's name and affiliation can be found on the first page of the published Article.

2. For electronic format permissions, Requestor agrees to provide a hyperlink from the reprinted APS material using the source material's DOI on the web page where the work appears. The hyperlink should use the standard DOI resolution URL, http://dx.doi.org/{DOI}. The hyperlink may be embedded in the copyright credit line.

3. For print format permissions, Requestor agrees to print the required copyright credit line on the first page where the material appears: "Reprinted (abstract/excerpt/figure) with permission from [(FULL REFERENCE CITATION) as follows: Author's Names, APS Journal Title, Volume Number, Page Number and Year of Publication.] Copyright (YEAR) by the American Physical Society."

4. Permission granted in this license is for a one-time use and does not include permission for any future editions, updates, databases, formats or other matters. Permission must be sought for any additional use.

5. Use of the material does not and must not imply any endorsement by APS.

6. APS does not imply, purport or intend to grant permission to reuse materials to which it does not hold copyright. It is the requestor's sole responsibility to ensure the licensed material is original to APS and does not contain the copyright of another entity, and that the copyright notice of the figure, photograph, cover or table does not indicate it was reprinted by APS with permission from another source.

7. The permission granted herein is personal to the Requestor for the use specified and is not transferable or assignable without express written permission of APS. This license may not be amended except in writing by APS.

8. You may not alter, edit or modify the material in any manner.

9. You may translate the materials only when translation rights have been granted.

10. APS is not responsible for any errors or omissions due to translation.

11. You may not use the material for promotional, sales, advertising or marketing purposes.

12. The foregoing license shall not take effect unless and until APS or its agent, Aptara, receives payment in full in accordance with Aptara Billing and Payment Terms and Conditions, which are incorporated herein by reference.

13. Should the terms of this license be violated at any time, APS or Aptara may revoke the license with no refund to you and seek relief to the fullest extent of the laws of the USA. Official written notice will be made using the contact information provided with the permission request. Failure to receive such notice will not nullify revocation of the permission.

14. APS reserves all rights not specifically granted herein.

15. This document, including the Aptara Billing and Payment Terms and Conditions, shall be the entire agreement between the parties relating to the subject matter hereof.

Figure 4.3

RightsLink

Sign in/Register

Photosensitization of Nanoporous TiO2 Electrodes with InP Quantum Dots

Author: A. Zaban, O. I. Mićić, B. A. Gregg, et al

Publication: Langmuir

Publisher: American Chemical Society

Date: Jun 1, 1998

PERMISSION/LICENSE IS GRANTED FOR YOUR ORDER AT NO CHARGE

This type of permission/license, instead of the standard Terms and Conditions, is sent to you because no fee is being charged for your order. Please note the following:

- Permission is granted for your request in both print and electronic formats, and translations.
- If figures and/or tables were requested, they may be adapted or used in part.
- Please print this page for your records and send a copy of it to your publisher/graduate school.
- Appropriate credit for the requested material should be given as follows: "Reprinted (adapted) with permission from {COMPLETE REFERENCE CITATION}. Copyright {YEAR} American Chemical Society." Insert appropriate information in place of the capitalized words.
- One-time permission is granted only for the use specified in your RightsLink request. No additional uses are granted (such as derivative works or other editions). For any uses, please submit a new request.

If credit is given to another source for the material you requested from RightsLink, permission must be obtained from that source.

BACK CLOSE WINDOW

How Trap States Affect Charge Carrier Dynamics of CdSe and InP Quantum Dots: Visualization through Complexation with Viologen

Author: Anoop Thomas, K. Sandeep, Sanoop Mambully Somasundaran, et al
Publication: ACS Energy Letters
Publisher: American Chemical Society
Date: Oct 1, 2018

PERMISSION/LICENSE IS GRANTED FOR YOUR ORDER AT NO CHARGE

This type of permission/license, instead of the standard Terms and Conditions, is sent to you because no fee is being charged for your order. Please note the following:

- Permission is granted for your request in both print and electronic formats, and translations.
- If figures and/or tables were requested, they may be adapted or used in part.
- Please print this page for your records and send a copy of it to your publisher/graduate school.
- Appropriate credit for the requested material should be given as follows: "Reprinted (adapted) with permission from {COMPLETE REFERENCE CITATION}. Copyright {YEAR} American Chemical Society." Insert appropriate information in place of the capitalized words.
- One-time permission is granted only for the use specified in your RightsLink request. No additional uses are granted (such as derivative works or other editions). For any uses, please submit a new request.

If credit is given to another source for the material you requested from RightsLink, permission must be obtained from that source.

BACK CLOSE WINDOW

Interfacial Charge Separation and Recombination in InP and Quasi-Type II InP/CdS Core/Shell Quantum Dot-Molecular Acceptor Complexes

Author: Kaifeng Wu, Nianhui Song, Zheng Liu, et al
Publication: The Journal of Physical Chemistry A
Publisher: American Chemical Society
Date: Aug 1, 2013

PERMISSION/LICENSE IS GRANTED FOR YOUR ORDER AT NO CHARGE

This type of permission/license, instead of the standard Terms and Conditions, is sent to you because no fee is being charged for your order. Please note the following:

- Permission is granted for your request in both print and electronic formats, and translations.
- If figures and/or tables were requested, they may be adapted or used in part.
- Please print this page for your records and send a copy of it to your publisher/graduate school.
- Appropriate credit for the requested material should be given as follows: "Reprinted (adapted) with permission from {COMPLETE REFERENCE CITATION}. Copyright {YEAR} American Chemical Society." Insert appropriate information in place of the capitalized words.
- One-time permission is granted only for the use specified in your RightsLink request. No additional uses are granted (such as derivative works or other editions). For any uses, please submit a new request.

If credit is given to another source for the material you requested from RightsLink, permission must be obtained from that source.

BACK CLOSE WINDOW

Fluorescence Resonance Energy Transfer Between Quantum Dot Donors and Dye-Labeled Protein Acceptors

Author: Aaron R. Clapp, Igor L. Medintz, J. Matthew Mauro, et al
Publication: Journal of the American Chemical Society
Publisher: American Chemical Society
Date: Jan 1, 2004

PERMISSION/LICENSE IS GRANTED FOR YOUR ORDER AT NO CHARGE

This type of permission/license, instead of the standard Terms and Conditions, is sent to you because no fee is being charged for your order. Please note the following:

- Permission is granted for your request in both print and electronic formats, and translations.
- If figures and/or tables were requested, they may be adapted or used in part.
- Please print this page for your records and send a copy of it to your publisher/graduate school.
- Appropriate credit for the requested material should be given as follows: "Reprinted (adapted) with permission from {COMPLETE REFERENCE CITATION}. Copyright {YEAR} American Chemical Society." Insert appropriate information in place of the capitalized words.
- One-time permission is granted only for the use specified in your RightsLink request. No additional uses are granted (such as derivative works or other editions). For any uses, please submit a new request.

If credit is given to another source for the material you requested from RightsLink, permission must be obtained from that source.

BACK CLOSE WINDOW

American Physical Society
Reuse and Permissions License

Figure 5.2

15-Jul-2024

This license agreement between the American Physical Society ("APS") and Pradyut Roy ("You") consists of your license details and the terms and conditions provided by the American Physical Society and SciPris.

Licensed Content Information

License Number:	**RNP/24/JUL/081332**
License date:	15-Jul-2024
DOI:	10.1103/PhysRevLett.89.186802
Title:	Spectrally Resolved Dynamics of Energy Transfer in Quantum-Dot Assemblies: Towards Engineered Energy Flows in Artificial Materials
Author:	S. A. Crooker et al.
Publication:	Physical Review Letters
Publisher:	American Physical Society
Cost:	USD $ 0.00

Request Details

Does your reuse require significant modifications: No

Specify intended distribution locations:	Worldwide
Reuse Category:	Reuse in a thesis/dissertation
Requestor Type:	Academic Institution
Items for Reuse:	Figures/Tables
Number of Figure/Tables:	1
Figure/Tables Details:	Figure 1
Format for Reuse:	Print and Electronic
Total number of print copies:	Up to 1000

Information about New Publication:

University/Publisher:	Indian Institute Of Science Education And Research Pune
Title of dissertation/thesis:	Light-Harvesting Studies in Electrostatically Bonded All-Quantum Dot Assemblies
Author(s):	Pradyut Roy
Expected completion date:	Sep. 2024

License Requestor Information

Name:	Pradyut Roy
Affiliation:	Individual
Email Id:	roy.pradyut@students.iiserpune.ac.in
Country:	India

American Physical Society
Reuse and Permissions License

TERMS AND CONDITIONS

The American Physical Society (APS) is pleased to grant the Requestor of this license a non-exclusive, non-transferable permission, limited to Print and Electronic format, provided all criteria outlined below are followed.

1. You must also obtain permission from at least one of the lead authors for each separate work, if you haven't done so already. The author's name and affiliation can be found on the first page of the published Article.

2. For electronic format permissions, Requestor agrees to provide a hyperlink from the reprinted APS material using the source material's DOI on the web page where the work appears. The hyperlink should use the standard DOI resolution URL, http://dx.doi.org/{DOI}. The hyperlink may be embedded in the copyright credit line.

3. For print format permissions, Requestor agrees to print the required copyright credit line on the first page where the material appears: "Reprinted (abstract/excerpt/figure) with permission from [(FULL REFERENCE CITATION) as follows: Author's Names, APS Journal Title, Volume Number, Page Number and Year of Publication.] Copyright (YEAR) by the American Physical Society."

4. Permission granted in this license is for a one-time use and does not include permission for any future editions, updates, databases, formats or other matters. Permission must be sought for any additional use.

5. Use of the material does not and must not imply any endorsement by APS.

6. APS does not imply, purport or intend to grant permission to reuse materials to which it does not hold copyright. It is the requestor's sole responsibility to ensure the licensed material is original to APS and does not contain the copyright of another entity, and that the copyright notice of the figure, photograph, cover or table does not indicate it was reprinted by APS with permission from another source.

7. The permission granted herein is personal to the Requestor for the use specified and is not transferable or assignable without express written permission of APS. This license may not be amended except in writing by APS.

8. You may not alter, edit or modify the material in any manner.

9. You may translate the materials only when translation rights have been granted.

10. APS is not responsible for any errors or omissions due to translation.

11. You may not use the material for promotional, sales, advertising or marketing purposes.

12. The foregoing license shall not take effect unless and until APS or its agent, Aptara, receives payment in full in accordance with Aptara Billing and Payment Terms and Conditions, which are incorporated herein by reference.

13. Should the terms of this license be violated at any time, APS or Aptara may revoke the license with no refund to you and seek relief to the fullest extent of the laws of the USA. Official written notice will be made using the contact information provided with the permission request. Failure to receive such notice will not nullify revocation of the permission.

14. APS reserves all rights not specifically granted herein.

15. This document, including the Aptara Billing and Payment Terms and Conditions, shall be the entire agreement between the parties relating to the subject matter hereof.

Electronic Coupling and Exciton Energy Transfer in CdTe Quantum-Dot Molecules

Author: Rolf Koole, Peter Liljeroth, Celso de Mello Donegá, et al
Publication: Journal of the American Chemical Society
Publisher: American Chemical Society
Date: Aug 1, 2006

PERMISSION/LICENSE IS GRANTED FOR YOUR ORDER AT NO CHARGE

This type of permission/license, instead of the standard Terms and Conditions, is sent to you because no fee is being charged for your order. Please note the following:

- Permission is granted for your request in both print and electronic formats, and translations.
- If figures and/or tables were requested, they may be adapted or used in part.
- Please print this page for your records and send a copy of it to your publisher/graduate school.
- Appropriate credit for the requested material should be given as follows: "Reprinted (adapted) with permission from {COMPLETE REFERENCE CITATION}. Copyright {YEAR} American Chemical Society." Insert appropriate information in place of the capitalized words.
- One-time permission is granted only for the use specified in your RightsLink request. No additional uses are granted (such as derivative works or other editions). For any uses, please submit a new request.

If credit is given to another source for the material you requested from RightsLink, permission must be obtained from that source.

BACK CLOSE WINDOW

Subdiffusive Exciton Transport in Quantum Dot Solids

Author: Gleb M. Akselrod, Ferry Prins, Lisa V. Poulikakos, et al
Publication: Nano Letters
Publisher: American Chemical Society
Date: Jun 1, 2014

PERMISSION/LICENSE IS GRANTED FOR YOUR ORDER AT NO CHARGE

This type of permission/license, instead of the standard Terms and Conditions, is sent to you because no fee is being charged for your order. Please note the following:

- Permission is granted for your request in both print and electronic formats, and translations.
- If figures and/or tables were requested, they may be adapted or used in part.
- Please print this page for your records and send a copy of it to your publisher/graduate school.
- Appropriate credit for the requested material should be given as follows: "Reprinted (adapted) with permission from {COMPLETE REFERENCE CITATION}. Copyright {YEAR} American Chemical Society." Insert appropriate information in place of the capitalized words.
- One-time permission is granted only for the use specified in your RightsLink request. No additional uses are granted (such as derivative works or other editions). For any uses, please submit a new request.

If credit is given to another source for the material you requested from RightsLink, permission must be obtained from that source.

BACK CLOSE WINDOW

Figure 5.3

Picosecond Energy Transfer in Quantum Dot Langmuir−Blodgett Nanoassemblies

Author: Marc Achermann, Melissa A. Petruska, Scott A. Crooker, et al
Publication: The Journal of Physical Chemistry B
Publisher: American Chemical Society
Date: Dec 1, 2003

PERMISSION/LICENSE IS GRANTED FOR YOUR ORDER AT NO CHARGE

This type of permission/license, instead of the standard Terms and Conditions, is sent to you because no fee is being charged for your order. Please note the following:

- Permission is granted for your request in both print and electronic formats, and translations.
- If figures and/or tables were requested, they may be adapted or used in part.
- Please print this page for your records and send a copy of it to your publisher/graduate school.
- Appropriate credit for the requested material should be given as follows: "Reprinted (adapted) with permission from {COMPLETE REFERENCE CITATION}. Copyright {YEAR} American Chemical Society." Insert appropriate information in place of the capitalized words.
- One-time permission is granted only for the use specified in your RightsLink request. No additional uses are granted (such as derivative works or other editions). For any uses, please submit a new request.

If credit is given to another source for the material you requested from RightsLink, permission must be obtained from that source.

BACK CLOSE WINDOW

Directed Energy Transfer in Films of CdSe Quantum Dots: Beyond the Point Dipole Approximation

Author: Kaibo Zheng, Karel Žídek, Mohamed Abdellah, et al
Publication: Journal of the American Chemical Society
Publisher: American Chemical Society
Date: Apr 1, 2014

PERMISSION/LICENSE IS GRANTED FOR YOUR ORDER AT NO CHARGE

This type of permission/license, instead of the standard Terms and Conditions, is sent to you because no fee is being charged for your order. Please note the following:

- Permission is granted for your request in both print and electronic formats, and translations.
- If figures and/or tables were requested, they may be adapted or used in part.
- Please print this page for your records and send a copy of it to your publisher/graduate school.
- Appropriate credit for the requested material should be given as follows: "Reprinted (adapted) with permission from {COMPLETE REFERENCE CITATION}. Copyright {YEAR} American Chemical Society." Insert appropriate information in place of the capitalized words.
- One-time permission is granted only for the use specified in your RightsLink request. No additional uses are granted (such as derivative works or other editions). For any uses, please submit a new request.

If credit is given to another source for the material you requested from RightsLink, permission must be obtained from that source.

BACK CLOSE WINDOW

Figure 6.2

High-Efficiency Förster Resonance Energy Transfer in Solid-State Dye Sensitized Solar Cells

Author: Gopal K. Mor, James Basham, Maggie Paulose, et al
Publication: Nano Letters
Publisher: American Chemical Society
Date: Jul 1, 2010

PERMISSION/LICENSE IS GRANTED FOR YOUR ORDER AT NO CHARGE

This type of permission/license, instead of the standard Terms and Conditions, is sent to you because no fee is being charged for your order. Please note the following:

- Permission is granted for your request in both print and electronic formats, and translations.
- If figures and/or tables were requested, they may be adapted or used in part.
- Please print this page for your records and send a copy of it to your publisher/graduate school.
- Appropriate credit for the requested material should be given as follows: "Reprinted (adapted) with permission from {COMPLETE REFERENCE CITATION}. Copyright {YEAR} American Chemical Society." Insert appropriate information in place of the capitalized words.
- One-time permission is granted only for the use specified in your RightsLink request. No additional uses are granted (such as derivative works or other editions). For any uses, please submit a new request.

If credit is given to another source for the material you requested from RightsLink, permission must be obtained from that source.

BACK CLOSE WINDOW